Universidad del País Vasco Euskal Herriko Unibertsitatea

NAZIOARTEKO BIKAINTASUN CAMPUSA
CAMPUS DE EXCELENCIA INTERNACIONAL

Role of Chaperone-Mediated Autophagy and Histone Deacetylases in Glioblastoma and Brain Aging – A focus on Stem Cell Maintenance

Jaione Auzmendi Iriarte

PhD thesis 2022

Role of Chaperone-Mediated Autophagy and Histone Deacetylases in Glioblastoma and Brain Aging – A focus on Stem Cell Maintenance

Jaione Auzmendi Iriarte

SUPERVISOR

Ander Matheu Fernández

PhD Thesis

2022

Nire familiari,

‘Energy and persistence conquer all things’

(Benjamin Franklin)

‘Kantu bat bizitako guztiari, kantu bat aurretik dugunari’

(Bulego)

Acknowledgments

Doktoretza tesi bat ikusi izan dudan bakoitzean, zuzenean joan izan naiz esker onen atala irakurtzera, eta beti pentsatu izan dut nik nirea ilusio eta emozioz beteta idatziko nuela. Eta halaxe nabil orain, sinestea ere zaila egiten zait. Izugarria da zenbat bizipen eta abentura izan ditudan urte hauetan, eta gehienbat zenbat ikasketa, ez bakarrik arlo profesionalean, baita pertsonalean ere. Noizbait galdetu izan didate, aukera izango bazenu atzera bueltatzeko, berriz ere aukeratuko zenuke doktoretza egitea? Nere erantzuna baiezkoa da. Etapa ez da erraza, gorabehera ugari azaltzen dira bidean, baina bizipen guztiek dute bere balorea eta ikasketa. Orain dela 5 urte eta erdiko Jaioneri begiratzen badiot, gaur egun, kanaren bat gehiagorekin (zergatik ote? jajaja), baina seguruago eta sendoago ikusten naiz, eta orduan bezala, kantu bat eskaintzen momentu orori.

Hay mucha gente a la que me gustaría agradecer su apoyo durante estos años, y que probablemente, las líneas aquí escritas se queden cortas para muchos de ellos. En primer lugar, gracias Ander por darme la oportunidad de realizar la tesis en tu grupo, y así poder dar mis primeros pasos en la investigación. He podido participar en varios trabajos, he asistido a congresos, y he podido hacer una estancia internacional (¡incluso en época de pandemia!). Gracias por esas comidas de grupo, les daba un toque especial a las celebraciones. De hecho, creo que aún tenemos alguna cosilla que celebrar… jajaja

Estefanía, mi compañera de batallas en el animalario, cuántos momentos habremos pasado allí abajo, y cuántas risas nos habremos echado. Gracias por tu ayuda y por los consejos que me has ido dando durante estos años. Y como no, junto con Ander y María, gracias por tomarte el tiempo de revisar esta tesis. Me alegro mucho de todas metas que has alcanzado durante estos años. Idoia, zurekin hasi nuen nire bidea taldean, masterreko proiektua zurekin egiteko aukera eman zenidan, eta asko eskertzen dizut hori. Urte gutxi izan badira ere elkarrekin egon garenak, zure aholkuak garrantzitsuak izan dira momentu askotan, beraz, mila esker. Paula, erreleboa hartu nizun taldean, gauza asko ikasi ahal izan nituen zurekin egondako momentu horietan, mila esker beraz! Oraindik ere ikusi izan gara kongresuren batean, eta tribunalarekin ere lagundu didazu! Laura, contigo coincidí poquito en Biodonostia, pero nos hemos juntado fuera en varias ocasiones y ha sido un placer conocerte, gracias por esos momentos.

Leire, oaindik goatzen naiz xaguen mundua erakutsi zenian garai hartaz, egia esanda gustoa hartzen nun zukin eondako momentu hoi, ilusioz ikasten nun zuk erakutsitakoa. Orduz geroztik momentu askotan lagundu izan diazu, proiektuakin aurrera nola jo ez nekinen, edota bizitzako aspektu filosofikotan. Zure etxeko atek ere ireki izan dizkiazu, bai Donostin eta baita Arrasaten ere, eskerrikasko horregatik, eta baita beti pijama bat prest eukitzeagatik netzat jajaja. Juncal, nere irakaslea izan zinen hasieran, eta lab meeting hartan esan nizun bezala, eskerrak ematen dizkizut horregatik. Zurekin oiartzuarra ikasiet (gutxi gorabehera), eta intxixuak zer dian deskubrituet, oaindik jutea pendiente dauket! Milesker opila ekartzeagatik, hori ere ohitura polita bihurtu zan! Momentu onak pasa ditugu elkarrekin, eta bizipen askori buruz hitz egin izan deu. Asko pozten naiz zure bidea aurkitu dezulako! Maddalen, zenbat hazi zean urte hauetan, zentzu guztitan! Beti esaten dizut, sinistu zure buruan, ta ikusikozu nola dena aurrea ateako dan, ta earki gainea! Milesker emandako apoyo guztiagatik, ta askotan entzuteagatik, lehen esandako gorabehera hoietan laguntza eskaintzeagatik. Paperra ere aurrea atea deu, ta ospatuko deu, noski! Bizi izandako beste momentu on asko bezela! Ta arroz esnea ze goxoa dan deskubritzea eskertu behar diot zure amai! Animo tesiko fase honetan! Miren, zure aholkuak ere ondo etorri izan zaizkit momentu askotan, milesker emandako laguntzagatik. Betiako geatukoa el "marcarse un Miren", zer dan gauzak zuzenen esatea! Jajaja sorpresa asegurada!

Mikel, also known as Maikel jajaja mi maju, ¡cuántos sustos me habrás pegado, y en cuántos momentos nos habremos reído! Has puesto el punto de humor a esta tesis en innumerables ocasiones, y eso ha sido genial. Gracias por tus consejos, y tu ayuda con nuestros amigos los mitotracker y mitosox. Por guardarme las babak aquel día en tu casa, por cantar conmigo "pa fuera lo malo", o por tus múltiples canciones mundialmente conocidas. Tantas cosas hijo mío… ¡y por muchas más! Ander, el sapiro maju, empezamos siendo glio team, y acabamos en brain team? Jajaja o algo parecido. Hemos ido a Madrid juntis, y ¡hemos vivido muchos buenos momentos! Siempre con tu punto musical, entre tu percusión y mis cantos, ¡el labo siempre tenía música de fondo! Jajaja transmites alegría e ilusión con muchas cosas, no pierdas eso :) Y a los dos juntos, deciros que siempre seréis mis ratitas, aunque a veces subáis un escalón y os volváis ratas máximas jajaja

María Álvarez., mi Maruxina, todo empezó en aquel sagardotegi en el que nos enseñaste la canción de la Maruxina, y de ahí te quedaste con el nombre. Me encanta tu forma de expresarte y de decir lo que piensas, ¡tan natural! Gracias por tu ayuda, con la tesis

e incluso cuando estuve preparando todo para la estancia, fue express y ¡tu ayuda fue esencial! Nos hemos reído muchísimas veces, y espero que siga siendo así. Diego, qué gracias me hizo preparar el videoclip para el vídeo de Mikel, me encanto tu rol jajaja también hemos podido disfrutar de buenos momentos, a pesar de la pandemia. Hemos ido a tomar unas cañas, o a comer por ahí, pero espero que esto se quede corto con lo que hagamos a partir de ahora, ¡al menos la sagardotetxi está asegurada! Gracias a los dos por enseñarnos los encantos de Galicia, ¡espero que podamos ir a disfrutar de ellos y sus aldeas!

Vero, tu incorporación fue un soplo de aire fresco en el grupo. Siempre con tu sonrisa, tu humor y tu ilusión por la ciencia. ¡Gracias por ello señora! Jajaja Sabrina, thanks for your advice, and for accepting the jokes as the one that we wrote saying 'it is what it is'. I wish you good luck in your life and scientific career :) Aizpea eta Joseba, zorte on tesiarekin, seguro nao oso ondo ingo dezuela! :) María García, ¡no olvidaremos tus aguacates! Alex A., cuántas risas también contigo, todos tenemos un serrinero y un mocasinero en nuestro interior jajaja Alejandro, gracias por enseñarme el proceso del clonaje de un gen, ¡tan complicado a veces!

Nuestros queridos médicos, Joaquín y Alex E., gracias por vuestra ayuda con las estereotaxias, y ¡por vuestra labor diaria! Es admirable veros venir con un café al labo, después de una guardia.

Ha pasado mucha gente por el grupo, pero hay muchos otros compañeros / amigos a los que me gustaría dedicar unas palabras. Carla, eres una de las personas que más contenta le veo trabajar, aunque te tires unos buenos overnights. He dejado de apuntar las IPadas, ¡pero estoy segura de que habrá habido más! Jajaja Gracias por tu ayuda con el citómetro, tus nociones fueron esenciales en aquel experimento. Y por supuesto, gracias por el apoyo, por transmitirme la ilusión que siempre tienes por hacer las cosas en la vida, por más pequeñas que sean. Hemos compartido grandes momentos, y espero que siga siendo así :) Vir, la florecilla, nuestros viajes en autobús y en el coche nos han hecho conocernos más la una la otra, y hemos compartido muchas cosas :) Me has intentado enseñar bailar la danza del vientre, aunque creo que aún necesitaría alguna clase más jajaja Gracias por los consejos de la vida, espero que seas feliz en esta nueva etapa. Bea, eres la alegría de la huerta, ¡auténtica! Me ha encantado conocerte, espero que compartamos muchos momentos más :) Araika, ezin ahaztu zure *burpee* -ak egiteko abilezia edo zure kafe eta bokadilo nahasketak!

Esther, urte batzuetan kointziditu genuen, ze graziosoa zen zure barre mota desberdinak entzutea! María Caffarel, gracias por contar conmigo en las múltiples actividades divulgativas que organizabas, ¡sabes que ha sido un placer! Y también por transmitirnos la ilusión por la ciencia. Andrea, autobuseko elkarrizketengatik. Giovanni, Angela, Maitane, Erika, María Arestín, Lorea, María Armesto. Gracias por los buenos momentos.

El grupo de bioingeniería. Laura Y, con su alegría y templanza. Héctor, con su humor. Haizea, Leire G., Sandra, Ainhoa y Paula.

El grupo de hepato. Aún me acuerdo de lo que pusisteis en la puerta del labo: "si con nosotros pasáis el rato, vas a ser feliz en hepato" jajaja pues tenéis razón. Paula, gracias por darme tu confianza, y por la ayuda. Por invitarme a aquel concierto de Aitana, o por las veces que hemos bailado juntas. Ainhoa L., nere gemelierra. Oain dala denbora bat ezagutu ginan, eta esan beharra dauket urte hauetan gehio ezautu geala! Eskerrikasko por tu locura y alegría, oso garrantzitsuk izaten día ta! Javi, recuerdo el momento en el que te dije que no controlaba a la gente de la primera planta porque no andabas mucho por Biodonosti en aquel momento, o aquella vez en la que vi unos falcon con anticuerpos de HDACs. Gracias por animarme cuando me llegaron todas las muestras de trizol descongeladas, y por todas las bromas que haces, me río mucho con ellas jajaja Pedro, no pierdas esa sonrisa, transmite muchísimo :) Aloña, Irene, Enara, Laura, Aitor, Álvaro, Ibone, Nuno, gracias a todos por los buenos momentos.

A las chicas de plataformas. Claudia, Alba, Ana A., Carmen, Nanda, Ana G. eskerrikasko por vuestra ayuda.

El grupo de neurociencias. Adolfo, gracias por aceptar ser mi tutor, y por los consejos que me has dado. Mónica, eres una terremoto, has hecho lo que has querido, y me alegro de que lo hayas conseguido :) Sonia, por las conversaciones en el autobús hablando del mundo científico y otras muchas cosas. Jon, kultibosen behin baino gehiotan kointziditu deu, beti eukizu "zemuz Jaione?" bat, zorte ona opa dizut tesiko etapa hontan, merezizu ta :) Jaione L., tokayi, por ese saludo tan nuestro de "hola qué hay?" Andrea I, gracias por tu ayuda con el citómetro y sus misterios. Lucía, por valorar mis cantos en cultivos. Tati, por los momentos vividos. Uxoa, por ayudarme con el ROS mitocondrial y sus antioxidantes. Haritz, Arantzazu, Gorka, Maddi, Haizpea, Leire I., Miren, Garazi, Martxel, Amaia E.

A Jose en la recepción, por tus emails originales. A los miembros del animalario Carlos, Eli, Iñaki, Jose, Mariasun.

I would also like to thank to all the people that I met in Leeds during my short stay. Ian, thanks for giving me the opportunity for working in your lab, and for evaluating my thesis. I really had a good time in Leeds. Zuleyha and Cihan, it has been a pleasure to meet you, we had great moments, you showed me Turkish culture and food, and we also visited beautiful parks. I was really emotional when you came to say goodbye to the train station, thanks for all, and also for those delicious biscuits :) Noelia, gracias por recibirme con los brazos abiertos en Leeds, y por invitarme a aquella excursion, fue un momento fantástico donde os conocí a todos. Eres una chica alegre, y con muchas ganas de conseguir tus metas, por lo que estoy segura de que lo harás :) Lynda, Vinzenzo, Sumi, Andrea. Thanks for all the good moments, each of you have something special :) Shrishti and Mugdha, we really enjoyed our time in the flat, in Leeds and in the trips to London and many others. Thanks for my birthday celebration, for the Zumba classes. Xuyuan, it was nice to meet you in Leeds.

I would not like to forget about nice people that I met in conferences. Anna, Nicola, Vir, Antonio, Daniela. We attended to great talks, but we also enjoyed our stay in Lyon, it was great to meet you all!

También me gustaría dedicar unas líneas a dos partes importantes de esta tesis. Por un lado, valorar los ratones que han participado en nuestros estudios, y en las puestas a punto de los mismos. Por otro lado, destacar también los datos de los pacientes de GB analizados en la presente tesis, los cuales han sido tratados con el mayor de los respetos. Sería fantástico que nuestro trabajo llegara a ayudar en el futuro, aunque sea en una mínima parte.

Tesi honetan, eta nire bizitzan orokorrean, ezinbestekoak direnei eskertzea gustatuko litzaidake azkenik. Ama, zer esan zuri, txikitatik erakutsi didazu neska gogorra izaten eta nahi dudanagatik borrokatzen, indar hori transmititu didazu. Beti egon zara laguntzeko prest, inongo dudarik gabe, eta hori beti eskertuko dizut. Eskerrikasko besarkada horiengatik, eta animoak emateagatik behar izan dudan guztietan :) Aita, mila esker zuri ere laguntza guztiagatik, zer moduz nagoen galdetzeko telefonoz deitu didazun bakoitzagatik, ilusio haundia egiten zidan hor zeundetela sentitzeak. Nire lorpen bakoitzarekin pozteagatik, eta karrera hasi nuenetik nahi nuena egiteko aukera emateagatik. Asko lagundu didazue biok, eta beti eskertuko dizuet emandako maitasun guztia, nik ere hala maite baitzaituztet. Hau

lortu badut, hein haundi batean, zuei esker izan da eta :) Aritz eta Iñigo, zuei ere eskerrak, animatzeagatik, laguntzeagatik behar izan deten guztitan. Ze ingo nuke abioia hartu behar nun egun hortan Aritzen laguntzaik gabe, edo tesi hontako formatoa ondo jartzen Iñigok lagundu gabe. Hoiek adibide txiki batzuk bakarrik dia, zuek uste baino gehio lagundu diazue, ta beti eskertukoizuet. Bizitzako momentu on guzti hoiengatik familia, eta datozen guztiengatik, guazen!!! :)

Itzi, mokorda, zenbat momentu bizi izan diteun oain dala urte askotatik. Zuk ikusituzu etapa hontako gorabeherak, baino garrantzitsuna da hor gaudela elkarri laguntzeko. Gure eskursiotxok, Tolosako rektak, eta bidaia desberdinak, hoiek ere lagundu diate animok eukitzen momentu askotan, mila esker horregatik. Ta baita zure hitz animoso ta besarkadangatik, ta aurretik dauzkaun abentura guztingatik :)

Aitor, morulin, mordof, milaka izen okurritzen zaizkit, gure hizkuntza espezial hontan gu ulertzen gea jajaja ezagutu ginanetik beti eon zea nere ondoan, apoyatzen, eta behar detenetan laguntzen. Morulinak gea, eta beti izango geala garbi dauket. Gure Donostiko kedadak irribarre bat baino gehio atera izan diate, eta seguro nao beste hainbat abentura bizi izango diteula. Gogoratu, bidaia bat daukaula pendiente! Esan izan dizut, oso harro nao zutaz, eta hartu dituzun erabakiez :) Marux, Feli, Itxungi, Maria, Andrea. Zuekin elkartzen naizen bakoitzen konturatzen naizelako Bilbok juntatu zuna ez dala inoiz separauko! Eskerrikasko bizipen guztingatik, plazer bat da zuekin eotea :) Baserria meeting point bihurtua, eta seguro beste asko eukiko diteula aurretik!

Kepatxo, zu izan zea egunerokotasunen bizi izan dezuna tesi hau. Ezinbestekoa izan da zure apoyoa urte hauetan, eztakizu zenbat laguntzen diten zure besarkada batek, edo zure hitz bakoitzak. Eskerrikasko denagatik, hartutako erabakitan laguntzeagatik, eta eskutik helduta biok batea aurrera pausoak emateagatik. Pila bat demostratu diazu urte hauetan, momentu desberdinetan, eta beti eon zea nire ondoan, eta bakit beti eongo zeala. Asko maiteizut, eskerrikasko, benetan. Eta eskerrak ebai zure amari, emandako laguntzagatik.

Azkenik, esker onen atal hau hasi deten bezela bukatzea gustatuko litzaidake. Eskerrak ematen orain dala 5 urte eta erdiko, eta urte hauetako Jaioneri. Inoiz amore ez emateagatik, indarra ateratzeagatik, eta zure buruan sinesteagatik. Azalean markatu dezun mezu hori inoiz ez ahaztu, eta hemendik aurrerakoetan ere betiko ilusioarekin bizi :)

Eskerrikasko denoi. Muchas gracias a todos. Thank you all.

Abstract

The brain is one of the most relevant and complex organs in the human body. With aging, cellular damage gets gradually accumulated, promoting a time-dependent functional decline of the brain. This fact leads to cognitive decline, neurodegeneration, and disease. In fact, brain aging constitutes one of the main risk factors in the development of glioblastoma (GB), the most common and aggressive form of glioma in adults, with a median patient survival of around 12-15 months.

GB tumors are characterized by a significant inter-tumor and intra-tumor heterogeneity at molecular and cellular level. Among the latest, the presence of a small subpopulation of glioma stem cells (GSCs) has been described as responsible for tumor initiation, progression, clonal heterogeneity, therapy resistance and tumor recurrence. This subpopulation is regulated by molecular and epigenetic mechanisms, which have been explored in the present doctoral thesis.

GB cells, and specifically, GSCs, need to maintain proteostasis in order to survive. For that, balanced activity of protein synthesis, folding, quality control and degradation is crucial. Regarding protein degradative systems, macroautophagy presents both tumor promoting and suppressor effects in GB, and it has been shown to regulate GSC activity. On the contrary, the impact of chaperone-mediated autophagy (CMA), a selective type of autophagy specialized in the individual degradation of targeted proteins after their binding to LAMP2A lysosomal transmembrane protein, on GB and GSCs remains elusive.

In this thesis, we have first characterized the expression of LAMP2A in GB, revealing its enrichment in the GSC subpopulation. In this line, we demonstrate for the first time that LAMP2A regulates tumorigenic properties of GSCs. Underlying molecular signature of CMA in GSCs comprises several proteomic and transcriptomic pathways, with special relevance of mitochondrial function, interferon pathway and extracellular matrix interactions. In fact, the effect of CMA in such pathways is translated into phenotypic alterations, as *LAMP2A* reduction impairs mitochondrial metabolism, cytokine secretion and migration and invasion abilities of GSCs. Remarkably, this effect is also translated into a clinical scenario, as samples from GB patients show increased expression of the gene *LAMP2* compared to healthy control tissue, being this expression positively associated with malignancy grade, Temozolomide (TMZ) resistance and lower patient survival. These results

reveal a novel function of CMA as an intrinsic regulator of GSC activity that highlights its relevance in GB progression.

Epigenetic mechanisms comprise reversible and heritable modifications in gene expression patterns, which do not constitute changes in DNA sequence. Among them, histone acetylation is based on the addition of an acetyl group into the lysine residues of histone tails. This modification is mainly associated with gene expression activation, and it is negatively regulated by the activity of histone deacetylases (HDACs). In fact, HDACs not only promote gene expression repression, but also non-histone protein deacetylation, modulating their activity and stability.

HDAC expression and activity is upregulated in multiples cancer types, including GB. In fact, currently available HDAC inhibitors (HDACi) have showed promising preclinical results in GB. However, the lack of specificity and therefore, the presence of side effects, significantly limit their therapeutic efficacy as anti-cancer treatment. In this line, HDAC6 is an interesting therapeutic target as, unlike other HDACs, *HDAC6* knock out mice are viable and fertile, with no apparent abnormalities, indicating that it may be a 'safe' target.

In the present work, we reveal upregulated levels of *HDAC6* in GB samples compared to healthy tissue. These levels correlate with glioma grade and poor prognosis in various large cohorts. Besides, we show that HDAC6 expression is enriched in the GSC subpopulation, and it correlates with stem molecular signature. Moreover, we have described a new small-molecule inhibitor of HDAC6, which presents stronger sensitivity for HDAC6 inhibition and exerts higher cytotoxic activity than the pan-inhibitor SAHA or the HDAC6-selective inhibitor Tubastatin A. Indeed, the new inhibitor significantly reduces tumor growth *in vivo*, even when administered after tumor occurrence. Transcriptomic analysis performed in treated GSCs confirms the increase in cell differentiation and cell death pathways, as well as a reduction in cell-cycle activity and cell division. Importantly, the novel HDAC6 inhibitor presents a remarkable cytotoxic effect both as a single agent or in combination with TMZ, indicating its potential in the preclinical setting.

At first sight, both aging and cancer seem to be opposite scenarios. However, their common origin based on the accumulation of cellular damage and their common molecular hallmarks indicate that they are different manifestations of the same underlying processes. In this sense, dysregulation in the stem cell pool and epigenetic modifications are two of the overlapping hallmarks in brain aging and cancer. Microenvironment contributes

to age-associated physiological neural stem cell (NSC) exhaustion. In particular, microglial cells play an important regulatory role in neurogenesis, as they phagocyte cell debris and apoptotic cells during this process and contribute to NSC self-renewal and differentiation in a paracrine manner. It has been described that HDACs regulate microglial function during development and neurodegeneration. However, no evidence has been published describing the role of HDACs in microglia during physiological aging. In this thesis, we show preliminary results suggesting that HDAC expression is upregulated upon microglial aging *in vitro* and *in vivo* in both mice and human samples. In the case of human samples, this upregulation is observed in different regions, including hippocampal neurogenic niche, where it shows a positive and significant correlation with microglial markers. These results highlight a possible role of HDACs in microglia with aging, which could influence NSCs and neurogenesis.

Overall, this thesis identifies two therapeutic strategies for GSC targeting, based on proteomic and epigenetic pathways. On the one hand, we demonstrate that CMA acts as GSC tumor promoting process, by regulating proteomic and transcriptomic pathways in a specific manner. On the other hand, we reveal the enrichment of HDAC6 in the GSC subpopulation, and we describe a novel small-molecule inhibitor of HDAC6 with great target selectivity and cytotoxic effect in GSCs, which is even more potent that other currently available HDACis. Furthermore, we extend the study of HDACs to the context of brain aging, showing preliminary evidence that highlights the upregulation of HDAC expression in several brain regions, such as, hippocampal neurogenic niche, which correlate with microglial aging.

Resumen

El cerebro es uno de los órganos más complejos del cuerpo humano, ya que coordina numerosas funciones importantes para el organismo. Con el paso de los años, el cerebro va acumulando daño celular que provoca un envejecimiento progresivo del tejido, su correspondiente pérdida de funcionalidad y la aparición de enfermedad. A su vez, el envejecimiento supone uno de los mayores factores de riesgo en el desarrollo de glioblastoma (GB), el glioma más común y agresivo en adultos. A pesar del tratamiento actual basado en la resección quirúrgica del tumor, seguido de radioterapia y quimioterapia con el agente alquilante Temozolomida (TMZ), los pacientes de GB presentan un pronóstico devastador, con una supervivencia media en torno a los 12-15 meses.

Los GB se caracterizan por una heterogeneidad inter-tumoral e intra-tumoral tanto a nivel celular como a nivel molecular. En relación a este último punto, se ha descrito la existencia de una subpoblación celular, llamada células madre de glioma (GSC, del inglés 'glioma stem cell'), responsable de la iniciación y progresión tumoral, además de la heterogeneidad clonal, resistencia a terapias y finalmente, recurrencia de los tumores. Esta subpoblación es estrictamente regulada por múltiples mecanismos moleculares y epigenéticos, procesos que han sido estudiados en esta tesis doctoral.

En las células de GB, y específicamente en las GSCs, la regulación de la proteostasis es vital. Para ello, procesos tales como la síntesis, el plegamiento, el control de calidad y la degradación de las proteínas deben estar estrictamente coordinados. Dentro de los procesos de degradación, mecanismos como la vía ubiquitina-proteasoma o la autofagia son de los más estudiados. En concreto, el interés por el proceso de autofagia ha aumentado en las últimas décadas. La autofagia es un proceso homeostático por el que las células degradan componentes dañados o innecesarios dentro del lisosoma. La macroautofagia (MA) fue el primer tipo de autofagia que se descubrió, y, en consonancia, es también el más estudiado hasta el momento. Este proceso se basa en la formación de autofagosomas para la captación de los orgánulos o moléculas diana, que posteriormente se fusionan con el lisososoma donde serán degradados. En el GB, la MA presenta un papel dual, tanto promoviendo como suprimiendo la progresión tumoral en los distintos estudios publicados. Además, la MA regula la actividad de las GSCs. Sin embargo, este tipo de autofagia, junto con la no tan conocida microautofagia, son procesos no-selectivos, centrados en la degradación

masiva de orgánulos y proteína dañadas. Por el contrario, la autofagia mediada por chaperonas (CMA, del inglés 'chaperone-mediated autophagy') es una forma selectiva de autofagia especializada en la degradación individual de proteínas diana. Aunque el proceso de CMA actúe como supresor tumoral en células sanas, en presencia de cierta acumulación de daño celular, las células tumorales elevan la actividad de CMA para su supervivencia. En este sentido, el aumento de la actividad de CMA se ha descrito en varios tipos de cáncer, pero no en el caso del GB, sobre el que se han publicado muy pocos estudios hasta el día de hoy.

El proceso de CMA consta de varios pasos. Por un lado, la proteína diana, de manera intrínseca, debe contener la secuencia consenso de aminoácidos "KFERQ", la cual será reconocida por la chaperona HSC70. Así, esta chaperona dirige la proteina al lisosoma, donde se unirá a la proteina transmembrana LAMP2A. A partir de este momento, LAMP2A se multimeriza, formándose un complejo por el cual la proteína diana desplegada podrá translocarse al lumen del lisosoma y ser degradada. Es importante destacar que, por el momento, el estudio de LAMP2A es una de las maneras más específicas de caracterizar el proceso de CMA, ya que proteínas como HSC70 también ejercen su función en otros procesos independientes.

En relación al estudio del CMA en GB, se ha mostrado recientemente que su desregulación en los pericitos tumorales contribuye a la progresión tumoral del propio GB. Aunque este estudio haya demostrado de manera interesante la función del proceso del CMA en el microambiente tumoral, su función en la heterogeneidad clonal dentro del mismo tumor aún no se ha llegado a explorar. En este sentido, se ha descrito que los tumores de pacientes tratados con TMZ presentan una mayor expresión de LAMP2A comparando con el estado de pre-tratamiento. Siendo este dato representativo de la resistencia a terapia y recurrencia del tumor, podría indicar una posible asociación entre la CMA y la subpoblación de GSCs. Sin embargo, hasta el momento, no se ha publicado ninguna evidencia sobre el papel de CMA en ningún tipo de célula madre tumoral.

En esta tesis doctoral, hemos caracterizado la expresión de LAMP2A en GB, revelando su enriquecimiento en la subpoblación de GSCs. En esta línea, demostramos por primera vez que la reducción en la expresión de *LAMP2A* disminuye la proliferación y la auto-renovación, e induce la apoptosis de las GSCs. Además, revelamos que la CMA también regula las propiedades tumorigénicas *in vivo* de las GSCs. Las alteraciones moleculares asociadas a

la reducción de los niveles de *LAMP2A* en las GSCs comprenden varias vías proteómicas y transcriptómicas, lo que indica el complejo papel regulador de la CMA en el mantenimiento de las GSCs. Entre las alteraciones más significativas, destacan el deterioro de la función mitocondrial, la vía del interferón y las interacciones con la matriz extracelular. El efecto de CMA en dichas vías a su vez se traduce en alteraciones fenotípicas, ya que la reducción de *LAMP2A* desregula el metabolismo mitocondrial, la secreción de citoquinas y la capacidad de migración e invasión de las GSCs. De manera destacable, este efecto se extiende a un escenario clínico, ya que muestras de pacientes de GB muestran mayor expresión del gen *LAMP2* que el tejido control sano, y se asocia positivamente con el grado de malignidad, resistencia a TMZ y una menor supervivencia. Así, nuestro trabajo revela la nueva función del proceso de CMA como regulador intrínseco de la actividad de las GSCs, e indica su revelancia en la progresión del GB.

Los mecanismos epigenéticos comprenden modificaciones reversibles y heredables en los patrones de expresión génica, sin alterar la secuencia del ADN. Entre ellos se encuentran mecanismos como la metilación del ADN, la regulación de las secuencias no codificantes del ARN, las variantes de las histonas, o las modificaciones post-transcripcionales en las histonas. Dentro de este último grupo encontramos la acetilación de las histonas. Este último mecanismo se basa en la adición de un grupo acetilo a residuos de lisina de las colas de las histonas. A nivel funcional, esta modificación está asociada principalmente a la activación de la expresión génica, y está regulada por varias enzimas. Por un lado, están las acetiltransferasas de histonas, las cuales catalizan dicha reacción. Por otro lado, se encuentran las deacetilasas de histonas (HDAC, del inglés 'histone deacetylase'), las cuales eliminan los grupos acetilo, catalizando la reacción contraria a la acetilación. De manera notable, las HDACs no sólo reprimen la expresión génica, sino que también promueven la deacetilación de proteínas no histónicas, modulando su actividad y estabilidad.

Tanto la expresión, como la actividad de las HDACs están elevadas en GB. De hecho, los inhibidores de HDACs (iHDAC) actualmente disponibles, como el SAHA, han mostrado resultados prometedores en ensayos preclínicos en GB. Sin embargo, la falta de especificidad de estos iHDAC puede presentar diversos efectos secundarios que repercuten directamente en la ventana terapéutica del compuesto y, así, en su eficacia como tratamiento anticanceroso. En esta línea, el interés por la HDAC6 como diana terapéutica está aumentando en los últimos años. A diferencia de otras HDACs, los ratones *knock out* de

HDAC6 son viables y fértiles, sin anomalías aparentes, dato que indica que podría ser una diana segura.

En el presente trabajo, mostramos que la expresión de *HDAC6* está aumentada en muestras de GB en comparación con tejido sano, asociándose además con el grado de malignidad y con un mal pronóstico en varias cohortes. Asimismo, revelamos que la expresión de HDAC6 está enriquecida en la subpoblación de GSCs, y se correlaciona con la expresión de varios marcadores específicos de célula madre. En esta línea, hemos descrito un nuevo inhibidor de HDAC6 que presenta una sensibilidad para la inhibición de HDAC6 y una actividad citotóxica superior al inhibidor no selectivo SAHA e incluso el inhibidor selectivo de HDAC6 Tubastatina A. Además, el nuevo inhibidor reduce significativamente el crecimiento tumoral *in vivo*, incluso al administrarse después de la aparición tumoral. En cuanto al efecto molecular de este compuesto, nuestro análisis transcriptómico realizado en GSCs tratadas revela un aumento de las vías de diferenciación y muerte celular, así como una disminución de la actividad del ciclo celular y de la división celular. Es importante destacar que el nuevo inhibidor de HDAC6 presenta un efecto citotoxico significativo no solo como tratamiento único, sino también en combinación con TMZ, hecho que indica su potencial en el contexto preclínico.

En un primer momento, los procesos de envejecimiento y cáncer podrían parecer opuestos. Sin embargo, el hecho de que compartan tanto la acumulación del daño celular como origen común, como un sello molecular similar, hace que se conviertan en dos manifestaciones distintas de los mismos procesos subyacentes. En este sentido, la desregulación del conjunto de células madre o las modificaciones epigenéticas constituyen dos de los procesos comunes en el envejecimiento y cáncer cerebral.

El envejecimiento se caracteriza por un fenotipo pro-inflamatorio generalizado, conocido por el término en inglés ‘inflammaging’. Además, el microambiente contribuye al agotamiento de las células madre neurales (NSC, del inglés ‘neural stem cell’) asociado a la edad, como es el caso de la microglia. En un contexto de homeostasis, la microglia desempeña un papel regulador importante en la neurogénesis, ya que fagocita los restos celulares y las células apoptóticas durante este proceso y contribuye a la auto-renovación y diferenciación de las NSC de forma paracrina. Sin embargo, con el envejecimiento, la población microglial va perdiendo su eficacia, disminuyendo su capacidad de fagocitosis y promoviendo la secreción aberrante de factores pro-inflamatorios. El estudio de los cambios

epigenéticos en las células microgliales está ganando interés en los últimos años. En concreto, se ha descrito recientemente que las HDACs regulan la función microglial durante el desarrollo y la neurodegeneración. Sin embargo, no se ha publicado ninguna evidencia que describa el papel de las HDACs durante el envejecimiento fisiológico. En esta tesis doctoral, mostramos resultados preliminares que sugieren que la expresión de las HDACs en la microglía se ve aumentada con el envejecimiento en un modelo *in vitro*. Además, caracterizamos la expresión de una serie de HDACs en hipocampos de individuos jóvenes y viejos, murinos y humanos, revelando su aumento con el envejecimiento. En el caso de muestras humanas, este incremento se observa en distintas regiones del cerebro, incluyendo el hipocampo, donde muestra una correlación positiva y significativa con marcadores microgliales. Estos resultados revelan el posible impacto de las HDACs en la microglia con el envejecimiento, hecho que podría afectar a las NSCs y al proceso de neurogénesis.

En definitiva, esta tesis revela dos estrategias terapéuticas basadas en vías proteómicas y epigenéticas dirigidas a la eliminación de la subpoblación de GSCs. Por un lado, demostramos que la CMA promueve la capacidad tumorigénica de las GSCs, regulando vías proteómicas y transcriptómicas asociadas a la proliferación, auto-renovación, metabolismo, respuesta immune e interacciones con la matriz extracelular. Por otro lado, revelamos el enriquecimiento de la expresión de HDAC6 en la subpoblación de GSCs, e identificamos un nuevo inhibidor de HDAC6 con gran selectividad de diana y efecto citotóxico en GSCs, incluso más potente que la de otros iHDAC actualmente disponibles. Además, ampliamos el estudio de las HDACs al contexto del envejecimiento cerebral, mostrando evidencias preliminares que indican el aumento en la expresión de las HDACs en varias regiones del cerebro, como es el caso del hipocampo, con el envejecimiento, correlacionando a su vez con el envejecimiento microglial.

Table of contents

Abbreviations

A	ACTB	Actin Beta
	ADP	Adenosine Diphosphate
	AGS	Astrocyte Growth Supplement
	AIF1	Allograft Inflammatory Factor 1
	AKB ligase / GCAT	2-amino-3-ketobutyrate coenzyme A ligase / Glycine C-acetyltransferase
	ANG	Angiogenin
	ASCL1	Achaete-Scute Family BHLH Transcription Factor 1
	ATCC	American Type Culture Collection
	ATP	Adenosine triphosphate
	ATRX	ATRX Chromatin Remodeler
	AUC	Area Under the Curve
B	BAX	Bcl-2 Associated X-protein
	BBB	Blood-Brain Barrier
	BCA	Bicinchoninic acid
	BHA	Butylated hydroxyanisole
	BLAST	Basic Local Alignment Search Tool
	BMI-1	BMI1 Proto-Oncogene, Polycomb Ring Finger
	BSA	Bovine Serum Albumin
	BSANP@JOC1	Bovine Serum Albumin Nanoparticles of JOC1
	BSC-A	Back Scatter-Area
C	C	Celsius
	CASA	Chaperone-Assisted Selective Autophagy
	CCT/TriC	Chaperonin Containing TCP-1 / T-complex protein Ring Complex
	CD133	Cluster of Differentiation 133
	CDK	Cyclin-Dependent Kinases
	CDKN2A	Cyclin Dependent Kinase Inhibitor 2A
	cDNA	Complementary Deoxyribonucleic Acid
	CDX	Caudal Type Homeobox
	CHK1	Checkpoint kinase 1
	Chr	Chromosome
	cIMPACT-NOW	Consortium to Inform Molecular and Practical Approaches to CNS Tumor Taxonomy
	CMA	Chaperone-Mediated autophagy
	c-Myc	MYC Proto-Oncogene, BHLH Transcription Factor
	CNS	Central Nervous System
	CO_2	Carbon Dioxide
	COL4A5	Collagen Type IV Alpha 5 Chain
	COX Vib-1	Cytochrome C Oxidase Subunit 6B1
	CSC	Cancer Stem Cell
	CSF1R	Colony Stimulating Factor 1 Receptor
	CSN2	Casein Beta
	CTSD	Cathepsin D
	CXCL10	C-X-C motif chemokine ligand 10

D	DAB	3,3'-Diaminobenzidine
	DEPC	Diethyl Pyrocarbonate
	DG	Dentate Gyrus
	DLL3	Delta-Like Ligand 3
	DLS	Dynamic Light Scattering
	DMEM	Dulbecco's Modified Eagle Medium
	DMSO	Dimethyl sulfoxide
	DNA	Deoxyribonucleic Acid
	dNTP	Deoxynucleotide Triphosphate
	DPBS	Dulbecco's Phosphate-Buffered Saline
	DPP1 /CTSC	Dipeptidyl Peptidase 1 / Cathepsin C
	DTT	Dithiothreitol
E	ECAR	Extracellular Acidification Rate
	ECM	Extracellular Matrix
	EDTA	Ethylenediamine Tetraacetic Acid
	EGF	Epidermal Growth Factor
	EGFR	Epidermal Growth Factor Receptor
	ESC	Embryonic stem cell
F	FASP	Filter-aided Sample Preparation
	FBS	Fetal Bovine Serum
	FCCP	Carbonyl cyanide 4-(trifluoromethoxy) phenylhydrazone
	FDA	Food and Drug Administration
	FDR	False Discovery Rate
	FGF	Fibroblast growth factor
	FN1	Fibronectin-1
	FSC-A	Forward Scatter-Area
	FSC-H	Forward Scatter-Height
	FSC-W	Forward Scatter-Width
	FWM	Forebrain White Matter
G	GAPDH	Glyceraldehyde 3-Phosphate Dehydrogenase
	GB	Glioblastoma
	GEO	Gene Expression Omnibus
	GFP	Green Fluorescent Protein
	GNS	Glioma Neural Stem cell
	GSC	Glioma Stem Cell
	GSEA	Gene Set Enrichment Analysis
	GSH	Glutathione
	GTP/GFAP/EF1α	Guanosine 5'-Triphosphate / Glial fibrillary acidic protein / Elongation factor 1-alpha
H	h	Hour
	H	Histone
	H_2O	Water
	HAT	Histone Acetyltransferases
	HBSS	Hank's Balanced Salt Solution
	HDAC	Histone Deacetylase
	HDACi	Histone Deacetylase inhibitor

	HIF1 α	Hypoxia-inducible Factor 1-alpha
	HIP	Hippocampus
	HIV-1	Human Immunodeficiency Virus-1
	HMC3	Human Microglial Clone 3
	HMGB1	High Mobility Group box 1
	HRP	Horse Peroxidase
	HSC	Hematopoietic Stem Cell
	HSC70	Heat Shock Cognate 70
I	IC_{50}	Half maximal inhibitory concentration
	IDH 1	Isocitrate dehydrogenase 1
	IFN-γ	Interferon Gamma
	IGFBP	Insulin-like Growth Factor-Binding Protein
	IgG	Immunoglobulin G
	IHC	Immunohistochemistry
	IL6	Interleukin 6
	IP10	Interferon γ-induced Protein 10 kDa
	ITGA/B	Integrin Subunit Alpha / Beta
	ITGAM	Integrin Subunit Alpha M
K	K	Lysine
	KEGG	Kyoto Encyclopedia of Genes and Genomes
	KFERQ	Lysine-Phenylalanine-Glutamic Acid-Arginine-Glutamine
L	LAMA/B/C	Laminin Subunit Alpha / Beta / Gamma
	LAMP2A/B/C	Lysosomal Associated Membrane Protein 2-A/B/C
	LC3B	Microtubule-associated proteins 1A/1B light chain 3B
	LC-MS	Liquid Chromatography-Mass Spectrometry
	LPS	Lipopolysaccharide
M	MA	Macroautophagy
	MARCHF5	Membrane Associated Ring-CH-Type Finger 5
	MGMT	O6-Methylguanine-DNA Methyltransferase
	MHC	Major Histocompatibility Complex
	MiDAC	Mitotic Deacetylase Complex
	min	Minute
	MKP1	Mitogen-activated protein kinase phosphatase
	MOI	Multiplicity Of Infection
	MRI	Magnetic Resonance Imaging
	mRNA	Messenger Ribonucleic Acid
	MR-PET	Magnetic resonance-Positron emission tomography
	MRP	Mitochondrial Ribosomal Protein
	mTOR	Mammalian Target Of Rapamycin
	mTORC2/PHLPP1/Akt	mTOR Complex 2 / PH domain leucine-rich repeats protein phosphatase 1 / Protein kinase B
	MTT	3-(4,5-Dimethylthiazol-2-Yl)-2,5-Diphenyltetrazolium Bromide
	MX1	MX Dynamin Like GTPase 1
N	Na_2HPO_4	Disodium hydrogen phosphate
	$Na_4P_2O_7$	Tetrasodium pyrophosphate

	NaCl	Sodium chloride
	NADH	Nicotinamide Adenine Dinucleotide
	NaF	Sodium fluoride
	NCoR	Nuclear Receptor Corepressor
	NDUFAF7	NADH:Ubiquinone Oxidoreductase Complex Assembly Factor 7
	NES	Nestin
	NF1	Neurofibromatosis 1
	NFAT1	Nuclear factor of activated T-cells-1
	NF-κB	Nuclear Factor Kappa light chain enhancer of activated B cells
	NHA	Normal Human Astrocytes
	NLS	Nuclear Localization Signal
	NPC	Neural Progenitor Cell
	NRF2	Nuclear factor erythroid 2-Related Factor 2
	NSC	Neural Stem Cell
	NuRD	Nucleosome Remodeling and Deacetylase complex
O	O_2	Oxygen
	OB	Olfactory Bulb
	OCR	Oxygen Consumption Rate
	OCT4	Octamer-binding Transcription factor 4
	Olig2	Oligodendrocyte Transcription Factor 2
	OXPHOS	Oxidative Phosphorylation
P	P/S	Penicillin / Streptomycin
	PARP	Poly (ADP-Ribose) Polymerase
	PCR	Polymerase Chain Reaction
	PCx	Parietal Neocortex
	PDGFRA	Platelet-Derived Growth Factor Receptor Alpha
	PDL	Population Doubling Level
	PEG400	Polyethylene Glycol 400
	PFA	Paraformaldehyde
	pH	Potential of Hydrogen
	PI3K	Phosphoinositide-3-Kinase
	PIK3CA	Phosphoinositide-3-Kinase Catalytic Subunit Alpha
	PIK3R1	Phosphoinositide-3-Kinase Regulatory Subunit 1
	PMSF	Phenylmethylsulfonyl Fluoride
	POU5F1	POU Class 5 Homeobox 1
	PTEN	Phosphatase and tensin homolog
R	RB	Retinoblastoma
	RCAN1	Regulator Of Calcineurin 1
	RCOR1/CoREST	Repressor element-1 silencing transcription factor Corepressor 1
	RILP	Rab Interacting Lysosomal Protein
	RMS	Rostral Migratory Stream
	RNA	Ribonucleic Acid
	RNAseq	RNA sequencing
	RND3/RhoE	Rho Family GTPase 3
	ROC	Receiver Operating Characteristic curve
	ROS	Reactive Oxygen Species

	rRNA	Ribosomal RNA
	RT	Reverse transcription
S	SAHA	Suberoylanilide Hydroxamic Acid
	SASP	Senescence-Associated Secretory Phenotype
	SA-β-galactosidase	Senescence-Associated-beta-galactosidase
	SDF1	Stromal cell-Derived Factor 1
	SDS-PAGE	Sodium Dodecyl Sulfate-Polyacrylamide Gel Electrophoresis
	SEM	Standard Error of the Mean
	SGZ	Subgranular Zone
	shRNA	Short hairpin RNA
	SIRT	Sirtuin
	SMRT	Silencing Mediumtor of Retinoic acid and Thyroid hormone receptor
	SOX	SRY-related HMG-box
	SPARC	Secreted Protein Acidic And Cysteine Rich
	STAT	Signal Transducer and Activator of Transcription
	SVZ	Subventricular Zone
T	TBI	Traumatic Brain Injury
	TBS-T	Tris Buffered Saline with Tween
	TCF4	Transcription Factor 4
	TCGA	The Cancer Genome Atlas
	TCx	Temporal neocortex
	TGF-β1	Transforming growth factor β1
	TIM23	Translocase of Inner Mitochondrial membrane 23
	TMA	Tissue Microarray
	TMZ	Temozolomide
	TNF	Tumor Necrosis Factor
	TP53	Tumor Protein 53
	Tris-HCl	Tris hydrochloride
	TSA	Trichostatin A
	TTF	Tumor Treating Fields
	TUBB3 / TUJ1	Beta-tubulin Class III
U	UCSC	University of California, Santa Cruz
	UKHC / KIF5B	Ubiquitous Kinesin Heavy Chain / Kinesin Family Member 5B
	UPLC	Ultra Performance Liquid Chromatography
V	VEGF	Vascular Endothelial Growth Factor
W	WHO	World Health Organization
Z	Zn^{2+}	Zinc (II) ion

Introduction

1. The brain

The human brain is a key organ of the central nervous system (CNS) which commands movement, emotions, communication, thinking and memory, among others [1]. Its development starts with the neurulation process from the ectodermic layer of the embryo, and it is completed 20-25 years after birth [2]. It consists of three main areas: (1) the cerebrum, which is the major part of the brain and takes control over motor and sensory information, (un)conscious behaviors, feelings, intelligence and memory; (2) the cerebellum, which controls the coordination of voluntary movement; and (3) the brainstem, which acts as a bridge that connects both cerebellum and cerebrum to the spinal cord, and contains the principal centers to perform autonomic functions such as breathing or heart rate [1]. In this doctoral thesis we will focus our attention on the cerebrum.

1.1. Main characters: glial cells and neurons

The brain is considered as one of the most structurally and functionally complex organs in mammals [3]. Human brain contains billions of neurons and hundreds of trillion nerve connections [4, 5]. Moreover, neurons are surrounded by vast number of glial cells, whose presence in the brain, compared with neuronal amount, is equivalent or even greater in some brain regions [5].

1.1.1. Glial cells

When glial cells were identified, they were suggested to only contribute to the structure of the brain, also reflected in their name, as '*glia*' from the ancient Greek means 'glue' in English [6]. However, research during the following decades has demonstrated that glial cells contribute to the correct neurotransmission, neural damage repair or even adult neurogenesis, among others [1, 7]. Main glial cells from CNS include oligodendrocytes, ependymal cells, astrocytes, and microglia [8]. In particular, in this thesis we will employ astrocytes and microglial cells.

1.1.1.1. Astrocytes

Human astrocytes comprise ~ 20% of glia with varying ratios to neurons depending on the CNS region [5]. Although they have been popularly defined as star-shaped

cells as its name indicates (‘*Astron’* from Greek means ‘star’), the truth is that astrocytes have a huge structural and functional diversity that makes human brain unique [9]. In line with this heterogeneity, astrocytes are implicated in a variety of structural, metabolic, and homeostatic functions [10]. In particular, processes such as metabolic regulation, support of synaptic transmission and blood-brain barrier formation [11] are tightly regulated by astrocytes.

1.1.1.2. Microglia

While astrocytes are formed from ectoderm germ layer in embryonic development, microglia are originated from the mesodermal-derived yolk sac macrophages [12]. Microglial progenitors infiltrate the brain during embryogenesis and early postnatal development and subsequently, they differentiate shifting from amoeboid to ramified morphology. Microglia stay in this ramified ‘resting’ state until activated, when processes such as chemotaxis, phagocytosis and cytokine secretion are induced [13]. Microglial function is focused in two key features. On the one hand, microglia are part of the innate immune system, playing a key role in the detection of signals of external danger such as invading pathogens and internal damaged or dying cells, and subsequent tissue repair. On the other hand, microglial function is also crucial for brain homeostasis through the control of neuronal proliferation and differentiation, as well as influencing formation of synaptic connections [14].

1.1.2. Neurons

Neurons are the structural and functional unit of the CNS, originated from ectoderm germ layer in embryonic development and composed by a cell body, dendrites, and an axon. As responsible for the processing and transmission of nerve impulses, neurons are electrically excitable, and they communicate between then and with other cells via synapsis [1]. In this sense, neuronal axons are covered with a multilamellar membrane of myelin, which facilitates rapid signal conduction promoting insulating properties [15]. Neuronal bodies are located in the grey matter of the cerebrum, whereas myelinated axons are mainly located in the white matter [1].

1.2. Concepts of radial glia and neural stem cells

During the mammalian embryonic formation of the CNS, neuroepithelial cells-derived radial glia give rise to neurons, and afterwards to astrocytes and oligodendrocytes [16, 17]. Afterwards, many radial glia differentiate directly into mature astrocytes, whereas radial glia-derived progenitors persist through adulthood, giving rise to adult neural stem cells (NSCs) [18]. In the adult mammalian brain, NSCs are mainly found in neurogenic niches, which comprehend the subventricular zone (SVZ) around the lateral ventricles and the subgranular zone of the dentate gyrus (DG) in the hippocampus (***Figure I1***). NSCs are characterized by stay dormant or in a quiescent state for prolonged periods, providing a reserve pool of cells available for tissue regeneration and cell replacement [19, 20]. In response to stimuli, NSCs get activated, triggering their proliferation and self-renewal. Activated NSCs give rise to neural progenitor cells, which have the potential to differentiate primarily into new neurons, and in smaller proportion, into astrocytes and oligodendrocytes [21].

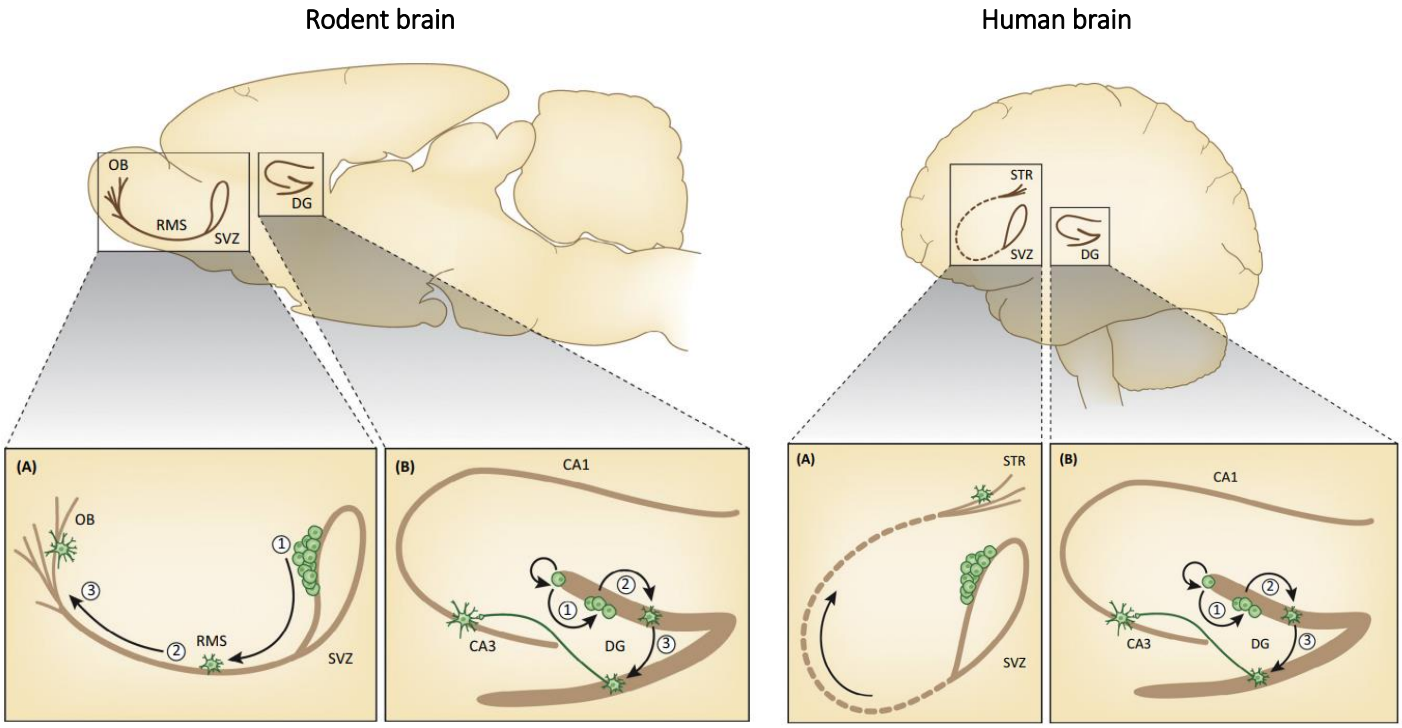

Figure I1. Sagittal view of rodent and human brain showing the neurogenic niches: the subventricular zone (SVZ) of the lateral ventricles and the subgranular zone (SGZ) of the dentate gyrus (DG) in the hippocampus. **(A)** In rodent brain (left), neural progenitor cells (NPC) generated in SVZ proliferate (1), migrate through the rostral migratory stream (RMS) (2) and differentiate in the olfactory bulb (OB) (3); in human brain (right), proliferated cells from the SVZ migrate into the striatum where they develop into mature neurons **(B)** In both rodent and human brain, NPCs generated in the SGZ of the DG proliferate (1), migrate into the granule cell layer (2) and mature into new neurons (3), extending projections into the CA3 region. *Modified from Borsini A. et al 2014*.

Importantly, these neurogenic niches are specialized microenvironments that, together with NSCs, contain a variety of other cell types, such as endothelial cells and microglia [22]. In particular, microglia significantly contribute to the maintenance of homeostasis in the adult hippocampal neurogenic niche. They eliminate by phagocytosis neural progenitor cells that undergo apoptosis before becoming neuroblast [23] and, during the process, they secrete factors that limit the production of new neurons [24].

1.3. The blood-brain barrier

The blood-brain barrier (BBB) is a diffusion barrier essential for the homeostasis and protection of the brain against external substances and pathogens. It is the central element of a tightly regulated neurovascular unit, composed by endothelial cells connected by tight junctions, surrounded by a specialized basal lamina shared with pericytes and astrocytic end-feet interconnected with neuronal endings and microglia [25]. The tight regulation of molecular influx and the existence of highly efficient efflux systems complicates the entry of therapeutic agents into the brain [26].

2. Brain cancer

According to GLOBOCAN 2020 database developed by the World Health Organization (WHO), cancer is one of the leading causes of death worldwide, accounting for 19.3 million new cases and 10 million deaths in 2020. It is estimated that cancer cases will increase in the following years, reaching approximately 30.2 million cases in 2040 (available in: https://gco.iarc.fr/today/home; accessed 20/01/2022).

In particular, tumors from the CNS account for a total of 308,102 new cases and 251,329 deaths in 2020 (available from: https://gco.iarc.fr/today/home; accessed 20/01/2022). Although incidence of brain cancer is not as high as breast, lung or colorectal cancer types, brain tumors are characterized by high morbidity and mortality caused by their delicate location and invasive growth [27]. Gliomas are the most common primary brain tumors, accounting for almost 30% of all primary tumors, and 80% of all malignant ones [27].

2.1. Gliomas and malignancy grades

The first recorded reports of primary CNS tumors were described based on gross morphological observations. Herein, Berns in 1800 and Abernety in 1804 defined them as diffuse tumors generated in the CNS, with no clear border with health tissue, but presenting significant differences with it. In this point, 'Medullary Sarcoma', 'Encephaloide' or 'Fungus Medullare' terms were attributed to these tumor types, in English, French and German literature, respectively [28]. The first comprehensive histo-morphological description was given in 1865 by the German pathologist Rudolf Virchow [29]. Using for the first time the term 'Glioma', he claimed that this tumor type is originated from the glial cells of the CNS, showing clear structural differences at tissue and cellular level, comparing to healthy brain tissue and invading neighboring structures. At that time, Virchow separated gliomas in two groups, according to their cellularity and general differences comparing to healthy brain tissue [29]. In 1926 the American neuropathologist Percival Bailey and the neurosurgeon Harvey Cushing, after histologically analyzing over 400 glioma sections, updated glioma classification. Herein, they described 14 glioma subtypes, which correlated with clinical outcome [30]. Those initial studies sustained the base of the current WHO glioma classification [31, 32].

Nowadays, gliomas are classified based on histological features, genetic alterations and location, among others. Among the histological features, the loss of structural and functional differentiation of cells, also known as anaplasia, has been classically used for associating malignancy WHO grade I to IV with tumor types, being considered grade I-II low grade and III-IV high grade gliomas [27]. Together with this, other pathological features such as mitotic activity, vascular proliferation, necrosis or proliferative potential have been associated with clinical course and treatment outcome [33]. Thus, while grade I tumors are often curable when surgically removed, grade IV tumors are highly malignant, presenting poor survival [32].

2.2. Glioblastoma: CNS WHO grade 4 glioma

2.2.1. Concept of glioblastoma: from its discovery to the present

The first specific comprehensive description of glioblastoma (GB, or GBM) was made by Strauss and Globus in 1925, assigning the name 'spongioblastoma' for it. They

reported that this tumor type presented intense vascularity, marked necrotic zones, large hemorrhagic *foci*, cystic degenerative changes, multiple growth centers at distant points and poor clinical outcome [34]. One year later, the histological classification of gliomas performed by Bailey and Cushing led to change the name to 'Glioblastoma Multiforme', defined as the most clinically malignant and histologically atypical form of glioma [35].

To date, GB is the most common and aggressive primary malignant tumors in the adulthood, considered as grade 4 glioma attending to the 2021 CNS WHO classification [32, 36]. The average incidence rate of GB is 3.19 per 100,000 population, whose median age of presentation is 64 years [37]. Although GB is considered a rare cancer type based on its low incidence, it presents a devastating prognosis. Patients diagnosed with GB show a median survival around 12 to 15 months, with a 5-year survival rate of 5% [36, 38].

2.2.2. Risk factors

The role of age as a negative prognostic factor in GB is well established. The incidence of GB is highest in patients around 65 years of age, and those over 70 years old present an even poorer prognosis, with a median survival of 4.5 months [39]. This is caused due to the aggressive biological features of the tumors, greater patient comorbidity and few therapeutic options [40]. Besides, GB is more common in Caucasians relative to other ethnicities, and males are slightly more affected than females [41]. Among other risk factors, previous familial glioma cases [42], ionizing radiation [43], the presence of rare syndromes such as Li-Fraumeni or neurofibromatosis I-II [44] and infection with cytomegalovirus [45] or Epstein-Barr virus [46] have been proposed.

2.2.3. Diagnosis

Among all GB cases, approximately 90% develop *de novo*, without evidence of a less malignant precursor lesion. These cases are classified as primary GBs. On the contrary, some other GB cases, named as secondary GBs, arise after the occurrence of a previous low-grade glioma [47]. This latter case is more common in younger patients, presents a slower progression and thus, carries a significantly better prognosis. On the contrary, primary GBs are very aggressive and present a dramatic clinical course [47, 48].

Most GBs are diagnosed following symptomatic presentation, as it expands, infiltrates, and affects brain structures rapidly [49]. The clinical presentation of GB varies depending on the size and location of the tumor, together with the degree of the peritumoral

edema [50]. Among common symptomatology, headache and focal or progressive neurologic deficits usually occur. Depending on the area where the tumor is located, these neurologic deficits may include persistent weakness, numbness, loss of vision, seizures, alteration of language, mood disorders or mild memory disorders, among others [51].

In the presence of symptoms, imaging techniques are the first step towards the diagnosis of a GB. Herein, gadolinium-enhanced magnetic resonance imaging (MRI) is the gold standard [52], where an irregular mass with a dense ring of enhancement and hypointense center of necrosis is observed [53]. Besides, surrounding vasogenic edema, hemorrhage and ventricular displacement may also be present on diagnostic image [54]. Together with MRI, positron emission tomography (PET) or magnetic resonance spectroscopy can also provide additional information about the tumor [49].

The next step in the diagnosis of a GB is the histological analysis of the tumor. GBs present astroglial appearance cellular polymorphism, nuclear atypia, high mitotic index, pseudopalisading necrosis, and microvascular hyperplasia or neovascularization [36]. In parallel, several molecular markers may be also analyzed by immunohistochemistry, fluorescence *in situ* hybridization or other techniques, due to their prognostic or predictive potential [55]. Among them, mutational status of isocitrate dehydrogenase-1 (IDH1) is relevant in the diagnosis of GB. IDH1 is a cytoplasmic enzyme which catalyzes the oxidative decarboxylation of isocitrate into alpha-ketoglutarate and nicotinamide adenine dinucleotide (NADPH). Mutated IDH1, which is unable to catalyze this reaction, and instead converts isocitrate into 2-hydroxyglutarate, occur more commonly in grade 2 and 3 adult gliomas and secondary GBs [56]. Besides, overexpression of epidermal growth factor receptor (EGFR) is detected in approximately 50% of GB patients [57]. EGFR is a transmembrane receptor with a cytoplasmatic domain containing a tyrosine kinase, which turns on oncogenic pathways. The specific EGFR vIII mutant, expressed in ~ 20-30% of GB cases, results in constitutive tyrosine kinase activity, promoting enhanced proliferation, therapy resistance, migration, and inhibition of apoptosis [58]. The proliferation marker Ki-67 has also been associated with higher glioma grade, and poorer progression-free survival and overall survival in GB patients [59]. On the contrary, ATRX mutations and 1p/19q chromosomal deletions are used for the identification of other glioma types [55].

2.2.4. Treatment

Since 2005, current standard therapy for GB patients includes maximal surgical resection of the tumor, followed by concurrent radiotherapy and chemotherapy based on the administration of temozolomide (TMZ) [36].

When possible, gross total or subtotal resection to immediately relieve the tumor-associated mass effect, delay recurrence and obtain tissue to confirm diagnosis is the first step in GB therapy. Indeed, a greater extend of surgical resection has been associated with better clinical outcome [53]. However, this process gets complicated when the tumor is located in eloquent areas, crucial in the control speech, motor function and the senses. Moreover, GB tumor cells are highly infiltrative, so that not all tumor cells can be removed by surgical procedure.

After craniotomy wound heal, the next step in the standard of care is post-operative radiotherapy and TMZ chemotherapy. This protocol was implemented in 2005, when Stupp R and collaborators demonstrated in a phase III clinical trial that patients who received TMZ and radiotherapy presented increased median survival [38] and 5-year term survival proportion [60]. TMZ is an alkylating agent, which methylates DNA at the O6, N3 and N7 positions, and produces DNA strand breaks [61]. In fact, in the same study Stupp R and collaborators indicated that TMZ response could depend on O6-methylguanine-DNA methyltransferase (MGMT) methylation status [38]. MGMT is a DNA repair enzyme that participates in the removal of the alkylation induced by TMZ, and whose methylation is associated with a reduced expression of the gene [62]. Thus, while methylated MGMT showed improved TMZ response, unmethylated MGMT reduced TMZ sensitivity due to the increased DNA repair mechanism [63, 64]. However, MGMT methylation has not shown predictive potential in other cohorts [65], suggesting that its potential as a therapy response biomarker is not complete.

2.2.5. Tumor recurrence

Despite the standard of care discussed above, prognosis of GB patients is still very poor, as almost all patients recur. Re-resection and additional radiotherapy are an option for some patients, but it is limited due to the uncertain benefit and increased risk of radiation necrosis [53]. In this context, in 2009, Bevacizumab, an anti-angiogenic humanized monoclonal antibody targeting vascular endothelial growth factor, was approved by the U.S.

Food and Drug Administration (FDA) for recurrent GB [66]. Besides, the novel therapeutic approach Optune® has been approved by the FDA both for recurrent (2011) and newly diagnosed supratentorial GB (2015) [67, 68]. This technology is based on a noninvasive portable device which delivers alternating electric fields (TTFs) to disrupt cell division [69]. Although this new device presents some benefit, its use has been limited due to cost and patient inconvenience [70].

Several efforts have been done in order to find successful treatments for GB therapy, but the vast majority have failed [36, 71]. In this sense, the huge tumor heterogeneity, and the poor BBB penetration of newly developed therapeutic agents represent main obstacles [71].

2.2.6. Tumor heterogeneity: responsible for therapy resistance

GB tumors from different patients comprise differences among them, representing a significant inter-tumor heterogeneity. Not only that, but the presence of distinct tumor clusters and genetic alterations within a specific tumor from a single patient have been also described, representing the relevant intra-tumor heterogeneity [72]. Huge efforts have been done in order to characterize this heterogeneity in GB patients with the aim of classifying them in specific tumor subtypes and thus, display potential personalized therapeutic strategies.

2.2.6.1. Molecular heterogeneity: classification of GB subtypes

In 2008 The Cancer Genome Atlas (TCGA) project sequenced more than 600 genes in more than 200 human tumors, revealing a complicated genomic landscape in GB [64]. Herein, alterations in the tumor suppressor protein p53, the receptor tyrosine kinase/Ras/phosphoinositide 3-kinase and retinoblastoma signaling pathways, as well as mutations in neurofibromin 1 (NF1), EGFR, PI3K complex and MGMT have been described [53, 64].

In 2011 Verhaak RGW and collaborators, based on transcriptomic features, reported a novel GB classification [73]. Herein, classical, mesenchymal, proneural and neural subtypes were addressed. However, although this original classification has been intriguingly informative, it included the transcriptomes of tumor-associated nonmalignant cells in the analysis. In fact, a previous study found that a high-grade astrocytoma tumor class displaying neuronal lineage markers presented exceptionally longer survival compared with others [74].

In this context, a subsequent transcriptomic study published in 2017 by Wang Q and collaborators, which presents more-stringent transcriptomic separation of tumoral and non-tumoral cells, have shown that neural subtype arose from contamination of the original samples with non-malignant cells [75]. Thus, currently three GB subtypes can be distinguished: classical, mesenchymal, and proneural (***Table I1***).

Table I1. Main characteristics of GB subtypes.

<table>
<tr><th></th><th>Mesenchymal</th><th>Classical</th><th>Proneural</th></tr>
<tr><td>Lineage enrichment</td><td>Astroglia, with microglial/macrophage gene signature</td><td>Astrocytic, with activated dendritic cell gene signature</td><td>Oligodendrocytic</td></tr>
<tr><td rowspan="7">Alterations</td><td>Focal hemizygous deletion at 17q11.2, containing NF1 / Lower NF1 expression / NF1 mutations</td><td>Chr 7 amplification / Chr 10 loss</td><td>Amplifications of the locus at 4q12 harboring PDGFRA / Mutations in PDGFRA</td></tr>
<tr><td>PTEN mutations</td><td>EGFR amplification / EGFR vIII mutation</td><td>Point mutations in IDH1</td></tr>
<tr><td rowspan="2">High expression of genes in TNF and NF-κB pathways</td><td>Lack TP53 mutations</td><td>Frequent TP53 mutations, loss of heterozygosity</td></tr>
<tr><td>Focal 9p21.3 homozygous deletion, targeting CDKN2A</td><td>Low CDKN1A expression</td></tr>
<tr><td rowspan="2">High overall necrosis and associated inflammatory infiltrates</td><td rowspan="2">RB pathway aberrations</td><td>PIK3CA/PIK3R1 mutations</td></tr>
<tr><td>High expression of oligodendrocytic development genes</td></tr>
<tr><td>Expression of mesenchymal markers</td><td>High expression of NES, and markers of Notch and Sonic Hedgehog signaling pathways</td><td>High expression of proneural development genes such as SOX, CDX, DLL3, ASCL1 and TCF4</td></tr>
<tr><td>Mediumn survival (months)</td><td>11.5</td><td>14.7</td><td>17</td></tr>
</table>

Sources: Verhaak RGW et al 2010 [73] and Wang Q et al 2017 [75].

Chr: chromosome.

Of note, proneural subtype is over-represented by younger patients, which show a better clinical outcome [73]. Indeed, younger age of the patient, together with *PDGFRA* abnormalities or *IDH1* and *TP53* mutations have been previously associated with secondary GB [76-78]. Overall, most known secondary GBs were classified as proneural [73]. In this sense, the new 2021 CNS WHO classification of gliomas and cIMPACT-NOW update 5 have distinguished the terms glioblastoma *IDH*-wildtype and astrocytoma *IDH*-mutant WHO grade 4 as different tumor types [32, 79].

It has been shown that GB presents phenotypic plasticity related to subtypes. In fact, proneural to mesenchymal subtype switching upon disease recurrence has been associated with therapy resistance [74, 80]. In this sense, Wang Q and collaborators, besides the update on GB subtypes, also performed a longitudinal study obtaining samples from patient at primary GB and recurrent status [75]. Herein, they observed that only 55% of GB samples retained their original subtype, reinforcing the idea of the huge plasticity of GB. In this line, in 2019, Neftel C and collaborators described four cellular states based on single cell ribonucleic acid (RNA) sequencing data of GB samples [81]: (i) neural progenitor-like, (ii) oligodendrocyte-progenitor-like, (iii) astrocyte-like and (iv) mesenchymal-like states. Importantly, authors show that relative frequency of each state varies between samples, and they demonstrate plasticity between different states.

Besides GB classification based on genomic and transcriptional data, other classifications based on DNA methylation [82, 83] or active biological functions [84] have been reported. These new classifications contributed to the better understanding of GB at diagnosis and prognosis level. However, its translation into treatment efficacy has not been successful so far, as GB present also a huge cellular heterogeneity.

2.2.6.2. Cellular heterogeneity: Concept of Cancer Stem Cells

A tumor is composed by heterogeneous populations of cells, which include malignant cancer cells, supportive cells and tumor infiltrating cells. This cellular heterogeneity is further enhanced by clonal variation and microenvironmental influences on cancer cells [85]. Regarding clonal variation, two models have been proposed (***Figure I2***).

The first theory is named clonal evolution model or stochastic model [85, 86], in which genetic instability of cancer cells leads to different clones of cells. Thus, mutations in genes such as oncogenes or tumor suppressors will contribute to carcinogenesis, and the

clone which outcompete other clones will become the driving cell population in a tumor, as a result of natural selection. Indeed, during the course of the disease or in response to a treatment, these clones may change spatially and temporally, generating a tumor-bulk composed by multiple subclones.

The second theory is the **cancer stem cell (CSC) model** [85]. This model suggests that only a small proportion of cancer cells, specifically the CSCs, can self-renew and initiate and maintain tumor growth. Thus, this model supports a hierarchical cellular structure, which is equivalent to normal tissue supported by healthy stem cells. On the one hand, CSCs present self-renewing ability. Thus, they divide symmetrically, generating cells with the same stemness capacity than the mother cell. On the other hand, CSCs asymmetric division leads to the maintenance of CSC pool, together with a heterogeneous progeny of differentiated cancer cells.

Although this latter model has been classically considered as unidirectional, the concept of cellular plasticity shows that this is not the case. In fact, terminally differentiated cells have shown the potential of dedifferentiating and gaining CSCs properties under specific conditions [87, 88].

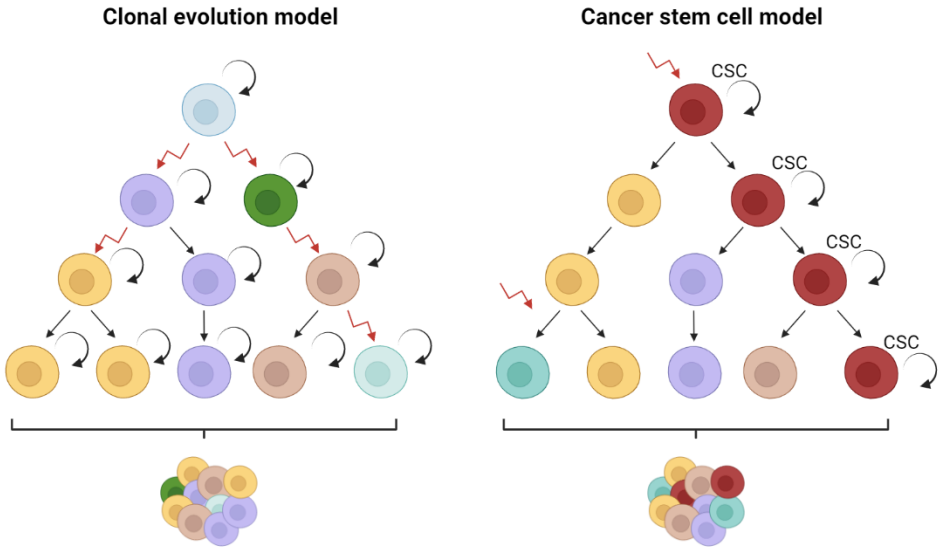

Figure I2. Main models for tumor heterogeneity. According to clonal evolution model (left), somatic alterations in a cell give rise to multiple clones which differ in sensitivity against therapy and proliferatiove rate. Genomic instability in such clones generate genetic alterations in the progeny, being all malignant cells able to maintain and expand the tumor. In contrast, cancer stem cell (CSC) model (right) claims that only a specific subpopulation of cells, named CSCs, are able to self-renew and proliferate, generating highly heterogeneous clones. Figure created with Biorender.com.

The connection between cancer and stem cells was firstly originated in the mid-19th century by Rudolf Virchow, as he observed that certain adult tumors and embryonic tissue present various histological similarities [89]. These observations culminated in a comprehensive 'embryonal rest' theory put forward by his student Julius Cohnheim in 1875. This theory stated that tumors may arise from embryonic cells that lie dormant in the adult tissue until activated to become malignant [89]. Since that theory, many studies have been published characterizing in further detail the link between stem cells and cancer, by the discovery of protein markers on the surface of these cells. The first experimental evidence proving the activity of CSCs was showed in 1994 by Lapidot T and collaborators in hematological malignances, in which $CD34^{+}/CD38^{-}$ subpopulation from acute myeloid leukemia was able to form leukemia after transplantation into NOD.SCID mice [90]. Following studies extended the presence of CSCs to additional cancer types, such as breast [91], prostate [92], colorectal [93, 94], pancreatic [95] and brain cancer [96-99], and currently they have been described in the majority of cancer types.

2.2.7. Glioma Stem Cells

2.2.7.1. Concept

Glioma stem cells (GSCs), also known as glioma initiating cells, are a small subpopulation of slow growing cells possessing tumor-propagating potential *in vivo*, sustained self-renewal and differentiation potential and infiltrative capacity [100, 101].

Quiescence is a main characteristic of GSCs, a dormant but reversible cellular condition in which cell-cycle entry and proliferation are prevented in the absence of specific stimuli. This feature hides GSCs from the cytotoxic effect of alkylating agents such as TMZ, and other therapeutic agents, which target highly proliferative cells [86, 102]. The high expression of drug transporters in the cellular membrane of GSCs makes even more challenging to target them, as a huge number of therapeutic agents are pumped out [103]. Chemotherapy resistance is also extended to radiotherapy, as GSCs activate DNA damage checkpoint response upon ionizing radiation, thus increasing DNA repair capacity more effectively than non-GSC tumoral cells [104]. Thus, GSCs have been proposed as key contributors towards therapy resistance and subsequently, tumor relapse.

2.2.7.2. Origin of GSCs: NSCs

GSCs share many features with adult NSCs at multiple levels and therefore, they have been proposed as the cells of origin of GB. On the one hand, both subpopulations present self-renewal and differentiation ability, crucial for their maintenance and generation of differentiated progeny [105]. Besides, both GSCs and NSC are quiescent cells, and they present a smaller size, reduced metabolic activity and substance efflux [105, 106]. On the other hand, since the discovery of CD133 as a cell surface antigen in GSCs [97], multiple signaling pathways involved in both normal NSC and GSCs biology have been identified, such as Notch, Bone Morphogenetic Protein, Wnt/β-catenin, Sonic Hedgehog, STAT3 or EGFR pathways [107]. Not only complete signaling pathways, but the activity of multiple transcription factors have been also observed to be common in the maintenance of NSCs and GSCs. Among them, Bmi1, c-Myc, Oct4, Nanog, Nestin and Olig2 have been described as regulators of the balance between 'stemness' and differentiation [107]. Together with these transcription factors, Sox family members are also crucial in the maintenance of embryonic and NSCs, which are aberrantly expressed in GBs and enriched in GSCs [108-110]. As an example, SOX2 and SOX9 expression has been linked to GSC activity and TMZ resistance [111].

In line with this, GSCs have been described to be originated from mutations in adult NSCs. This idea arises from experimental evidence obtained from the genetic manipulation of oncogenes or tumor suppressor genes in murine models. Herein, the overexpression of the oncogenic forms of *Ras*, *Akt*, *EGFR*, *PDGFR*, in some cases in combination with *Ink4A*/*Arf* or *Pten* deletion, in embryonic or early postnatal cells resulted in astrocytoma formation in mice [112-114]. On the other hand, knock out mice for tumor suppressor genes such as *p53*, *Pten* and *Nf1* also gave rise to astrocytoma [115, 116]. Subsequent analysis of these mice revealed that lesions were located in the SVZ, suggesting that mutations in NSCs have an impact on tumor formation. For testing directly this hypothesis, the same strategy was applied directly into NSCs and their progeny, using *Cre* recombinase [117]. In this approach, mice developed tumors, indicating that NSC may be the origin of GB. In fact, a recent publication by Lee JH and collaborators provides direct evidence which demonstrates that driver mutations within NSCs direct the origin of GB [118, 119].

On the other hand, GSCs can be originated from the de-differentiation of mature cells, such as astrocytes, neurons, or oligodendrocytes. In this line, the transduction of *Ras* [120] or *Nanog* [121] oncogenes in p53-deficient mice directed the de-differentiation of astrocytes into GSCs. This effect has been also observed in *vivo* by the inactivation of *Nf1* and

p53 in astrocytes and neurons [122]. Besides, Mario L. Suvà and collaborators, using an epigenomic mapping of the chromatin status, identified POU3F2, SOX2, SALL2 and OLIG2 stem cell transcription factors to be able to reprogram differentiated tumor cells into GSCs in proneural GB [123]. These factors were essential for the maintenance of tumorigenic properties of GSCs, indicating that stem cell mediators are crucial in the activity of GSC subpopulation.

2.2.7.3. Plasticity of GSCs

GSCs constitute a highly dynamic and adaptative cellular type at multiple levels, which compromises patient outcome. As an example, GSCs can intrinsically shift between different metabolic pathways, allowing them to survive nutrient deprivation [124]. GSC can also modulate their microenvironment for their own maintenance, generating a niche which contributes to their proliferation, cell-fate decisions, and protection from environmental insults such as therapeutic agents [125, 126]. In this sense, extracellular matrix (ECM) protein secretion, and perivascular and hypoxic niches have been shown to sustain maintenance of GSCs [127-129]. Hypoxia can also enhance the trans-differentiation of GSCs into endothelial-like cells contributing to blood vessel formation and thus, tumor growth [130]. Conversely, dedifferentiation of non-GSCs towards GSC phenotype can also occur, induced by several stimuli such as environment acidification [131], metabolic stress [132] or even hypoxia [133]. Recent studies have also revealed the direct interaction of GSCs with immune cells, promoting a pro-tumorigenic inflammatory environment [134]. All this evidence highlights the complex regulation of GSC maintenance and its interaction with the microenvironment.

The crucial role of GSC subpopulation in GB, and its relevant characteristics (***Figure I3***) make it a promising therapeutical target. Thus, its elimination, or at least, differentiation, could improve treatment outcome. Understanding the molecular regulatory mechanisms that control GSC maintenance is therefore critical in the development of novel anti-tumor therapies that success in the complete and lasting tumor elimination.

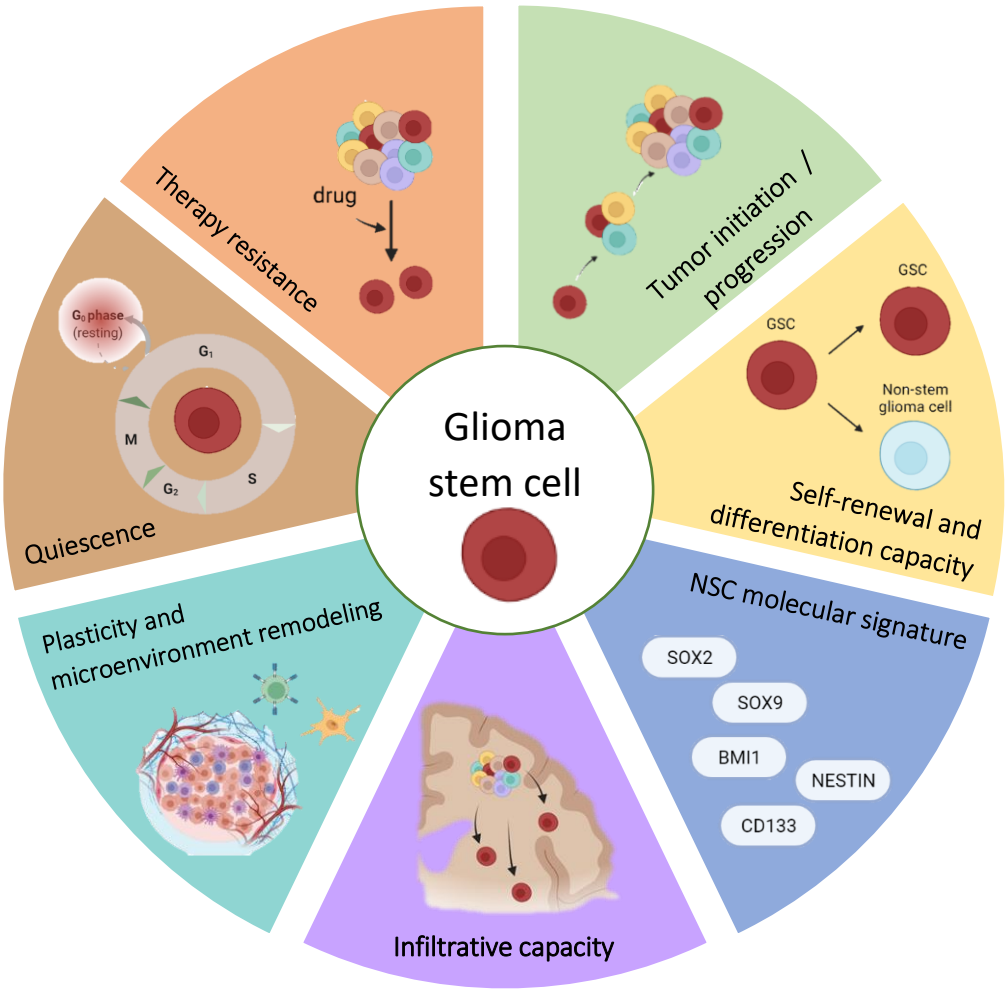

Figure I3. Characteristics of glioma stem cells (GSC). GSCs are a small subpopulation of cells responsible for tumor initiation and progression. In this sense, they present self-renewal and infiltrative capacities, and they share many molecular pathways with NSC. Besides, they are responsible for therapy resistance, as they are quiescent or 'dormant' cells, which hides them from alkylating agents. GSCs also present a huge plasticity, and they can modulate their microenvironment for their maintenance. Figure created with Biorender.com.

3. Cancer and aging: overlapping processes

For most cancer types, incidence and mortality increase with age, as it is the case of CNS tumors. Indeed, while the incidence of both benign and malignant primary CNS tumors is 18.16 per 100,000 individuals in the general population, it reaches up to 63.75 per 100,000 individuals in the age range of 75 to 84 years old. Moreover, advanced age is a well-known prognostic factor linked to poor survival in brain tumors [135].

The effect of aging as a risk factor can be observed at two levels. On the one hand, chronological aging provides time for intrinsic and extrinsic factors to exert their effects. On the other hand, the generalized decline in cellular and molecular functions observed upon biological aging has been strongly associated with cancer formation [136].

Cancer and aging may seem opposite processes, as cancer is the consequence of an aberrant gain of cellular fitness, whilst aging is based on its loss. However, cancer and aging share a common origin: accumulation of cellular damage [137]. Indeed, both hallmarks of aging [137] and cancer [138] show numerous overlaps between them, such as genomic instability, telomere attrition, epigenetic alterations, loss of proteostasis, mitochondrial dysfunction, deregulated nutrient sensing, cellular senescence, stem cell exhaustion and altered intercellular communication [136]. Thus, cancer and aging have been proposed to behave as two manifestations of the same underlying processes [137, 139].

4. Brain aging

Aging is a time-dependent functional decline of organs and tissues of most living organisms occurred due to the gradual accumulation of cellular damage [137, 140]. In the last two centuries, human life expectancy has doubled in most developed countries [141]. However, this increase in life expectancy contributed to the onset of many common diseases, such as neurodegenerative diseases or cancer, with death rates rising significantly with advancing age [142].

Although human aging affects the entire organism, brain aging is especially distinctive. At macroscopic level, aging alters human brain structure, as it shrinks grey and white matter volume, and subsequently enlarges the ventricles [143]. At cellular level, the majority of neurons are highly differentiated postmitotic cells whose lifespan is almost equivalent to the one of the whole organism [140], making them susceptible to aging process. Thus, brain aging is characterized by the loss of nerve fibers and their demyelination, the reduction of dendritic length and branching or the partial loss of synapses [144]. Besides neurons, aging also affects to other cell types, such as NSCs and glial cells [145] [146]. All these changes contribute to a decline in cognitive abilities, sensory perception, and motor function and coordination [147].

4.1. NSC aging

The decline of the stem cell pool is one of the nine hallmarks of aging described in 2013 by López-Otín and collaborators [137]. Specifically in the brain, in homeostatic conditions, impaired neurons could be partially replaced and compensated through the neurogenesis process occurred in the neurogenic niches. In rodents, during aging, the ability of NSCs to proliferate and differentiate into new neurons decreases in a devastating manner [145, 148]. This decline in neurogenesis observed in both SVZ and hippocampus involves processes such as increased NSC dormancy, decreased self-renewal, reduced neural differentiation, and induced cell death [145]. Human hippocampal neurogenesis occurs at postnatal stages, although there are discrepancies regarding its activity during the adulthood and upon aging [149-152]. Importantly, besides the dysregulation of intrinsic pathways crucial for NSC maintenance, external factors have been also described to have an impact on neurogenesis.

4.2. Microglial aging: a pro-inflammatory signature

Aging alters overall intercellular communications, which indeed constitute another hallmark of aging [137]. One of the most prominent alterations is 'inflammaging', the pro-inflammatory phenotype that an organism adopts with age. It might present various causes, such as the accumulation of pro-inflammatory tissue damage, dysfunction of the immune system or the secretion of pro-inflammatory cytokines by senescent cells [137].

Glial cells are the first cells responding to stress signals in CNS, being quite susceptible to brain aging. In fact, a gene expression study has demonstrated that glial-specific genes predict age with greater precision than neuron-specific genes, as their regional specific pattern is shifted upon human brain aging [146]. Interestingly, studies performed in rats and monkeys reported that microglial cells presented more dramatic alterations than other glial cell types upon aging, in terms of number of inclusions, and overall number of cells [153, 154]. Those alterations were also observed in mice, as well as morphological changes such as increased soma volume and shortening of processes, in old animals compared to young ones [155]. Human brains show a distinctive microglial morphology upon aging, with beaded and fragmented processes and a disrupted cytoplasmic structure [156]. As this phenotype reflects the degeneration of microglia, the difference observed in mice and

human aged brains could be partly explained by the different lifespan of each species [157]. Regarding microglial function, both murine and human aged microglia adopt an aberrant activation (primed) and pro-inflammatory status, accompanied by dysfunction in phagocytosis and impaired *in vivo* motility, among others [147, 158]. Overall, these alterations in microglial cells contribute to the aged phenotype of other cell types, altogether limiting brain function [147].

4.3. Impact of aged microglia in NSCs

The microenvironment present within the neurogenic niches is necessary for the maintenance and function of NSCs. In fact, NSCs transplanted beyond this brain regions lose their ability to self-renew and differentiate into new neurons [159]. During aging, cellular composition of neurogenic niches and their response to local or systemic signals changes significantly [145]. Importantly, microglial phagocytosis is impaired in brain aging, which may contribute to the accumulation of debris and aggregates in the NSCs niches [145]. Besides, the aberrant pro-inflammatory factor secretion by aged microglia reduces NSC proliferation in both SVZ and hippocampus [160-162]. These studies may suggest that the removal of aged microglia may be a promising strategy for delaying NSC decline. In this sense, the rapid depletion of aged microglia by the administration of an inhibitor of the colony-stimulating factor 1 receptor (CSF1R) in mice, and subsequent natural cell repopulation showed improved spatial learning and increased hippocampal dendritic spine density and neurogenesis [163]. Thus, the pro-inflammatory status of microglia in aged neurogenic niches impairs NSC activity and neurogenesis, which eventually contribute to cognitive decline (***Figure I4***).

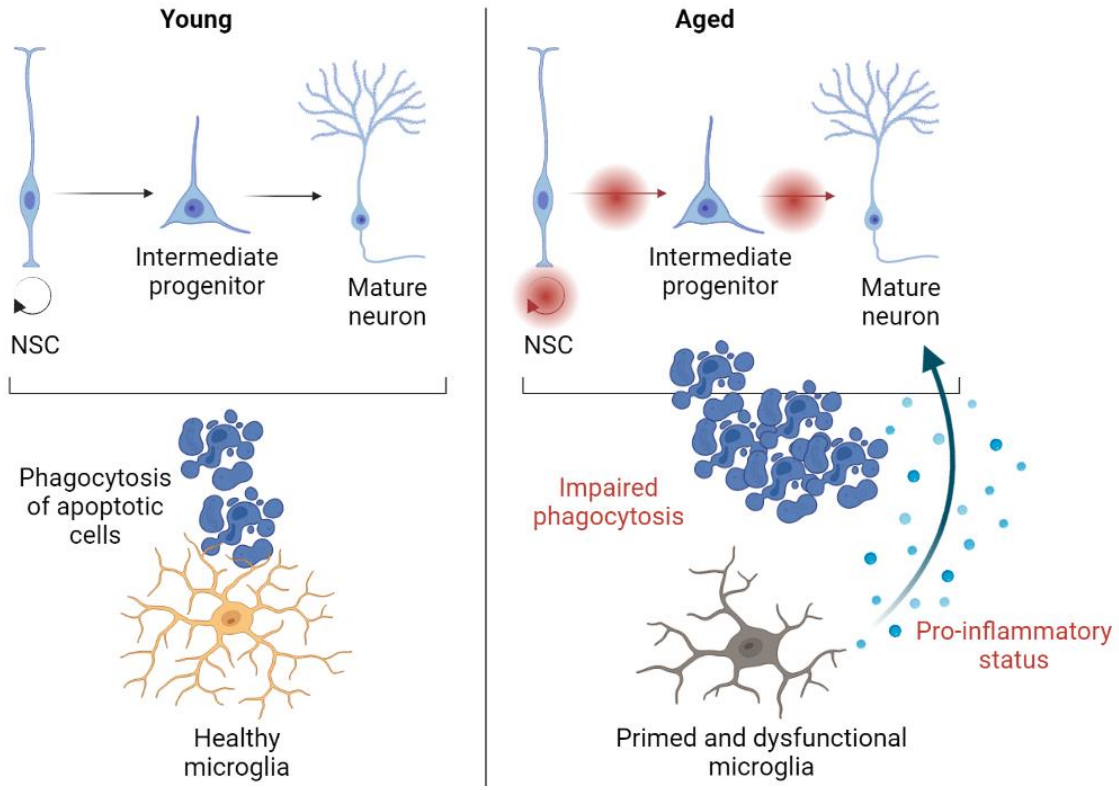

Figure I4. Changes in microglial activity in neurogenic niches upon aging. Microglia participate in the elimination of apoptotic cells and cell debris in the process of neurogenesis. Upon aging, microglial cells adopt a pro-inflammatory phenotype and present impaired phagocytosis, affecting to NSC proliferation and differentiation process. Figure created with Biorender.com.

Overall, a proper homeostasis of the cell is essential for the correct function of the organ. In this sense, dysregulation of proteomic and epigenetic processes have been linked to the development of GB and physiological brain aging.

5. Proteostasis in GB: role of chaperone-mediated autophagy

5.1. The concept of proteostasis

Protein homeostasis, also named proteostasis, refers to the ability of cells to maintain a correct balance between protein synthesis, folding and degradation [164]. A correct preservation of proteostasis is essential for optimal proteome renewal, cell growth and adaptation to environmental conditions [165]. Several stressors, such as heat shock, oxidative stress or aging-related modifications, cause protein misfolding, aggregation and a general imbalanced proteostasis, triggering the development of several diseases [165]. In this

context, a balanced activity of protein quality control orchestrated by molecular chaperones, together with the degradative ubiquitin proteasomal system and autophagy processes is crucial [165].

5.2. Autophagy

Autophagy, term that originally comes from the Ancient Greek meaning 'self-eating', refers to the catabolic process that cells use to recycle their own constituents or to eliminate damaged proteins, within the lysosome [166, 167]. So far, three main types of autophagy have been described (***Figure I5***).

The first discoveries were based on the bulk trapping of the cargo, such as damaged organelles or protein aggregates, in double-membrane autophagosomes that fuse with lysosomes, process that afterwards was named 'macroautophagy' (MA) [168]. This type of autophagy has been the most studied one since its discovery, showing a great implication in cancer and aging processes [169, 170]. Further studies indicated the existence of a second type of autophagy, named 'microautophagy'. This process involves the uptake of soluble or membrane-bound material directly into the lysosome by invagination [171, 172]. In contrast to MA, the role of microautophagy in cancer and aging is still poorly understood.

Both MA and microautophagy overall represent mainly non-selective forms of autophagy, although recent studies have reported selective forms within them [173]. Among them, 'chaperone-assisted selective autophagy' (CASA) is a selective-type of MA, which targets ubiquitin-positive protein aggregates via autophagosomes [174]. Besides, the 'endosomal-microautophagy' process is based on a mechanism in which cytosolic proteins enter endosomal compartments inside vesicles generated at the surface of the late endosomes [175]. The study of these subtypes of autophagy is still a young field, with very few evidence in the fields of cancer and aging.

In 1986 Dice JF and collaborators described a third main type of autophagy, nowadays known as 'chaperone-mediated autophagy' (CMA), which is selective for protein degradation, and whose impact on cancer and aging has been established. This finding came from the identification a pentapeptide region on ribonuclease A required for its enhanced degradation during serum deprivation [176], a well-established inductor of CMA process. Importantly, among all currently known forms of autophagy, CMA is the only process that

enables the direct translocation of an individual cargo protein across the lysosomal membrane for its degradation [177].

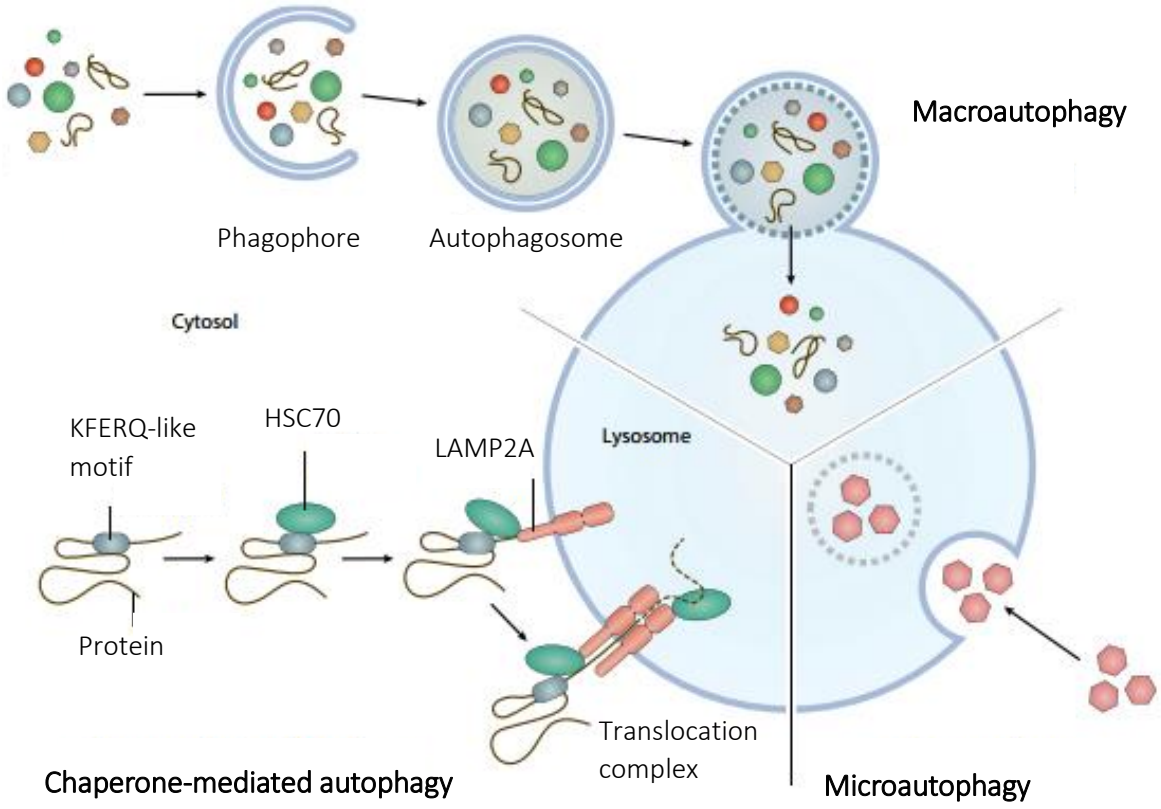

Figure I5. Main types of autophagy: macroautophagy (MA), microautophagy and chaperone-mediated autophagy (CMA). MA is specialized in the bulk degradation of damaged organelles and protein aggregates by the formation of phagophore and autophagosomes. These autophagosomes fuse with lysosomes, where cargo is degraded. Microautophagy is based on the bulk degradation of soluble or membrane bound material by direct invagination of lysosomal membrane. CMA is a unique selective form of autophagy. Proteins containing a KFERQ-like motif are recognized by the chaperone HSC70, which eventually targets the protein to the lysosomal membrane. Herein, protein is bound to lysosome-associated membrane protein type 2A (LAMP2A) protein, which subsequently is multimerized. Unfolded protein is finally translocated through the complex and it is degraded in the lysosomal lumen. Modified from https://www.ibric.org/myboard/read.php?id=156992&Page=298&Board=new_protech&

5.3. CMA process

5.3.1. Mechanism of action

The targeting and degradation of proteins through CMA process comprehend a subset of critical steps (***Figure I5***).

The first requirement for a protein to be a CMA substrate is that it must contain a KFERQ-like motif, which consist of a sequence of amino acids with specific charge and hydrophobicity [177]. In fact, post-translational modifications, such as phosphorylation or ubiquitination, can recreate this motif conferring the necessary properties, or they can induce conformational changes that expose or mask an existing motif [177, 178]. Next, this KFERQ-like motif is recognized by a heat shock cognate 71kDa protein (HSC70), which subsequently is going to target the protein to the lysosome [179]. Within the lysosomal membrane, the substrate binds to the cytosolic tail of the lysosome-associated membrane protein type 2A (LAMP2A) [180]. After this interaction, two processes occur. First, the substrate acquires an unfolded state to be translocated into the lumen of the lysosome [181]. Herein, HSC70 and other co-chaperones located in the surface of the lysosome are thought to be mediating this process [182]. Second, LAMP2A monomers are multimerized, in order to form the translocation complex [183]. As lysosomal membrane is enriched in proteases, heat shock cognate 90 kDa (HSC90) chaperone stabilizes the complex from the luminal part, hiding the protease-sensitive regions of LAMP2A. When these two latter steps are fulfilled, the substrate enter the lumen of the lysosome through LAMP2A complex, where degradation occurs. This process is facilitated by a form of HSC70 located in the lumen, which pulls the substrate and prevents its return into the cytosol [184].

5.3.2. Biological processes

The best characterized function of CMA is its role in cellular protein quality control, promoting the degradation of misfolded or unfunctional proteins [185]. As a consequence, CMA inhibition turns cells sensitive to oxidative stress, or protein-damaging chemicals, leading to the accumulation of oxidized and aggregated proteins [186, 187].

Cellular energetics has been linked to CMA since its discovery, as it is upregulated upon starvation [188]. At that time, this effect was proposed to be caused by the need of free amino acids for the synthesis of essential proteins. Further advances in the field have revealed that CMA selectively degrades fully functional key enzymes in lipid and glucose metabolism, affecting the activity of these pathways [189].

CMA also contributes to cell cycle regulation in the presence of stressors. In this line, after DNA repair, CMA induces cell cycle re-entry through the degradation of Chk1, a protein required for checkpoint mediated cell cycle arrest [190]. Thus, in CMA-deficient cells nuclear phospho-Chk1 gets aberrantly accumulated, thus disrupting DNA repair machinery

[190]. In hypoxic conditions, CMA also regulates cell cycle through the degradation of HIF1α [191, 192].

The implication of CMA in immune function has been also emerged, having observed that CMA targets the ubiquitin ligase Itch and the calcineurin inhibitor RCAN1 for degradation to maintain activation status in T cells [193].

Very recent studies have revealed the role of CMA in stem cell maintenance. Low activity of CMA promotes self-renewal in embryonic stem cells (ESC), whereas its upregulation enhances their differentiation [194]. On the contrary, CMA has been shown to be crucial in sustaining quality control, appropriate energetics, and overall long-term function in adult hematopoietic stem cells (HSC) [195]. In fact, CMA function decreases with age, being its genetic or pharmacological activation able to restore the functionality of old mouse and human HSCs [195]. This evidence highlights the dual role of CMA in stem cell maintenance in embryonic and adult stages of an organism.

5.3.3. CMA regulation

LAMP2A activity is the best criteria to determine specifically CMA activity [177], as other proteins, such as HSC70 also participate in other processes [174, 175]. LAMP2A is one of the three splicing variants of the *LAMP2* gene, which contains a cytosolic tail that differs from its isoforms LAMP2B and LAMP2C. However, none of these two additional isoforms can compensate LAMP2A absence and its role in CMA process [196].

In the process of CMA, regulation of the expression, trafficking, and stability of LAMP2A are crucial. Regarding its expression, transcription factors such as NFAT1 [193] or NRF2 [197], or PI3K/AKT/mTOR pathway [198] modulate *LAMP2A* expression *de novo*. LAMP2A trafficking to the lysosomal membrane is also important, where cystinosin, Rab11 and Rab7/RILP proteins play a key role [198]. Besides, in resting conditions, LAMP2A monomers are located in lipid-enriched microdomains within the lysosomal membrane, whereas their multimerization occurs outside these regions [199]. These microdomains make LAMP2A more susceptible to proteolytic cleavage and degradation. The stability of the translocation complex is also a relevant point in the regulation of CMA. Herein, GTP/GFAP/EF1α [200] and mTORC2/PHLPP1/Akt [201] axes play a crucial role. Recent studies also indicate the impact of post-translational modifications on HSC70 and HSC90, and subsequently, in CMA activity [202].

Compensatory mechanisms between CMA, MA or ubiquitin-proteasomal systems have been described in the literature [202], which reflects the complex scenario of interactions between the distinct protein degradative systems within the cell.

A proper regulation of CMA process is crucial for the homeostasis of a cell, so that its dysregulation has been linked to aging and cancer. Upon physiological aging, functionality of CMA process declines [203], whereas the activation of an extra copy of LAMP2A in aging liver reduces damaged proteins and improves organ function [204]. Regarding malignant transformation, CMA presents anti-oncogenic effects in untransformed cells [205]. In this context, the decline in CMA upon aging may also be a risk factor for carcinogenesis. However, once transformation occurs due to damage accumulation, malignant cells activate CMA constitutively, promoting cancer progression [205]. The tumor promoting role of CMA has been identified in several cancer-types, such as lung, liver, or breast cancer [206].

5.4. Role of CMA in GB and brain aging

Most of the evidence linking autophagy to human brain aging field are focused on MA process, describing an age-related decline of this form of autophagy in animal models [207]. However, current knowledge regarding the impact of CMA on brain aging is limited to few preliminary studies [202]. Among them, a significant decline in HSC70 [208] and little changes in *LAMP2* [209] concentration have been found in cerebrospinal fluid. In brain disease, research in the field of CMA has been focused on its role of in neurodegenerative diseases, being Parkinson's disease the first disorder associated with this form of autophagy [202].

When studying the implication of autophagy in brain cancer, most of the efforts have also focused on MA [210]. In fact, MA shows a dual role in GB, both suppressing or promoting tumor progression [211]. While it has been demonstrated that MA promotes apoptosis in response to several stressors in glioma cells [212], others have shown that, during advanced stages, MA promotes cell survival, providing metabolic support and preventing senescence [213].

Nevertheless, the study of CMA in brain cancer is still a relatively new field. In this context, surgical samples from patients after TMZ chemotherapy have shown induced

expression of LAMP2A, together with MA markers LC3B and LAMP1, compared to pre-treatment samples [214]. Besides, a recent study showed that GB-induced upregulation of CMA activity in pericytes is essential for their effective interaction with GB cells that help tumor growth [215]. Besides, this study shows that a GB mouse model grafted with CMA-defective pericytes exhibits reduced GB proliferation and effective immune response when comparing to others grafted with control pericytes [215].

The regulatory role of MA in GSC metabolism and maintenance has been described [216, 217]. Regarding CMA, the high levels of LAMP2A in TMZ resistant samples could suggest that it is involved in the regulation of GSC subpopulation. However, no evidence has been published studying the intrinsic function of CMA in GSC or in any CSC type.

6. Epigenetics in the brain: role of histone deacetylases

6.1. Concept of epigenetics

The concept of epigenetics, which was firstly introduced by Waddington C. in the early 1940s, refers to the study of changes in gene expression patterns that are heritable and do not constitute a change in DNA sequence [218]. Processes such as the conversion of a pluripotent stem cell into a differentiated cell-type are therefore explained by epigenetic mechanisms [219]. Differences in environmental and lifestyle factors have been also described as modulators of the epigenetic landscape, which suggests the relevance of epigenetics during adulthood and in physiological aging [137, 220, 221]. To date, DNA methylation [222], noncoding RNAs [223], histone variants [224] and histone modifications are the mainly described epigenetic processes. Importantly, although heritable, epigenetic modifications have been described as dynamic and reversible, making them targets for the development of strategies against neurodegenerative diseases and brain cancer, among others [138, 225-227].

The role of histones in gene expression and chromatin structure has been widely described, as they are a key component of the basic structure of the chromatin unit known as the nucleosome. The nucleosome is a unit composed by 146 bp DNA wrapped around an octamer consisting of two copies of H2A, H2B, H3 and H4 core histones, and held together with the linker histone H1 [228]. Structure of nucleosome arrays can form euchromatin or

heterochromatin conformations, which represent lax and active chromatin, or tight and repressed chromatin, respectively [224]. Histones are subjected to modifications such as phosphorylation, methylation, ubiquitination, biotinylation, sumoylation, ADP ribosylation, and acetylation on the amino-terminal tails, which can modify configuration and accessibility of the chromatin [229]. Thus, by modulating electrostatic charge of the histone and its affinity for the DNA, recruitment of transcriptional regulators can be altered, which eventually may modify gene expression. Among these modifications, histone methylation and acetylation are the most prevalent ones. Herein, while methylation of lysine residues may be either associated with transcriptional repression or activation depending on the amino acid and to what extend (mono-/di-/tri-methylation) the residue is modified, all acetylation of lysine residues on H3 and H4 have been associated with transcriptional activation [230].

6.2. Histone acetylation

Acetylation of lysine residues of histone tails neutralizes their positive charge, decreasing the ionic interactions between histones and the negatively charged DNA. The main consequence of this histone modification is the conversion into a more relaxed chromatin state and transcriptional activation [231]. As the other main epigenetic modifications, histone acetylation is regulated by 'writers' or enzymes that establish the epigenetic change, and 'erasers' or enzymes that remove these modifications [232]. Acetylation is controlled by two antagonistic enzyme families: the 'writers' histone acetyltransferases (HAT) and the 'erasers' histone deacetylases (HDAC). HDACs catalyze the removal of acetyl groups from histone tails and thus provoke a 'compacted' chromatin status, while HATs have the opposite effect (***Figure I6***).

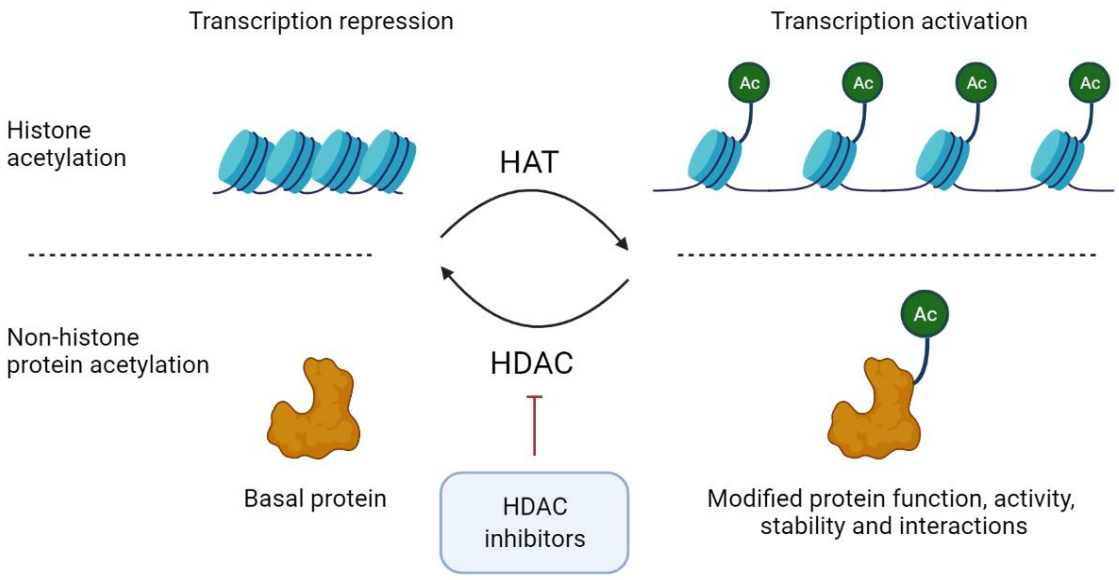

Figure I6. Regulation of histone and non-histone protein acetylation. Acetylation is regulated by the balanced activity of histone acetyltransferases (HAT) and histone deacetylases (HDACs). HATs act as 'writers', adding an acetyl group to these proteins, whereas HDACs act as 'erasers', removing the acetyl groups. The addition of acetyl groups into histone tails neutralizes the positive charge of lysines, reducing their interaction with the negatively charged DNA. Thus, chromatin structure changes, which gets more accessible to transcription factors, and thus, transcription can be activated. Non-histone protein acetylation regulates protein function, activity, stability, and interaction with other proteins. HDACis negatively regulate the function of HDACs. Figure created with Biorender.com.

6.3. Histone deacetylases

The enzymatic activity of deacetylation of histones was firstly discovered by Inoue A and Fujimoto D in 1969, in calf thymus extract [233]. In the following years, various molecular studies on HDACs were performed in *Saccharomyces cerevisiae* yeast organism [234]. The first human HDAC was identified in 1998, which was named HDAC1 [235]. Since then, research on HDACs exploded, being human HDAC11 the last member of human HDAC family, discovered in 2002 [236, 237].

Besides the initially discovered and best studied epigenetic activity of HDACs, recent studies revealed that certain HDACs can also modulate the acetylation status of numerous cytoplasmatic proteins and transcription factors, thus regulating their stability and function [238] (***Figure I6***). As an example, HDAC6 catalyzes α-tubulin deacetylation [239], whereas HDAC1,2 and 3 present this effect in p53 tumor suppressor [240].

6.3.1. Human HDAC classification

To date, 18 human HDACs have been identified (***Table I2***), which are classified in four groups based on sequence similarity with yeast HDACs. Among them, class I, II, and IV HDACs, also known as classical HDACs, depend on Zn^{2+} ion located in their catalytic pocket, whereas class III HDACs, known as Sirtuins (SIRTs), are nicotinamide adenine dinucleotide (NAD^+)-dependent enzymes [241].

Table I2. Classification of human HDACs.

Group	Class	Name	Location in cell
Zn^{2+} dependent	Class I	HDAC1, 2, 3, 8	Mainly nucleus (HDAC8 mainly cytoplasm)
	Class IIa	HDAC4, 5, 7, 9	Nucleus / cytoplasm (HDAC7 also in mitochondria)
	Class IIb	HDAC6, 10	Mainly cytoplasm (HDAC10 also in the nucleus)
	Class IV	HDAC11	Nucleus / cytoplasm
NAD^+ dependent	Class III	SIRT1-7	Nucleus/ cytoplasm/ mitochondria

Source: Shukla S & Tekwani BL 2020 [241].
HDAC: histone deacetylase; SIRT: sirtuin; NAD: nicotinamide adenine dinucleotide

Class I HDACs, which are homologous to Rpd3 in yeast, include HDAC1, 2, 3 and 8. Their catalytic activity depend on their respective co-repressor complexes. Based on the similar structure of both HDAC1 and HDAC2, they are often recruited to the same co-repressor complexes, such as NuRD, RCOR1/CoREST, Sin3A and MiDAC [231]. On the contrary, HDAC3 associates with NCoR and SMRT complexes [231]. HDAC8 has the unique property of accommodating substrates with a flexible L1 loop in its N-terminal region, which is absent in the rest of HDACs [231].

Class II HDACs, which are homologous to yeast Hda1, are further divided in two subgroups: class IIa and IIb. Class IIa includes HDAC4, 5, 7, and 9, while class IIb includes HDAC6 and 10. Members of class IIa include an extended N-terminal domain that contains conserved serine residues, which can be phosphorylated by several kinases and eventually, facilitate nuclear export of HDACs [231]. For the opposite effect, class IIa HDACs contain

nuclear localization sequences (NLS), indicating their ability to shuttle between the nucleus and the cytoplasm. Within class IIb HDACs, HDAC6 is predominantly localized in the cytoplasm and contains two catalytic domains, conferring differential substrate recognition [242]. Besides, it contains zinc-finger ubiquitin binding domains that negatively regulate polyubiquitin chain turnover [243]. Furthermore, HDAC10 contains leucine-rich domain, a deacetylase domain, and an inactivity domain [244]. As class IIa HDACs, HDAC10 associates with HDAC2, HDAC3, SMRT and NCOR2 to enhance transcriptional repression [231].

Class III HDACs, or SIRTs, are homologous to yeast Sirt2 and include SIRT1-7. While SIRTs such as SIRT1 are distributed in the cytoplasm, nucleus, and mitochondria [231, 245], others such as SIRT3 are primarily found in the mitochondria [246].

Class IV HDACs include only HDAC11, which might be predominantly involved in the fatty acylation of proteins compared to its weak deacetylation capacity [231, 247].

6.3.2. Biological functions of HDACs

HDACs are implicated in a wide range of processes, as a result of the direct and indirect modulation of multiple histone and non-histone protein acetylation [231, 248]. In fact, knock out mice of almost all HDACs present embryonic and perinatal aberrations and lethality [238], indicating the pivotal role of HDACs in cellular homeostasis. In particular, knock out mice for *HDAC1, 3* and *7* present embryonic lethality. Other HDACs dysregulation presents a milder but still significant effect, as it is the case of *HDAC2, 5* and *9*, whose knock out mice present cardiac defects, or *HDAC4* knock out, which show premature and ectopic ossification [238]. On the contrary, knock out mice for *HDAC6*, which show a global tubulin acetylation, are viable and do not present significant defects [249].

The epigenetic activity of HDACs mainly results in the negative regulation of gene transcription, forming a complex with transcription factors or by indirectly regulating their transcription or acetylation [250]. As an example, HDACs regulate p53 tumor suppressor pathway, crucial for mediating gene expression, by modulating its activity [251, 252]. In addition to transcription factors, HDACs also modulate the activity of super enhancers [253], and the maintenance of DNA methylation [253].

HDACs are often involved in cell cycle checkpoints, regulating G1/S and G2/M transitions. In this line, HDACs regulate the expression of key cell-cycle regulation proteins, being $p21^{CIP1}$ the main target [254]. Other regulators such as $p27^{KIP1}$ [255] and Cyclin A [231]

have been also described to be modulated by HDACs. In fact, *HDAC6* knock down results in reduced proliferation and induction of cell cycle arrest [256]. Moreover, HDACs also regulate apoptosis, mediated in part by their effect in p53 expression and acetylation [231, 240]. Interestingly, the inhibition of HDACs induces cell differentiation [257]. In this sense, it has been shown that the target of HDACs, $p27^{Kip1}$, directly represses Sox2 stem cell factor during ESC differentiation [258]. Together with these functions, HDAC activity has been also associated with the regulation of migration, metabolism, hypoxia, angiogenesis, oxidative stress, DNA damage response, degradative systems such as autophagy and immune functions [231, 259].

6.3.3. HDAC inhibitors

The development of HDAC inhibitors (HDACi) has facilitated the understanding of molecular and phenotypical functions of HDACs. In the 1970s, sodium butyrate was identified as the first HDACi [260], and since then, multiple natural and synthetic HDACis have been discovered. At present, HDACi are classified into four categories: (i) hydroxamic acids or hydroxamates, such as Suberoylanilide hydroxamic acid (SAHA), Trichostatin A (TSA), Panobinostat and Belinostat; (ii) cyclic peptides, including Depsipeptide; (iii) benzamides, such as Chidamide; and (iv) short chain fatty acids, including Valproic acid [231].

From preclinical studies to clinical trials, HDACis have demonstrated potent therapeutic effects in various cancers. In fact, SAHA (2006) and Belinostat (2014) have been already approved by the FDA for the treatment of relapsed cutaneous and peripheral T-cell lymphomas, respectively [231]. However, most of the currently available HDACis are unselective, inhibiting various HDAC members [231]. Therefore, they present numerous side effects, affecting directly to their clinical efficacy.

6.1. HDACs in GB

A typical characteristic of human cancer is the deregulation of histone modifications, which has fatal consequences at gene transcription level. Indeed, the loss of acetylated lysine 16 (K16-H4) and trimethylated lysine 20 (K20-H4) of histone H4 is a common event in human cancer [261]. These histone marks are a result of the aberrant expression or activity of enzymes involved in adding, removing, or signaling histone modifications. In this

line, overexpression of HDACs is frequently observed in cancer patients [262], regulating both histone and non-histone proteins.

In GB, the overexpression of HDACs, such as HDAC1 or HDAC6, has been associated with aberrant proliferation, invasion, tumor growth and TMZ resistance [263-267]. Interestingly, elevated expression and activity of HDAC4, HDAC6 and several SIRTs has been reported in GSCs compared to non-stem cancer cells or NSCs, correlating with glioma progression [268-271]. In this context, the interest of using HDACis as a promising anticancer strategy in GB has been increased in the last years. HDACis such as SAHA have been shown to reduce GSC subpopulation by modulating their stemness, proliferation, differentiation, cell cycle arrest, apoptosis, autophagy and vasculogenic mimicry, among others [272, 273]. The potential of several HDACis, most prominently SAHA, has been tested in preclinical and even clinical trials in GB, with promising results [274]. Not only as single agents, but also in combination with other anti-cancer agents such as TMZ or bevacizumab, and in some cases with radiotherapy, are being tested in various clinical trials of GB patients [274]. However, the lack of specificity of pan-inhibitors still remains a clinical issue since high and, for some cases, active doses elicit deleterious side effects.

HDAC6 is becoming an attractive pharmacological target in cancer, also in GB. Besides its relevant role in GB tumor initiation and progression, *HDAC6* could be considered a 'safe' target, as its homozygous knock out mice, in contrast to class I, II and III knock out conditions, remain viable and fertile, with no clear developmental alterations [249]. This fact indicates that the use of HDAC6-specific inhibitors could offer a wider therapeutic window than other pan-HDACis.

6.2. HDACs in brain aging

Epigenetic mechanisms are increasingly appreciated to be crucial for a variety of processes related to aging, such as cellular and organismal senescence, genomic instability, and carcinogenesis [275].

Among all HDAC classes, although the role of SIRTs is better established [276], several evidence have suggested the impact of classical HDACs on brain function and aging. In this sense, recent studies performed in rodent models have revealed that both classical HDAC expression [277, 278] and activity [279] are increased with age in hippocampus. In this

line, HDAC1, 3, 5, and 7 are highly expressed in NSCs, whereas HDAC2 is more widespread in the brain [280, 281]. Importantly, treatment of adult NSCs with HDACis induce differentiation and upregulates neuronal-specific genes, such as NeuroD, Neurogenin 1, and Math1 [282], altogether indicating the relevance of classical HDAC activity in NSC maintenance. Consistent with this, HDAC1 [283], HDAC2 [284], HDAC3 [285], HDAC4 [286] and HDAC6 [287] play a key role in associative and spatial memory, learning, and synaptic plasticity. However, the exact mechanism and the affected cell-types that are consequently dysregulated remain to be elucidated.

The impact of HDAC enzymes is also extended to the maintenance of other cell-types, such as microglia, which, as discussed in a previous section, are relevant in the maintenance and activity of NSCs. Particularly, HDAC1 and HDAC2 regulate microglial function during development and neurodegeneration [288]. However, the implication of HDACs in microglial aging and their effect in NSCs has not been explored.

Hypothesis and objectives

Hypothesis

Given the role of CMA in tumor formation and progression, we hypothesize that this process may be involved in GB and may regulate GSC maintenance and activity. Besides, the selective inhibition of the oncogenic histone deacetylase 6 may present strong cytotoxic and anti-tumor effect in GSCs, possibly in a safer way than other pan-HDACis. Finally, the role of HDACs in microglia and its paracrine effect in hippocampus may have an impact on physiological aging.

Objectives

1. To determine the role of CMA in GSC subpopulation
   1.1. To characterize the expression of LAMP2A and activity of CMA in GB and GSCs
   1.2. To study the role of LAMP2A in GSC activity
   1.3. To unravel the underlying proteomic and transcriptomic pathways of LAMP2A in GSCs
   1.4. To associate the molecular signature of LAMP2A impairment with phenotypic alterations
   1.5. To establish the impact of LAMP2A expression on patient survival

2. To study the potential of a novel HDAC6 inhibitor against GSCs and GB progression
   2.1. To characterize the expression of HDAC6 in GB and GSCs
   2.2. To test the target specificity and cytotoxic activity of a novel small-molecule inhibitor of HDAC6 in GB cell lines and GSCs
   2.3. To compare the activity of the novel HDAC6 inhibitor with currently available HDACis
   2.4. To determine the effect of the novel HDAC6 inhibitor in tumor initiation and progression *in vivo*
   2.5. To develop a vehiculation strategy for the novel HDAC6 inhibitor

3. To characterize the expression of HDACs in aged brain and explore its implication in microglial aging
   3.1. To study the expression of HDACs in microglial aging *in vitro*
   3.2. To determine the expression of HDACs in young and aged, murine, and human, hippocampus and correlate it with microglial markers
   3.3. To extend the characterization of HDACs and microglial marker expression to other brain regions

Materials and Methods

1. Human samples

1.1. GB samples

Control and glioma patient clinical and transcriptomic data have been partly collected from GlioVis database (http://gliovis.bioinfo.cnio.es/) [289]. RNA sequencing (RNAseq) and microarray results from TCGA (10 controls, 226 grade II, 244 grade III and 528 grade IV or GB), Rembrandt (28 controls, 98 grade II, 85 grade III and 219 grade IV or GB), Phillips (76 GB) and Joo (57 GB) cohorts were extracted for the study of *HDACs* and *LAMP2* expression and its impact on patient survival. Expression cutoffs for Kaplan Maier curves have been designated as optimal by GlioVis database. For the specific characterization of *LAMP2* gene expression among distinct subpopulations of cells within GB tumors, data from single cell RNAseq of 11 GB primary tumors obtained from UCSC Cell Browser (https://cells.ucsc.edu/?ds=gbm) [290] were analyzed. Moreover, for the analysis of the impact of *LAMP2* in TMZ response, microarray data from 319 GB samples from ROC plotter online tool (http://www.rocplot.org/) [291] were included, which comprise gene expression data from 154 non-responder and 165 responder patients.

Association studies have been developed based on transcriptomic data from TCGA cohort using the website 'R2: Genomics Analysis and Visualization Platform' (http://r2.amc.nl) and cBioPortal database (https://www.cbioportal.org/) [292, 293].

In the first chapter of this doctoral thesis, all clinical data obtained from publicly available databases constantly refer to *LAMP2* gene expression; they do not contain information regarding any specific isoform, as it is the case of *LAMP2A, B* and *C*. Thus, in order to see whether the results obtained in these cohorts could be attributable to *LAMP2A* transcript by itself, *LAMP2A* expression was studied in a total of 20 frozen biopsies at mRNA level and 98 biopsies by tissue microarray (TMA) immunohistochemical analysis, which were obtained from patients seen at Donostia University Hospital (San Sebastian, Spain) and diagnosed as primary GB according to the WHO criteria. All participants of the study signed an informed consent form approved by the Clinical Research Ethics Committee. For the mRNA expression analysis, total human brain RNA (AM7962, Invitrogen™) was used as healthy control tissue.

Given the acquisition timeline of the tumor specimens and associated clinical long-term follow-up that predate the 2016 WHO classification [294], the definition of glioblastoma, IDH wildtype is not as strict as currently defined in the upcoming 2021 WHO classification of central nervous system tumors [32].

2. Healthy brain samples of young and aged individuals

For the study of the expression of *HDACs* and microglial markers, hippocampal samples from 33 individuals from the Basque Country were analyzed. In particular, this cohort comprises young individuals ranged from 27-45 years old (female n=8, male n=8) and elderly people from 76 to 96 (female n=8, male n=9).

RNAseq data from white matter of forebrain, hippocampus, parietal neocortex and temporal neocortex from aged individuals were obtained from 'Aging, Dementia and TBI Study' (https://aging.brain-map.org/rnaseq/search) [295]. This cohort encompasses 54 participants from 78 to 100+ years old (female n=22, male n=32), among which 24 presented dementia (Alzheimer's disease, vascular dementia, multiple etiologies, or other medical dementia), while other 30 did not present any of these disorders.

For the study of the expression of *HDACs* directly in microglia, RNAseq data originated from the bulk human dorsolateral prefrontal cortex (n=540) and from purified human microglia (n=10) from the same brain region were studied (http://shiny.maths.usyd.edu.au/Ellis/MicrogliaPlots/) [296].

3. Experimental mouse models

Several mouse strains have been used for the development of this doctoral thesis, whose main characteristics and application have been summarized in ***Table M1***.

Table M1. Mice strains used in this work.

Name in this thesis	Strain	Description	Assay	Source
Foxn1^{nu}/Foxn1^{nu}	Hsd:Athymic Nude-*Foxn1^{nu}*	Athymic and hairless mice, T-cell deficient	Generation of subcutaneous glioma xenografts subjected to intraperitoneal treatment	Envigo, order code 069
NOD.SCID	NOD.CB17-*Prkdc*^{scid}/NCrHsd	Altered T- and B-lymphocyte development. Reduced NK, macrophage and granulocyte numbers and function	Generation of orthotopic glioma xenografts	Envigo, order code 170
C57BL6	C57BL/6J	No genetic alterations	Study of the expression of *HDAC* and microglial markers in neurogenic niches	The Jackson Laboratory, *Stock. No. 000664*

All mice have been housed in specific pathogen-free barrier areas of the Biodonostia Health Research Institute, maintained in ventilated racks, under controlled humidity, light cycle, temperature, food, and water.

Experiments have been performed in age-matched mice paired by sex, and blind to the experimental condition. According to the principles of bioethics in animal experimentation, for intracranial injection of tumor cells analgesia with 0.07 mg/kg Buprenorphine (CN 679588) was applied prior the surgical procedure and anesthesia with isoflurane (880393HO, Abbvie) during the process. Ophthalmic gel was also applied in the eyes of the mice to avoid dryness. In all experiments mice weight and wellbeing were monitored, and experimental endpoint was considered when > 10-20% weight loss [297] or in the presence of other cognitive or motor alterations. For brain and subcutaneous tumor

extraction, mice were anesthetized with isoflurane and culled by either CO_2 or decapitation, depending on the collected tissues.

Animal research regulations specified in the European Union Directive [2010/63/EU] and guidelines from the Animal Care and Use Committee from Biodonostia Health Research Institute have been followed and fulfilled in this work.

Together with these experimental models, *in situ* hybridization data were obtained from sagittal sections of P56 male adult C57BL6 mice from Allen Brain Atlas data portal (https://mouse.brain-map.org/) [298].

4. Cell culture

GB cell lines U87, U373, U251, T98, and A172, and the embryonic kidney cell line HEK293T were obtained from the American Type Culture Collection (ATCC) (***Table M2***). All these adherent cell lines were cultured in treated culture plates (130182, Thermo Scientific), in Dulbecco's Modified Eagle Medium (DMEM, 41966029, Gibco), supplemented by 10 % Fetal Bovine Serum (FBS, 10270106, Gibco), 2 mM L-Glutamine (25030024, Gibco), 100 U/mL penicillin and 100 µg/mL streptomycin (P/S, 15140122, Gibco). For cell splitting, 0.05 % trypsin-EDTA (25300054, Gibco) was used, with incubations of 2-5 min at 37 °C. DPBS was used for cell wash (14190094, Gibco), and cells were centrifuged at 1,500 rpm for 5 min.

Glioma Neural Stem 166 (GNS166), 179 (GNS179) and 144 (GNS144) cell lines (***Table M2***) were kindly provided by Dr. Steve Pollard (MRC Centre for Regenerative Medicine and Edinburgh Cancer Research Centre, University of Edinburgh). These cell lines were cultured in adhesion in treated culture plates, in Dulbecco's Modified Eagle Medium/Nutrient Mixture F-12 (DMEM/F-12) medium (31331028, Gibco), supplemented by 2 µg/mL laminin (L2020, Sigma-Aldrich), 1 % N2 (11520536, Gibco), 2 % B27 (11500446, Gibco), 1.34 % D-(+)-Glucose solution 45 % (G8769, Sigma-Aldrich), 2 mM L-Glutamine, 100 U/mL penicillin, 100 µM/mL streptomycin, 20 ng/mL basic fibroblast growth factor (bFGF, PHG0023, Gibco) and 20 ng/mL epidermal growth factor (EGF, A15E9644, Sigma-Aldrich). This medium was also employed for culturing GB cell lines in suspension and generation of oncospheres, but in this case, in absence of laminin and using non-treated 6-well plates (351146, Becton Dickinson). In the same way, GB2 cell line, which was generated previously in our group [111], was also cultured in suspension, generating oncospheres in the mentioned medium with double

concentrated bFGF and EGF. For both splitting GNS cell lines, or disaggregating GB2 cells or oncospheres, accutase (11599686, Gibco) was used, with incubations of 2-5 min at 37 °C. DPBS was used for cell wash, and cells were centrifuged at 1,200 rpm for 4 min.

Normal human astrocytes (NHA) from cerebral cortex were purchased in ScienCell (*Table M2*). This cell line was cultured in adhesion in culture plates pre-treated with 15 µg/mL poly-L-lysine (0413, ScienCell) for 1 h. Astrocyte medium kit (1801, ScienCell) was employed, which contains supplements such as FBS, P/S and astrocyte growth supplement (AGS). For cell splitting, 0.05 % trypsin-EDTA was used, with incubations of 2 min at 37 °C. DPBS was used for cell wash, and cells were centrifuged at 1,000 rpm for 5 min.

Human microglial cells (HMC3) were purchased from ATCC (*Table M2*). This cell line was cultured in adhesion in treated culture plates, in StableCell™ DMEM – high glucose medium (D0819, Sigma-Aldrich), supplemented by 10 % FBS, 2 mM L-Glutamine and 100 U/mL penicillin and 100 µM/mL streptomycin. For cell splitting, 0.05 % trypsin-EDTA was used, with incubations of 2 min at 37 °C. DPBS was used for cell wash, and cells were centrifuged at 1,000rpm for 5 min.

All cell lines were maintained in standard culture conditions, at 37 °C, 95 % humidity, 21 % O_2 and under 5 % CO_2 pressure. All cell culture procedures were performed in class II security laminar flow hoods (Class II Biohazard Safety Cabinets, ESCO). Cell lines were tested regularly for Mycoplasma (90021, Biotools).

Table M2. Main characteristics of cell lines used in this thesis.

Cell line	Origin	Culture medium	Reference
U87-MG (U87)	GB	DMEM + 10 % FBS	ATCC® HTB-14™
U373-MG (U373)	GB	DMEM + 10 % FBS	ATCC® HTB-17™
U251-MG (U251)	GB	DMEM + 10 % FBS	ATCC
T98-G (T98)	GB	DMEM + 10 % FBS	ATCC® CRL-1690™
A172	GB	DMEM + 10 % FBS	ATCC® CRL-1620™
GNS166	GSC	DMEM/F12 + EGF/FGF	Dr. Steve Pollard (MRC)
GNS179	GSC	DMEM/F12 + EGF/FGF	Dr. Steve Pollard (MRC)
GNS144	GSC	DMEM/F12 + EGF/FGF	Dr. Steve Pollard (MRC)
GB2	GSC	DMEM/F12 + EGF/FGF (x2)	Generated in our lab
NHA	Normal human astrocytes from cerebral cortex	NHA medium	ScienCell 1800
HMC3	Human embryo microglia	DMEM + 10 % FBS	ATCC® CRL-3304™
HEK293T	Embryonic kidney	DMEM + 10 % FBS	ATCC® CRL-1573™

5. Treatments

During this work, several compounds have been used, whose main characteristics are summarized in ***Table M3***. Bleomycin was dissolved in DPBS, whereas all other free compounds were dissolved in DMSO (D2650, Sigma-Aldrich).

The new molecule studied in this PhD thesis was designed to selectively inhibit HDAC6 activity, as previously described [299]. The name was changed to JOC1 for strategy purposes [300]. For the vehiculization of JOC1, which has been performed in Dr. Aitziber Cortajarena's laboratory at CIC biomaGUNE (San Sebastian, Spain), bovine serum albumin (BSA) based nanoparticles (NPs) have been used (BSANP@JOC1). Thus, BSANP@JOC1 were formulated following a coprecipitation method based on the FDA approved Paclitaxel formulation [301]. 40 mg/mL BSA (Sigma-Aldrich) was dissolved in phosphate buffer 50 mM NaCl, 10 mM Na_2HPO_4 pH 11.5 (PBS-11.5) and incubated under continuous stirring at 27 °C for 5 min. Then, reduced L-Glutathione (GSH, Thermo Fisher) was added in excess at 1:80

(BSA:GSH) molar ratio to reduce the intramolecular di-sulfide bonds. This solution was incubated under stirring during 3–5 h, and then dialyzed (3.5 kDa cutoff membrane) in PBS-11.5 overnight at room temperature in order to eliminate the GSH. The dialyzed solution was incubated under stirring at 27 °C during 5 min and JOC1 was added at 10 mg/mL. When JOC1 was properly dissolved, 96% ethanol (Scharlau) was added at 1:3 (v/v) and incubated for 10 min. Then, microparticles were eliminated by centrifugation (1.5×10^4 g, 5 min) and the non-encapsulated JOC1 and ethanol were eliminated by dialysis (6–8 kDa cutoff membrane) in phosphate buffer at pH 7.4 (50 mM NaCl, 10 mM Na_2HPO_4 pH 7.4). Samples were stable for at least 1 week at room temperature.

For the characterization of BSANP@JOC1, size distribution was measured by Dynamic Light Scattering (DLS) in NanoSizer (Malvern Nano-Zs, UK) with 173° scattering angle at 25 °C directly from the final formulation in PBS pH 7.4 and the data were analyzed in Zetasizer Software 7.11. The amount of JOC1 loaded was determined after BSANP@JOC1 digestion in acetonitrile (1:19) by liquid chromatography-mass spectrometry (LC-MS) using an Ultra Performance Liquid Chromatography (UPLC) linked to a LCT XE time-of-flight mass spectrometer at the Mass Spectroscopy Platform in CIC biomaGUNE.

Table M3. List of compounds used in this study and their main characteristics.

Name in this thesis	Complete name of the compound	Function	Tested conditions	Reference
JOC1	JOC1	HDAC6 inhibitor	*In vitro:* 0.01-100 µM, 48 h-72 h *In vivo:* 40-50 mg/kg, 5 days on, 2 days off. 16-30 days.	Previously described in [299]
BSANP@JOC1	BSANP@JOC1	BSA-bound HDAC6 inhibitor	*In vitro:* 0.01-6 µM, 48-72 h	CIC BiomaGUNE
SAHA	Suberoylanilide hydroxamic acid, Vorinostat	Pan-HDACi	*In vitro:* 0.01-100 µM, 48-72 h	Cayman, 10009929
Tubastatin A	Tubastatin A	HDAC6 inhibitor	*In vitro:* 0.01-18 µM, 48-72 h	Cayman, 15785
TMZ	Temozolomide	Alkylating agent	*In vitro:* 50-250 µM, 72 h	Sigma-Aldrich, T2577
BHA	Butylated hydroxyanisole	ROS scavenger	*In vitro:* 100 µM, 24 h	Sigma-Aldrich, B1253
Bleomycin	Bleomycin sulfate	Senescence inductor	*In vitro:* 50 µg/mL, 24 h	BioServ, BS-7621A
LPS	Lipopolysaccharide	Microglial activator	*In vitro:* 1 µg/mL, 12 h	Sigma-Aldrich, LPS25

6. Transfections and lenti-/retroviral infections

In order to modulate the expression of those genes studied in this thesis, lentiviral and retroviral infections have been performed. Main characteristics of the plasmids used are summarized in ***Table M4***. We took advantage of ampicillin resistance of the plasmids to amplify them by transforming DH5α™ competent *Escherichia coli* (18265017, Thermo Fisher). Plasmid extraction was then performed using NucleoBond Xtra Midi Plus kit (740412.50, Macherey-Nagel).

In particular, for the study of *MKP1* overexpression, we used empty *pLXSN* and *pLXSN-MKP1* plasmids, which have been kindly provided by Dr. Rosario Perona (***Table M4***).

Retroviruses were generated in the Viral Vector Unit of Inbiomed (San Sebastian, Spain). $3 \cdot 10^5$ U87 cells were retrovirally infected with a multiplicity of infection (MOI) of 10 for 6 h at 37°C and 5 % CO_2 in DMEM medium supplemented by 2 µg/mL polybrene (H9268, Sigma-Aldrich). At 48 h post-infection, 1.5 mg/mL geneticin (G-418, A1720, Sigma-Aldrich) was added for other 48 h in order to select infected cells.

For *LAMP2A* downregulation, short hairpin RNA (shRNA) technique was employed. In particular, lentiviral green fluorescent protein (GFP) containing empty vector *pGK* and *pGK-shL2A* plasmid have been used, kindly provided by Dr. Ana María Cuervo (***Table M4***). In this case, lentiviruses were generated by transfection of the HEK293T cell line with third generation lentiviral packaging plasmids. Herein, $3 \cdot 10^6$ HEK293T cells were seeded in 100 mm diameter culture plates (130182, Thermo Fisher). After 24 h, transfection mix was prepared with 0.6 mL DMEM medium, 8 µg *pGK* or *pGK-shL2A*, 5.2 µg *MDL*, 2.8 µg *VSV-g*, 2 µg *REV* and 30 µL transfection agent TurboFect (R0531, Thermo Fisher), and incubated at room temperature for 20 min. HEK293T medium was replaced by 6 mL fresh DMEM medium and transfection cocktail was added dropwise. HEK293T cells were transduced for 6 h at 37°C and 5% CO_2, and consecutively, medium was replaced by 4 mL DMEM + 10% FBS. After 48 h, lentiviral HEK293T supernatant was filtered with 0.45 µm filters (17598K, Sartorius), supplemented by 2 µg/mL polybrene and transferred to $4 \cdot 10^5$ cells of interest plated 24 h before in 100 mm diameter culture plates, for 6 h. This procedure was repeated with HEK293T lentiviral supernatant at 72 h post-transduction, as a reinfection step, in order to increment infection efficiency. When infecting GNS166 or GNS179, viral supernatants were previously incubated overnight at 4 °C with 1 mL lenti-X concentrator (631231, Clontech Takara) per 3 mL of viral supernatant. After this step, viral medium was centrifuged at 1,500 g for 40 min at 4 °C, so that generated virus formed a pellet and could be resuspended in the appropriate culture medium for the GNS. 5 days after re-infection, which comprises the estimated half-life of LAMP2A protein, transduction efficiency was certified by observing GFP signal under a Nikon Eclipse TS-100 microscope. In the case of rescue experiments, where LAMP2A was upregulated using *PAMC1* plasmid kindly provided by Dr. Ana María Cuervo (***Table M4***), viral supernatants were generated following the same protocol, and they were stored at -80 °C until LAMP2A downregulation was verified. Once this occurred, LAMP2A overexpression viral supernatants were thawed and 2 µg/mL polybrene was added. After

infection and re-infection steps, cells were incubated 48 h at 37 °C and 5 % CO_2 and experiments were performed.

For *HDAC1* and *HDAC2* overexpression in microglia, transient transfections were performed, using empty *pGal4*, *pGal4-HDAC1 OE* and *pGal4-HDAC2 OE* plasmids, kindly provided by Dr. Ian C. Wood (***Table M4***). Thus, $7 \cdot 10^5$ HMC3 cells were seeded in one 100 mm treated plate and after 24 h at 37 °C and 5 % CO_2, transfection protocol was performed. Herein, 10 µg plasmid and 1.5 mL DMEM without FBS were firstly incubated for 5 min at room temperature. Meanwhile, 25 µL lipofectamine™ 2000 (11668019, Invitrogen™) and 1.5 mL DMEM without FBS were incubated for 5 min at room temperature. After this time, both cocktails were mixed and incubated for 20 min at room temperature. Next, HMC3 cells were washed with DPBS and 5 mL DMEM without FBS were added. Finally, transfection cocktail was added dropwise to the cells, which were then incubated for 4 h at 37 °C. After this time, cell medium was replaced by 8 mL DMEM 10 % FBS and cells were incubated overnight at 37 °C and 5 % CO_2 till bleomycin and/or LPS treatments.

Table M4. Plasmids used in this thesis.

Name of the plasmid	Transgene	Selection (bacterial / mammalian)	Origin
pLXSN	Control, empty vector	Ampicillin / Geneticin (G-418)	Dr. Rosario Perona (CSIC/UAM, Spain) [302]
pLXSN-MKP1	Overexpression of MKP1	Ampicillin / Geneticin (G-418)	Dr. Rosario Perona (CSIC/UAM, Spain) [302]
pGK	Control, empty vector	Ampicillin / GFP	Dr. Ana María Cuervo (Albert Einstein College of Medicine, USA) [185]
pGK-shL2A	shRNA for LAMP2A	Ampicillin / GFP	Dr. Ana María Cuervo (Albert Einstein College of Medicine, USA) [185]
PAMC1	Overexpression of LAMP2A	Ampicillin	Dr. Ana María Cuervo (Albert Einstein College of Medicine, USA) [185]
pGal4	Control, empty vector	Ampicillin	Dr. Ian C Wood (University of Leeds, UK) [303]
pGal4-HDAC1 OE	Overexpression of HDAC1	Ampicillin	Dr. Ian C Wood (University of Leeds, UK) [303]
pGal4-HDAC2 OE	Overexpression of HDAC2	Ampicillin	Dr. Ian C Wood (University of Leeds, UK) [303]

7. Functional assays

7.1. Proliferation assay

To assess cell proliferation, cells were plated in duplicate in 6-well-treated plates (3506, Corning™) in appropriate culture medium (***Table M2***), in a density of $2.5 \cdot 10^4$ cells per well in 2 mL, and counted with Neubauer chamber at day 1, 3 and 5 after seeding. To test the

effect of a compound in cell proliferation, treatment was applied once cells got attached into the surface of the culture plate, which was considered as day 0. For cell dissociation 0.05 % trypsin-EDTA or accutase were used and data have been represented indicating the total number of cells per experimental condition in each time point.

7.2. Senescence assays

7.2.1. Replicative senescence measurement

Microglia were cultured in 6-well-treated plates in a density of $3 \cdot 10^4$ cells per well, appropriate culture medium (***Table M2***) with vehicle or 50 µg/mL bleomycin. This culture was maintained for 48 h and subsequently, cells were counted. Next, cells were seeded again in the same density, and the procedure was repeated for another 48 h. With these data, cumulation of population doubling level (ΔPDL) was calculated, which represents the number of times in which cells were doubled. For that, the following formula was used: PDL = Log_{10} (number of HMC3 at day 2/number of HMC3 at day 0)/Log_{10} (2).

7.2.2. Senescence-associated-β-Galactosidase assay

For the analysis of the activity of β-galactosidase in senescent cells, a commercial kit was used (9860S, Cell Signaling). This kit measures the activity of this enzyme at pH6, which is a distinctive characteristic of senescent cells. Thus, the substrate X-Gal is metabolized by senescent cells, generating a blue and insoluble product visible by optical microscope. For the performance of the assay, manufacturer's instructions were followed. Briefly, $2.5 \cdot 10^4$ HMC3 cells were seeded in 6-well-treated plates in 2 mL of appropriate culture medium (***Table M2***) with vehicle or 50 µg/mL Bleomycin. After 48 h of treatment, cells were washed with PBS and fixation and staining steps were performed. In particular, staining was done keeping cell plates overnight with the pH 6-adjusted-staining-reagent in a non-CO_2 incubator. Finally, blue cells were observed in an optical microscope, and quantification was done.

7.3. Oncospheres formation assay

For the performance of this assay, conventional cells were first washed with DPBS in order to eliminate all FBS from the previous culture medium, as it can induce the differentiation of GSCs. Next, cells were harvested with 0.05 % trypsin-EDTA, counted and centrifuged for pellet obtention. Then, cells were plated in non-treated 6-well plates in a

density of 7,000-10,000 cells per well resuspended in DMEM/F12 medium supplemented by 20 ng/mL hEGF and hFGF, in triplicate. Primary oncosphere culture was maintained for 10 days, adding 300 µL fresh stem cell medium three times a week. After this time, oncospheres were counted in an optical microscope.

In order to measure self-renewal properties, primary oncospheres were disaggregated by mechanical and chemical digestion during 2 min with 200 µL accutase per three wells at 37 °C. After that, accutase was removed by centrifugation and cells were seeded in non-treated 6-well plates at the same density as in the previous assay. This culture was also maintained for other 10 days, renewing culture medium as explained before, and afterwards, secondary oncospheres were counted following the same procedure.

To test the effect of a compound, treatment was applied directly in oncosphere assay culture medium at the day of experiment seeding.

7.4. Colony formation assay

For colony generation, $5 \cdot 10^2$ cells were seeded in 6-well-treated plates in appropriate culture medium (***Table M2***), in triplicate. Cells were maintained in culture for 9 days and during this time, fresh medium was added twice a week. At day 9, cells were fixed with 0.5 mL formaldehyde 37 % (104002, Merck Millipore) for 30 min under stirring at room temperature. After that, medium was removed, and cells were stained with 10 % Giemsa (1.09204.0500, Merck) diluted in DPBS for 30 min at room temperature in agitation. Excess of staining was washed with distilled water, colonies were dried and then, they were manually counted.

7.5. Cell viability and half maximal inhibitory concentration (IC_{50}) measurement

In order to measure the effect of compounds previously mentioned in ***Table M3*** on cell viability, colorimetric MTT assay was performed. This assay is based on the reduction of a yellow tetrazolium salt (3-(4,5-dimethylthiazol-2-yl)-2,5-diphenyltetrazolium bromide or MTT) to purple formazan crystals by metabolically active cells. Viable cells contain NAD(P)H-dependent oxidoreductase enzymes that reduce the MTT to formazan.

Thus, depending on the cell type, $1.5 \cdot 10^3$ or $8 \cdot 10^3$ cells per well were seeded in 96-well-treated plates (3585, Corning™), in appropriate culture medium (***Table M2***), in sextuplicate. After 24 h, treatments were applied (***Table M3***) at concentrations and timings indicated in each experiment. After this time, 30 µL of 1.9 mg/mL MTT reagent (M2128, Sigma-Aldrich) were added per well and incubated at 37 °C and 5 % CO_2 during 3.5 h. Consecutively, medium was removed and 150 µL DMSO were added per well in order to dissolve formed crystals. Absorbance at 570 nm was measured by Halo LED 96 microplate reader (Dynamica) and data were relativized against DMSO control condition.

To test the cytotoxic efficacy of a compound, the half maximal inhibitory concentration (IC_{50}) parameter was calculated, which is representative of the concentration needed for eliminating 50 % of total cells. For that, different concentrations of each compound were chosen and after 72 h, absorbance was measured and IC_{50} was calculated by Graphpad software.

7.6. Analysis of metabolic activity by Seahorse assay

For the study of both mitochondrial and glycolytic metabolism, XF96 Extracellular Flux Analyzer (Seahorse Bioscience) was used, which measures simultaneously the oxygen consumption rate (OCR) and extracellular acidification rate (ECAR) of living cells.

7.6.1. Mitochondrial function

For mitochondrial metabolism detection, XF Cell Mito Stress (103015, Seahorse Bioscience) kit was used, and manufacturer's instructions were followed. Thus, $1.5 \cdot 10^4$ cells were seeded in appropriate culture medium (***Table M2***) the day prior to the experiment, in a XF 96-well plate. This plate was pre-coated by 10 µg/mL laminin (L2020, Sigma-Aldrich) for 3 h in the case of GNS166 cells, and by 15 µg/mL poly-L-lysine (0413, ScienCell) for 1 h in the case of U251 cell line at 37 °C and 5 % CO_2. After 24 h, culture medium was replaced by Mito Stress medium pH 7.4 (***Table M5***), and basal levels of OCR and ECAR were measured. Next, in order to modulate the activity of several mitochondrial effectors, a set of compounds were injected into the wells in the following order: (1) Oligomycin, (2) Trifluoromethoxy carbonylcyanide phenylhydrazone (FCCP) and (3) a combination of Rotenone and Antimycin

A (*Table M6*). Three measurements of OCR and ECAR were performed after the injection of each compound, and mean values were analyzed.

Table M5. Composition of Mito Stress assay medium.

Compound	Concentration	Reference
DMEM	0.83 g in 100 mL	D5030, Sigma-Aldrich
Glucose	10 mM	G8769, Sigma-Aldrich
Pyruvate	1 mM	11360070, Gibco
L-Glutamine	2 mM	25030024, Gibco

After experiment completion, cell plates were stained with crystal violet, in order to normalize values to total cell number. For that, cells were washed twice with DPBS and stained with 0.5 % crystal violet (HT90132, Sigma-Aldrich)-4%formaldehyde (818708, Merck Millipore) for 20 min. To eliminate the remaining staining, cell plates were washed with water, and dried. Stained cells were then dissolved in 5 % glacial acetic acid (1.00063, Merck Millipore) and absorbance was measured at 570 nm in Halo LED 96 microplate reader (Dynamica).

Table M6. Main characteristics of compounds used in Mito Stress assay.

Compound	Target	Result	Concentration	Reference
Oligomycin	ATP synthase (complex V)	Decreases electron flow through the ETC, resulting in a reduction in mitochondrial respiration, and ATP production	1 µM	75351, Sigma-Aldrich
Carbonyl cyanide-4 (trifluoromethoxy) phenylhydrazone (FCCP)	Proton gradient and mitochondrial membrane potential	Electron flow through ETC is uninhibited and oxygen consumption by complex IV reaches the maximum	1 µM	C2920, Sigma-Aldrich
Rotenone	Complex I	This combination shuts down mitochondrial respiration and enables the calculation of respiration driven by processes outside the mitochondria	1 µM	R8875, Sigma-Aldrich
Antimycin A	Complex III		1 µM	A8674, Sigma-Aldrich

ETC: Electron Transport Chain.

Thus, several parameters associated with mitochondrial function were obtained:

- Basal respiration: Oxygen consumption used to meet cellular ATP demand resulting from mitochondrial proton leak, under baseline conditions.
- ATP production: The decrease in OCR upon injection of the oligomycin represents the portion of basal respiration that was being used to drive ATP production.
- Proton leak: Remaining basal respiration not linked to ATP production.
- Maximal respiration: The maximal OCR attained by adding FCCP. FCCP mimics a physiological "energy demand" by stimulating the respiratory chain to operate at maximum capacity, which causes rapid oxidation of substrates (sugars, fats, and amino acids) to meet this metabolic challenge.
- Spare respiratory capacity: Capability of the cell to respond to an energetic demand as well as how close the cell is to respire at its maximum level.

- Non-mitochondrial respiration: Oxygen consumption that persists due to cellular enzymes that continue consuming oxygen after the addition of Rotenone and Antimycin A.

7.6.2. Glycolysis activity

In this case, XF Glycolysis Stress kit (103020, Seahorse Bioscience) was used, following again manufacturer's guidelines. Thus, 1.5 $\cdot 10^4$ GNS166 cells were seeded in DMEM/F12 + EGF/FGF medium the day prior to the experiment, in a XF 96-well plate pre-coated by 10 µg/mL laminin (L2020, Sigma-Aldrich) for 3 h at 37 °C and 5 % CO_2. After 24 h, culture medium was replaced by Glyco Stress medium pH 7.4 (***Table M7***) and basal level of ECAR was measured. In this case, in order to analyze glycolytic activity, a set of compounds were injected (***Table M8***), in an ordered manner: (1) Glucose, (2) Oligomycin and (3) 2-deoxy-D-glucose. Three measurements of ECAR were performed after the injection of each compound, and mean values were analyzed. As in the case of Mito Stress assay, for data normalization against total cell number, crystal violet staining was performed and absorbance at 570 nm was measured in Halo LED 96 microplate reader (Dynamica).

Table M7. Composition of Glyco Stress assay medium.

Compound	Concentration	Reference
DMEM	0.83 g in 100 mL	D5030, Sigma-Aldrich
L-Glutamine	2 mM	25030024, Gibco

This assay gave us data about the following points:

- Glycolysis: It is defined as the process of converting glucose to pyruvate. It is measured as the ECAR rate reached by a given cell after the addition of saturating amounts of glucose.
- Glycolytic capacity: The maximum ECAR rate reached by a cell following the addition of oligomycin, shutting down oxidative phosphorylation and driving the cell to use glycolysis to its maximum capacity.

- Glycolytic reserve: This measure indicates the capability of a cell to respond to an energetic demand as well as how close the glycolytic function is to maximum level.

Table M8. Main characteristics of compounds used in Glyco Stress assay.

Compound	Target	Result	Concentration	Reference
Glucose	Glycolysis	Saturating conditions of glucose induce glycolytic pathway, producing ATP, NADH, water and protons, increasing rapidly ECAR	10 mM	G8769, Sigma-Aldrich
Oligomycin	ATP synthase (complex V)	Inhibition of mitochondrial ATP production and thus, shift of the energy production to glycolysis. ECAR associated with cellular maximum glycolytic capacity	1 µM	75351, Sigma-Aldrich
2-Deoxy-D-Glucose	Hexokinase	This glucose analog inhibits glycolysis, resulting in a decreased ECAR	50 mM	D6134, Sigma-Aldrich

7.7. Analysis of mitochondrial polarization and reactive oxygen species (ROS)

Mitochondrial depolarization and ROS production were studied by flow cytometry (SH800, Sony). For that, MitoTracker™ Red FM dye (M22425, Invitrogen™), which stains active and polarized mitochondria, and MitoSox™ Red dye (M36008, Invitrogen™), whose mitochondrial oxidation by superoxide produces red fluorescence, were employed. Both dyes were diluted in HBSS (14025050, Gibco) and studied separately to avoid spectral overlapping. Thus, infected GNS166 were collected with accutase, centrifuged and incubated with control HBSS, 5 µM MitoSox or 0.2 µM MitoTracker for 25 min at 37 °C at a density of $2 \cdot 10^5$ cells per condition. After this time, cells were centrifuged, resuspended in 200 µL HBSS and analyzed with Cell Sorter Software version 2.1 (Sony). First, the population was gated by backward scatter-area (BSC-A) *vs*. forward scatter-area (FSC-A), and doublets were excluded by forward scatter-height (FSC-H) *vs*. forward scatter- width (FSC-W). As both GNS166 *pGK* and *shL2A* conditions were GFP^+, manual compensation was applied, where, besides MitoSox

and MitoTracker unstained controls, wild type GNS166 cells were used as a negative control for GFP. Thus, gates were set for both dyes and analysis were performed reaching 10^4 final events per condition. Fluorescence intensity percentage was represented, which comprises the number of positive events multiplied by the mean fluorescence intensity of them. For ROS scavenging experiment, cells were incubated for 24 h with 100µM Butylated hydroxyanisole (***Table M3***) antioxidant agent and/or 10 µM Antimycin A (***Table M6***) as positive control of ROS induction.

7.8. Migration and invasion assays

7.8.1. Migration assay

In order to assess cell migration capacity, 6.5 mm Transwell® chambers with 8.0 µm pore polycarbonate membrane inserts (3422, Corning™) were used, pre-coated with 2 µg/mL laminin for 3 h at 37 °C and 5 % CO_2. Inserts were then placed in 24-well plates with 500 µL DMEM/F12 medium without EGF nor FGF per well and other 300 µL of the same medium were added inside each insert, so that they get humidified for 2 h at 37 °C and 5 % CO_2. After that, $2.5 \cdot 10^4$ GNS166 *pGK* or *shL2A* cells were seeded per insert, in 100 µL DMEM/F12 medium without EGF nor FGF. After 12 h, inserts were placed in new 24-well plates (P24, 3527, Corning™), which, in this case, contain 500 µL DMEM/F12 medium with 40 ng/µL EGF and 40 ng/µL FGF per well. These two growth factors were used as chemoattractant, so that cells would migrate through the polycarbonate membrane. Cells were incubated for 72 h at 37 °C and 5 % CO_2.

Cells that migrated through the inserts were next stained with 300 µL cell stain solution (90144, Millipore) in a 24-well-plate, for 20 min at room temperature under stirring. Inserts were then washed with distilled water and cotton swabs for elimination of remaining staining, and dried. Pictures were taken by Eclipse TS100 (Nikon) microscope and for quantification of migrated cells, 200 µL extraction buffer (90145, Millipore) was applied in a new 24-well-plate for 15 min at room temperature under stirring. Absorbance at 570 nm was measured in Halo LED 96 microplate reader (Dynamica).

7.8.2. Invasion assay

For the study of the invasion capacity, 8µm pore collagen cell invasion assay (ECM551, Merck Millipore) was performed, whose inserts were pre-coated with 2 µg/mL

laminin for 3 h at 37 °C and 5 % CO_2. Inserts were then placed in 24-well plates with 300 µL DMEM/F12 medium without EGF nor FGF per well and other 300 µL of the same medium were added inside each insert, so that they get humidified for 2 h at 37 °C and 5 % CO_2. Next, $2.5 \cdot 10^4$ GNS166 *pGK* or *shL2A* cells were seeded per insert, in 500 µL DMEM/F12 medium without EGF nor FGF. Next, inserts were placed in new 24-well-plates (3527, Corning™), which, in this case, contain 750 µL DMEM/F12 medium with 40 ng/µL EGF and 40 ng/µL FGF per well. As in the case of migration assay, these two growth factors were used as chemoattractant, so that cells would degrade collagen matrix, invading the insert. Cells were incubated for 72 h at 37 °C and 5 % CO_2.

For insert staining, the same procedure as for migration assay was performed.

8. Protein analysis

8.1. Protein extraction and quantification

For protein extraction, cells were collected in conical centrifuge tubes, centrifuged, and washed with DPBS. Resulting cell pellets were lysed in 100-120 µL lysis buffer (1% NP-40, 150 mM NaCl, 5 mM EDTA, 50 mM NaF, 30 mM $Na_4P_2O_7$, 1 mM Na_3VO_4, 50 mM Tris-HCl pH 7.4), supplemented by 100 µM protease inhibitor cocktail (P8340, Sigma-Aldrich), 100 µM phosphatase inhibitor mix (P5726, Sigma-Aldrich) and 100 µM serine protease inhibitor Phenylmethanesulfonyl fluoride (PMSF, P7626, Sigma-Aldrich), for 30 min on ice. After that, cell lysates were centrifuged at $1.2 \cdot 10^4$ g for 10 min at 4 °C in order to precipitate cell debris. Supernatants containing whole cell protein extracts were then collected and placed in new tubes.

For protein quantification, colorimetric bicinchoninic acid (BCA) assay (Pierce BCA Protein Assay 23227, Thermo Fisher) was used. This process combines the reduction of Cu^{++} to Cu^{+} by proteins in an alkaline medium with the highly sensitive colorimetric detection of the Cu^{+} by BCA. Thus, following manufacturer's instructions, 1 µL whole protein extract was incubated with BCA for 20 min at 37 °C and colorimetric intensity was measured at 560 nm in a Halo LED 96 microplate reader (Dynamica). In parallel, a calibration line was performed with five different concentrations of BSA provided by the kit in order to extrapolate protein concentration of the samples of interest. Protein samples were stored at -80 °C until use.

8.2. High-throughput proteomic study

High-throughput proteomic study was performed by the Proteomics Facility at CIC bioGUNE (Derio, Spain). Cellular pellets obtained as previously mentioned were sent to this department, and they followed the protocol detailed in the next lines.

Samples were incubated in 7 M urea, 2 M Thiourea, 4 % CHAPS detergent and 5 mM dithiothreitol (DTT) for 30 min at room temperature under agitation, and digested following the previously described filter-aided sample preparation (FASP) protocol [304] with minor modifications. Trypsin was added to a trypsin:protein ratio of 1:50, and this mixture was incubated overnight at 37 °C, dried out in a RVC2 25 speedvac concentrator (Christ), and resuspended in 0.1 % formic acid. Peptides were desalted and resuspended in 0.1 % FA using C18 stage tips (Millipore).

Samples were then analyzed in a novel hybrid trapped ion mobility spectrometry – quadrupole time of flight mass spectrometer (timsTOF Pro with PASEF, Bruker Daltonics) coupled online to a nanoElute liquid chromatograph (Bruker). A sample of 200 ng was directly loaded in a 15 cm Bruker nanoelute FIFTEEN C18 analytical column (Bruker) and resolved at 400 nL/min with a 100 min gradient. Column was heated to 50 °C using an oven.

Protein identification and quantification was carried out using MaxQuant software with default settings. Searches were carried out against a database consisting of human protein entries (Uniprot/Swissprot), with precursor and fragment tolerances of 20ppm and 0.05 Da. Only proteins identified with at least two peptides at false discovery rate (FDR)<1% were considered for further analysis. Data were loaded onto Perseus platform [305] and further processed (log_2 transformation, imputation). Significantly differentially expressed proteins ($p<0.05$) with a ratio>1.5 in either direction were analyzed using DAVID (https://david.ncifcrf.gov/) in order to characterize the biological pathways they are involved in. Processes enriched with a $p \leq 0.05$ were considered as significantly correlated to the set of differential proteins.

8.3. Western Blot

In western blot experiments 20 ng protein were usually used. Thus, the appropriate sample volume was collected, to which one fifth loading buffer 5X (312.5 mM Tris pH 6.8, 10 % sodium dodecyl sulfate (SDS), 50 % glycerol, 0.5 % bromophenol blue and 5

% β-mercaptoethanol) was added. For protein denaturation, samples were then heat-shocked by incubating them 5 min at 95 °C and immediately after placed on ice.

For protein separation by their molecular weight, sodium dodecyl sulphate-polyacrylamide gel electrophoresis (SDS-PAGE) technique was performed. Herein, 1.5 mm thick polyacrylamide gels were used, composed by stacking gel (4.5 % polyacrylamide) and separating gel (10-15 % polyacrylamide, depending on the molecular weight of the protein of interest). Electrophoresis was performed using electrophoresis buffer (Tris 20 mM, glycine 0.2 M, SDS 0.1 %, pH 8.3) and buckets (Mini-PROTEAN® Tetra Cell Precast, Bio-Rad). The power supply BioRad HC Power Pac was run first for 10 min at 90 V and then, for 60-90 min at 120 V and room temperature, depending on the molecular weight of the protein of interest.

After this process, proteins were transferred into a nitrocellulose membrane (Amersham Protran 0.2 µm NC; 10600001, GE Healthcare Life Science). This membrane is positively charged so that, in the presence of differential potential, proteins migrate from the gel into the membrane. For this, humidified transfer was performed in the first years of this PhD project, in transfer buffer (25 mM Tris, 192 mM glycine, 20 % methanol pH 6.8, 0.05 % SDS) for 90 min at 90 V and 4 °C. However, thanks to the acquisition of a semi-dry transfer apparatus (Trans-Blot Turbo Transfer System, Bio-Rad), protein transfers were then performed at 1.3 A, 25 V in 7 min. For that, pre-cast 0.2 µm nitrocellulose transfer packs were used (1704158, Bio-Rad). For verification of the efficiency of the protein transfer, Ponceau staining was used (P7170, Sigma-Aldrich).

In order to avoid unspecific bindings of primary antibodies, membranes were incubated with blocking solution (Tris Buffered Saline 0.1 M-0.01 % Tween 20 (TBS-T), 5 % powder milk) for 1 h in agitation at room temperature. Once membranes were blocked, they were incubated for 14-18 h at 4 °C with corresponding primary antibodies (***Table M9***) diluted in blocking solution and following manufacturer recommendations. After this incubation, membranes were washed with TBS-T for 5 min 3 times in agitation and horseradish peroxidase (HRP)-conjugated secondary antibodies (***Table M9***) were applied for 1 h in blocking solution at room temperature. Three washes with TBS-T were then performed.

Proteins were finally detected by chemiluminescence. In particular, NOVEL ECL Chemi Substrate (WP20005, Thermo Fisher) was used for highly expressed proteins, whereas SuperSignal West Femto Maximum Sensitive Substrate (34096, Thermo Fisher) was used for

detection of low expressed proteins. Signal was captured and recorded by iBrightFL1000 imaging system (Invitrogen).

Table M9. Primary and secondary antibodies used in Western Blot technique.

Type of antibody	Recognized antigen	Applied for	Working dilution	Produced in	Supplier	Reference
Primary antibody	HDAC1	Human	1/1000	Rabbit	Abcam	ab109411
	HDAC6		1/1000	Rabbit	Cell Signaling	7558S
	Acetyl-α-tubulin (Lys40)		1/1000	Mouse	Abcam	ab24610
	α-tubulin		1/1000	Rabbit	Abcam	ab52866
	Acetyl-histone H3 (Lys9)		1/1000	Rabbit	Cell Signaling	9649
	Histone H3		1/1000	Rabbit	Novus	NB500-171
	PARP		1/500	Rabbit	Abcam	ab32064
	BMI1		1/500	Mouse	Millipore	05-637
	SOX2		1/250	Rabbit	Millipore	AB5603
	SOX9		1/1000	Rabbit	Millipore	AB5535
	LAMP2A		1/500	Rabbit	Abcam	ab18528
	p-STAT1		1/1000	Rabbit	Cell Signaling	9167S
	STAT1		1/1000	Rabbit	Cell Signaling	14994S
	p-STAT3		1/1000	Rabbit	Cell Signaling	9145S
	STAT3		1/1000	Mouse	Cell Signaling	9139
	MX1		1/500	Rabbit	Abcam	ab95926
	TIM23		1/1000	Rabbit	Proteintech	11123-1-AP
	MRP-S23		1/500	Rabbit	Sigma-Aldrich	SAB2701383
	ITGA6		1/250	Rabbit	Cell Signaling	3750S
	ITGB4		1/500	Rabbit	Sigma-Aldrich	HPA036348
	p-AKT		1/1000	Rabbit	Cell Signaling	9271S
	AKT1/2/3		1/200	Rabbit	Santa Cruz Biotechnology, inc.	sc-8312
	β-actin		1/100,000	Mouse	Sigma-Aldrich	A5441
Secondary antibody	Goat anti-rabbit		1/2000	Goat	Cell Signaling	7074S
	Horse anti-mouse		1/2000	Horse	Cell Signaling	7076S

8.4. Cell immunofluorescence

1-2 ·10^4 cells were seeded in 8-well immunofluorescence chambers (154534, LabTek Thermo), and after cell adhesion or treatment completion, cells were fixed with 4% paraformaldehyde (PFA, 158127, Sigma-Aldrich) for 10 min at room temperature. Cells were then washed 3 times with 1X PBS (44592, BioSystems) and blocked and permeabilized with 1X PBS-0.3 % Triton X-100 (T8787, Sigma-Aldrich) supplemented by 5 % FBS for 1 h at room temperature. Later on, they were incubated with primary antibodies (***Table M10***) diluted in 1X PBS 0.3 % Triton X-100 overnight at 4 °C. Afterwards, 3 washes with 1X PBS were done and cells were incubated with fluorophore-conjugated secondary antibodies (***Table M10***) diluted in 1X PBS 0.3 % Triton X-100 for 1 h in darkness at room temperature. After other three washes as previously described, chromatin was stained with 1 µg/mL Hoechst (33342, Sigma-Aldrich) for 1-2 min. Next, two washes with 1X PBS and a final wash with distilled water were performed. Finally, slides were mounted with mounting medium Fluoro-Gel (17985, Aname). Immunofluorescence was evaluated with Eclipse 80i microscope and processed with NIS Element Advances Research (Nikon) software. In the case of experiments with compounds, cells were seeded and after adhesion, treatments were applied for other 48 h.

Table M9. Primary and secondary antibodies used in cell immunofluorescence.

Type of antibody	Recognized antigen	Working dilution	Produced in	Supplier	Reference
Primary antibody	p-histone H3	1/2000	Mouse	Abcam	ab14955
	Cleaved-caspase 3	1/500	Rabbit	R&D Systems	AF835
Secondary antibody	Alexa Fluor® 555 Goat anti-mouse IgG (H+L)	1/500	Goat	Invitrogen	A21422
	Alexa Fluor® 555 Donkey anti-rabbit IgG (H+L)	1/500	Donkey	Invitrogen	A31572

8.5. Cytokine array

Cytokine expression from supernatants of GNS166 cells was determined by C-Series Human Cytokine Array 5 (AAH-CYT-5, RayBiotech), following manufacturer instructions. Cell culture medium did not contain FBS, so no interferences occurred in the development of this assay. Thus, supernatants were collected and immediately frozen at -80 °C until the day of the experiment.

Prior starting the assay, supernatant samples were thawed and centrifuged at 10,000 rpm for 5 min to eliminate possible cell debris or particulates that could interfere the detection of the cytokines. After blocking membranes with blocking buffer provided in the kit for 30 min at room temperature, 1 mL undiluted sample was pipetted into each membrane and incubated overnight at 4 °C. Membranes were then washed and incubated with a biotinylated antibody cocktail overnight at 4 °C. After this incubation, membranes were again washed and incubated with 1X HRP-Streptavidin overnight at 4 °C. Finally, a last wash was performed and chemiluminescent signal was detected by iBright FL1000 imaging system (Invitrogen). All incubation and wash steps were performed under gentle rotation in the incubation tray provided by the manufacturer. Spot signal density values were extracted by ImageJ as previously described in the literature [306] and then, background subtraction and positive control normalization were performed by the analysis tool for AAH-CYT-5 (S02-AAH-CYT-5, RayBiotech).

8.6. CMA activity measurement assay

For direct measurement of CMA activity, GB cells were transduced with lentivirus carrying the KFERQ-PS-Dendra reporter [307]. This reporter acts as a CMA substrate, as it contains the KFERQ-like sequence needed for the recognition by the HSC70 chaperone and posterior degradation by CMA process. Thus, activation of CMA increases the association of the reporter with lysosomes, which can be visualized as a change in the intracellular fluorescence.

Once cells were transduced, they were photoactivated by exposure to a 3.5 mA (current constant) light emitting diode (LED: Norlux, 405nm) for 3 min and then plated in glass-bottom 96-well plates. At the desired times, cells were fixed with 4 % PFA and imaged using high-content microscopy (Operetta system, Perkin Elmer). Images were quantified

using the manufacturer's software in a minimum of 1,500 cells per well. In all cases, focal plane thickness was set at 0.17 µm and sections with maximal nucleus diameter were selected for quantification. Values are presented as number of puncta per cell section that in our acquisition conditions represents 10-20 % of the total puncta per cell.

9. Gene expression

9.1. Ribonucleic acid extraction and quantification

Total RNA was extracted from cell lysates and fresh brain tissues. In the case of tissues, samples were firstly homogenized by a tissue-lyser (Qiagen Retsch MM300) with 1 mL TRI Reagent Solution (AM9738, Life Technologies). In the case of cellular pellets, 1 mL TRI Reagent Solution was added as a first step. Once cell lysis was performed, the same protocol was applied for both cases. First, 200 µM chloroform (C2432, Sigma-Aldrich) were added, and after gently mixing the samples, they were incubated 10 min at room temperature. Samples were then centrifuged at 12,000 rpm for 10 min at 4 °C, so that three phases were separated. Thus, aqueous phase was collected in a new tube and 500 µL 2-propanol (I9516, Sigma-Aldrich) and 1 µL 5 µg/µL glycogen (AM9510, Ambion) were added. Samples were gently mixed, incubated for 10 min at room temperature and centrifuged at 12,000 rpm for 22 min at 4 °C for RNA precipitation. Supernatants were discarded and two washes with 75 % ethanol (Scharlau) were done to increase purity of the sample. Finally, RNA pellet was dried at room temperature and resuspended in H_2O DNase/RNase free (10977035, Invitrogen). All procedures with RNA were performed in tubes treated for 24 h with diethyl pyrocarbonate (DEPC, 159220, Sigma-Aldrich) for inhibiting RNases.

RNA concentration and purity were determined by measuring absorbance at 260 nm and 280 nm in Nanodrop-100 spectrophotometer (Thermo Fisher). RNA samples were stored at -80 °C until use.

9.2. RNAseq study

RNAseq was performed by CD Genomics company (Shirley, New York). Integrity and quality of RNA samples was tested using Agilent RNA 6000 Nano kit, obtaining integrity values higher than 8. After this check point, RNA samples were sent to the company and the

following protocol was performed. After performing quality control of the samples by Agilent 2100 Bioanalyzer, 200 ng of high-quality total RNA was proceeded to library construction. Magnetic beads with Oligo (dT) were used to isolate messenger RNA (mRNA). The mRNA was then fragmented randomly by adding fragmentation buffer, and cDNA was synthesized by using mRNA template, random hexamers primer, dNTPs, RNase H and DNA polymerase I by ABI StepOnePlus Real-Time polymerase chain reaction (PCR) System. Short fragments were next purified and resolved with EB elution buffer for end repair and single nucleotide adenine addition. After that, the short fragments were connected to sequencing adapters. The double-stranded cDNA library was completed through size selection and PCR enrichment. Qualified RNA-seq libraries were sequenced using Illumina NovaSeq6000 after pooling according to its effective concentration and expected data volume. The sequencing was paired end 150 bp.

Regarding data analysis, FastQC tool was used to perform basic statistics on the quality of raw reads. Then, sequencing adapters and low-quality data of sequencing data were removed by Trim Galore. For alignment, HISAT2 software was used, having human GRCh38 as the reference genome. HTseq software and DESeq were used to quantify transcripts and differential gene expression levels using mapped reads' positional information on the gene. During the process, fold change ≥ 2 and FDR <0.01 were set as screening criteria. KEGG pathway analysis results have been represented.

9.3. Microarray expression study

Whole-transcriptome analysis was performed from 300 ng of RNA using Clariom^{TM} S Assay (902927, Applied Biosystems), which covers > $2 \cdot 10^4$ well-annotated genes, by the Genomics Facility at Biodonostia Health Research Institute. Raw data were first checked for quality purposes through TAC software v4.0. Then, data were normalized using the Robust Multi-array Average and analyzed by Limma tool. Probesets with FDR corrected p-values smaller than 0.05 were selected. Functional enrichment on Gene Ontology (GO) biological processes was performed on a smaller subset of the differentially expressed genes (corrected p-value < 0.001) by means of Broad Institute GSEA. Terms with an FDR-corrected p-value smaller than 0.05 were treated as significantly enriched. The data that support this study have been deposited in NCBI´s Gene Expression Omnibus and are accessible through GEO series accession number GSE143887.

9.4. Reverse transcription

For the obtention of complementary desoxyribonucleic acid (cDNA) from RNA samples, reverse transcription (RT) was performed by Maxima First Strand cDNA Synthesis Kit (K1671, Thermo Fisher), which comprises a first step for double strand DNA degradation by DNase to avoid contamination. The employed protocol was based on manufacturer's instructions, and BioRad C1000 thermocycler was used to perform the next incubation steps: 10 min at 25 °C, 30 min at 50 °C and 5 min at 85 °C. Immediately after, samples were placed on ice and diluted to final concentration of 2-4 ng/µL in DNase/RNase free H_2O. cDNA samples were stored at -20 °C until use.

9.5. Quantitative Real-Time PCR

In order to measure the expression level of those genes of interest, quantitative real-time PCR (qRT-PCR) was used. Herein, an initial amount of 10-20 ng cDNA as reaction template, 10 mM of each gene-specific forward and reverse primer (***Table M10***) and 6 µL Power SYBR® Green Master Mix (4368706, Applied Biosystem) were included per reaction. Primer sequences were obtained from PrimerBank database (https://pga.mgh.harvard.edu/primerbank/) and from previously published research articles. In both cases, primer specificity was verified first by Primer-BLAST tool (https://www.ncbi.nlm.nih.gov/tools/primer-blast/) and by melting curve analysis in each qRT-PCR experiment.

Reactions were performed in triplicate in CFX384 Touch Real-Time PCR Detection System (BioRad), following the next incubation cycles: 1 cycle of 2 min at 50 °C, 1 cycle of 10 min at 95 °C, 41 cycles of 15 seconds at 95 °C and 1 min at 60 °C, and a last cycle of 10 seconds at 95 °C followed by 1 min at 60 °C and 1 second at 97 °C. As internal control to correct possible variations in cDNA levels, glyceraldehyde 3-phosphate dehydrogenase (GAPDH) and 18S ribosomal RNA (18S rRNA) housekeeping genes were used in the case of human samples, whereas β-actin was used in mice samples. As GAPDH is a well-defined substrate of CMA process, 18s rRNA was used in *LAMP2A* knock down experiments.

Relative quantification was calculated using the $2^{-\Delta\Delta Ct}$ formula, which is based on the normalization of the expression of the gene of interest with respect to the expression of

the housekeeping gene and the sample of reference. Results were represented as fold change.

Table M10. Primer sequences used in qRT-PCR reactions.

Species	Gene	Forward primer sequence (5' → 3')	Reverse primer sequence (5' → 3')
Human	*HDAC1*	CGC CCT CAC AAA GCC AAT G	CTG CTT GCT GTA CTC CGA CA
	HDAC2	ATG GCG TAC AGT CAA GGA GG	GCG GAT TCT ATG AGG CTT C
	HDAC3	CAC CCT ATG AAG CCC CAT CG	GAG ACC GTA ATG CAG GAC CAG
	HDAC6	AAG AAG ACC TAA TCG TGG GAC T	GCT GTG AAC CAA CAT CAG CTC
	HDAC7	GCA CCC AGC AAA CCT TCT AC	AGC CCC TAC CTC ATC CAC AG
	SIRT1	TCG CAA CTA TAC CCA GAA CAT AGA CA	CTG TTG CAA AGG AAC CAT GAC A
	SIRT3	CAA GGA GCT GTA CCC TGG AAA	CGA CAC TCT CTC AAG CCC ATC
	CD68	CTT CTC TCA TTC CCC TAT GGA CA	GAA GGA CAC ATT GTA CTC CAC C
	ITGAM	ACT GGT GAA GCC AAT AAC GCA	TCC GTG ATG ACA ACT AGG ATC TT
	AIF1	AGA CGT TCA GCT ACC CTG ACT T	GGC CTG TTG GCT TTT CCT TTT CTC
	BAX	CAT GTT TTC TGA CGG CAA CTT	CCA GAT CAC GCC ATT TCA C
	MKP1	CCT GTC CAC TCC ACG AAC AGT	GCT GGG AGA GGT CGT AAT GG
	TUJ1	GCG AGA TGT ACG AAG ACG AC	TTT AGA CAC TGC TGG CTT CG
	SOX2	TAC AGC ATG TCC TAC TCG CAG	GAG GAA GAG GTA ACC ACA GGG
	SOX9	AGC GAA CGC ACA TCA AGA C	CTG TAG GCG ATC TGT TGG GG
	NESTIN	AGA CTT CCC TCA GTT TAG G	CAG GTG TCT CAA GGG TAG CAG
	$p21^{Cip1}$	GAC ACC ACT GGA GGG TGA CT	CAG GTC CAC ATG GTC TTC CT
	$p16^{INK4a}$	GGG GGC ACC AGA GGC AGT	GGT TGT GGC GGG GGC AGT T
	CHK1	ATG GCA GGG GTG GTT TAT CT	ACT GTT GCC AAG CCA AAG TC
	LAMP2A	TGA CGA CAA CTT CCT TGT GC	AGC ATG ATG GTG CTT CAG AC
	IGFBP2	CAC CGG CAG ATG GGC AA	GAA GGC GCA TGG TGG AGA T
	IGFBP4	GAG CTG GGT GAC ACT GCT TG	CCC ACG AGG ACC TCT ACA TCA
	ANG	CTG GGC GTT TTG TTG TTG GTC	GGT TTG GCA TCA TAG TGC TGG
	Eotaxin-3	CTT CCA ATA CAG CCA CAA GCC	GAT GGG TAC AGA CTT TCT TGC
	SDF1	ATT CTC AAC ACT CCA AAC TGT GC	ACT TTA GCT TCG GGT CAA TGC
	IP10	GTG GCA TTC AAG GAG TAC CTC	TGA TGG CCT TCG ATT CTG GAT T
	VEGF	ACA TCT TCC AGG AGT ACC C	CTT GGT GAG GTT TGA TCC G
	IL6	CCA GGA GCC CAG CTA TGA AC	CCC AGG GAG AAG GCA ACT G
	IGFBP1	TTT TAC CTG CCA AAC TGC AAC A	CCC ATT CCA AGG GTA GAC GC
	IL1α	AGT AGC AAC CAA CGG GAA GG	TGG TTG GTC TTC ATC TTG GG
	ITGA3	TGT GGC TTG GAG TGA CTG TG	TCA TTG CCT CGC ACG TAG C
	ITGA6	GGC GGT GTTATGTCCTGAGTC	AATCGCCCATCACAAAAGCTC

	ITGAV	GCT GTC GGA GAT TTC AAT GGT	TCT GCT CGC CAG TAA AAT TGT
	ITGB3	CAT GAA GGA TGA TCT GTG GAG C	AAT CCG CAG GTT ACT GGT GAG
	ITGB4	CTC CAC CGA GTC AGC CTT C	CGG GTA GTC CTG TGT CCT GTA
	LAMC1	ACT GCC ACT GAC ATC AGA GTA	GCT TGC GTG TCC ATT ACA TTT AC
	COL4A5	TGG ACA GGA TGG ATT GCC AG	GGG GAC CTC TTT CAC CCT TAA AA
	FN1	GAG AAT AAG CTG TAC CAT CGC AA	CGA CCA CAT AGG AAG TCC CAG
	PIK3CA	AGT AGG CAA CCG TGA AGA AAA G	GAG GTG AAT TGA GGT CCC TAA GA
	mTOR	TCC GAG AGA TGA GTC AAG AGG	CAC CTT CCA CTC CTA TGA GGC
	PDGFRA	TGG CAG TAC CCC ATG TCT GAA	CCA AGA CCG TCA CAA AAA GGC
	PTEN	TGA GTT CCC TCA GCC GTT ACC T	GAG GTT TCC TCT GGT CCT GGT A
	CYCLIN A	AGA GCG TGA AGA TGC CCT	GTG ATG TCT GGC TGT TTC T
	GAPDH	ATG GGG AAG GTG AAG GTC GG	GAC GGT GCC ATG GAA TTT GC
	18S rRNA	CGC GGT TCT ATT TTG TTG GT	CGG TCC AAG AAT TTC ACC TC
Mouse	*Hdac1*	AGT CTG TTA CTA CTA CGA CGG G	TGA GCA GCA AAT TGT GAG TCA T
	Hdac2	ATG GCG TAC AGT CAA GGA GG	GCG GAT TCT ATG AGG CTT C
	Hdac3	TCAT CGC CTG GCA TTG ACT C	CTC AGA ATG GAA GCG GCA CA
	Hdac6	GGA GAC AAC CCA GTA CAT GAA TGA A	CGG AGG ACA GAG CCT GTA G
	Hdac7	TGG TGT CTG CTG GGT TTG ATG	ACC CAA AAC ATT TGG CAG AAA CAT
	Sirt1	ATG ACG CTG TGG CAG ATT GTT	CCG CAA GGC GAG CAT AGA T
	Sirt3	CCC AAT GTC ACT CAC TAC TT	GGG ATC CCA GAT GCT CTC T
	Aif1	ATC AAC AAG CAA TTC CTC GAT GA	CAG CAT TCG CTT CAA GGA CAT A
	p16^{ink4a}	CCC AAC GCC CCG AAC T	GCA GAA GAG CTG CTA CGT GAA
	p21^{Cip1}	GTG GGT CTG ACT CCA GCC C	CCT TCT CGT GAG ACG CTT AC
	β-actin	GGC ACC ACA CCT TCT ACA ATG	GTG GTG GTG AAG CTG TAG CC

10. *In vivo* assays

10.1. Carcinogenesis assays

10.1.1. Subcutaneous assay

Subcutaneous tumor formation assays were performed in 4-8 weeks old immunocompromised Foxn1^{nu}/Foxn1^{nu} mice (***Table M1***). These mice present an autosomal recessive mutation in the *Foxn1* gene, impairing the development of the thymus and hair. Thus, they are hairless and mature T-cell deficient, not presenting graft versus host response.

Injection of U87 cells was performed subcutaneously in the four flanks. For this, cells were harvested with 0.05 % trypsin-EDTA, counted, washed with DPBS, and resuspended in DPBS at the concentration of interest. 100 µL of cell preparation was inoculated in each flank. From this point, two types of experiments were performed in this thesis. For tumor initiation assay, $3.5 \cdot 10^5$ cells per flank were injected, and then, mice were treated intraperitoneally with vehicle or 40 mg/kg JOC1 since the following day of cell inoculation on a schedule of 5 days on / 2 days off for 30 days. Conversely, for tumor growth assay, $5 \cdot 10^5$ cells per flank were injected, and mice were started being treated only when tumor volume reached 50 mm^3. In that moment, mice were sorted into two different groups of treatment with vehicle and 50 mg/kg JOC1 on a schedule of 5 days on / 2 days off for 16 days. In both assays, mice weight was measured daily, and external calipers were used to measure tumor size twice a week. From these measurements, tumor volume was estimated by $V = L \cdot W^2 \cdot 0.5$; where L is tumor length and W is the tumor width. JOC1 was dissolved in 10 % DMSO: 35 % PEG400: 55 % sterile water, while vehicle condition comprised the same formulation in the absence of JOC1.

10.1.2. Orthotopic intracranial injection assay

The induction of brain tumors *in vivo* was performed in 4-8 weeks old NOD.SCID mice (***Table M1***). The homozygous mice for the severe combined immune deficiency spontaneous mutation (*Prkdc*^{scid}) are characterized by the absence of functional T and B cells. Thus, this model accepts allogeneic and xenogeneic grafts.

Prior injection, GNS166 *pGK* and *shL2A* cells were harvested with accutase, counted, washed with DPBS and resuspended in DPBS. Final samples were prepared so that $2 \cdot 10^5$ cells of interest in 5 µl were injected per mice.

For cell injection, instead of performing a classical individual stereotaxic surgery, a novel technique was used. Herein, up to 10 mice could be intracranially injected simultaneously [308, 309]. Briefly, after applying analgesia and anesthesia to the mice as previously mentioned in section 2, a small incision in the skin of the head was made, so that coronal and sagittal sutures of the skull got exposed. Then, a 1 x 1 mm deep hole was done by a manual drill (DH-1, Plastics One; drill-bit: D60, Plastics One) at 2.5mm lateral and 1mm anterior to bregma, directly above the caudate nucleus. Here, a bolt (C212SG, Plastics One) was inserted by a screwdriver (1253, Quick-Wedge) until flush with the skull (***Figure M1***). Next, Hamilton syringes (1701 N, Hamilton) were loaded with the cells of interest and

positioned inside the bolts and sustained by an infusion pump (PHD ULTRA™ Harvard Apparatus). When surgical process of a total of 8-10 mice was finalized, cell infusion was performed, by an infusion rate of 0.5µl / min (***Figure M1***). Finally, skin glue (1050044, Braun Surgical) was used to close the wounds. All the procedure was performed ensuring the correct temperature of the mice, using a circulating water blanket warmed at 37 °C (TP-700, Stryker Gaymar).

Figure M1. Representative images of surgical procedure for the insertion of the bolt above the caudate nucleus (left, modified from Lal S et al, 2000) and the posterior intracranial injection of cells simultaneously to 8 mice (right, prepared by the PhD candidate).

Mice weight and welfare was monitored during the experiment. In the presence of any sign associated with the formation of a brain tumor, such as, cognitive or motor failure or weight loss, mice were culled. Brains of mice were extracted and fixed in 3.7 % formaldehyde (104002, Merck Millipore) for 48 h for posterior studies. Survival distributions were determined using the log-rank test and GraphPad Prism 8 software.

11. Tissue analysis

In order to characterize the expression of proteins of interest in human biopsies and mice xenografts immunohistochemistry was performed.

11.1. GB patient biopsies

Expression of LAMP2A was studied in 98 human GB biopsies prepared as TMAs. TMA blocks were kindly generated and processed by the Pathological Anatomy Department from Donostia University Hospital following a standard protocol and staining for LAMP2A protein was performed (***Table M11***). Quantification of the staining was measured and categorized based on LAMP2A positive signal percentage. Thus, samples were classified in three groups: '-' (≤ 20 %), '+' (20-40 %) and '++' (≥40 %).

11.2. Subcutaneous mice xenografts

Once subcutaneous tumors generated in mice reach the above-mentioned endpoint, tumors were extracted and fixed with 3.7 % formaldehyde for 48 h at room temperature. Next, they were moved to DPBS solution at 4 °C no more than a week, until they were embedded in paraffin. Posterior tumor processing and immunohistochemistry was performed by the Histology Platform from Biodonostia Health Research Institute, following standard protocols. Herein, 4 µm sections done using a microtome (HM355S, Thermo Scientific) were then deparaffined and rehydrated with increasing concentrations of alcohol. Heat-induced antigen retrieval was performed, and subsequently, blocking solution (PBS-0,3 %-Triton X-100-5 % FBS) was applied to the sections. Next, sections were incubated overnight with primary antibodies of interest (***Table M11***) at 4 °C. After this time, sections were washed and secondary antibody was applied (***Table M11***), incubating it for 1 h at room temperature. Finally, 10 min incubation with 3,3'-Diaminobenzidine (DAB, ab64238, Abcam) was performed at room temperature, so that DAB got oxidized and could be visualized by its brown color. Staining was captured by Eclipse 80i microscope and processed by the NIS Elements Advances Research software (Nikon).

Table M11. Primary and secondary antibodies used in tissue immunohistochemistry.

Type of antibody	Recognized antigen	Produced in	Supplier	Reference
Primary antibody	Ki-67	Rabbit	Abcam	ab15580
	Acetyl-α-tubulin (Lys40)	Mouse	Abcam	ab24610
	LAMP2A	Rabbit	Abcam	ab18528
Secondary antibody	Anti-Rabbit IgG H&L (HRP)	Goat	Abcam	ab6721
	MACH 3 Rabbit HRP-Polymer	Rabbit	BioCare Medical	M3R531
	MACH 3 Mouse HRP-Polymer Detection	Mouse	BioCare Medical	M3M530H

12. Statistical analysis

Data presented in this doctoral thesis show mean values ± standard error of the mean (SEM), indicating in each graph symbols representing each individual experiment and the number of independent experiments (n) in the figure legend. Mean values were compared by t test statistical parameter, where $p \leq 0.1$, $p \leq 0.05$, $p \leq 0.01$ and $p \leq 0.001$ are represented as #, *, ** and ***, respectively. In the case of data from GlioVis, pairwise comparisons with corrections for multiple testing (p-values with Bonferroni correction) have been performed.

For correlation analysis, after performing normality test, Spearman coefficient was indicated in non-normal distributions, whereas Pearson coefficient was used for normal distributions.

In the case of orthotopic intracranial injection assay and data from TCGA, Rembrandt, Phillips and Joo cohorts, survival curves were compared by using log-rank (Mantel-Cox) test. In these last cohorts, cutoffs for Kaplan Meier curves have been designated as optimal by GlioVis database.

All data were represented by GraphPad software 8.

Results

1. CMA maintains GSC activity controlling different proteomic and transcriptomic pathways

1.1. *LAMP2A* is overexpressed in human GSCs and GB

In order to get the first insights regarding the impact of CMA on GSCs, we started characterizing the expression of the key protein in this process LAMP2A in a set of conventional GB cell lines and patient-derived GSCs. Herein, all studied GB cells presented detectable expression of LAMP2A, which varied between cell lines (***Figure R1A***). Interestingly, patient-derived GSCs were the ones with highest levels of LAMP2A. Indeed, LAMP2A expression positively correlates with the stem cell marker SOX2 and shows a tendency for the same effect with SOX9 (***Figure R1A, B***). As conventional GB cell lines are representative of the tumor bulk, we next moved to test whether the expression of LAMP2A could be enriched in the GSC pool of these GB cells. For that, we cultured conventional cell lines in GSC medium, and performed oncosphere assays. After 20 days in culture, with a dissection step at day 10, we observed that generated oncospheres (2^{ry} CSCs) presented higher expression of LAMP2A in all the cases (***Figure R1C***). Indeed, this *in vitro* result was also validated *in vivo*, as the subcutaneous xenograft of 2^{ry} CSCs originated from U87 and U373 cells presented higher levels of LAMP2A compared to subcutaneous tumors originated from parental cells (***Figure R1D***).

With the aim of analyzing the translation of *LAMP2* association with GSCs into clinical data, we checked *LAMP2* gene expression, as well as several stem cell markers, in GB samples from TCGA cohort. It is noteworthy to say that the following clinical data refer to *LAMP2* gene expression, as there is not any specific information regarding each isoform in TCGA and Rembrandt cohorts. First, we confirmed that *LAMP2* positively correlated with the GSCs markers *SOX2*, *SOX9*, *BMI1* and *POU5F1* (***Figure R1E***). Moreover, single cell RNAseq data from GB patients available in USCS Browser revealed immature astrocytes, glycolytic progenitors and radial glia cells as the cell types with most prominent expression of *LAMP2* within GB tumor bulk (***Figure R1F***). All these data reveal *LAMP2* enrichment in GSCs.

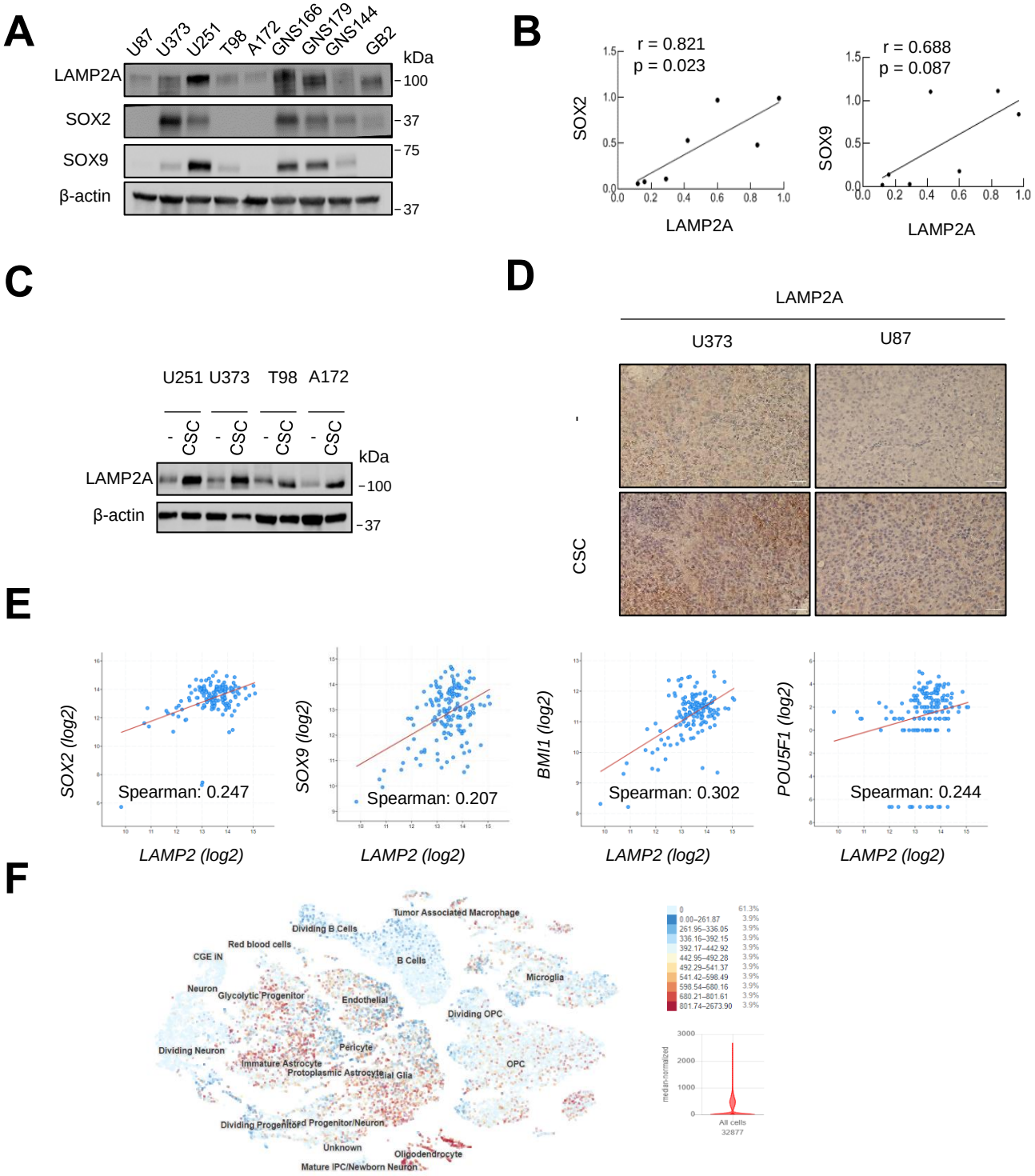

Figure R1. LAMP2A is overexpressed in GSCs. (A) Representative immunoblots of LAMP2A, SOX2, SOX9 and β-actin in conventional GB (U87, U373, U251, T98, A172) and patient-derived GSC (GNS166, GNS179, GNS144, GB2) lines (n=3); **(B)** Correlation analysis of LAMP2A with SOX2 (left) and SOX9 (right), based on intensities on **A**; **(C)** Immunoblot of LAMP2A in parental and 2^{ry} CSCs of GB cell lines (n=3); **(D)** Representative images of immunohistochemical staining of LAMP2A in subcutaneous tumors from parental U373 (left) and U87 (right), and their respective 2^{ry} CSCs (n=2), scale bar= 100 µm; **(E)** Association study of *LAMP2* with stem cell markers *SOX2* (p=2.197e-03), *SOX9* (p=0.0103), *BMI1* (p=5.707e-05) and *POU5F1* (p=2.456e-03) in TCGA cohort (cBioPortal for cancer genomics, https://www.cbioportal.org/); **(F)** Single cell RNAseq results for the expression of *LAMP2* among different cell types in GB samples (https://cells.ucsc.edu/?ds=gbm).

Next, we wondered whether LAMP2A expression could be also associated with malignant properties and therapy resistance in the clinic. In order to test this idea, we firstly studied *LAMP2* gene expression in both TCGA and Rembrandt cohorts. Herein, we determined that *LAMP2* expression was higher in GB samples compared to healthy control tissue in both cohorts (***Figure R2A***). Next, we explored the expression according to glioma grades, observing that grade IV glioma (GB) displayed higher expression of *LAMP2* than grade III in both cohorts, and grade II in TCGA cohort (***Figure R2B***). In order to see if any molecular subtype within GB present any difference in *LAMP2* expression, we analyzed data from classical, mesenchymal and proneural subtypes, where we saw that patients with mesenchymal subtype GB presented the highest expression of *LAMP2* (***Figure R2C***). Regarding therapy resistance, we took advantage of a cohort of GB patients, which comprised TMZ non-responder and responder individuals. Herein, non-responder patients presented higher levels of *LAMP2* compared to responder ones (***Figure R2D***), with a significant area under the curve (AUC) in ROC analysis (***Figure R2E***). All these data confirm that *LAMP2* gene expression is elevated in GB and correlates with malignant features of GB.

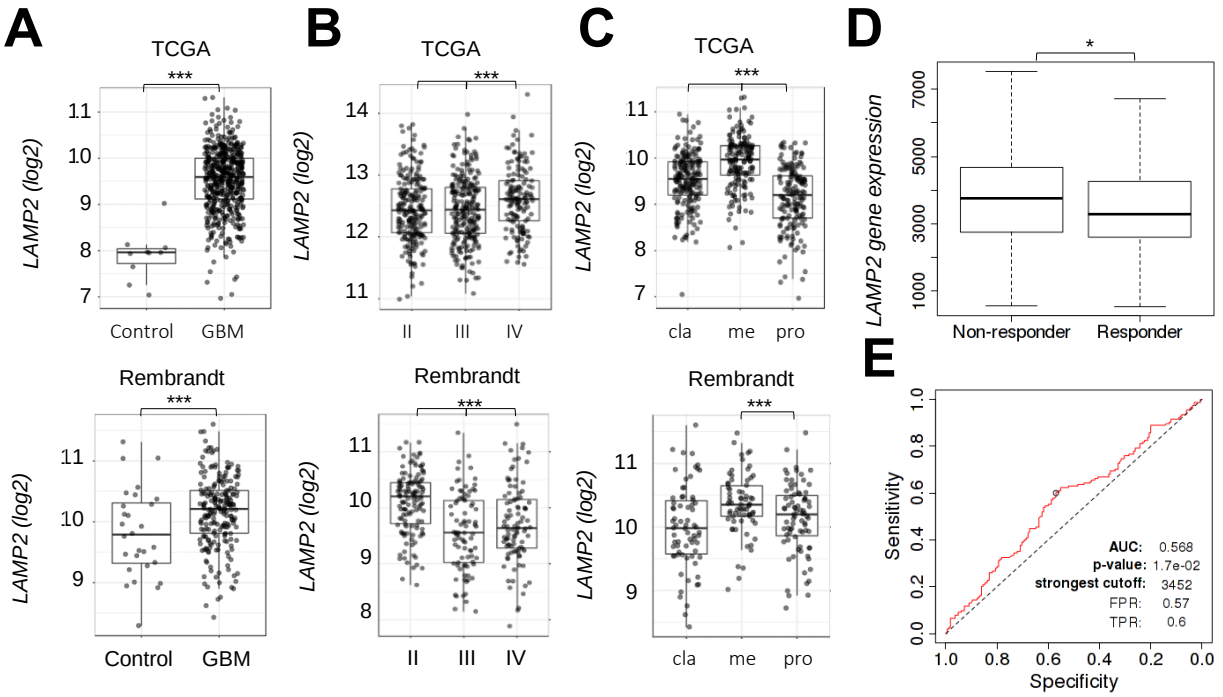

Figure R2. ***LAMP2*** **expression is associated with malignant phenotype in TCGA and Rembrandt cohorts. (A)** *LAMP2* mRNA expression in control and GB samples in TCGA (p=2.4e-13) and Rembrandt (p=4.5e-03) cohorts; **(B)** *LAMP2* mRNA expression in grade II, III and IV of glioma in TCGA (p II-III =n.s., p II-IV =1.3e-02, p III-IV =7.5e-03) and Rembrandt (p II-III =n.s, p II-IV=3.5e-05, p III-IV=3.1e-08) cohorts; **(C)** mRNA expression of *LAMP2* in classical (cla), mesenchymal (me) and proneural (pro) subtypes of GB from TCGA (p cla-me=2.9e-09, p cla-pro=2.9e-08, p me-pro=4.5e-27) and Rembrandt cohorts (p cla-me=4.8E-02, p cla-pro=n.s., p me-pro=6.3E-04); **(D)** *LAMP2* expression in TMZ treatment non-responder (n=154) and responder (n=165) GB patients (http://www.rocplot.org/). Mann-Whitney test p-value: 0.036; **(E)** ROC curve of *LAMP2* gene expression in GB patients treated with TMZ (n=319, http://www.rocplot.org/).

As *LAMP2* gene expression is representative of the three isoforms *LAMP2A*, *LAMP2B* and *LAMP2C*, we decided to study specifically *LAMP2A* expression in an additional cohort from Donostia Hospital. First, we characterized the mRNA expression of the three isoforms of *LAMP2* gene in GB samples compared to healthy control tissue. Our results demonstrated that both *LAMP2A* and *LAMP2B* were augmented in GB samples (***Figure R3A***). Next, we measured LAMP2A protein expression in GB TMAs, where we determined that 60% of the samples presented ≥40% of positive staining, whereas only 13% of the samples presented ≤20% or no staining (***Figure R3B***).

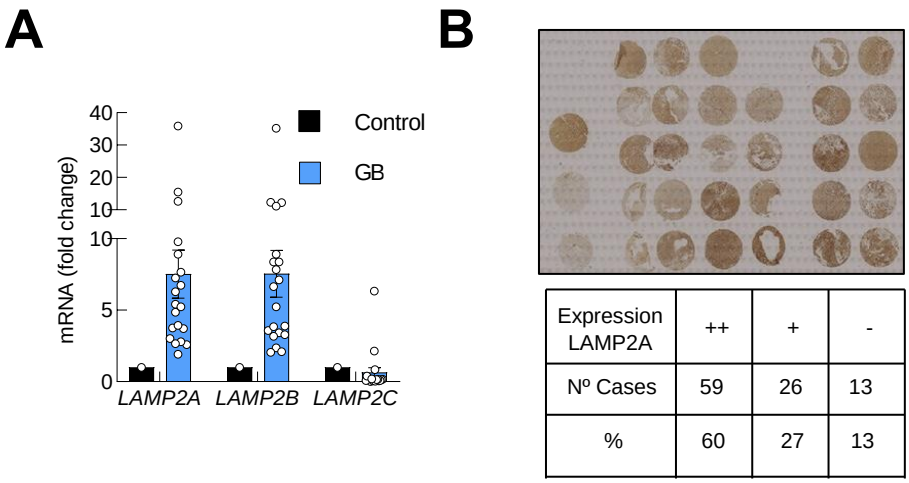

Expression LAMP2A	++	+	-
Nº Cases	59	26	13
%	60	27	13

Figure R3. LAMP2A expression is upregulated in GB samples from Donostia Hospital cohort. (A) mRNA expression of *LAMP2A*, *LAMP2B* and *LAMP2C* in GB samples (n=20) compared to healthy brain tissue; **(B)** Representative TMA and overall quantification for LAMP2A protein expression in GB samples (n=98).

In order to further confirm CMA activity in GSCs, we decided to use a photo-switchable KFERQ-Dendra CMA reporter [307]. This reporter acts as a CMA substrate, so that, when CMA is active, fluorescence puncta can be detected. Thus, we observed that GNS166 and GNS179 cells present more than three times higher puncta intensity per cell compared to control cells (***Figure R4A***). Indeed, conventional GB cell lines, representative of tumor-bulk, also presented higher CMA activity than control cells, but in most of the cases not as much as GSC lines (***Figure R4B***). All these data together confirm that LAMP2A and CMA activity are increased in GB and enriched in the GSCs population.

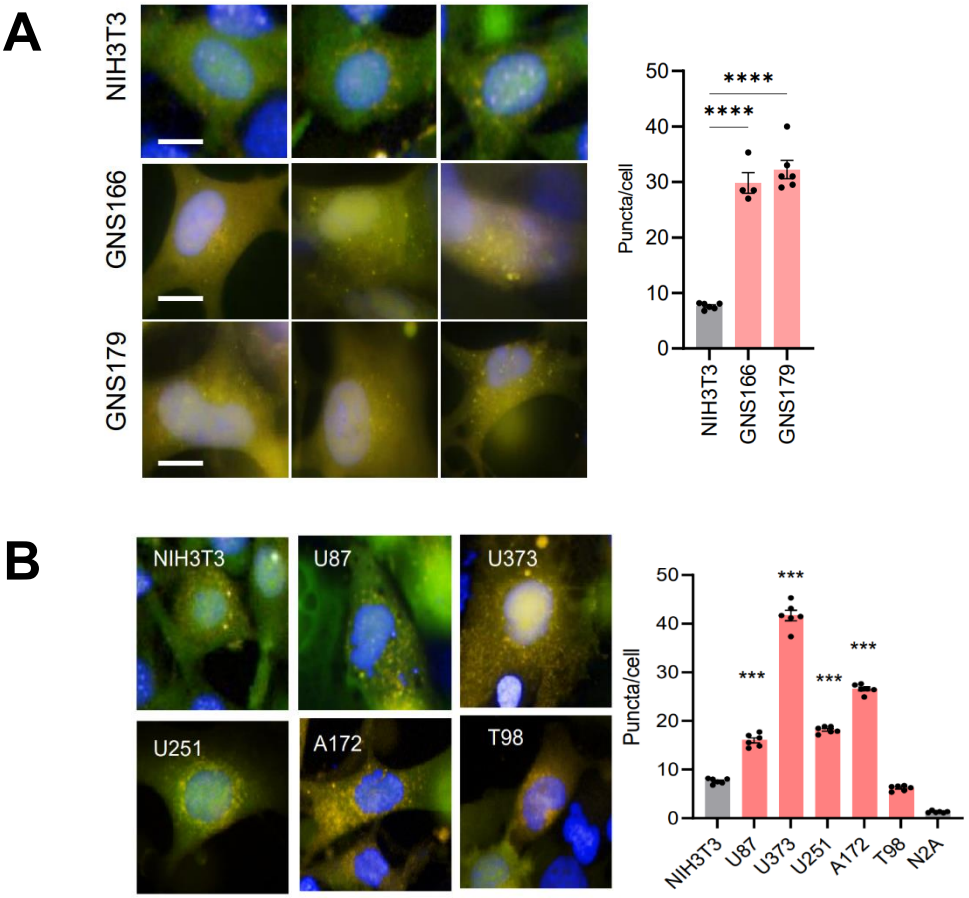

Figure R4. CMA activity is increased in GSC and GB cell lines. (A) Representative images (left) and quantification (right) of KFERQ-Dendra reporter puncta per cell fluorescence intensity in GNS cells and **(B)** conventional GB cell lines, compared to control cells NIH3T3 (mouse embryonic fibroblasts) and N2A (mouse neuroblasts) cells (n≥4). Yellow fluorescence is representative of CMA activity.

1.2. *LAMP2A* knock down suppresses patient-derived GSCs activity

Once we revealed that CMA is highly enriched in GSCs, we decided to further characterize its role in this subpopulation. With this aim, we firstly performed short hairpin RNA technique-mediated lentiviral knock down of *LAMP2A* in U251, as it was the conventional cell line with highest LAMP2A expression (***Figure R1A***). Once we validated *LAMP2A* knock down (*shL2A*, ***Figure R5A, E***), we proceeded to study its impact on oncosphere formation and self-renewal, a major characteristic of GSCs. In this sense, we saw that *shL2A* cell presented a reduction of an ~ 80% in colony formation ability (***Figure R5B***), which represents a diminished capacity of the cell to grow in limiting dilutions. Moreover, we found

that *shL2A* cells presented a ~ 60% diminishment in the ability to form 1^{ry} and 2^{ry} oncospheres (***Figure R5C***), confirming impaired proliferation and self-renewal capacities. This reduction in oncosphere generation was also observed in U373 cells (***Figure R5D***), but not so drastically, probably due to the lower basal expression of LAMP2A. Accordingly, these results were accompanied by a significant decrease in the expression of *SOX2* and *SOX9* stem cell markers in *shL2A* U251 cells (***Figure R5E***).

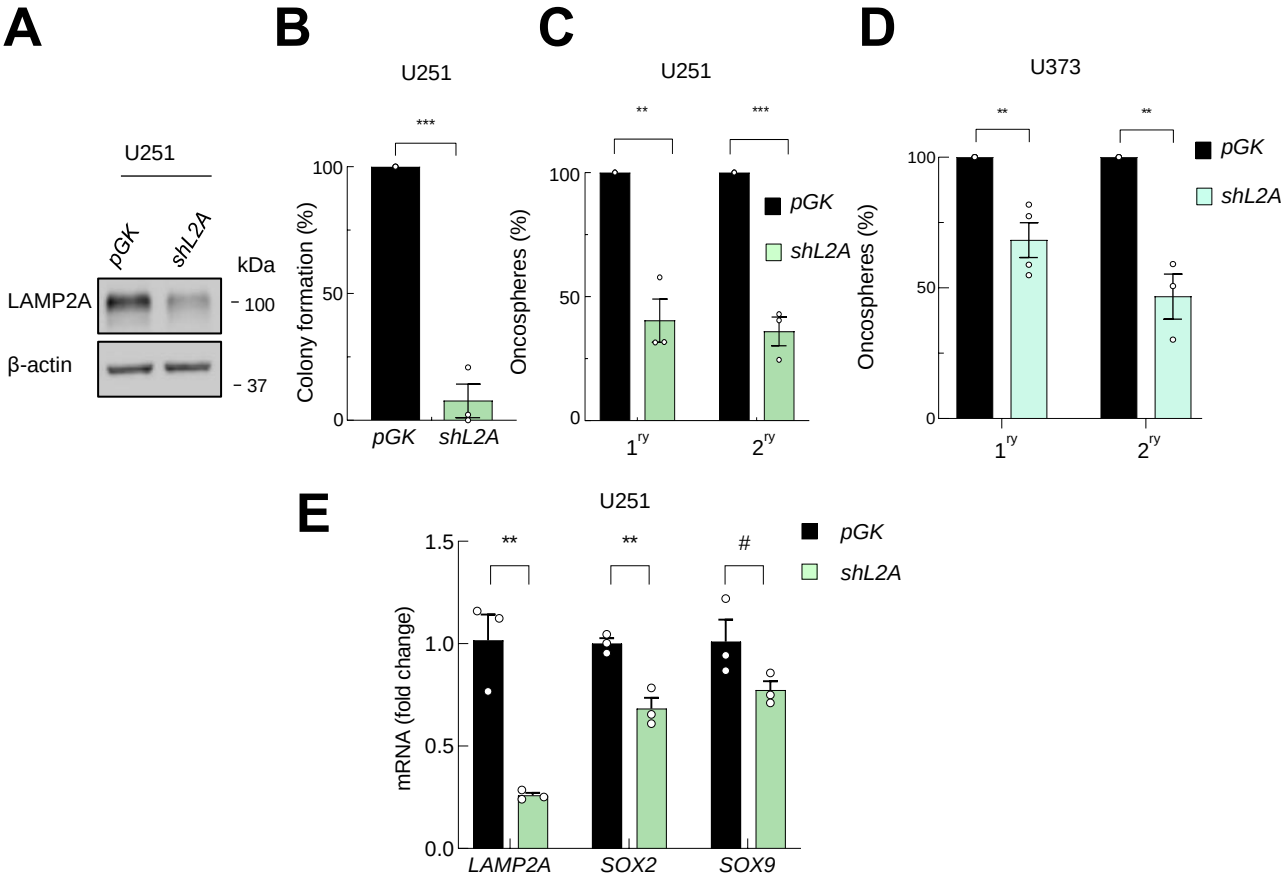

Figure R5. *LAMP2A* silencing reduces self-renewal of GSCs. (A) Representative western blot for LAMP2A and β-actin in *pGK* and *shL2A* U251 cells (n=3); **(B)** Relative number of colonies formed by *pGK* and *shL2A* U251 cells (n=3); **(C)** Relative number of 1^{ry} and 2^{ry} oncospheres generated at 10 and 20 days, respectively, by *pGK* and *shL2A* U251 (n=3) and **(D)** U373 (n≥3) cells; **(E)** Relative mRNA expression of *LAMP2A*, *SOX2* and *SOX9* in *pGK* and *shL2A* U251 cells (n=3).

To further confirm the impact of CMA on self-renewal of U251, we exogenously upregulated LAMP2A in control and *shL2A* cells. Herein, we found that *LAMP2A* overexpressing *pGK* U251 cells presented an enhanced oncosphere generation ability (***Figure R6A***). Moreover, LAMP2A restoration in *shL2A* cells reverted the impairment in oncosphere

and colony formation abilities (***Figure R6A, C***). All these data suggest the relevance of CMA in the regulation of GSCs activity.

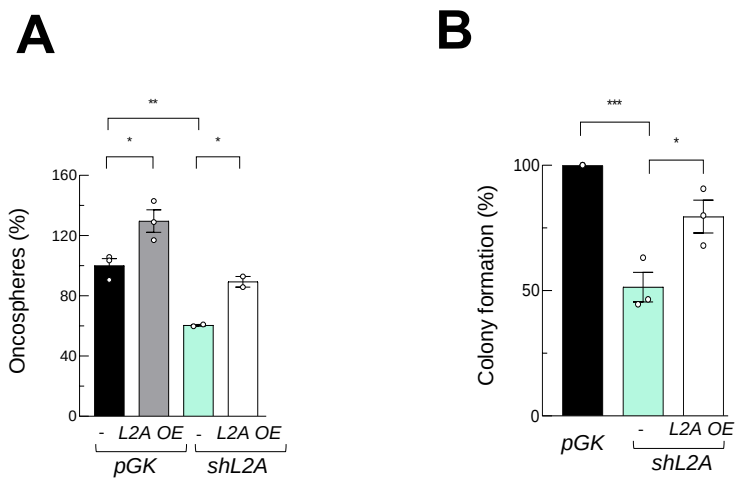

Figure R6. *LAMP2A* upregulation increases self-renewal of U251. (A) Relative number of primary oncospheres generated by control and *LAMP2A* overexpressing cells in *pGK* or *shL2A* U251 (n=3); **(B)** Relative number of colonies formed by *pGK*, *shL2A* and *LAMP2A* rescued *shL2A* U251 (n=3).

To directly unravel the impact of CMA on GSC population, we carried out the same strategy of silencing *LAMP2A* in two patient-derived GSCs (GNS166 and GNS179). Thus, after validating *LAMP2A* knock down in both GSCs (***Figure R7A***), we firstly studied the proliferative capacity. Herein, we determined that *shL2A* GSCs proliferated significantly less than *pGK* control cells, measured by cell counting (***Figure R7B***) and number of positive cells for the mitosis marker phosphor-histone3 (p-H3) by immunofluorescence (***Figure R7C***). Similar results were observed in U251 and U373 cells in these experiments (***Figure R7B, C***). Of note, impaired proliferation was rescued by LAMP2A overexpression in U251 (***Figure R7D***). Reduced proliferation was accompanied by an induction of apoptosis, as the number of cells positive for active Caspase-3 (Casp3) was increased in *shL2A* GSCs. Moreover, *shL2A* GSCs presented significantly reduced expression of the stem cell markers *SOX2*, *SOX9* and *NESTIN* (***Figure R7F***), indicating that *LAMP2A* knock down impairs GSC maintenance.

Since GSC are responsible for therapy resistance, we next measured the response to TMZ of *LAMP2A* knocked down GSCs. We found that these cells were more sensitive to TMZ treatment than control cells (***Figure R8A, B***). This result was similarly observed in U251 cell line (***Figure R8A, B***), whose oncosphere generation ability was even more reduced when *shL2A* cells were treated with TMZ (***Figure R8C***). Altogether, these results reveal the relevant role of LAMP2A in GSC activity and therapy response.

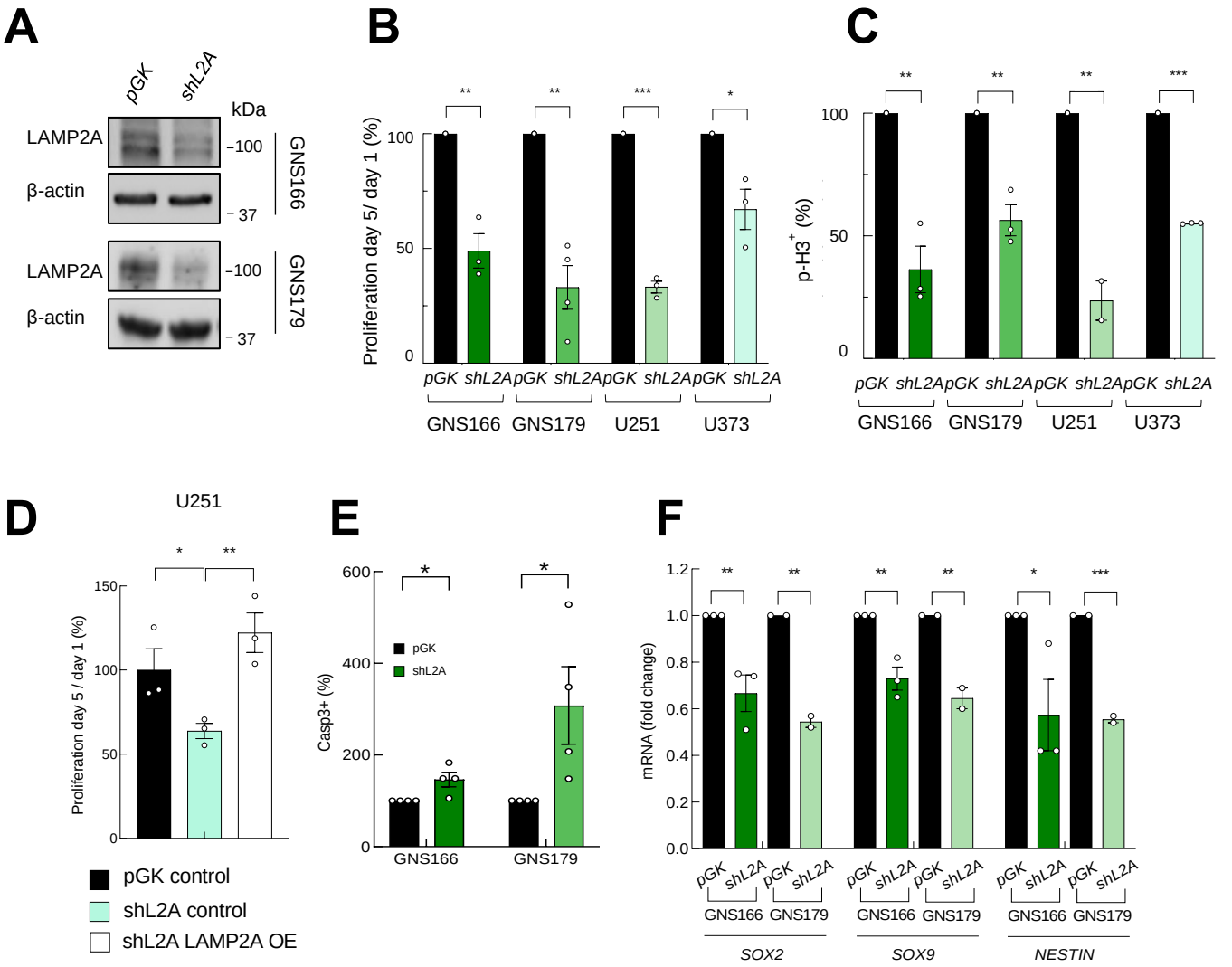

Figure R7. *LAMP2A* silencing reduces patient-derived GSC proliferation and stem properties. (A) Immunoblot of LAMP2A in *pGK* and *shL2A* GNS166 and GNS179 cells (n=3); **(B)** Number of proliferating cells at day 5 relative to day 1 in *pGK* and *shL2A* indicated cells (n≥3); **(C)** Quantification of immunofluorescence of p-H3 in *pGK* and *shL2A* GNS166 (n=3) GNS179 (n=4), U251 (n=2) and U373 (n=3) cells; **(D)** Number of proliferating cells at day 5 relative to day 1 after LAMP2A expression rescue (n=3); **(E)** Quantification of immunofluorescence of caspase-3 in *pGK* and *shL2A* GNS166 and GNS179 cells (n=4); **(F)** Relative mRNA expression of GSC markers *SOX2*, *SOX9* and *NESTIN* in *pGK* and *shL2A* GNS166 (n=3) and GNS179 cells (n=2).

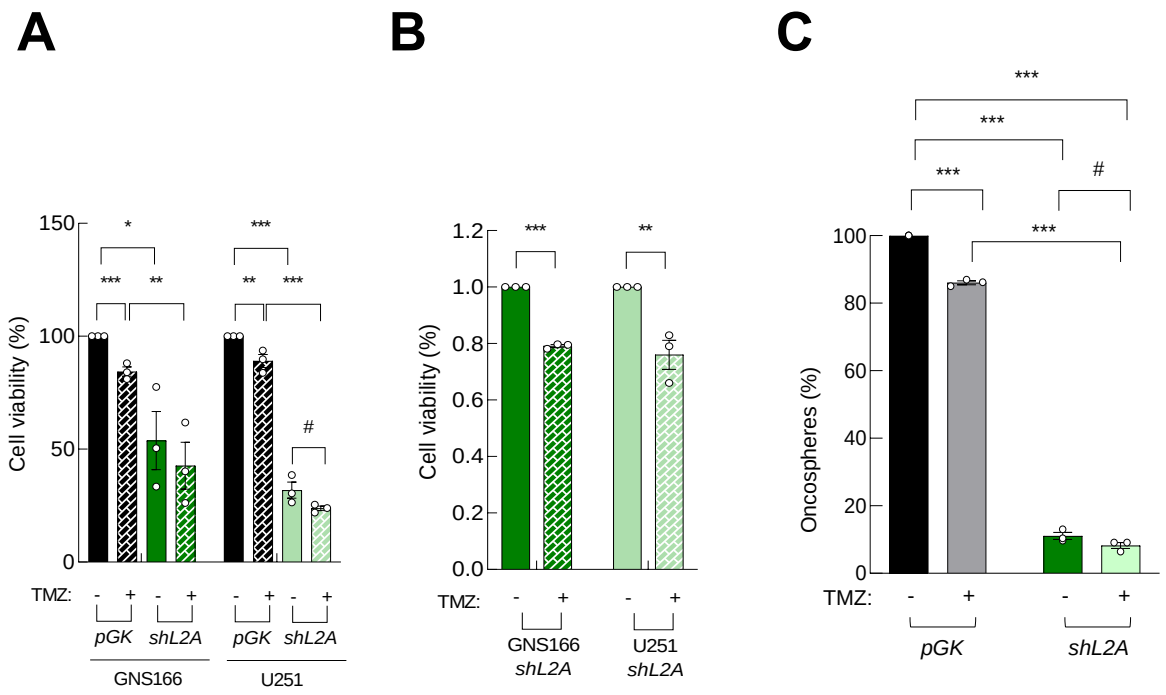

Figure R8. *LAMP2A* silencing increases TMZ sensitivity in GSCs. (A) Relative cell viability of *pGK* and *shL2A* GNS166 and U251 cells after 72 h with control and 2 mM or 250 µM TMZ treatment, respectively (n=3); **(B)** Relative cell viability of *shL2A* in **A**; **(C)** Relative primary oncospheres generated by *pGK* and *shL2A* U251 cells, after 50 µM TMZ treatment (n=3).

1.3. Proteome and transcriptome studies reveal multiple pathways altered in *LAMP2A* knocked down GSCs

In order to get a deep view regarding molecular changes associated with LAMP2A downregulation in GSCs, we next performed a high throughput proteome study in control and *shL2A* GNS166 cells. Herein, we observed a total of 273 significantly altered proteins, among which 172 were downregulated and 101 upregulated (***Figure R9A***). Of note, previously described CMA substrates such as Annexin A6 [310] and HSC70 [311] proteins were found upregulated (***Figure R9B***) further validating the inhibition of CMA process. Moreover, proteins such as CD44, CD109 and EGFR, whose implication in GB and GSC proliferation and maintenance has been previously reported [312-314], appeared to be downregulated in our analysis (***Figure R9C***). With the aim of having a general overview of proteomic pathways altered by *LAMP2A* knock down, we performed an ontology analysis of all significantly altered proteins (***Figure R9D***). Herein, chaperone function and protein translation associated pathways were altered, which could be expected as we were reducing the activity of a protein quality control system. Intriguingly, pathways related to extracellular

matrix (ECM) interaction, interferon (IFN) signaling, and antigen presentation, mitochondrial metabolism and others were also differentially expressed (***Figure R9D***).

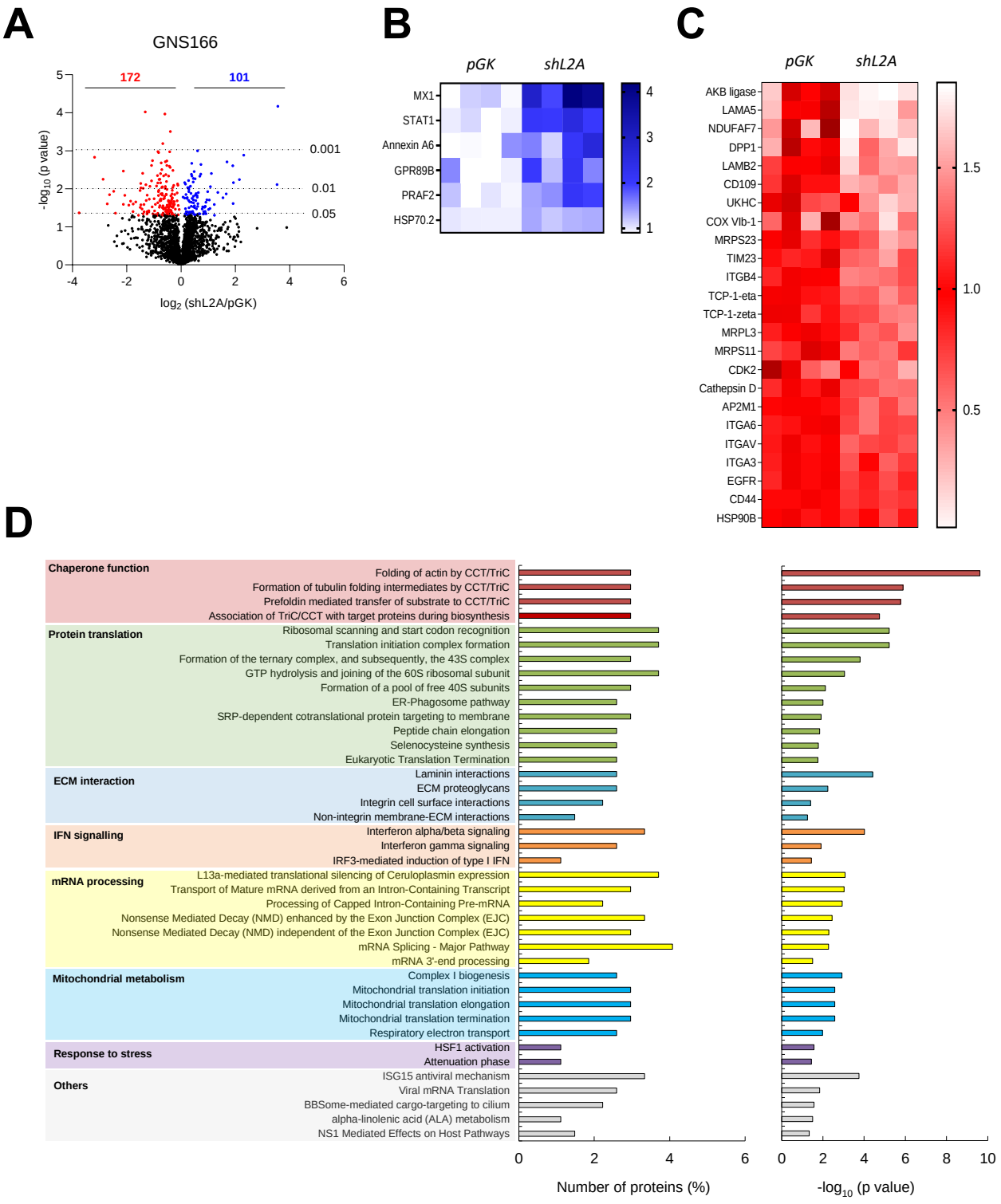

Figure R9. *LAMP2A* silencing in GNS166 alters crucial proteomic pathways. (A) Volcano plot of upregulated and downregulated pathways in proteome study of GNS166 pGK vs shL2A cells (n=4); **(B)** Representative heat map of upregulated and **(C)** downregulated proteins in the proteome study; **(D)** Ontology analysis based on Reactome database of altered proteome in **A**.

With these results in mind, we next wondered whether this altered proteomic signature could be specific for GSCs, or instead, it could be extended to bulk GB cells. To test this idea, we performed the same proteomic study in control and *shL2A* U251 cells. Herein, a total of 464 proteins appeared to be differentially expressed, among which 284 were downregulated and 180 upregulated (***Figure R10A***). Of note, only 60 common altered proteins were found when comparing proteomic studies from control and *shL2A* GNS166 and U251 cells (***Figure R10B***), indicating that CMA regulates distinctly the proteome of bulk tumor and GSCs.

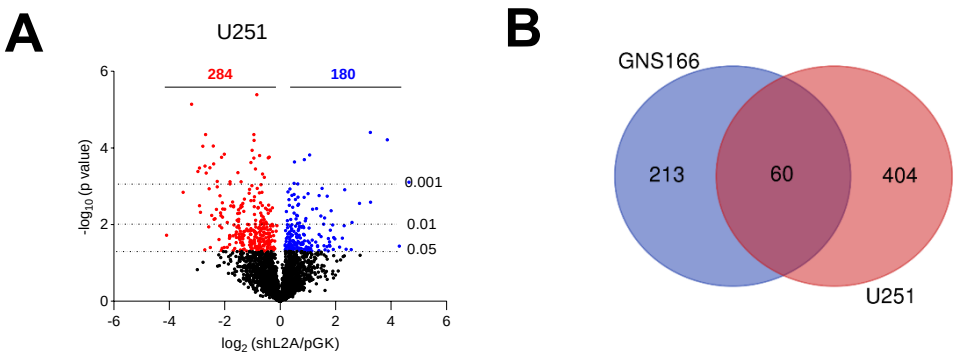

Figure R10. *LAMP2A* silencing alters common and unique proteins in U251 and GNS166. (A) Volcano plot of upregulated and downregulated proteins in U251 *pGK* vs *shL2A* proteomics (n=4); **(B)** Venn diagram representing the comparison of proteins altered in GNS166 and U251 proteomic studies.

In line with this, when performing ontology analysis of significantly altered proteins in U251, processes associated with DNA damage, cell cycle, protein transport and degradation, and other signaling pathways seemed to be uniquely altered (***Figure R11***). On the contrary, chaperone function and protein translation, as well as ECM interactions, antigen presentation, and mitochondrial metabolism were also significantly altered (***Figure R11***). These data reveal that, although proteome regulation is not identical in tumor bulk and GSCs, CMA is involved in some common crucial processes in both populations.

Figure R11. *LAMP2A* silencing alters crucial proteomic pathways in U251. Ontology analysis based on Reactome database of altered proteome in *pGK* and shL2A U251 (n=4).

Among dysregulated pathways in the proteomic studies, mRNA processing was also highlighted (***Figure R9D, R11***), suggesting that *LAMP2A* downregulation may also alter the transcriptome of GSCs. Thus, we performed an RNAseq study in control and *shL2A* GNS166 cells. Of note, a total of 2,972 transcripts were dysregulated, among which 1,299 were downregulated and 1,673 upregulated (***Figure R12A***).

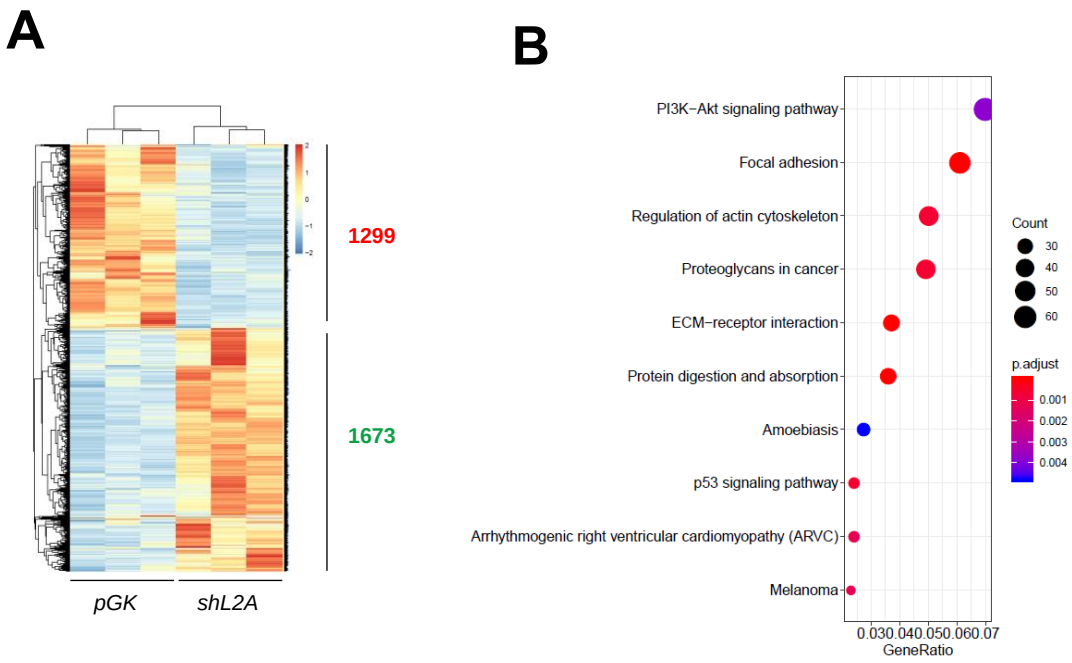

Figure R12. *LAMP2A* silencing alters transcriptome of GNS166. (A) Representative heat map of upregulated and downregulated transcripts in RNAseq study of *pGK* vs *shL2A* GNS166 cells (n=3); **(B)** Dotplot representation of the main altered biological processes after gene ontology analysis of RNAseq study on **A**.

Of note, gene ontology analysis of significantly altered transcripts showed changes in processes such as PI3K-Akt or p53 signaling pathways (***Figure R12B***), whose relevance in GSCs proliferation and maintenance has been previously reported [315, 316]. Consistent with functional studies presented before, *shL2A* GNS166 and U251 cells presented diminished mRNA levels of the cell cycle regulator *Cyclin A* (***Figure R13A***), confirming the downregulation of proliferation also at molecular level. Moreover, we observed and further validated augmented mRNA levels of *PI3KCA* and *mTOR* (***Figure R13B***) in *shL2A* cells of both GNS166 and U251. Accordingly, we found an upregulation in the phosphorylated form of AKT protein (***Figure R13C***), indicating an overactivation of the pathway. Conversely, significant downregulation in mRNA expression of *PDGFRA* and the negative regulator *PTEN* were also detected in both cell lines upon *LAMP2A* downregulation (***Figure R13D***), suggesting a more complex regulatory system of the pathway.

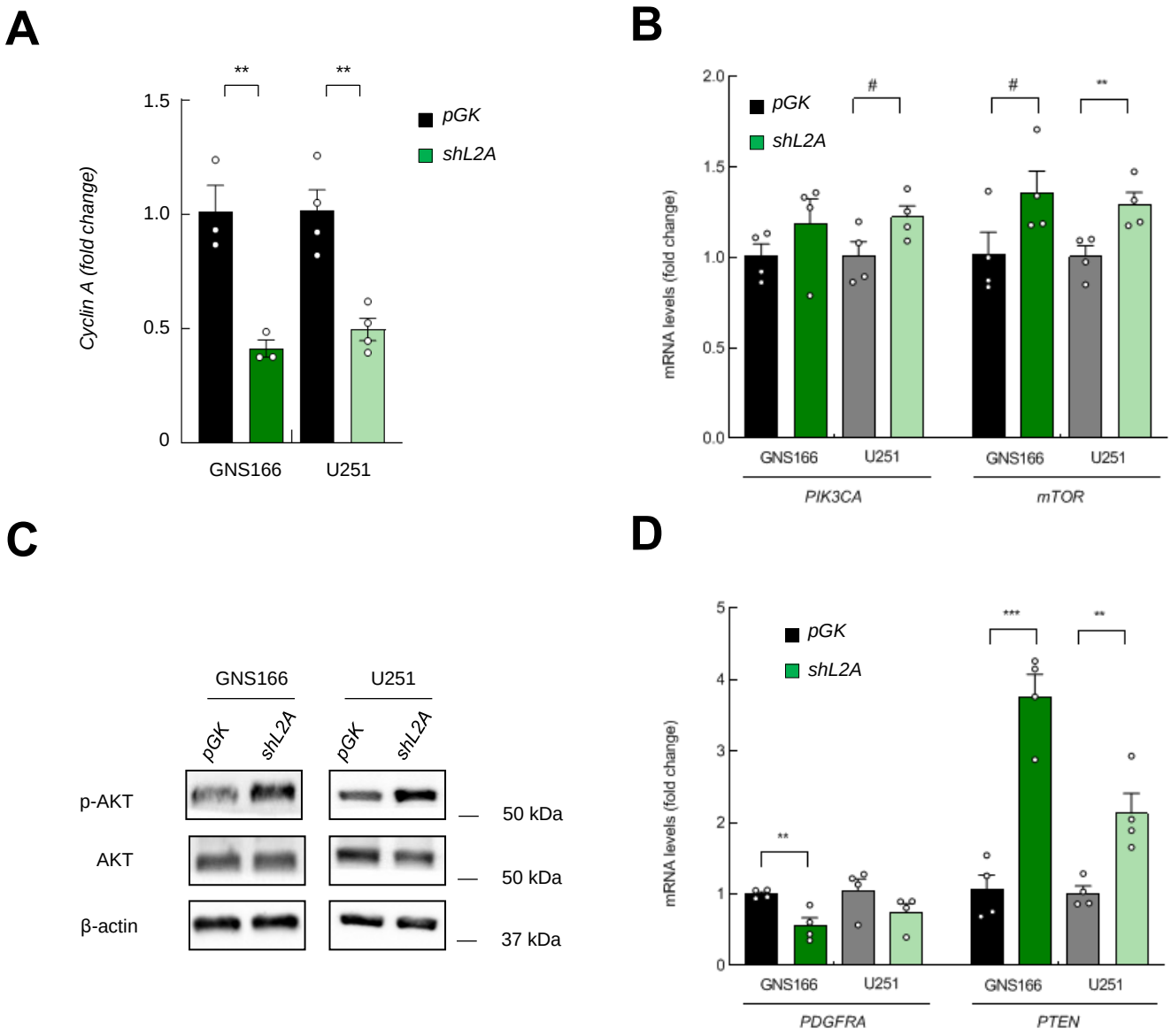

Figure R13. ***LAMP2A*** **knock down alters Cyclin A and PI3K/AKT/mTOR pathway. (A)** Relative mRNA expression of *Cyclin A* in both GNS166 (n=3/4) and U251 (n=4) *pGK* vs *shL2A*; **(B)** Relative mRNA expression of *PIK3CA* and *mTOR* in both GNS166 and U251 *pGK* vs *shL2A* (n=4); **(C)** Representative immunoblots of p-AKT and total AKT in both GNS166 and U251 *pGK* vs *shL2A* (n=3); **(D)** Relative mRNA expression of *PDGFRA* and *PTEN* in both GNS166 and U251 *pGK* vs *shL2A* (n=4).

Interestingly, processes associated with the regulation of actin cytoskeleton, proteoglycans, focal adhesion, and ECM interactions also appeared to be highly altered in RNAseq study (***Figure R12B***). Notably, pathways related to ECM interactions were also dysregulated at proteome level, indicating that CMA regulates multiple pathways at distinct levels.

1.4. *LAMP2A* knock down impairs mitochondrial metabolism in GSCs

CMA can promote the selective degradation of enzymes operating in glucose or lipid metabolism pathways and, therefore, regulate energy homeostasis [189]. In our proteomic study, *LAMP2A* knock down in GNS166 cells showed an impairment in mitochondrial metabolism (***Figure R9D, R11***). However, these cells, instead of an accumulation, presented a downregulation of mitochondrial ribosomal proteins such as MRP-S23, MRP-S11 or MRP-L3, and proteins regulating mitochondrial functionality such as TIM23, COX VIb-1, NDUFAF7 and AKB ligase (also known as GCAT) (***Figure R9C***). Indeed, immunoblot studies further corroborated the diminishment in *shL2A* cells of TIM23 and MRP-S23 not only in GNS166, but also in GNS179 and U251 (***Figure R14A***). Accordingly, these results were also translated into clinical data, as *LAMP2* presented significant positive correlation with *MRP-L3, MRP-S23, MRP-S11, COX6B1, NDUFAF7* and *GCAT* in GB samples from TCGA cohort (***Figure R14B***). These results demonstrate that *shL2A* GSCs present proteomic changes indicative of a possible mitochondrial impairment.

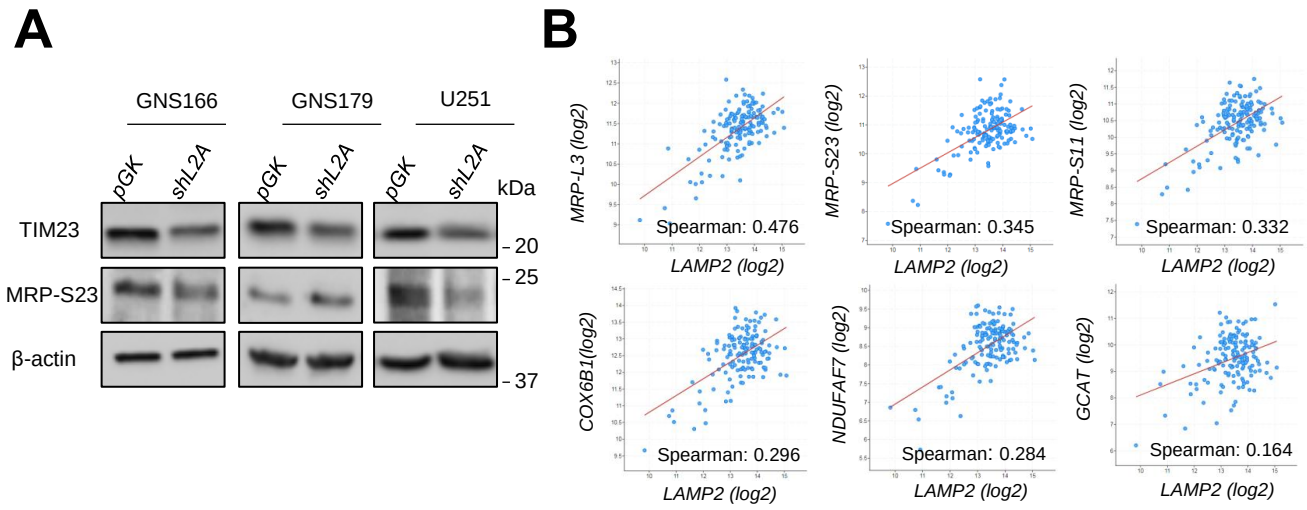

Figure R14. *LAMP2A* silencing impairs the expression of mitochondrial markers. (A) Immunoblot of mitochondrial markers TIM23 and MRP-S23, and β-actin in *pGK* and *shL2A* GNS166, GNS179 and U251 (n≥3) cells; **(B)** Association study of *LAMP2* with mitochondrial metabolism genes *MRPS23* (p=1.336e-05), *MRPS11* (p=2.972e-05), *MRPL3* (p=5.80e-10), *COX6B1* (p=2.086e-04), *NDUFAF7* (p=3.970e-04) and *GCAT* (AKB ligase, p=0.0430) in TCGA cohort (cBioPortal for cancer genomics, https://www.cbioportal.org/).

In order to confirm these molecular results, we decided to carry out mitochondrial functional assays using Agilent Seahorse XF technology. Based on the measurement of oxygen consumption rate (OCR) of both control and *shL2A* GNS166 cells (***Figure R15A***), we firstly studied the functionality of the oxidative phosphorylation system

(OXPHOS). In particular, we found that *LAMP2A* knocked down GNS166 cells presented a reduction of ~ 40% of basal respiration (***Figure R15B***) and a diminishment of ~ 60% in maximal respiration in response to the uncoupler of mitochondrial oxidative phosphorylation FCCP (***Figure R15C***). These alterations lead to a reduction of ~ 75% in the spare respiratory capacity of these cells (***Figure R15D***). As a key product of OXPHOS is the adenosine triphosphate (ATP), the observed impairment in respiratory capacity of *shL2A* cells also triggered a diminishment of ~ 45% in OXPHOS-mediated ATP production (***Figure R15E***). Moreover, this assay also showed that *shL2A* cell presented reduced non-mitochondrial oxygen consumption in a ~ 50% (***Figure R15F***). Altogether, these results demonstrate that CMA is relevant for the maintenance of OXPHOS functionality. Besides, similar results were observed in U251 cells (***Figure R15B-F***), extending the impact of CMA on the regulation of mitochondrial metabolism also to differentiated GB cells.

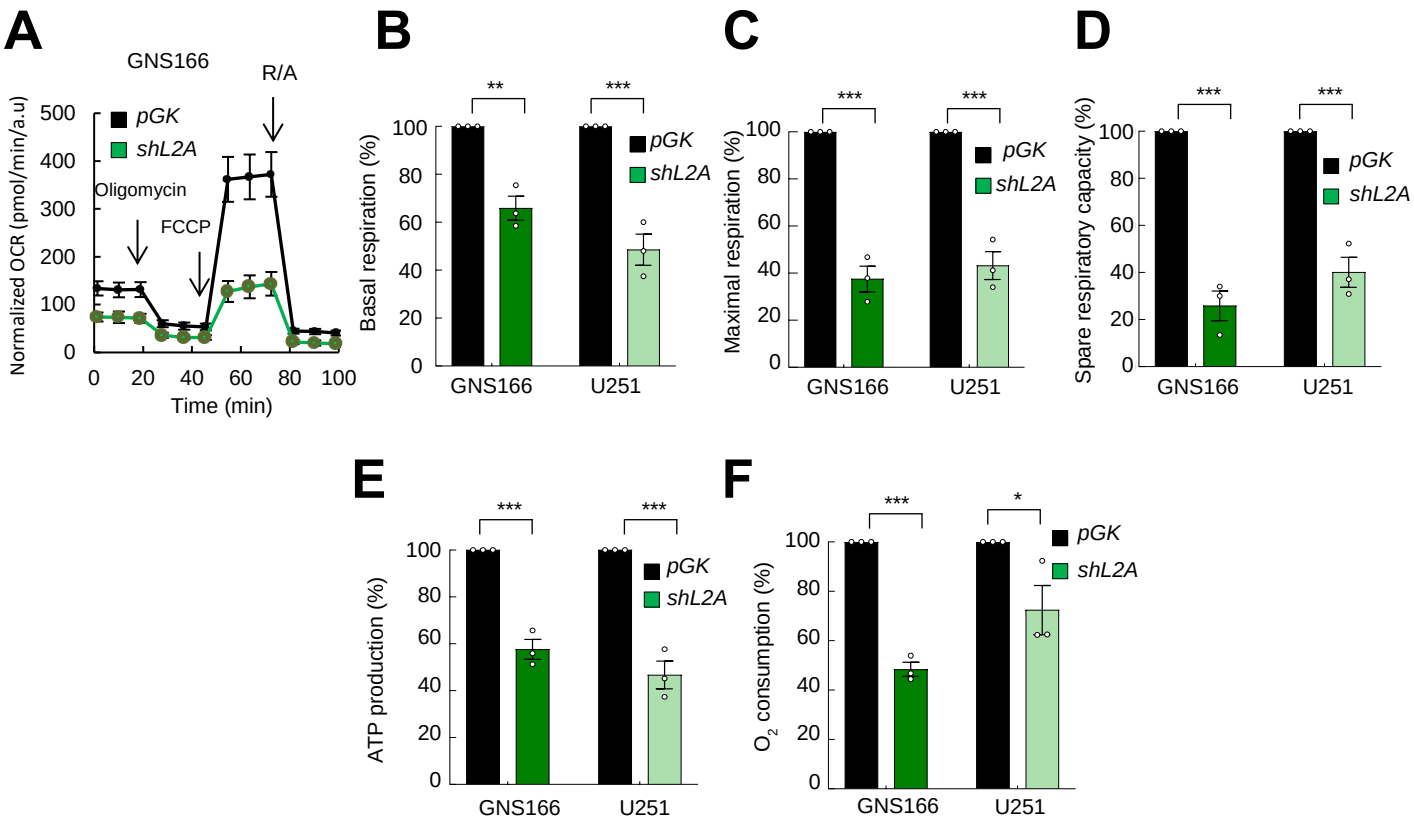

Figure R15. *LAMP2A* silencing impairs mitochondrial metabolism of GNS166 and U251. (A) Normalized OCR response in *pGK* and *shL2A* GNS166 in basal conditions and after consecutive addition of 1 µM Oligomycin, 1 µM FCCP and 1 µM Rotenone/Antimycin A. A representative experiment in GNS166 is shown from a total of n=3; **(B-F)** Quantification of mitochondrial respiratory functions of *pGK* and *shL2A* GNS166 and U251 (n=3).

An impaired OXPHOS system can give rise to alterations in mitochondrial polarization and generation of reactive oxygen species (ROS) within the mitochondria [317]. With the aim of studying whether OXPHOS impairment observed in *shL2A* GNS166 cells could be extended to a generalized mitochondrial damage, we next decided to study these two characteristics by flow cytometry. Herein, we observed that *shL2A* GNS166 cells showed more depolarized mitochondria (***Figure R16A***) and accumulated more mitochondrial ROS (***Figure R16B***), being this latter partially rescued with the antioxidant agent butylated hydroxyanisole (BHA) (***Figure R16C***). Together, these results demonstrate a clear impairment of mitochondrial functionality in *LAMP2A* knocked down GSCs.

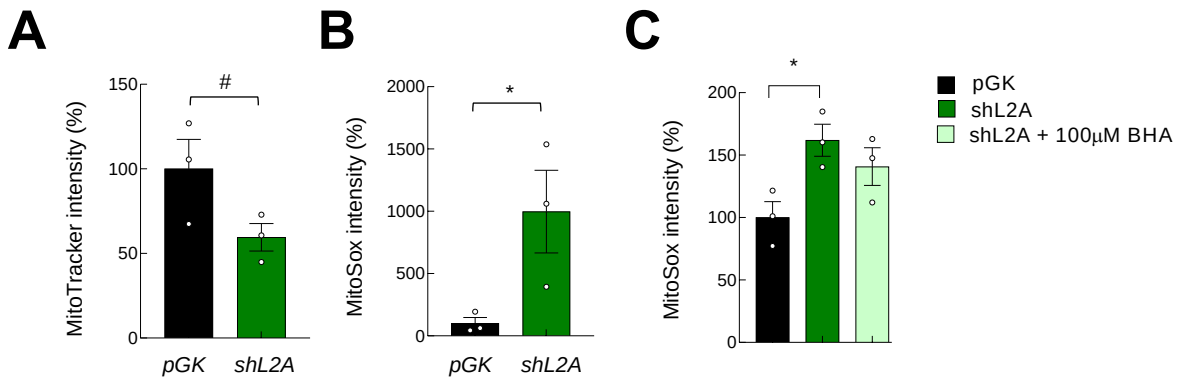

Figure R16. *LAMP2A* silencing alters mitochondrial polarization and induces ROS in GNS166. (A) Relative quantification of mitochondrial polarization measured by fluorescent intensity of MitoTracker™ Red FM dye via flow cytometry (n=3); **(B)** Relative quantification of mitochondrial ROS analysed by MitoSox™ Red via flow cytometry (n=3); **(C)** Relative quantification of mitochondrial ROS by MitoSox™ Red of *pGK* and *shL2A* GNS166, after treatment with antioxidant 100 μM BHA (n=3).

GSCs are metabolically heterogeneous and adaptative cell population able to shift between glycolytic and oxidative phenotypes [124]. Thus, we next wanted to unravel if, together with the mitochondrial impairment, *shL2A* GSCs could present any other type of metabolic alteration. In this line, we decided to study glycolysis, a major metabolic pathway for cancer cells. For that, we again used Agilent Seahorse XF technology, but this time, taking advantage of the measurement of extracellular acidification (ECAR). Intriguingly, and contrary to previous reports in bulk cancer cells [206], *shL2A* GNS166 cells displayed a ~ 50% increase on the levels of glycolysis in glucose saturating conditions (***Figure R17A***). Moreover, when

OXPHOS is completely inhibited, both control and *shL2A* GNS166 cells present no differences in glycolytic capacity (***Figure R17B***). Together, these data could indicate that *LAMP2A* knocked down GNS166 cells upregulate glycolysis, in part, to compensate OXPHOS impairment and maintain the necessary ATP production. In this context, *shL2A* GNS166 cells presented a significantly lower glycolytic reserve (***Figure R17C***), which could be detrimental as the mitochondria or other metabolic pathways further degenerate.

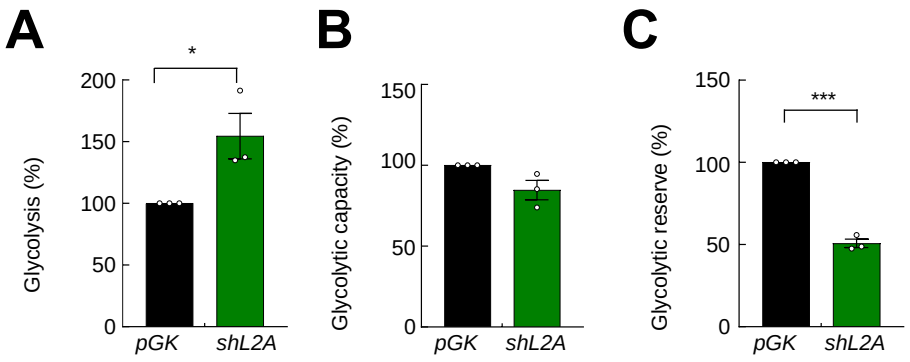

Figure R17. *LAMP2A* silencing upregulated glycolysis in GNS166. Relative quantification of glycolytic functions based on kinetic normalized ECAR response of *pGK* and *shL2A* GNS166 in basal conditions and after consecutive addition of glucose 10 mM, Oligomycin 1 µM and 2-D-Deoxy-Glucose 50 mM (n=3).

1.5. *LAMP2A* knock down impairs inflammatory and immune response in GSCs

Among altered proteomic pathways in *shL2A* GSCs, IFN signaling, and antigen presentation were also significantly dysregulated (***Figure R9C, D, R11***). In particular, a total of 10 IFN signaling proteins were upregulated, including relevant mediators such as STAT1 or MX1 (***Figure R9C***). These results were confirmed by immunoblot and extended to GNS179 and U251 cell lines (***Figure R18A***). Indeed, not only increased the total amount of STAT1, but the phosphorylated form was also augmented (***Figure R18A***), indicating the post-transcriptional activation of the pathway. Accordingly, we found that *shL2A* cells of both GSC and U251 presented elevated mRNA expression of IFN-γ compared to control cells (***Figure R18B***). Together with the IFN pathway, proteomic study revealed significant reduction in proteins associated with MHC class II antigen presentation, such as AP2M1, UKHC (also known as *KIF5B*), DPP1 (also known as Cathepsin C or CTSC) and Cathepsin D (CTSD) (***Figure R9C***). Notably, clinical data from TCGA cohort corroborated the positive correlation between *LAMP2* and *CTSD*, *AP2M1*, *CTSC* and *KIF5B* (***Figure R18C***). Surprisingly, however, *STAT1* and *MX1* also showed a positive correlation with *LAMP2* in these GB patients (***Figure R18C***), which

is contrary to what was expected from the results obtained in *LAMP2A* knocked down glioma cells.

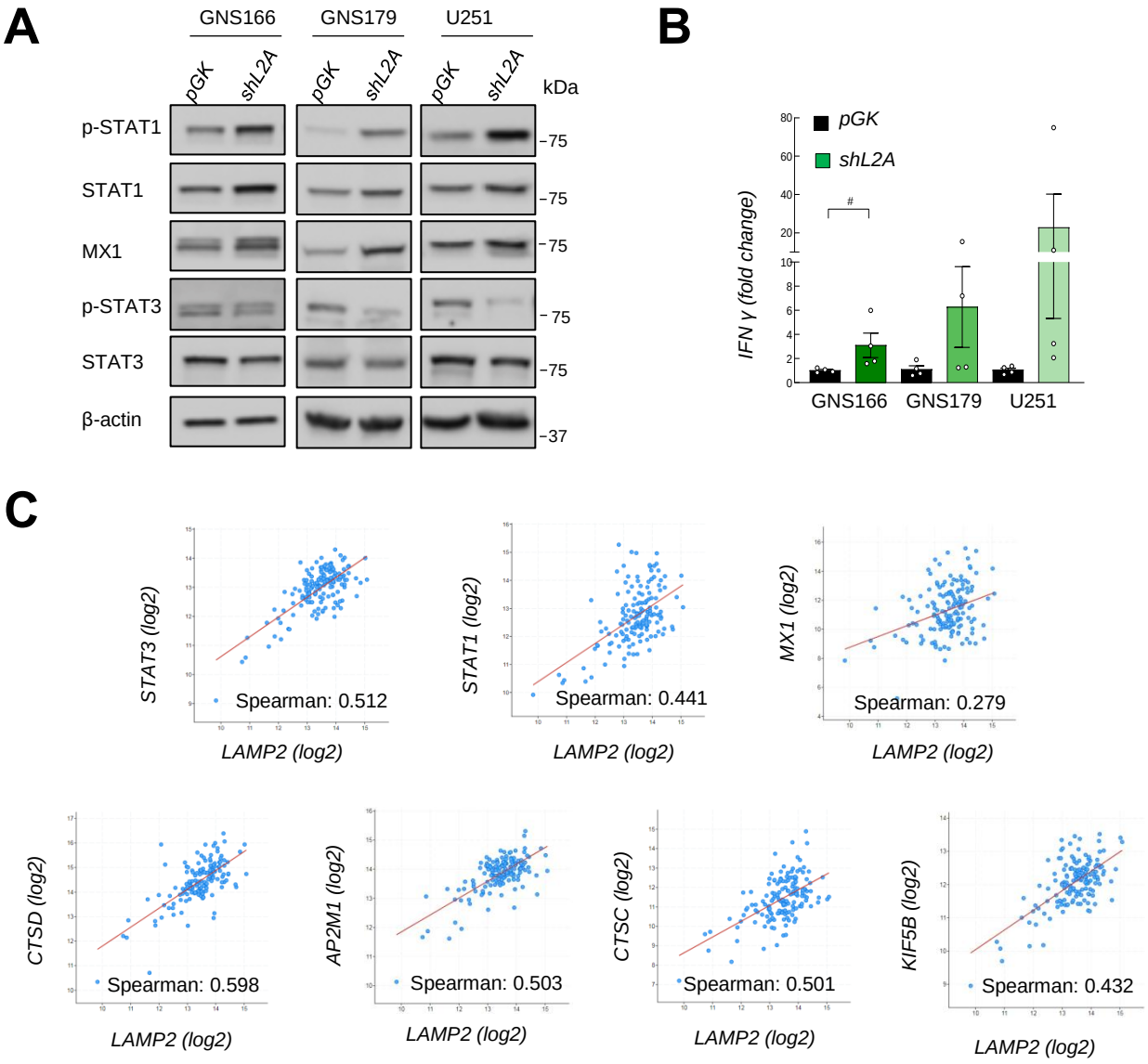

Figure R18. *LAMP2A* silencing activates IFN signalling and reduces antigen presentation in GSCs. (A) Representative immunoblots of indicated proteins in *pGK* vs *shL2A* GNS166, GNS179 and U251 (n≥3); **(B)** Relative mRNA expression of *IFN-γ* in *pGK* and *shL2A* GNS166, GNS179 and U251 cells (n=4); **(C)** Association study of *LAMP2* with *STAT3* (p=1.64e-11), *STAT1* (p=1.32e-08) and *MX1* (p=4.960e-04), and *CTSD* (Cathepsin D, p=4.07e-16), *AP2M1* (p=3.86e-11), *CTSC* (DPP1, p=4.78e-11) and *KIF5B* (UKHC, p=2.82e-08) in TCGA cohort (cBioPortal for cancer genomics, https://www.cbioportal.org/).

Interestingly, together with IFN signaling and antigen presentation, we also found an upregulation of the phosphorylated form of STAT3 (***Figure R18A***), a major modulator of inflammation and immune system, and well stablished downstream effector of cytokines and growth factors in GB [318]. Of note, TCGA GB samples also showed a positive correlation between *LAMP2* and *STAT3* (***Figure R18C***). These data suggest that STAT3 may be associated with CMA process, but further studies would be needed to elucidate their relationship in detail.

Having this in mind, and in order to further characterize the impact of CMA blockage on immune response, we next studied the comprehensive profile of cytokines secreted by *shL2A* GSCs. For this, we performed a cytokine array with supernatants of control and *shL2A* GNS166 cells. Overall, a total of 50 cytokines were significantly reduced, being IGFBP-4, Angiogenin (ANG), VEGF, SDF-1, IL-8, IL-6, IGFBP-2, Eotaxin-3 and TGF-β1, among the most diminished ones (***Figure R19A***). On the contrary, IP10, also known as CXCL10 and which is secreted in response to IFN-γ, was clearly upregulated in *shL2A* cells (***Figure R19A***). Accordingly, the altered expression of *IGFBP2, IGFBP4, ANG, Eotaxin-3, SDF1* and IP10 was also validated at mRNA level, not only in GNS166 cells (***Figure R19B***), but also in GNS179 (***Figure R19C***). Nevertheless, VEGF, IL6 and IGFBP1 mRNA expression was upregulated in *shL2A* cells (***Figure R19D***), suggesting distinct regulatory processes among different cytokines. We next wondered whether the reduction of the validated cytokines in *shL2A* could be translated into clinical data. Thus, we took advantage of TCGA cohort GB data, and we found a positive correlation between *LAMP2* and *ANG, Eotaxin-3, SDF-1,* and *IGFBP-4* (***Figure R20A***). Together with this, the comparative KEGG analysis of *LAMP2* high and low expressing GB patients from TCGA cohort highlighted inflammation-associated pathways as the most differentially expressed ones (***Figure R20B***). All these data indicated that CMA regulates GSCs inflammatory and immune response.

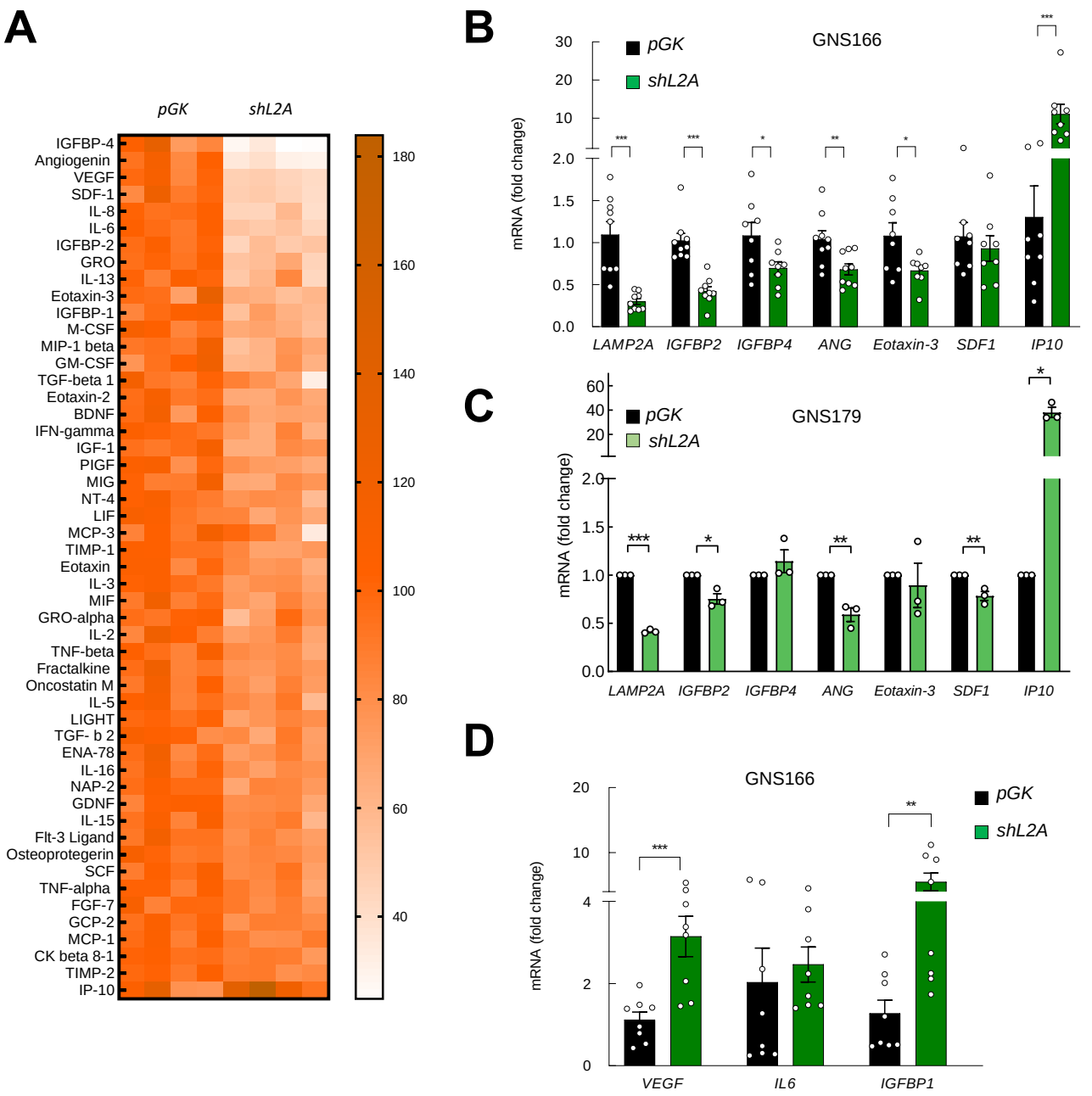

Figure R19. *LAMP2A* silencing reduces the secretion of cytokines in GSCs. (A) Representative heat map of the altered secretion of cytokines from supernatants of GNS166 *pGK* and *shL2A* ($p<0.05$, n=4); **(B)** Relative mRNA expression of *LAMP2A*, *IGFBP2*, *IGFBP4*, *ANG*, *Eotaxin-3*, *SDF-1* and *IP10* in *pGK* and *shL2A* GNS166 (n=8) and **(C)** GNS179 (n=3); **(D)** Relative mRNA expression of *VEGF, IL6, IGFBP1* and *IL1α* in GNS166 *pGK* and *shL2A* (n=8).

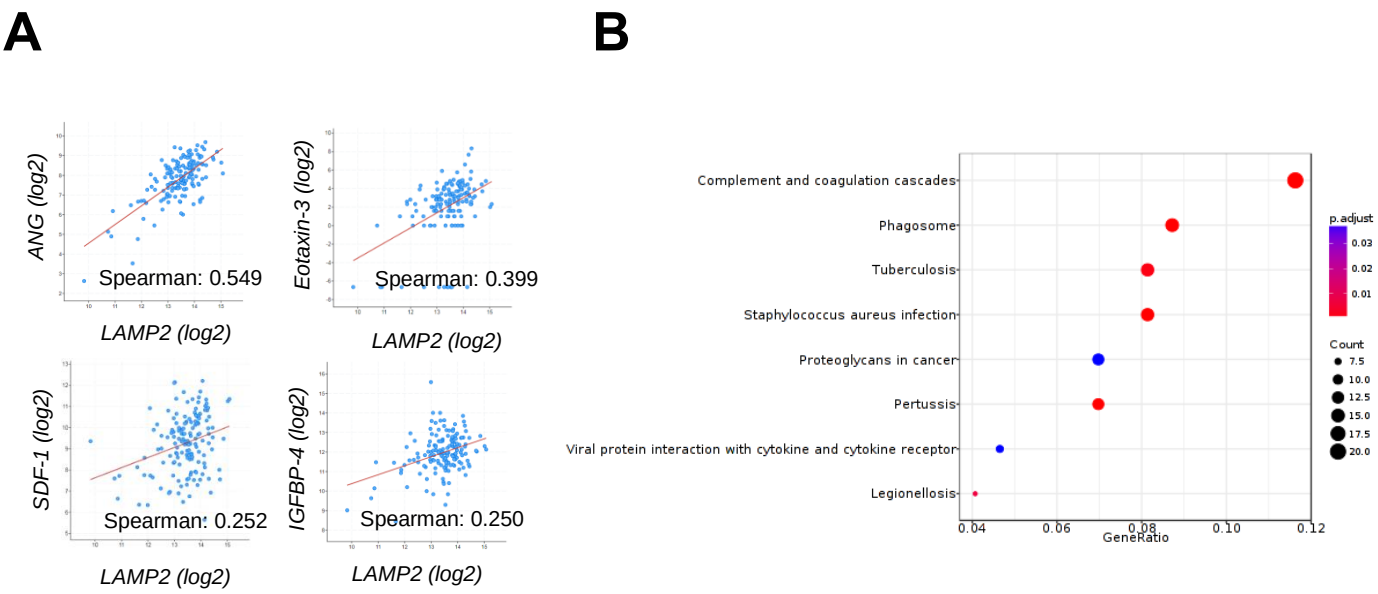

Figure R20. *LAMP2* correlates with inflammation in TCGA cohort. (A) Association study of *LAMP2* with *ANG* (p=2.40e-13), *Eotaxin-3* (p=3.56e-07), *SDF-1* (p=1.701e-03) and *IGFBP-4* (p=1.904e-03) in the TCGA cohort (cBioPortal for cancer genomics, https://www.cbioportal.org/); **(B)** Dotplot of KEGG enrichment analysis of *LAMP2* high vs low in the TCGA cohort (p<0.05).

1.6. *LAMP2A* knock down alters ECM related pathways in GSCs

ECM interaction associated processes appeared to be significantly dysregulated both in the proteomic (***Figure R9D, R11***) and transcriptomic studies (***Figure R12B***). Among dysregulated proteins, several integrin subunits such as ITGB4, ITGA6, ITGAV or ITGA3, and ECM components as LAMA5 or LAMB2, were found diminished (***Figure R9C***). Of note, immunoblot studies validated the reduction in ITGA6 and ITGB4 in GNS166 and U251 cells (***Figure R21A***). Moreover, we also looked at the mRNA expression of some dysregulated transcripts in RNAseq study, validating the reduction of *ITGA3, ITGA6, ITGAV, ITGB3, ITGB4, LAMC1, COL4A5* and *FN1* in GNS166, GNS179 and U251 (***Figure R21B, C***). Interestingly, all these markers presented significant positive correlation with *LAMP2* in GB samples from the TCGA cohort (***Figure R21D***).

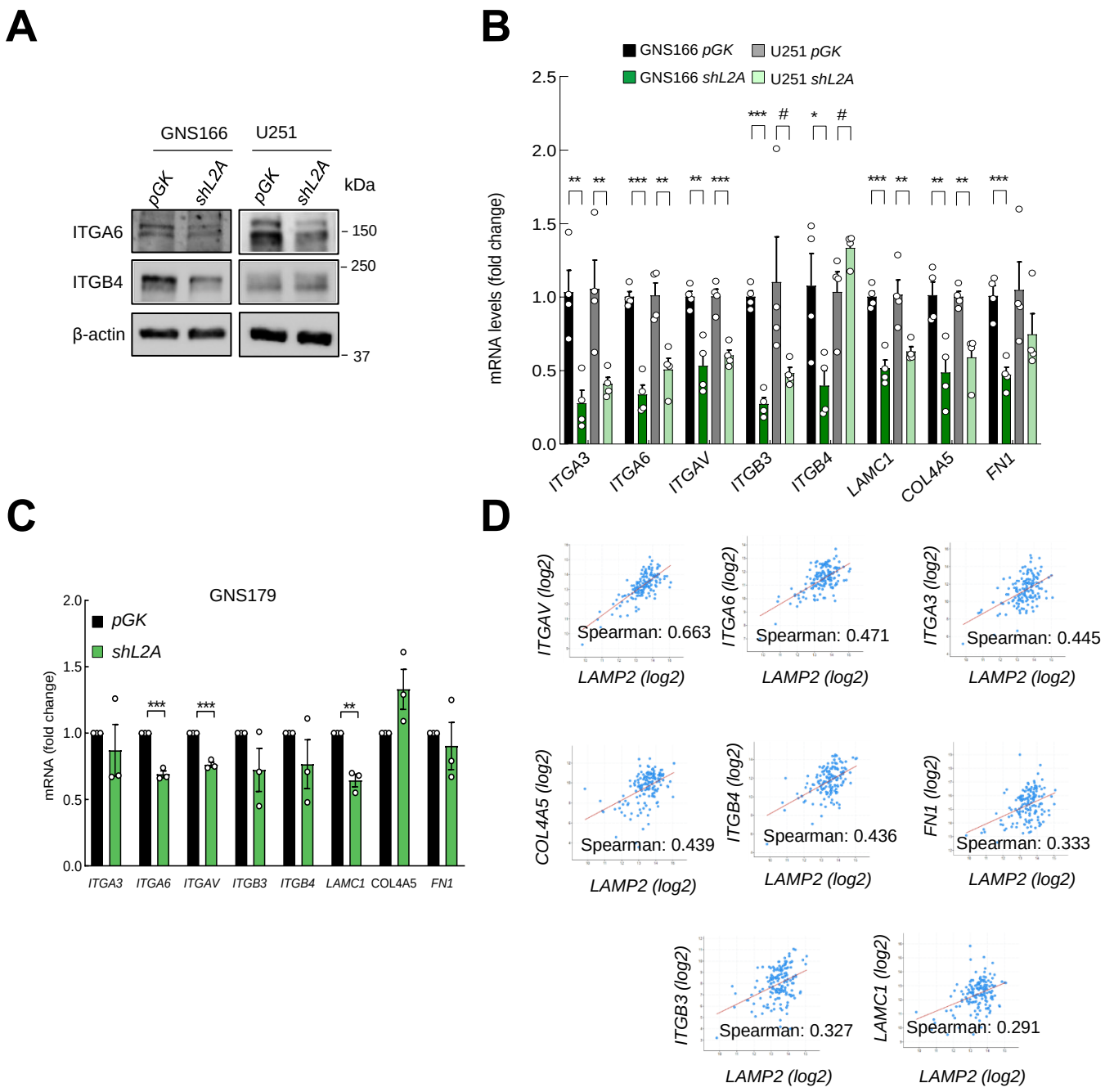

Figure R21. *LAMP2A* silencing reduces ECM interaction and content markers in GSCs. (A) Representative immunoblot of ITGA6, ITGB4 and β-actin in GNS166 (n=4) and U251 (n=3) cells; **(B)** Relative mRNA expression of ECM interaction markers *ITGA3*, *ITGA6*, *ITGAV*, *ITGB3*, *ITGB4*, *LAMC1*, *COL4A5* and *FN1* in *pGK* and *shL2A* GNS166, U251 (n=3/4) and **(C)** GNS179 (n=3) cells; **(D)** Association study of *LAMP2* with *ITGAV* (p= 1.31e-20), *ITGA6* (p= 8.90e-10), *ITGA3* (p= 8.92e-09), *COL4A5* (p= 1.57e-08), *ITGB4* (p=1.98e-08), *FN1* (p= 2.787e-05) , *ITGB3* (p= 3.949e-05) and *LAMC1* (p= 2.826e-04) in the TCGA cohort (cBioPortal for cancer genomics, https://www.cbioportal.org/);

It has been previously reported that ECM regulates migratory response of GSCs [319]. Having seen the impact of CMA modulation on ECM interaction in GSCs, we decided to study migration and invasion abilities of CMA impaired GSCs. For that we performed transwell migration and collagen invasion assays in control and *shL2A* GNS166 cells. Herein, we found that *shL2A* cells presented ~ 60% reduced migration (***Figure R22A***) and ~ 40% diminishment in invasion (***Figure R22B***) capacities. All these data indicate that CMA regulates GSC interaction with ECM and its content, having an impact on migratory and invasion ability of the cells.

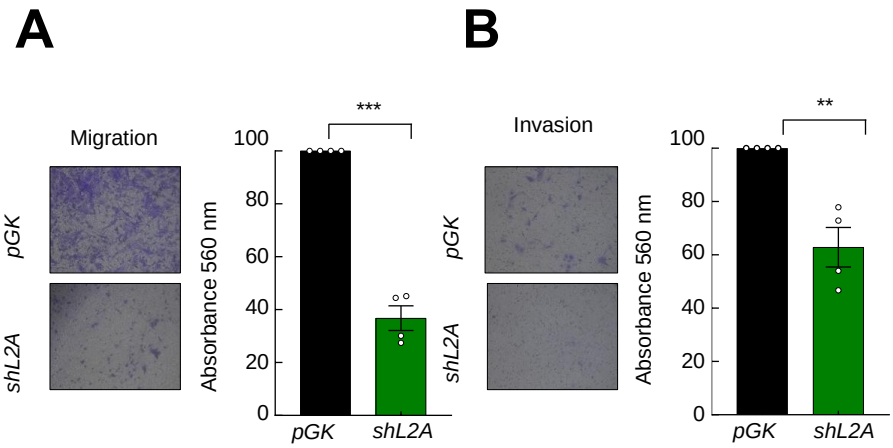

Figure R22. *LAMP2A* knock down impairs migration and invasion in GSCs. **(A)** Representative images (left) and quantification (right) of migration and **(B)** invasion of *pGK* and *shL2A* GNS166 cells (n=4).

1.7. *LAMP2A* levels modulate GB survival

After having demonstrated the role of LAMP2A and CMA in GSC maintenance *in vitro*, we finally moved to study its relevance in an *in vivo* scenario. For that, we injected control and *shL2A* GNS166 cells intracranially into the caudate nucleus of immunodeficient NOD.SCID mice for the evaluation of tumor formation and survival rates. Impressively, *shL2A* GSCs generated delayed and less tumors than controls, leading to significantly extended mice survival (***Figure R23A***). Of note, while control cells formed tumors from day 64 onwards, *LAMP2A* knocked down GSCs did not until day 114 post-inoculation. Indeed, at day 130, 75% of control cells generated tumors, whereas only 22% of *shL2A* GSCs did so. This relevant result indicates that LAMP2A and CMA regulate GSCs maintenance and tumorigenicity not only *in vitro*, but also *in vivo*.

With the goal of elucidating directly the impact of CMA on human GB survival, we analyzed data from TCGA and Rembrandt cohorts. Herein, in line with the results obtained in immunodeficient mice, GB patients with higher levels of LAMP2 expression presented decreased overall survival in both cohorts (***Figure R23B***).

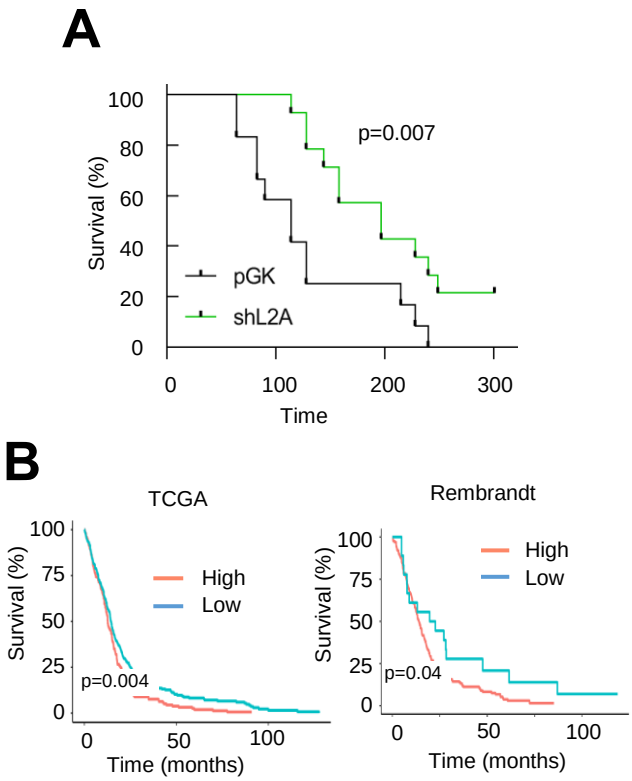

Figure R23. ***LAMP2*A correlates with poor overall survival in GB. (A)** Kaplan Meier survival curve of orthotopic intracranial xenograft of GNS166 *pGK* and *shL2A* cells in NOD.SCID immunodeficient mice (n=12 per condition); **(B)** Kaplan Meier curves representing survival of patients with low vs high expression of *LAMP2* in TCGA (left, n=340 vs n=185, respectively) and Rembrandt (right, n=18 vs n=185, respectively) cohorts. Optimal cutoff points for Kaplan Meier curves were designated by GlioVis database.

The results obtained in this first chapter of the doctoral thesis demonstrate for the first time that LAMP2A and thus, CMA regulates intrinsic activity of a CSC population. In particular, LAMP2A controls mitochondrial metabolism, inflammatory response and interactions with ECM in GSCs, having a direct impact on their maintenance and tumorigenicity, and eventually, in patient overall survival.

2. Characterization of a new small-molecule inhibitor of HDAC6 in GB

2.1. HDAC6 is overexpressed in human GB and GSCs

In order to determine the expression of the 11 human *HDAC*s in GB samples, we firstly took advantage of Rembrandt cohort samples (n=247). Herein, we saw that *HDAC1, 3, 6, 7* were significantly upregulated in GB comparing to healthy control tissue (***Figure R24A***). With the purpose of extending these results to an additional cohort, we analyzed these four HDACs in GB samples from the TCGA cohort (n=160), finding very similar results (***Figure R24B***). Among the four HDACs, *HDAC1* and *HDAC6* were of special interest, based on their distinct cellular localization, and thus, possible different targetome [238]. Thus, we next decided to explore the association of their expression with GB patient survival. Data from Rembrandt, Phillips and Joo cohorts showed that high expression of *HDAC6* (***Figure R24C***) or *HDAC1* (***Figure R24D***) seemed to correlate with poor overall patient survival, with significant results in some of the cases.

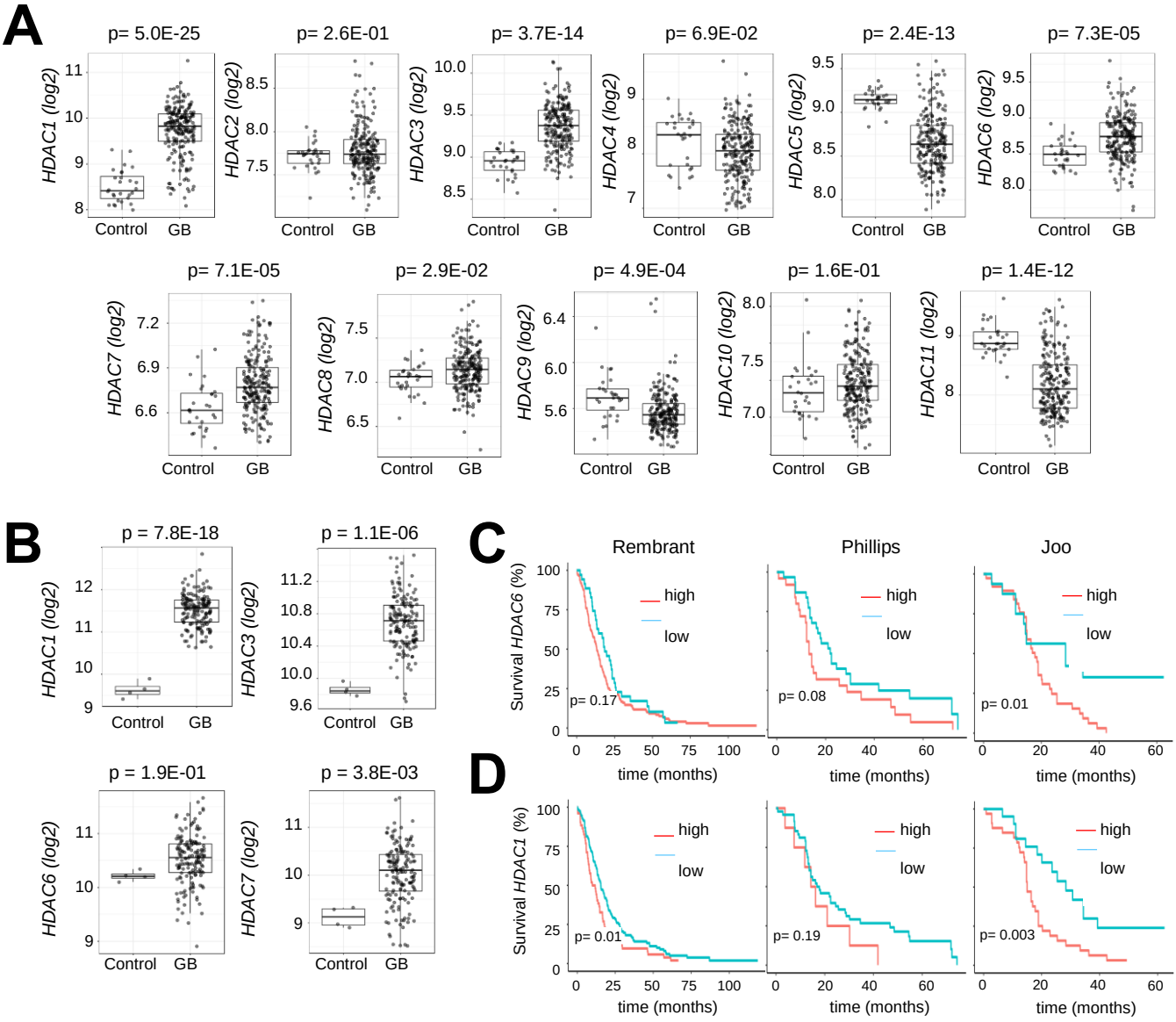

Figure R24. *HDAC6* is overexpressed in GB samples. (A) mRNA expression of the 11 human *HDACs* in control and GB samples from Rembrandt cohort (GlioVis, http://gliovis.bioinfo.cnio.es); **(B)** mRNA expression of human *HDAC1, 3, 6* and *7* in control and GB samples from TCGA cohort; **(C)** Kaplan-Meier curves representing survival of patients with low vs. high expression of *HDAC6* and **(D)** *HDAC1* in Rembrandt (n=33 vs. n=139; n=121 vs. n=51; respectively), Phillips (n=26 vs. n=24; n=42 vs. n=8; respectively) and Joo cohorts (n=10 vs. n=35; n=14 vs. n=31; respectively). Optimal cutoff points were designated by GlioVis database.

With this results in mind, we next characterized the expression of both HDAC6 and HDAC1 in a set of conventional GB cell lines and two patient-derived GSCs. GB cell lines presented variable expression of both HDAC6 and HDAC1 (***Figure R25A***). Of note, both patient-derived GSCs highly expressed HDAC6. Accordingly, oncospheres generated from conventional GB cell lines also presented upregulated expression of both *HDAC1* and *HDAC6*, being *HDAC6* more prominently expressed (***Figure R25B***). Interestingly, clinical data from GB

patients from the TCGA cohort showed a significant positive correlation of *HDAC6* expression with GSC markers *SOX2*, *SOX9*, *NANOG*, *NESTIN*, *OCT4* and *CD133* (***Figure R25C***), whereas *HDAC1* did not with none of them (***Figure R25D***).

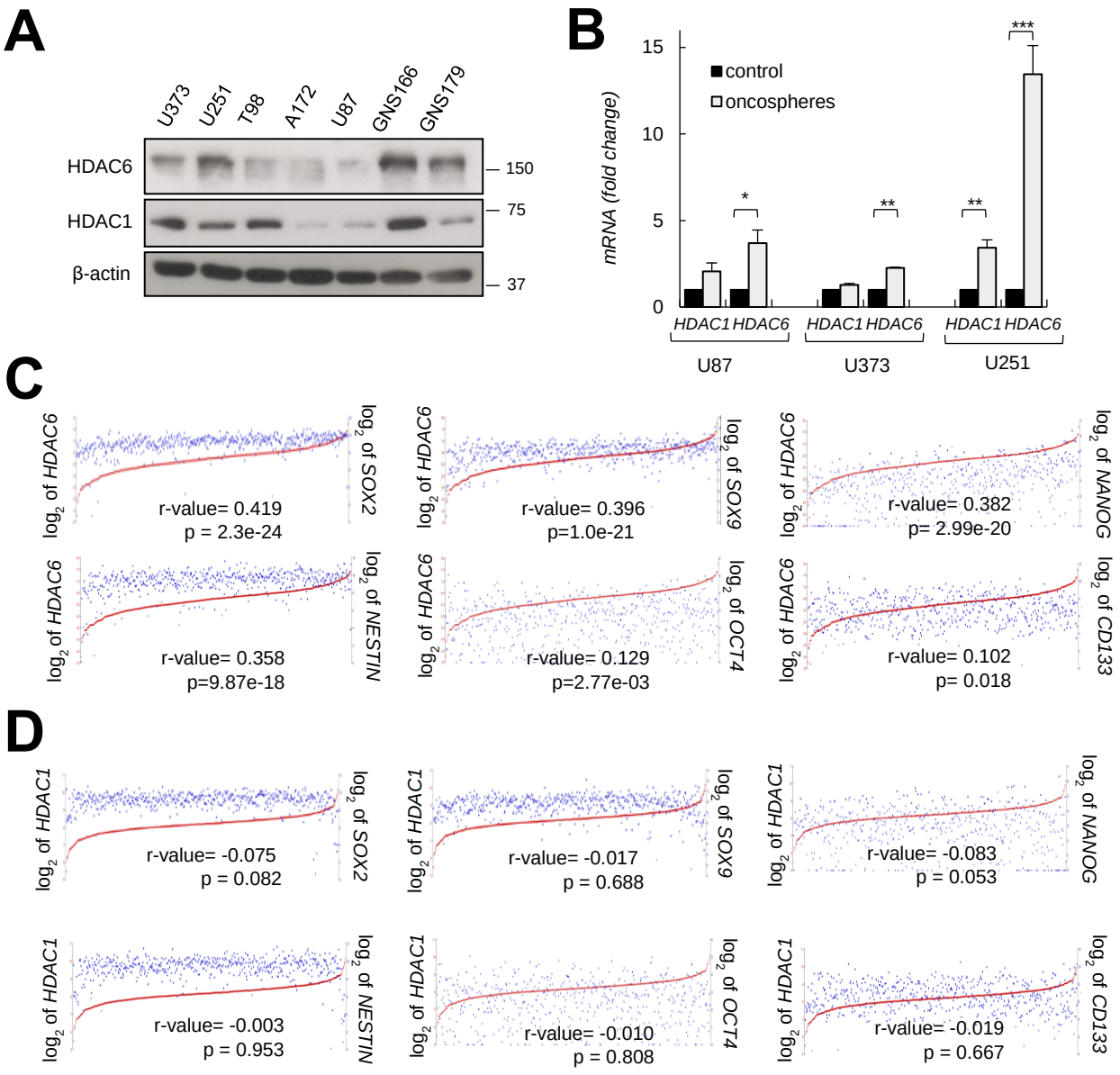

Figure R25. ***HDAC6* is enriched in GSCs. (A)** Representative immunoblots of HDAC1 and HDAC6 expression for a set of glioma cell lines, including patient-derived GNS166 and GNS179 stem cells (n=2); **(B)** *HDAC1* and *HDAC6* mRNA expression in U87, U373 and U251 cells cultured in serum and stem cell conditions (n=4); **(C)** Association analysis of *HDAC6* and **(D)** *HDAC1* mRNA expression with *SOX2*, *SOX9*, *NANOG*, *NESTIN*, *OCT4* and *CD133* in TCGA cohort (R2: Genomics Analysis and Visualization Platform: https://r2.amc.nl).

Altogether, these results demonstrate that both *HDAC1* and *HDAC6* are highly expressed in GB and are associated with poor overall survival. Moreover, HDAC6 is significantly enriched in GSC subpopulation, correlating positively with many stem cell markers. Thus, HDAC6 may be a potential therapeutical target in GSCs.

2.2. The novel HDAC6 inhibitor JOC1 reduces GB cell viability

The pharmacological strategy for inhibiting HDACs have been tested in various types of cancer, including GB (https://clinicaltrials.gov/). However, their lack of selectivity causes several side effects, limiting the therapeutic window of the compounds and eventually, their effectiveness. Thus, we decided to collaborate with a company that had recently developed an HDAC6 inhibitor with promising preclinical results in mantle cell lymphoma [299]. For strategy purposes of the company, the name of the compound in this doctoral thesis and in the resulting publication [300] changed to JOC1.

We firstly tested the capacity of JOC1 for inhibiting HDAC6 in GB cells. For that, we studied the expression of HDAC6 and the acetylated form of its main substrate α-tubulin. Our results revealed that increasing concentrations of JOC1 clearly induced the acetylation of α-tubulin in both U87 conventional GB cells and the patient-derived GNS179 cells (***Figure R26A***), indicating the efficient inhibition of HDAC6 activity. Indeed, JOC1 does not change total expression of HDAC6 protein (***Figure R26A***), which could be expected as this compound acts as an inhibitor of HDAC6 function. Of note, we also found an upregulation of the acetylated form of histone 3 (H3) (***Figure R26A***), a main substrate of nuclear HDACs. However, this effect was not as strong as α-tubulin acetylation, indicating that the activity of JOC1 is more selective inhibiting HDAC6 than nuclear HDACs. This result agrees with *in vitro* enzymatic studies previously performed, which demonstrated an exceptional specificity for decreasing HDAC6 enzymatic activity (IC_{50} < 1nM), being nuclear HDAC1 the second member of the family whose activity was more inhibited, with an IC_{50} value over 50 nM [299].

After verifying the HDAC6 inhibitor function of JOC1, we next studied the effect of the compound in the viability of GB cell lines. For that, we used a set of conventional GB cell lines and compared their sensitivity to the one exhibited by control normal human astrocytes (NHA). After 72 h of treatment with increasing concentrations of JOC1, we

observed that all GB cell lines presented remarkably lower IC_{50} values than NHA cells (***Figure R26B***), indicating that JOC1 cytotoxic effect is higher in GB cells than in control ones.

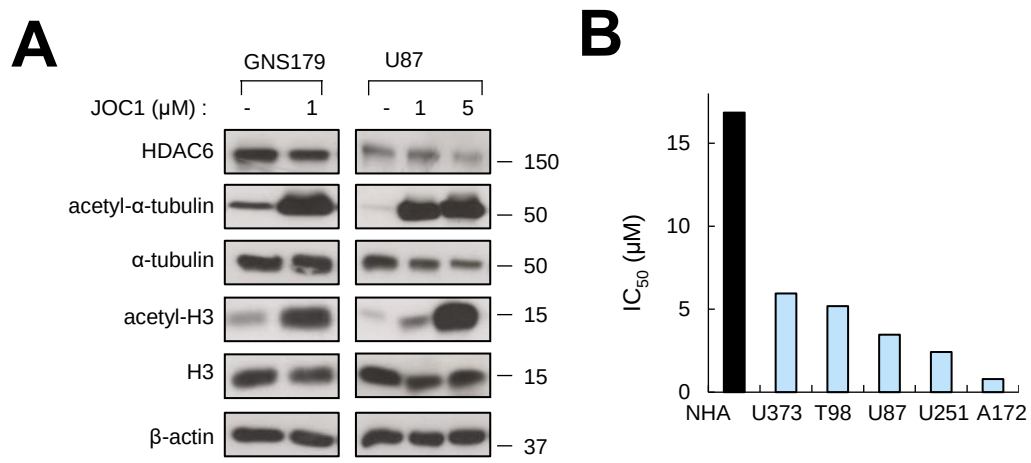

Figure R26. JOC1 compound inhibits GB cell viability by inhibiting HDAC6. (A) Representative immunoblots of HDAC6, its main target (acetyl-) α-tubulin and nuclear HDAC target (acetyl-) histone-3 (H3) after 48 h of control, 1 μM and 5 μM JOC1 treatment in patient-derived GNS179 and U87 cells (n=3); **(B)** IC_{50} values (μM) measured by MTT assay (n=3), after 72 h of increasing concentrations of JOC1 treatment in control (NHA, normal human astrocytes) and glioma cell lines.

2.3. The novel HDAC6 inhibitor is more efficient than other HDACi available

In order to assess the potential of JOC1 as an antitumor agent, we next compared its efficacy to the pan-HDACi SAHA and the HDAC6-selective inhibitor Tubastatin A. For that, we treated U251 cell line with low concentrations of the three compounds for 48 h and we studied their effect in HDAC function. Importantly, we found that only JOC1 was able to induce α-tubulin acetylation at the concentration of 10 nM, whereas SAHA and Tubastatin A were not (***Figure R27A***). Moreover, 100 nM JOC1 promoted stronger α-tubulin acetylation than the other HDACi studied (***Figure R27A***), indicating its remarkable efficacy as an HDAC6 inhibitor. As previously mentioned, in this experiment we also observed the upregulation of the acetylated form of H3, being this effect similar at 10 nM of all three compounds studied, and lower than the α-tubulin hyperacetylation in both concentrations (***Figure R27A***). Interestingly, this molecular pattern was also translated into cellular effects, as JOC1 presented greater cytotoxic efficacy in all seven GB cell cultures studied (***Figure R27B***). In line with this, JOC1 also promoted higher induction of apoptosis, measured by cleaved PARP (***Figure R27A***), reinforcing its potency as a cytotoxic agent.

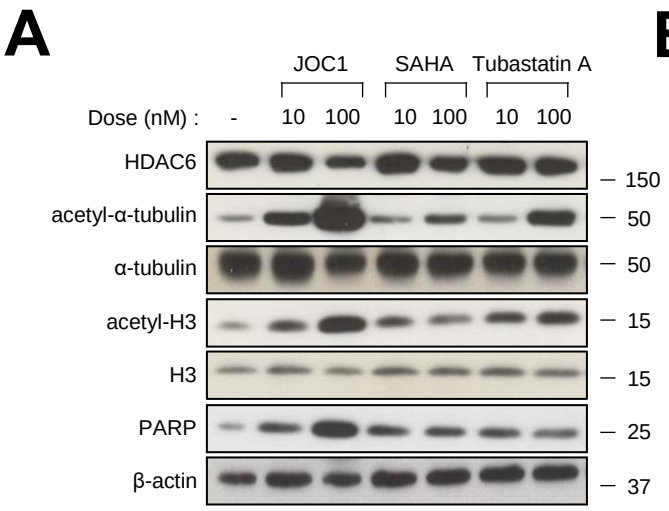

B

IC_{50} (µM)	JOC1	SAHA	Tubastatin A
U87	3.46	9.99	23.67
U251	2.42	22.07	26.27
U373	5.95	47.10	13.19
T98	5.19	4.69	104.30
A172	0.79	4.29	52.50
GNS166	12.48	41.09	26.37
GNS179	5.26	11.24	175.40

Figure R27. JOC1 compound is more efficient than other HDACis available. (A) Western blot analysis of the expression of HDAC6, (acetyl-)α-tubulin, (acetyl-) H3 and cleaved PARP in U251 cell line after 48 h treatment of control, 0.01 µM and 1 µM of JOC1, pan-inhibitor SAHA and HDAC6-selective-inhibitor Tubastatin A; **(B)** Cell viability IC_{50} values (µM) of JOC1, SAHA and Tubastatin A at cell viability level of conventional and patient-derived GSCs, at 72 h (n≥3).

The use of combined therapy as a pharmacological strategy enables treating the tumor through various molecular pathways. Thus, we next wondered whether JOC1 could be a good candidate for combining it with the gold standard treatment in GB, TMZ. To test this idea, we treated U87 cell line with TMZ alone, and in combination with JOC1 or SAHA for 72 h. Herein, we saw that both combinations presented increased cytotoxic activity than TMZ alone, having the combination of JOC1 plus TMZ the strongest effect (30% viability vs. 50% SAHA/TMZ and 85% TMZ alone) (***Figure R28***). These results confirm the potential of JOC1 compound as a cytotoxic agent in GB, being more efficient than other available HDACis, even in combination with TMZ.

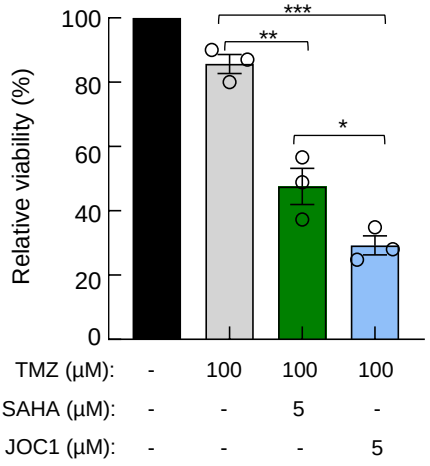

Figure R28. Combinational therapy of TMZ with JOC1 is more effective than the one with SAHA. Comparative study of cell viability in combinational treatments of TMZ and JOC1 or SAHA, after 72 h in U87 (n=3).

2.4. The novel HDAC6 inhibitor JOC1 suppresses GSC activity *in vitro*

To test the effect of JOC1 directly in GSC subpopulation, we studied the cellular properties of patient-derived GNS179 in response to increasing concentrations of JOC1. Notably, JOC1 reduced the proliferation of GNS179, measured both by immunofluorescence analysis of the mitosis marker phosphorylated H3 (***Figure R29A***) and by cell counting (***Figure R29B***).

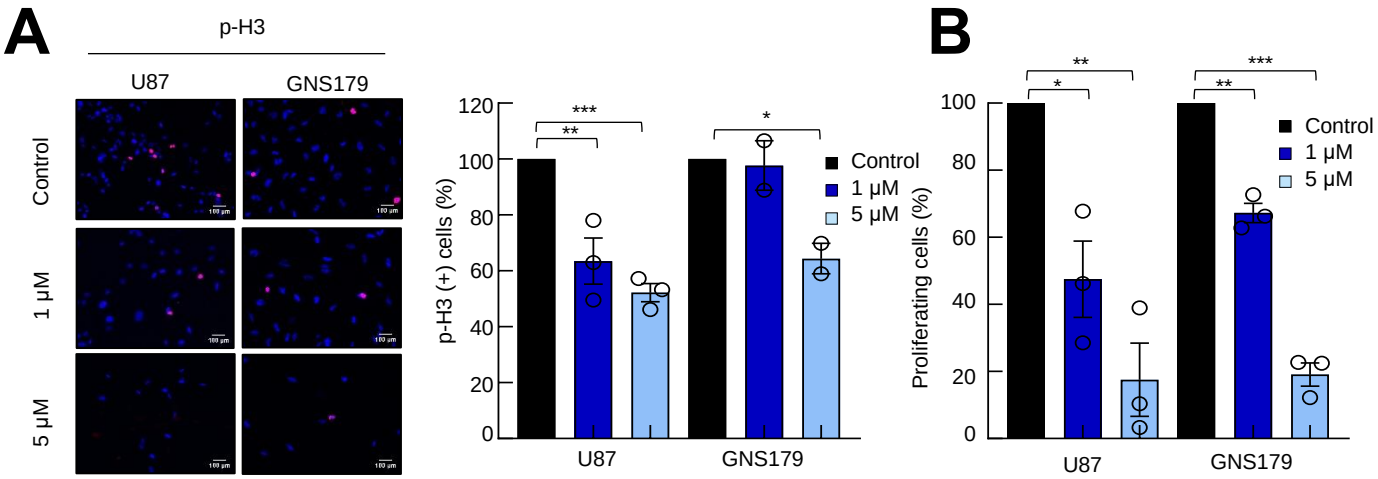

Figure R29. JOC1 inhibits proliferation of GSCs. (A) Representative images and quantification of phospho-histone-3 (p-H3) positive cells with increasing dosage of JOC1 in both U87 and GNS179 cells, at 48 h (n=3); **(B)** Proliferating cell percentage comparing U87 and GNS179 cells, after vehicle, 1 µM and 5 µM JOC1 72 h treatment (n=3).

Similar results were observed in U87 (***Figure R29A, B***), indicating an effect also in tumor bulk. In order to study more deeply the GSC subpopulation, we next performed oncospheres assay in the presence of increasing concentrations of JOC1 in U87. Accordingly, we found that JOC1 significantly impairs the generation of both 1^{ry} CSCs (reduction of ~ 50 % at 1 µM / ~ 95 % at 5 µM) (***Figure R30A***) and 2^{ry} CSCs (reduction of ~ 80 % at 1 µM / ~ 90 % at 5 µM) (***Figure R30B***), demonstrating a robust effect in self-renewal of GSCs. Supporting these results, we observed that 48 h of treatment with 1 µM JOC1 reduced the protein expression of GSC markers BMI-1, SOX9 and SOX2 in GNS179 (***Figure R30C***). Similar results were obtained for BMI-1 in U87 cells (***Figure R30C***), a model whose basal expression of SOX9 and SOX2 is not detectable [111].

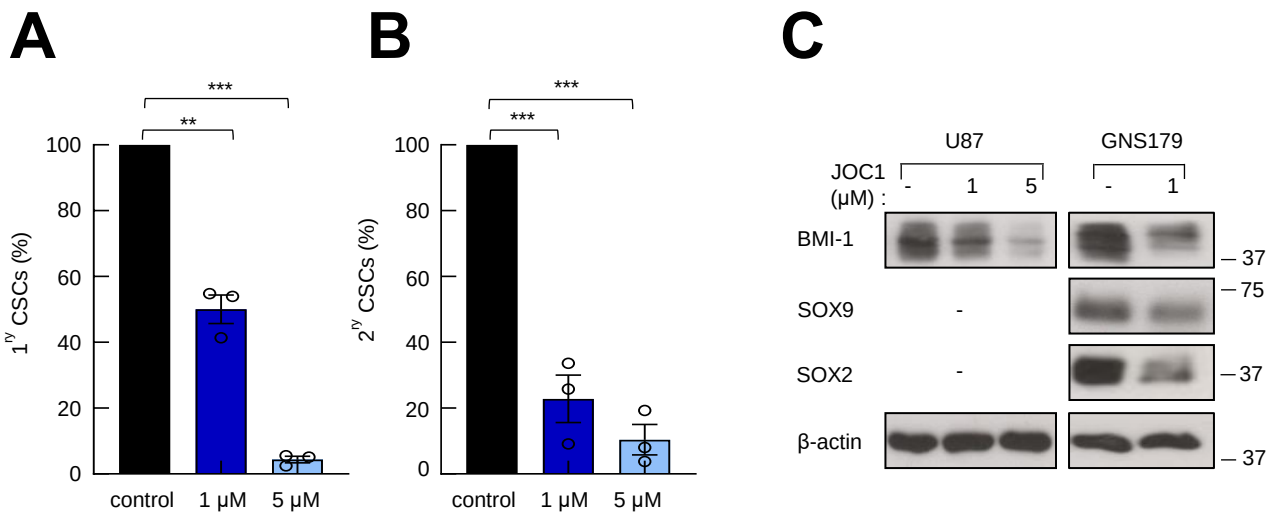

Figure R30. JOC1 inhibits self-renewal and molecular markers of GSCs. (A) Relative quantification of 1ry **(B)** and 2ry CSCs forming capacity with increasing dosage of JOC1, in U87 cells (n=3); **(C)** Western blot assay of BMI-1 SOX9 and SOX2 after 48 h with control, 1 µM or 5 µM JOC1 treatment in GNS179 and U87 cells (n=3).

The potential GSC differentiating effect of JOC1 was further confirmed with the dose-dependent induction of *MKP1* expression (***Figure R31A***), which we had previously associated with impaired GSCs activity and enhanced differentiation [302]. With the purpose of elucidating the involvement of *MKP1* in JOC1 response, we examined cell viability of U87 transduced with control or *MKP1* overexpressing vector, in the presence of the combination of TMZ plus JOC1 (***Figure R31B***). Herein, we determined that high levels of *MKP1* sensitized U87 to the tested therapeutic strategy, revealing that MKP1 mediates, at least in part, the activity of JOC1.

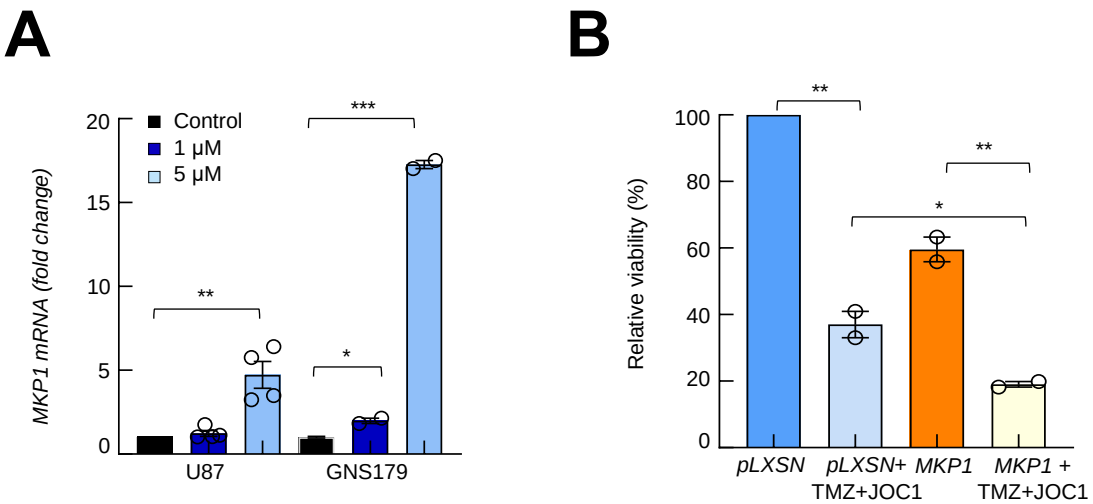

Figure R31. JOC1 induces *MKP1* differentiation marker expression. (A) *MKP1* mRNA expression in U87 and GNS179 cells treated with control, 1 µM and 5 µM JOC1 for 48 h (n=4); **(B)** MTT cell viability assay of U87 cells infected with empty vector *pLXSN* or *MKP1* overexpression, treated with 100 µM TMZ and 1 µM JOC1 for 72 h (n=2).

Together with differentiation of GSCs, we wondered whether JOC1 could also induce apoptosis. With this aim, we firstly studied caspase-3 activation by immunofluorescence, observing that 48h of increasing concentrations of JOC1 promoted dose-dependent gain of this marker in GNS179 (***Figure R32A***). This result was accompanied by the upregulation of PARP cleavage (***Figure R32B***) and *BAX* mRNA expression (***Figure R32C***). These results show that JOC1 impairs GSC activity inducing both differentiation and apoptosis.

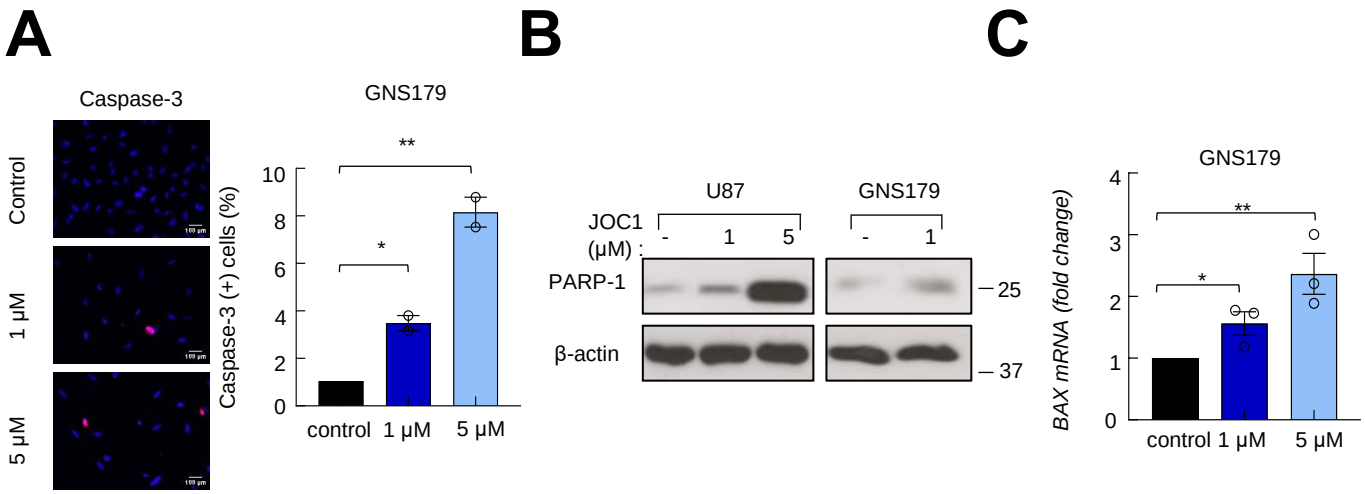

Figure R32. JOC1 induces apoptosis in GSCs. (A) Representative images and quantification of Caspase-3 positive cells after 48 h of control, 1 µM or 5 µM JOC1 in GNS179 cells, by immunofluorescence (n=3); **(B)** Immunoblot of cleaved PARP-1 after 48 h with control, 1 µM or 5 µM JOC1 treatment in GNS179 and U87 cells (n=3); **(C)** *BAX* mRNA expression in GNS179 after increasing dosage of JOC1 treatment for 48 h (n=3).

2.5. The novel HDAC6 inhibitor JOC1 promotes differentiation and cell death, and inhibits cell cycle in GSCs

In order to characterize the comprehensive profile of transcriptional alterations induced by JOC1 treatment, we performed a microarray gene expression analysis in patient-derived GNS166 in the absence and presence of 5µM of the novel compound. Overall, a total of more than 1,000 genes were significantly dysregulated by JOC1. For getting a general landscape of altered pathways, we carried out a gene ontology analysis of dysregulated transcripts. Interestingly, the top canonical pathways within the upregulated networks were associated with cell differentiation, cell death, protein modifications, signaling, motility, transport, and others, being cell differentiation the most remarkable one (***Figure R33A***). On

the contrary, among downregulated pathways, processes associated with cell cycle were clearly the most abundant ones, with a few pathways linked to transcriptional regulation and others (***Figure R33B***). Supporting these data, we observed a dose-dependent induction of the differentiation marker *TUJ1* (***Figure R33C***) and the cell cycle inhibitor $p21^{Cip1}$ (***Figure R33D***) mRNA expression in GNS179 after 48 h of JOC1 treatment.

The microarray results obtained in GNS166 treated with JOC1 were in line with the cellular and molecular alterations that we had seen in GSCs. Accordingly, GB samples from TCGA also supported these results, as they presented the previously mentioned significant positive correlation of *HDAC6* with GSC markers (***Figure R25C***), as well as with cell cycle regulators *CDK11, Cyclin D2, CDK19* and *EGFR*, and a negative correlation with $p21^{Cip1}$ (***Figure R34A***). Of note, there was not significant correlation with almost any of the markers in the case of *HDAC1* (***Figure R25D, R34B***). These data reinforce the potential of HDAC6 as a promising therapeutic target in GB and demonstrates that JOC1 is an effective and selective inhibitor of it.

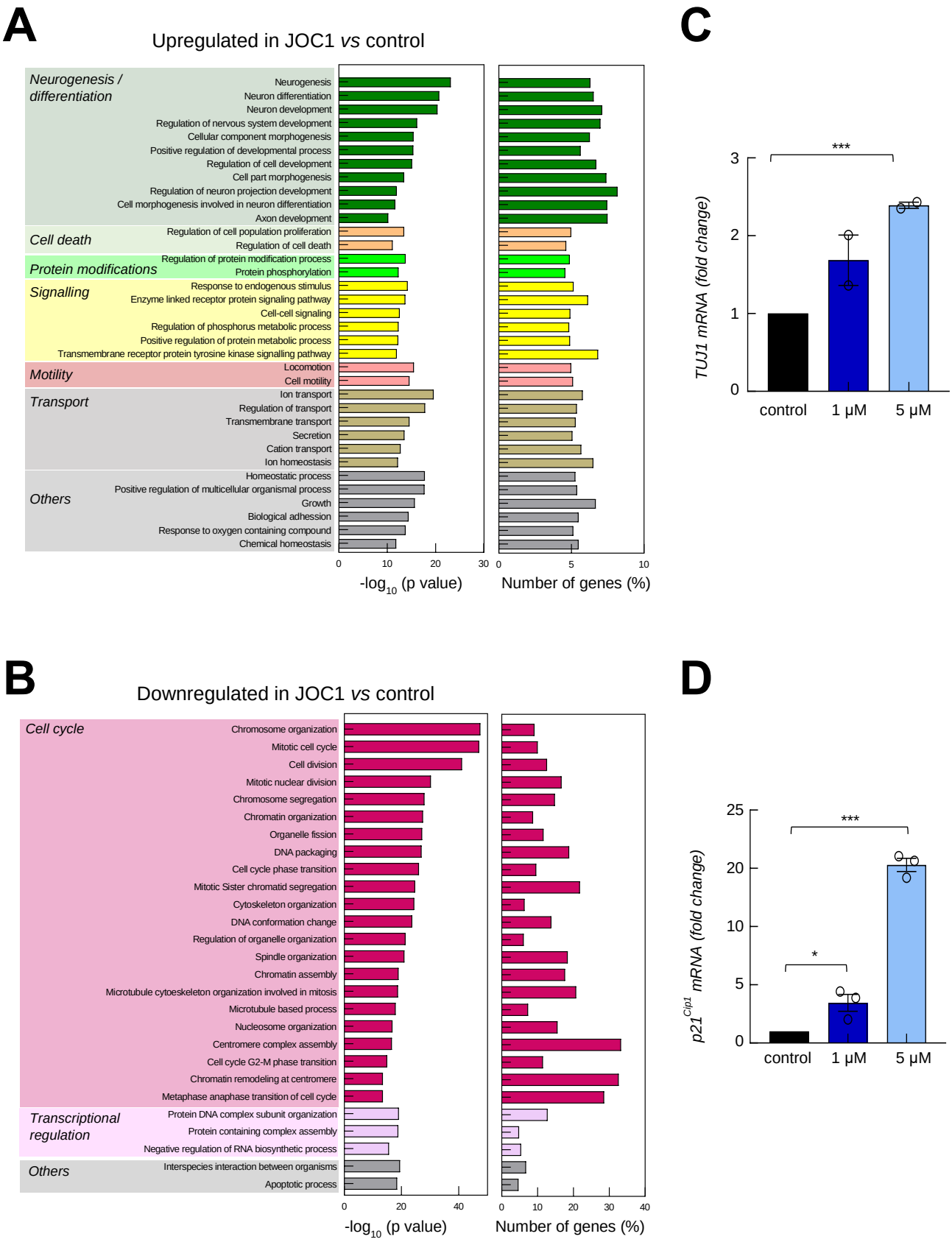

Figure R33. JOC1 treatment induces cell differentiation and reduces cell cycle associated transcriptomic pathways. (A) Representative bar plots of biological processes up-regulated and **(B)** down-regulated by 48 h of 5 µM JOC1 in GNS166 cells (n=3), after gene ontology analysis of microarray results. All genes selected for gene ontology analysis presented fold change >1.5 and p value < 0.001 in the microarray; **(C)** *TUJ1* and **(D)** $p21^{Cip1}$ mRNA expression in GNS179 cells treated with control, 1 µM or 5 µM JOC1 for 48 h (n=3).

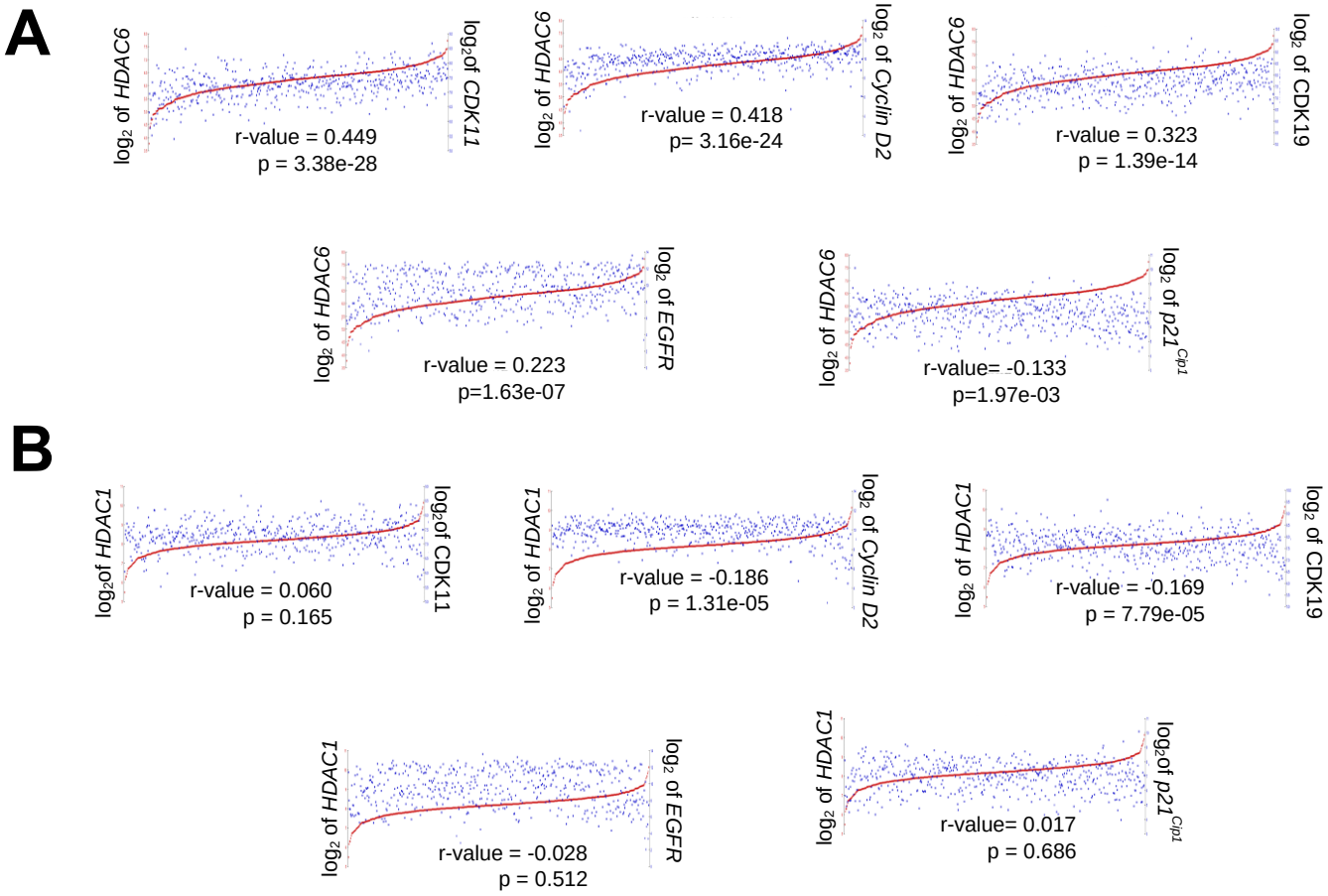

Figure R34. *HDAC6*, but not *HDAC1*, correlates positively with cell cycle regulator markers. (A) Association analysis of *HDAC6* and **(B)** *HDAC1* with *CDK11*, *Cyclin D2*, *CDK19*, *EGFR* and *p21*^{Cip1} in TCGA cohort (R2: Genomics Analysis and Visualization Platform: https://r2.amc.nl).

With the aim of further characterizing the difference between JOC1 and the pan-HDACi SAHA, we performed the same microarray analysis in GNS166 cells upon treatment with 5 µM SAHA for 48 h. We found that both JOC1 and SAHA shared a total of 1,822 upregulated and 1,427 downregulated transcripts, indicating huge similarities in their targetome (***Figure R35A, B***). Notably, however, JOC1 upregulated and downregulated a higher number of genes, which might suggest a wider mechanism of action of JOC1. When performing gene ontology analysis, although both compounds presented very similar altered pathways, such as differentiation and cell cycle, based on obtained q-values, JOC1 altered them more significantly than SAHA (***Figure R35C***). Accordingly, immunoblots corroborated the greater potency of JOC1 compared to SAHA in GNS166, as it triggered higher α-tubulin hyperacetylation and PARP cleavage (***Figure R36***), whereas it showed more decreased expression of the GSC marker BMI-1. These results reveal advanced mechanistic insight of JOC1 functionality, which further supports its antitumor activity at molecular level.

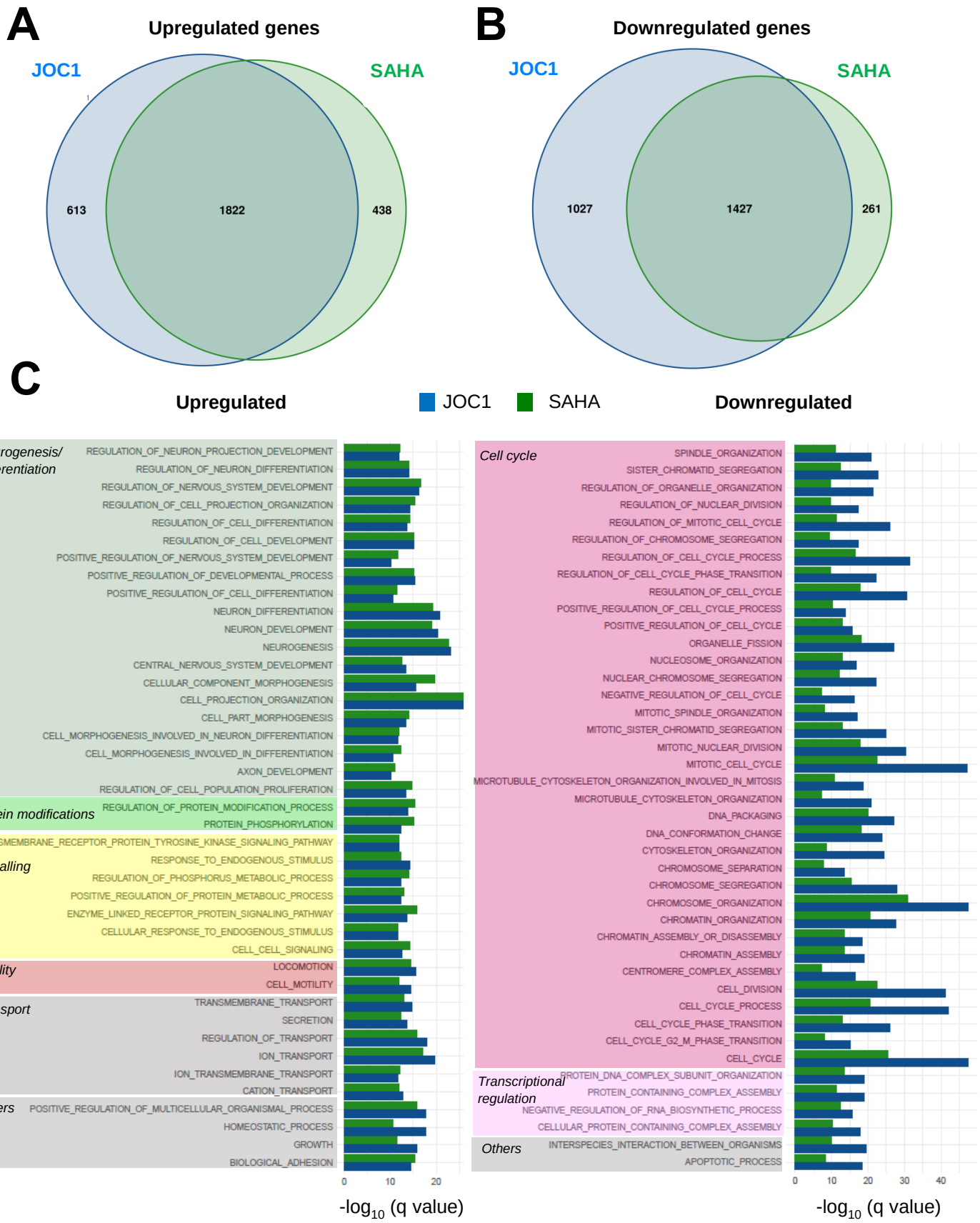

Figure R35. JOC1 treatment presents more potent anti-oncogenic molecular pattern than SAHA. (A) Venn diagram of genes upregulated and **(B)** downregulated in DMSO vs JOC1, DMSO vs SAHA and DMSO-JOC1 vs DMSO-SAHA; **(C)** Comparison of gene ontology analysis of upregulated and downregulated genes, for JOC1 and SAHA drugs, based on q-values (n=3).

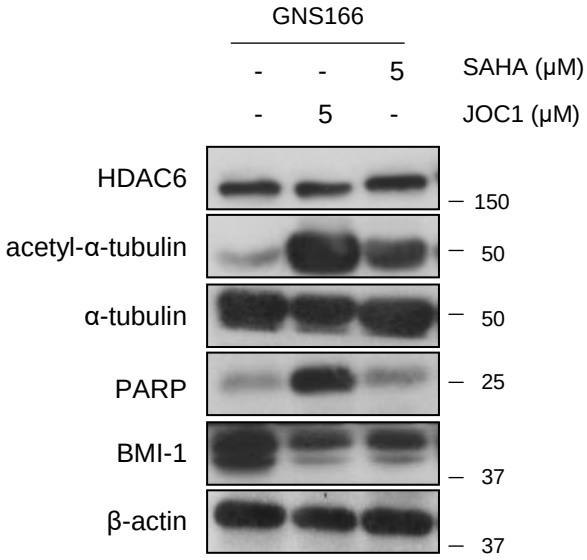

Figure R36. JOC1 is more potent than the pan-inhibitor SAHA in GSCs. Immunoblots for the validation of samples treated with control, 5 μM JOC1 or 5 μM SAHA used for microarray analysis (n=3).

2.6. The novel HDAC6 inhibitor JOC1 reduces GB tumorigenicity *in vivo*

Having reported the *in vitro* potential of JOC1 as an antitumoral agent in GB, we decided to analyze its effect in an *in vivo* scenario. For that, we carried out two different experiments. First, we studied the effect of the novel compound in tumor initiation *in vivo* (***Figure R37A***). For that, we injected $3.5 \cdot 10^5$ U87 cells subcutaneously in the flanks of *Foxn1^{nu}/Foxn1^{nu}* mice and we subsequently started to treat the mice with vehicle or 40 mg/kg JOC1, intraperitoneally. The treatment schedule followed during the experiment comprised 5 consecutive days of treatment and 2 days off, for a total of 30 days (***Figure R37A***). Mice weight was controlled during the experiment, not observing significant changes in any of the time points (***Figure R37B***). Interestingly, we determined that JOC1 treatment delayed tumor initiation and reduced tumor growth (***Figure R37C***). Indeed, after 30 days of experiment, tumors from mice treated with JOC1 presented a reduction of ~30% of the final volume, compared to control ones (***Figure R37D***). Thus, these results indicate that, JOC1 reaches subcutaneous tumors by intraperitoneal administration, reducing tumor initiation and growth, without affecting mice weight.

Next, we performed immunohistochemical studies of the generated tumors in order to confirm the effect of JOC1 molecularly. Meaningfully, tumors from treated mice presented higher expression of acetylated α-tubulin (***Figure R37E***) and reduced number of

cells positive for the proliferation marker Ki-67 (***Figure R37E, F***). These results confirm the specificity and anti-tumor effect of JOC1 *in vivo*.

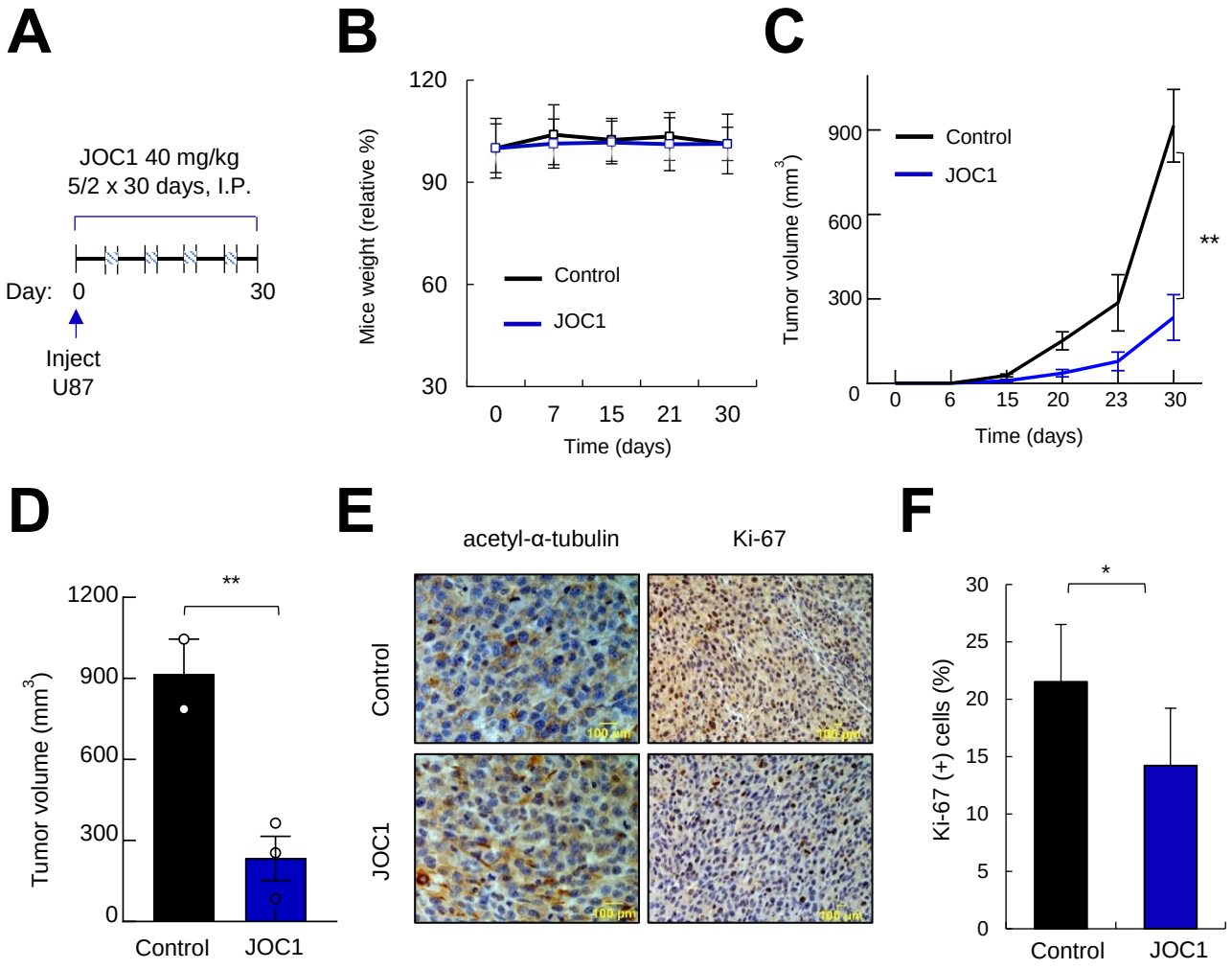

Figure R37. JOC1 treatment slows down tumour initiation *in vivo*. **(A)** Schematic representation of tumour initiation assay. 3.5x10^5 U87 cells were injected *Foxn1^{nu}/Foxn1^{nu}* nude mice and since then, vehicle or 40 mg/kg JOC1 treatment was applied intraperitoneally by 5 days of dosing/2 days off, for 30 days; **(B)** Body weight changes of mice relative to their initial status. Each bar represents mean% ± SE; **(C)** Tumour volume scored at the indicated time points (n=12); **(D)** Measurement of tumour volume at final time point of the experiment; **(E)** Representative images of acetyl-α-tubulin and Ki-67 IHC staining from tumours obtained in **D** (n=4); **(F)** Quantification of Ki-67$^+$ cells in **E** (n=4).

With the purpose of performing an *in vivo* experiment that could be closer to what is observed in the clinic, we planned a second *in vivo* model where the compound was administrated once tumors were formed. In this case, we injected 5 ·10^5 U87 cells subcutaneously in the flanks of *Foxn1^{nu}/Foxn1^{nu}* and, once detectable tumors were formed, mice were grouped for receiving vehicle or 50 mg/kg JOC1 treatment (***Figure R38A***). We followed the same treatment schedule as in the previous *in vivo* experiment, so that we did not detect significant changes in mice weight (***Figure R38A, B***). Of note, JOC1 diminished

tumor growth, causing a reduction of ~50% in the final volume of tumors generated compared to the ones from vehicle-treated mice (***Figure R38C, D***). Similarly, immunohistochemical analysis of the formed tumors presented hyperacetylation of α-tubulin and reduced number of Ki-67 positive cells upon JOC1 treatment (***Figure R38E, F***), confirming its function at molecular level. Together, these data reveal that JOC1 treatment presents potent antitumorigenic activity *in vivo*, even when treatment is initiated once tumors are formed, and seems not to alter mice weight.

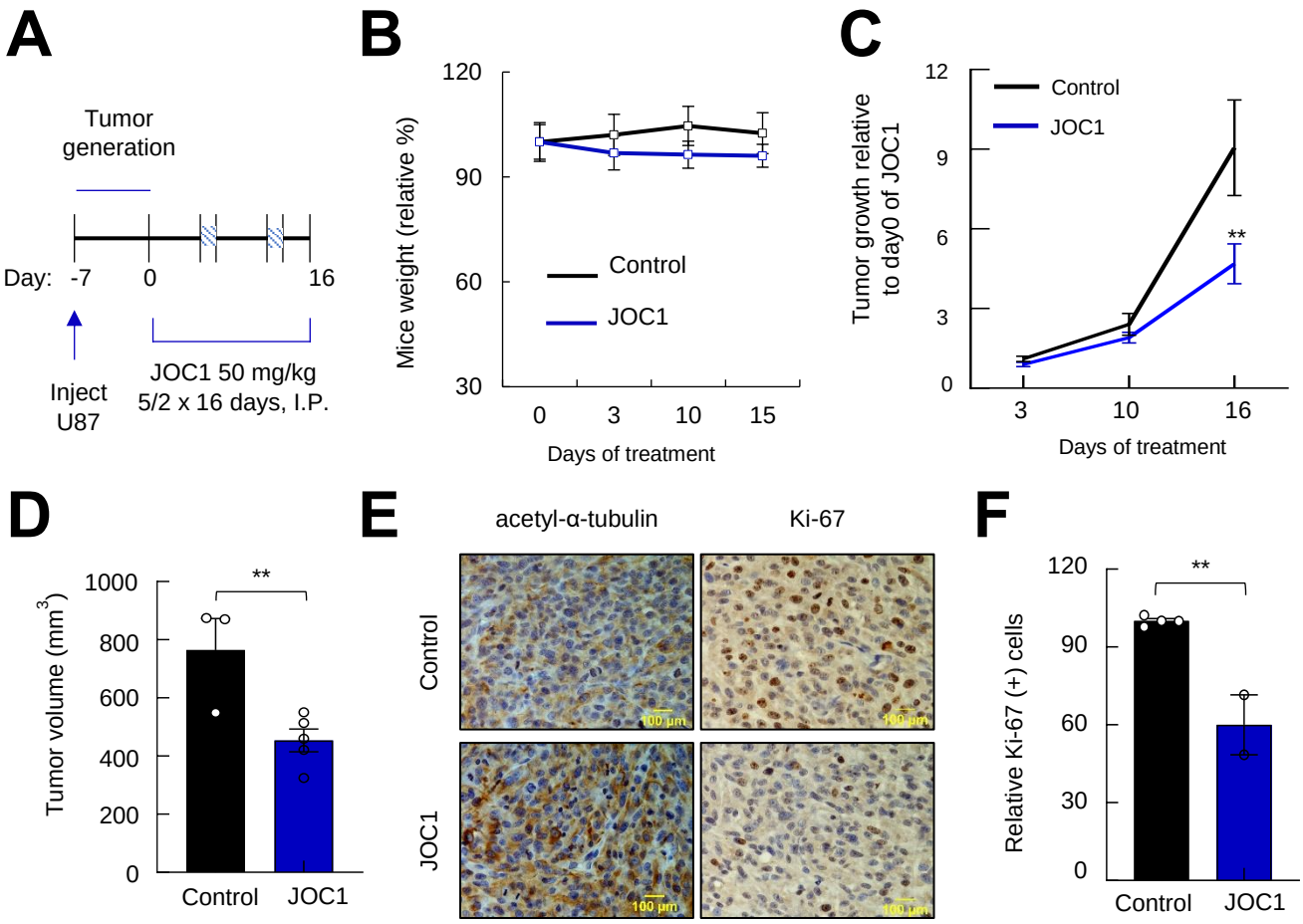

Figure R38. JOC1 treatment reduces tumour growth *in vivo*. **(A)** Schematic representation of tumour growth assay. $5{\cdot}10^5$ U87 cells were injected in *Foxn1*^{nu}/*Foxn1*^{nu} nude mice and, after tumour occurrence, mice were treated with vehicle or 50 mg/kg JOC1 treatment, for 16 days; **(B)** Body weight changes of mice relative to their initial status. Each bar represents mean% ± SE; **(C)** Tumour growth relative to tumour volume at the beginning of JOC1 treatment at the indicated time points; **(D)** Tumour volume measured at the end of experiment; **(E)** Representative images of acetyl-α-tubulin and Ki-67 staining from tumours in **D**; **(F)** Relative quantification of Ki-67$^+$ cells in JOC1 treated compared to control tumours (n=3).

2.7. The vehiculation of JOC1 using protein nanoparticles improves its efficacy

Every compound designed for treating brain disorders have to meet certain characteristics, including the ability of crossing the BBB. Although the *in vivo* potential of JOC1 compound seemed to be promising, its structure and solubility hampered reaching into the brain. Thus, in collaboration with Aitziber Cortajarena's group in CIC biomaGUNE (San Sebastian, Spain), we decided to develop a vehiculation strategy of JOC1 based on nanoparticles of BSA. Herein, JOC1 was added to the reduced BSA solution and then ethanol was added in order to form the nanoparticles (BSANP@JOC1) by coprecipitation. Notably, encapsulation yield increased more than 100 times from pH 7.4 to 11.5, whereas nanoparticle size decreased significantly (***Figure R39A, B***). Thus, following nanoparticle synthesis were done in pH 11.5. Interestingly, the final BSANP@JOC1 nanoformulation had high encapsulation yields and a size below 100 nm (***Figure R39B***), which is ideal for nanodelivery applications. Thus, we finally succeeded in generating ~1mg/mL JOC1 concentration in BSANP@JOC1 form, which presented a homogeneous size distribution (***Figure R39C***). Then, we compared the efficacy of the nanoformulation to the one of the free compound *in vitro*. In particular, we calculated IC_{50} cell viability parameter for each formulation upon 72 h of treatment in U87 cells. Notably, the encapsulation presented a tendency for improving free compound efficacy (IC_{50} BSANP@JOC1=1.819 vs. IC_{50} JOC1 free=2.364) (***Figure R39D***), which demonstrated the successful vehiculation of JOC1.

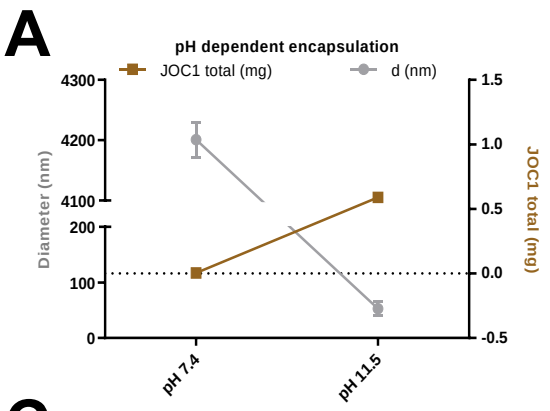

B

	Diameter	PdI	Encapsulation yield
pH 7.4	4201 ± 28.84 nm	0.177	0.08 %
pH 11.5	52.62 ± 12.38 nm	0.022	11.8 %

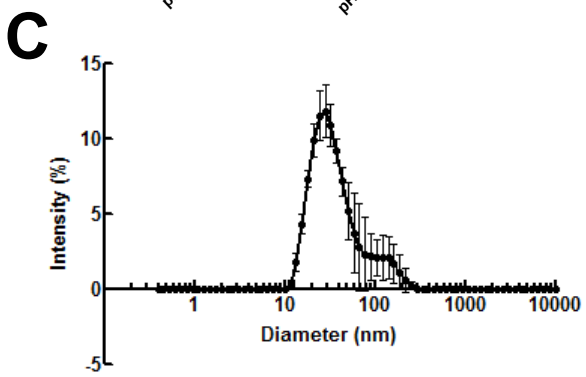

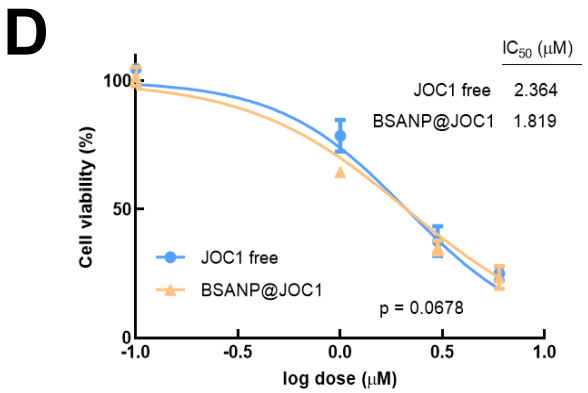

Figure R39. BSA-based encapsulation of JOC1 increases free-compound solubility and efficacy. (A) Representation and **(B)** values of encapsulation yields and size of BSANP@JOC1 at pH 7.4 and 11.5; **(C)** Size-distribution of synthesized BSANP@JOC1, at pH 11.5 and 1 mg/mL JOC1; **(D)** Cell viability of U87 cells after 72 h of control, free JOC1 and BSANP@JOC1 treatment (n=3).

Data generated in this second chapter reveal the potential of HDAC6 as prognostic biomarker and therapeutic target in GB, and describe the antitumor effect of a novel HDAC6 inhibitor, JOC1, in GB, with special emphasis in targeting the population of GSCs.

3. HDAC expression correlates with microglial aging

3.1. HDAC expression is associated with microglial senescence *in vitro*

As a first approach for characterizing the impact of HDACs on microglial aging, we aimed to recapitulate it by an *in vitro* model in which we induced senescence in HMC3 microglial cells with the senescence inductor bleomycin [320]. Herein, we confirmed that 48 h of bleomycin treatment induced the number of HMC3 cells positive for the senescence-associated β-galactosidase activity staining (***Figure R40A***), validating the model. In fact, bleomycin stopped proliferation of HMC3 cells, and induced cell death, as we got negative values for the cumulative population doubling level (ΔPDL) parameter at day 2 and 4 of treatment (***Figure R40B***). In order to study molecular changes preceding this phenotypic effect, we studied HMC3 cells upon 24 h of bleomycin treatment. Treated microglia presented significant upregulation of the cell cycle inhibitor $p21^{Cip1}$ (***Figure R40C***) and *IL6* expression, a marker of senescence-associated secretory phenotype (SASP) [321] on these cells (***Figure R40C***). In this context, we checked the expression of *HDACs*. We selected *HDAC1, 2, 3, 6, 7* and SIRT1, based on their link with age-associated brain disorders [322-327]. Interestingly, bleomycin treated microglia presented a slight upregulation of *HDAC1*, *HDAC3* and *Sirt1* mRNA levels, with a similar tendency but not significant in the case of *HDAC6* and *HDAC7*. (***Figure R40C***). Of note, when activating both control and senescent microglia with lipopolysaccharide (LPS) for 12 h, *IL6* expression was increased in both cases, but no clear changes were observed in any of the studied HDACs (***Figure R40C***). These data may suggest that *HDAC* expression increases upon induction of microglial senescence, but not activation.

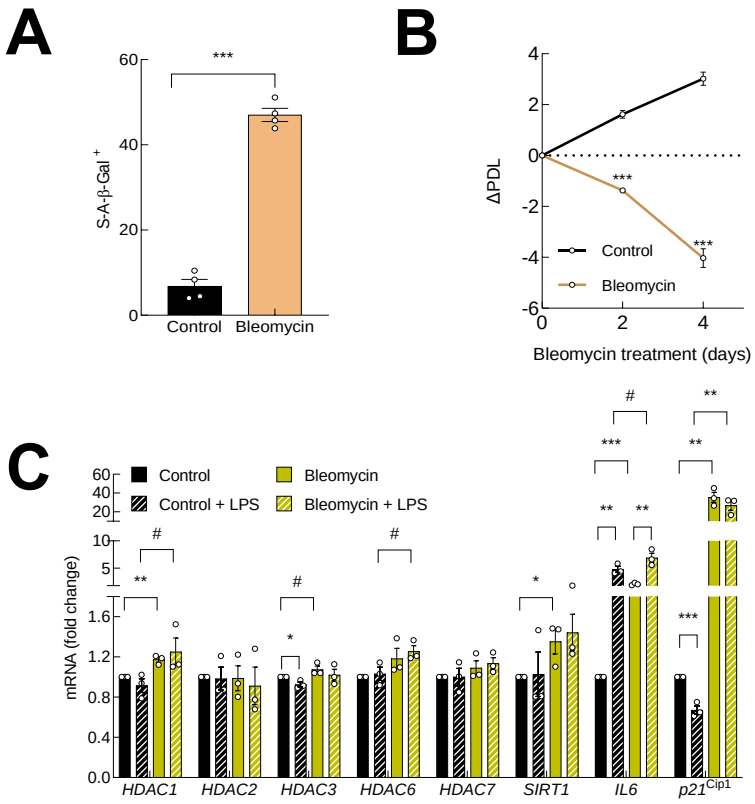

Figure R40. ***HDAC* expression is slightly upregulated with microglial senescence. (A)** Quantification of microglial cells positive for senescence-associated β-galactosidase (S-A-β-Gal) activity staining upon 48 h treatment of 50 µg/mL bleomycin (n=4); **(B)** Cumulative population doubling level (PDL) at day 2 and day 4 treatment of bleomycin (n=4); **(C)** Relative mRNA expression of the indicated transcripts after 24 h with control, 1 µg/mL LPS, 50 µg/mL bleomycin or 50 µg/mL bleomycin plus 1 µg/mL LPS (n=3).

With these results in mind, we next wondered if the upregulation of HDACs could have any impact on microglial senescence. Among HDACs studied, *HDAC1* was the most significantly dysregulated one upon bleomycin treatment, whereas *HDAC2*, although not altered in our study, share some redundant functions with HDAC1 [328]. Thus, we performed their individual ectopic overexpression in HMC3. After validating the upregulation of both transcripts (***Figure R41A***), we studied the expression of $p21^{Cip1}$ in these cells. No changes were observed at basal level, but interestingly, when treating cells with bleomycin, *HDAC1* or *HDAC2* overexpressing cells presented a tendency for a greatest induction of $p21^{Cip1}$ compared to control cells (***Figure R41B***).

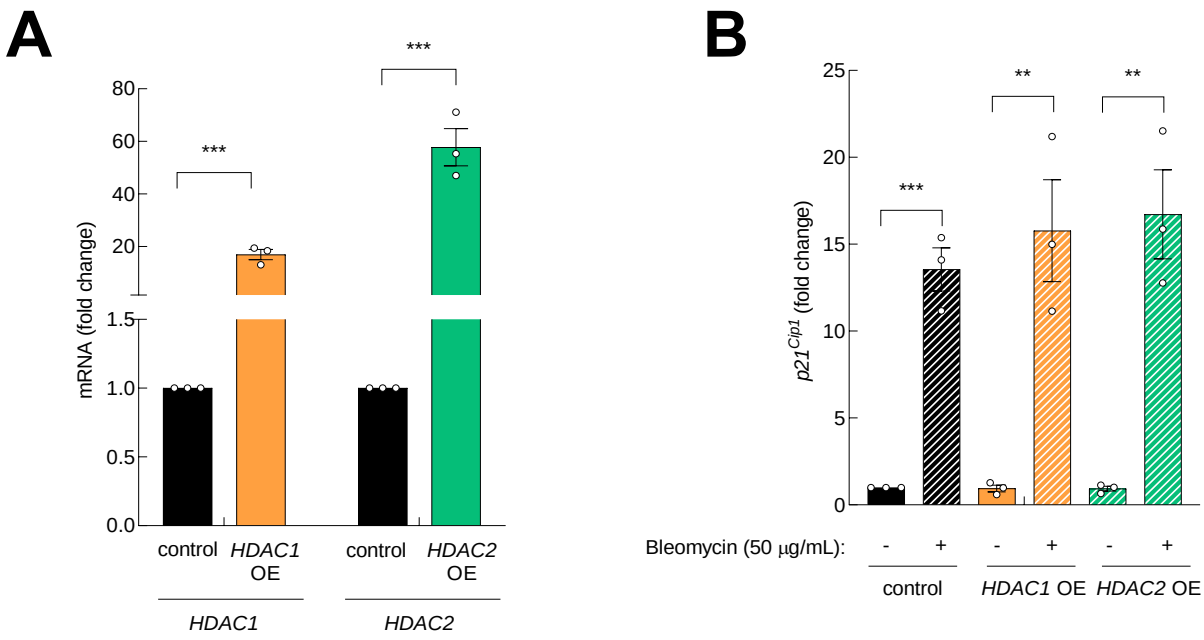

Figure R41. Upregulation of *HDAC1* and *HDAC2* tend to increase $p21^{Cip1}$ in microglia. (A) Relative mRNA expression of *HDAC1*, *HDAC2* and **(B)** $p21^{Cip1}$ in HMC3 transfected with control and HDAC1 or HDAC2 overexpression (OE) plasmids, and treated with control or 50 µg/mL bleomycin for 24 h (n=3).

3.2. HDAC and microglial marker expression is upregulated in aged DG

Aging is a multifactorial process that affects distinct cell types along the brain. Consequently, we decided to move to *in vivo* scenario. First, we studied the expression of *HDACs* in adult mice brain sections. Of note, hereafter we included Sirt3 in our study, based on its recent link with microglial senescence upon HIV-1 infection [329]. Interestingly, we found that *Hdac1, 2, 3, 6, 7* and *Sirt3* were highly expressed in the DG from adult C57BL6 mice (***Figure R42A***). Indeed, *Hdac2* and *Hdac3* were also expressed in other regions of the brain, but in a lower intensity. When studying microglial marker expression, *Cd68* expression was as well highly enriched in the DG, whereas no clear signal was detected for *Aif1* (***Figure R42B***), suggesting a putative association between microglia and *Hdac* expression in this brain region.

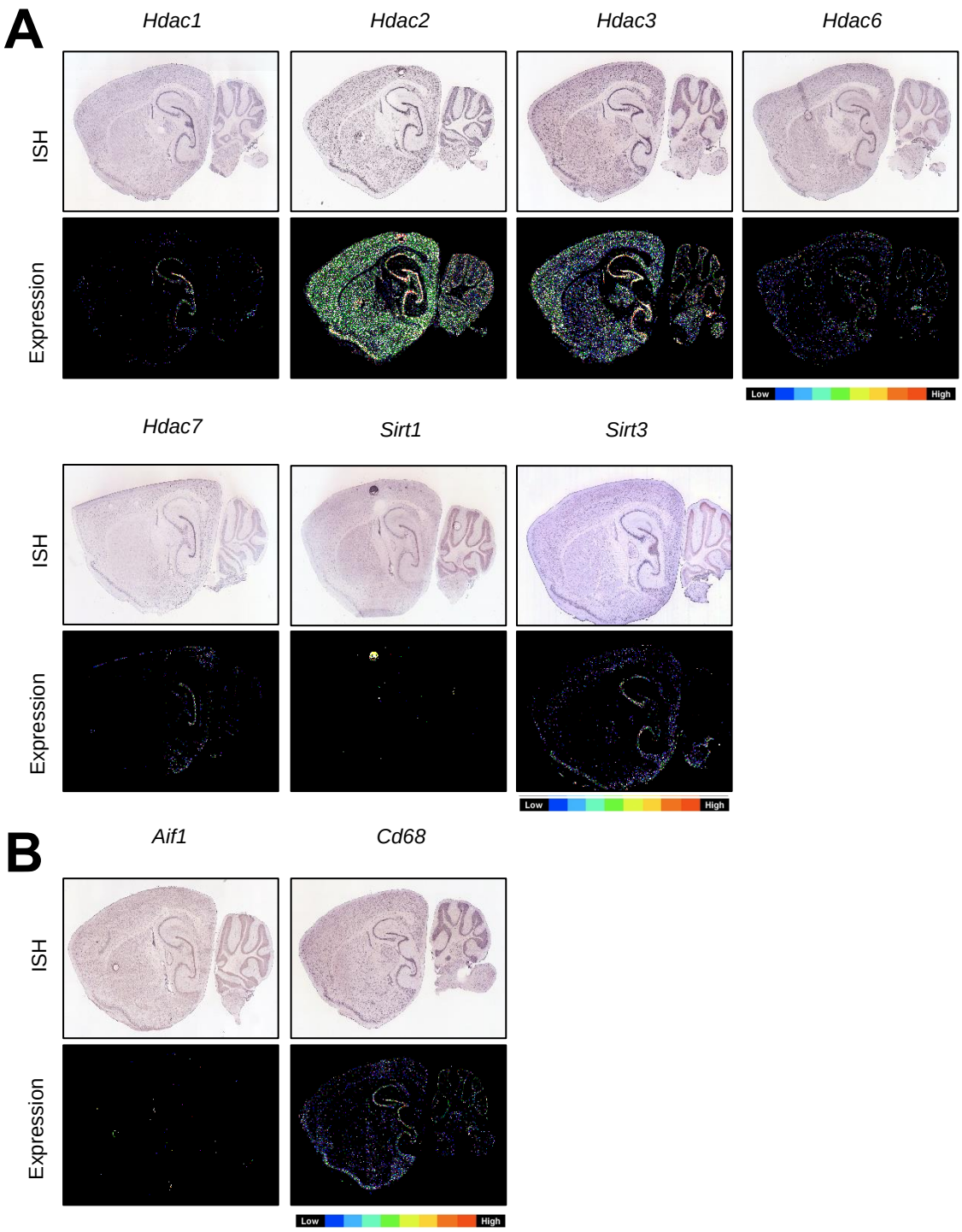

Figure R42. HDAC expression is enriched in dentate gyrus of adult C57BL6. (A) Images of *in situ* hybridization (up) and expression (down) of *Hdac1, 2, 3, 6, 7* and *Sirt1 ,3* and **(B)** microglial markers *Aif1* and *Cd68* in brain sections from P56 C57BL6 mice.

Thus, we subsequently moved to study DG samples from a set of young and aged mice. Although variability between samples was high, aged mice DG samples presented a tendency for increased expression of the senescence marker *p16*^{INK4a} and the cell cycle

inhibitor *p21*^{Cip1} (***Figure R43A***). Interestingly, similar tendency was observed in *Hdac1, 2, 3, 6, 7* and *Sirt1* expression (***Figure R43A***). Moreover, we observed that *Aif1* microglial marker was upregulated in aged mice compared to young ones (***Figure R43A***), supporting the idea of a possible link between *Hdac* expression and microglial aging in this brain region.

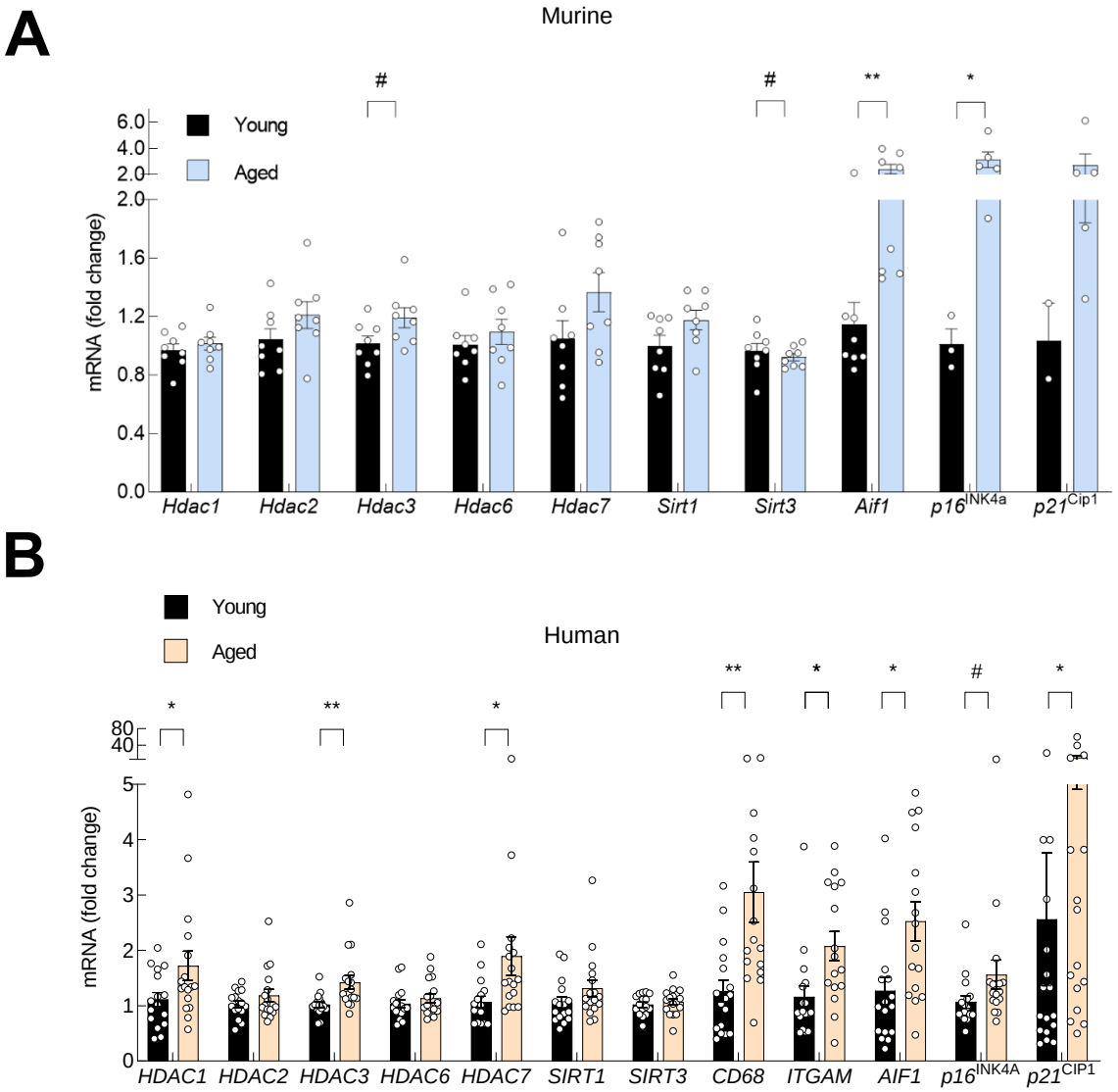

Figure R43. ***HDAC*** **and microglial marker expression is upregulated in aged mice and human hippocampus. (A)** Relative mRNA expression of the indicated *Hdac* transcripts, together with the microglial marker *Aif1,* senescence marker *p16*^{INK4a} and cell cycle inhibitor *p21*^{Cip1} in dentate gyrus from young (2 months) and aged (24 months) C57BL6 mice (n=7 *vs.* n=9, respectively) and **(B)** in hippocampus from young (27-45 years old) and aged (76-96 years old) human individuals (n=16 vs n=17, respectively). *CD68* and *ITGAM* microglial markers were also analyzed in human samples.

With the aim of translating the obtained results into human samples, we analyzed the same set of *HDACs* in hippocampal samples from young and aged human individuals. Herein, we found that aged individuals presented general increase on the

expression of *HDACs*, with significant results in the case of *HDAC1, 3* and 7 (***Figure R43B***). Indeed, aged hippocampus also showed significant upregulation of the microglial marker *AIF1*, and the senescence markers $p16^{INK4A}$ and $p21^{CIP1}$ in aged individuals.

For the characterization of microglial content, in addition to *AIF1*, we included other microglial markers, such as *CD68* and *ITGAM*. Notably, all microglial markers appeared to be significantly upregulated in hippocampus samples from aged individuals compared to young ones. Intriguingly, almost all studied *HDACs* showed positive and significant correlation with *CD68* (***Figure R44A***), *ITGAM* (***Figure R44B***) and *AIF1* (***Figure R44C***), being *HDAC1, HDAC7* and *SIRT1* the ones with strongest Spearman correlation coefficients. These data indicate a significant association between HDACs and microglia in human hippocampus with aging.

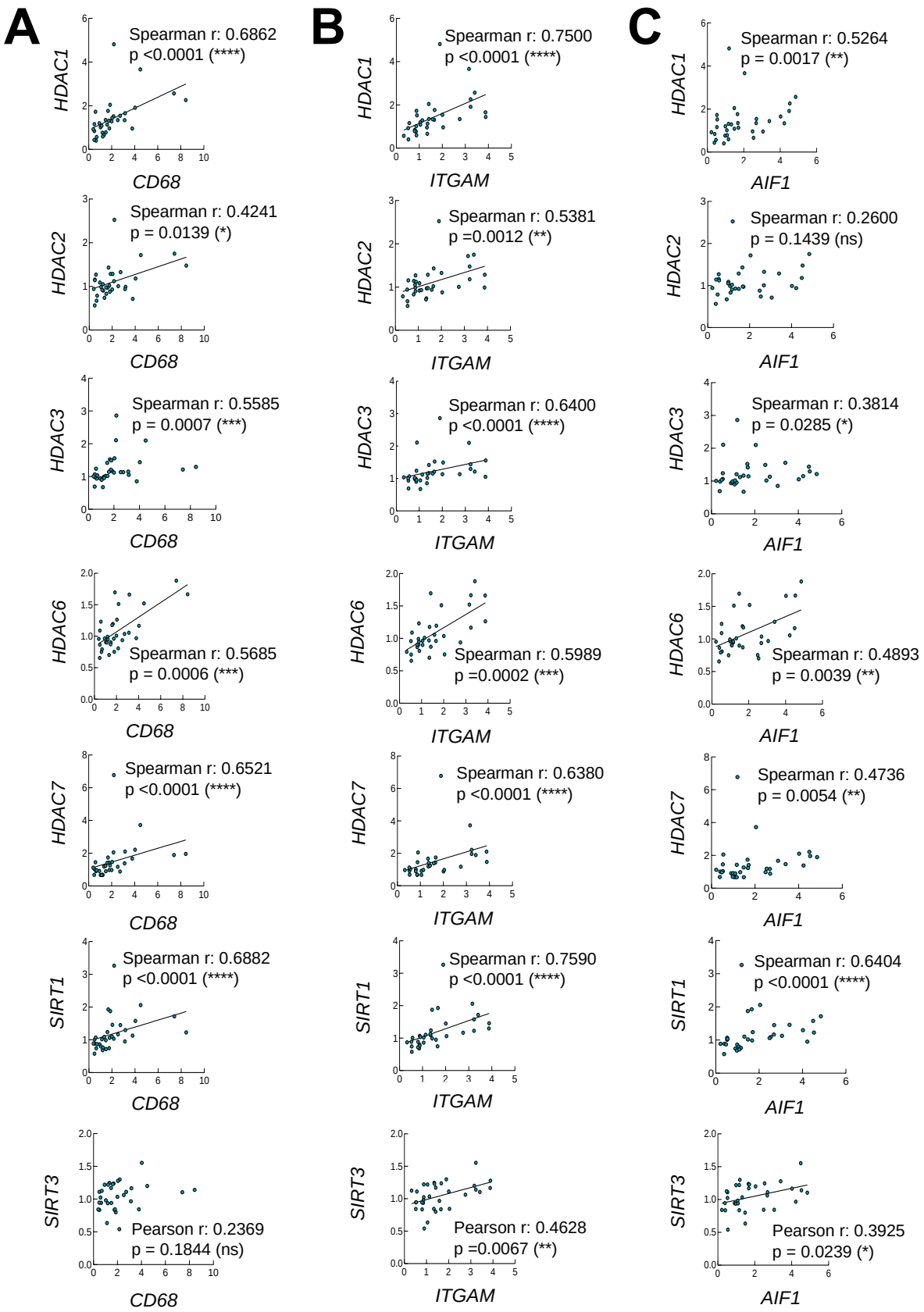

Figure R44. *HDACs* correlate positively with microglial markers in human hippocampus. (A) Correlation analysis of *HDAC1, 2, 3, 6, 7, Sirt1* and 3 with *CD68*, **(B)** *ITGAM* and **(C)** *AIF1* microglial markers in young and aged human hippocampus (n=33). Linear regression is shown when significant.

Taking advantage of data from RNAseq studies in publicly available datasets, we further characterized the expression of HDACs in human aged individuals. Herein, we firstly found that the expression of *HDAC1* and *HDAC2* was enriched in the hippocampus (***Figure R45***). Similarly, *CD68*, *ITGAM* and *AIF1* microglial markers appeared to be enriched in this brain region (***Figure R45***), reinforcing the positive correlation between HDAC expression and microglia. Additionally, *HDAC1, 2, 6, 7* and *SIRT1* expression was also enriched in white matter of forebrain, where glial cells are predominantly found (***Figure R45***). Accordingly, the high expression of microglial markers was also observed in this brain region (***Figure R45***).

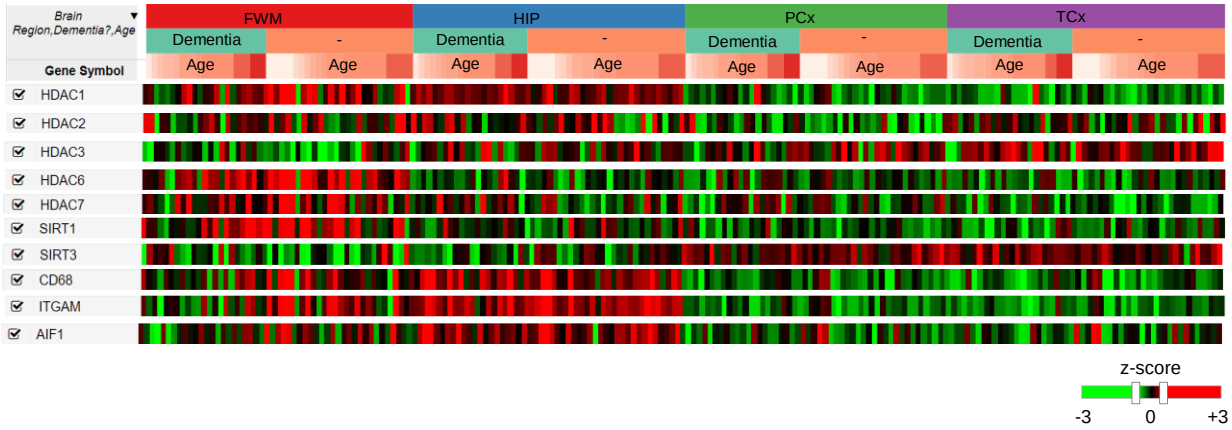

Figure R45. HDAC and microglial marker expression is highly enriched in hippocampus and white matter in aged human individuals. RNAseq results for *HDAC1, 2, 3, 6, 7, SIRT1, SIRT3* and microglial markers *CD68, ITGAM* and *AIF1* expression represented by z-score in white matter of forebrain (FWM), hippocampus (HIP), parietal neocortex (PCx) and temporal neocortex (TCx) of aged human individuals ranged between 78-100+ years old (n=30 no-dementia *vs*. n=24 dementia). Dementia was presented as vascular, multiple etiologies, Alzheimer's disease or other medical form. Data obtained from https://aging.brain-map.org/rnaseq/search.

Next, we decided to check *HDAC* expression directly in aged microglia. For that, we took advantage of RNAseq data from aged human bulk dorsolateral prefrontal cortex samples and purified microglia from the same region. Herein, as expected, we observed that microglial markers *CD68, ITGAM* and *AIF1* were clearly enriched in microglia compared to

bulk cortex (***Figure R46A***). Interestingly, we found that the expression of *HDAC1, 2* and *3* was also enriched in microglia (***Figure R46B***), supporting their association with microglial aging.

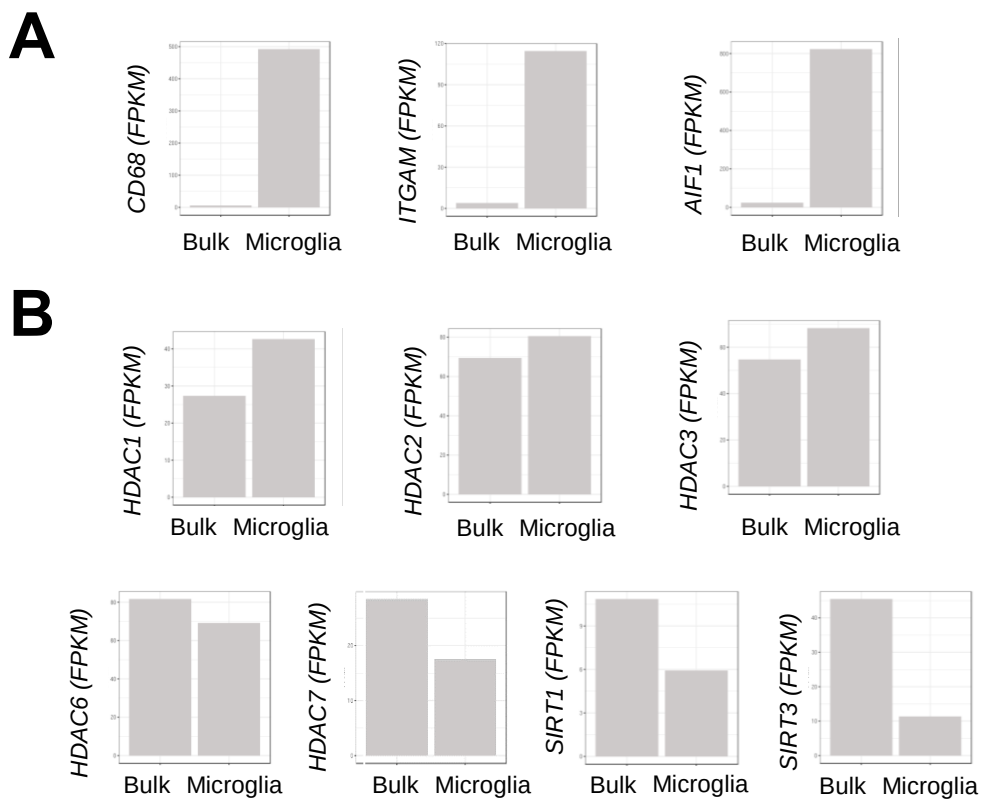

Figure R46. *HDAC1, 2* and *3* are enriched in aged microglia from human dorsolateral prefrontal cortex. RNAseq data for the expression of microglial markers *CD68, ITGAM* and *AIF1*, and **(B)** *HDAC1, 2, 3, 6, 7, SIRT1, SIRT3* in bulk dorsolateral prefrontal cortex (n=540) *vs.* purified microglia from the same region (n=10). Data obtained from http://shiny.maths.usyd.edu.au/Ellis/MicrogliaPlots/.

In this third and last chapter of the doctoral thesis we found that *HDAC* expression correlates positively with microglial aging in an *in vitro* model and *in vivo* samples of aged DG. Among all studied HDACs, HDAC1 seem to be the strongest member associated with microglial aging, as it followed the positive tendency in almost all experiments and cohorts analyzed.

Discussion

Cancer and aging may be considered opposite processes in terms of cellular fitness. However, some evidence suggests that the link between them is strong. First, both processes share a common origin: accumulation of DNA damage [137]. Second, they present similarities in their main hallmarks, but represented as two different manifestations [137, 330]. Moreover, incidence of most cancer types increases notably with age, as it is the case of GB [331]. In this doctoral thesis, we focused our attention on the intrinsic and extrinsic dysregulation of stem cell pool observed within the brain in both scenarios.

Control of processes modulating proteostasis, as well as regulation of epigenetic mechanisms are crucial in stem cell maintenance and activity [145, 330, 332]. In the present doctoral thesis, we aimed to study their impact on GB and brain aging. Regarding proteostasis, we studied CMA, a unique and selective protein degradative system, whose implication in CSCs was completely unknown [202]. In terms of epigenetic mechanisms, instead, we put our focus on HDACs, enzymes that catalyze the removal of acetyl groups, regulating both chromatin structure and function of non-histone proteins [333]. On the one hand, we studied the impact of HDAC expression on GB malignancy and GSC subpopulation, and revealed the potential of a novel compound selective for the inhibition of HDAC6 as an anti-oncogenic agent for targeting GSCs. On the other hand, we characterized the expression of a subset of HDACs in aged brain regions and studied its correlation with microglia in aging.

1. CMA maintains GSC activity

1.1. CMA is upregulated in GSCs and GB tissues

Fast growing GB cells contain numerous misfolded proteins, causing imbalanced proteostasis. [211]. In this context, how autophagy affects to GB progression and GSC activity is still under research. MA, the most studied type of autophagy, presents a dichotomous effect in GB. In particular, it has been shown to promote apoptosis in response to several stressors [212], whereas, in advanced stages of the disease, it contributes to cell survival, providing metabolic support and preventing senescence [213]. CMA also presents a dual role in cancer, being protective in malignant transformation and promoter of cancer progression [205]. Thus, CMA activity has been associated with tumor progression in various types of cancer [205], but its role is still very poorly understood in the case of GB and completely unknown in CSCs.

In the first chapter of this doctoral thesis, we revealed that LAMP2A expression and CMA process were enriched in GSCs. In fact, we found that LAMP2A correlated with GSC markers in different GB cell models *in vitro* and *in vivo*. Moreover, our results were extended into clinical samples of GB, where we found that total mRNA levels of *LAMP2* were positively associated with stem cell signature, and were enriched in GSC-like cells [290]. Although changes in the abundance of LAMP2A in lysosomes usually correlate with CMA activity [334], we took advantage of the photoswitchable KFERQ-Dendra reporter to reveal that GB cells, and specially GSCs, presented higher CMA activity than non-transformed cells. This reporter acts as a CMA substrate, so that, when CMA is active, the association of the reporter with lysosomes increases, changing intracellular fluorescence [307]. Thus, using different approaches we unraveled a novel link between CMA and GSCs.

Malignancy in the clinics of GB appeared to be associated with total mRNA levels of *LAMP2* in our work. Thus, *LAMP2* gene was overexpressed in GB compared to control human tissue in two large and independent cohorts. As this analysis could not distinguish the different isoforms of *LAMP2* gene, we studied specifically *LAMP2A* expression in an additional cohort. Thus, we revealed that GB samples showed higher mRNA expression of *LAMP2A* compared to control tissue, and 60% of GB samples presented very high LAMP2A protein expression, indicating the upregulation of CMA process in GB. In the same line, other reports have shown similar results in smaller cohorts of GB samples at protein level [335, 336], extending our results into additional cohorts. Our work also confirmed that GB samples presented an enhanced mRNA expression of *LAMP2B* isoform, which participates in MA process and thus, validates also the previously described upregulation of MA in GB [337]. Moreover, we revealed that high *LAMP2* expression was associated with increased glioma grade, mesenchymal GB subtype that shows the worst prognosis [338], and poor overall survival in GB patients. Altogether, these data suggest that *LAMP2* may present a prognostic value in GB, as it has been previously proposed for gastric [339] and breast cancer [340] patients.

1.2. *LAMP2A* regulates GSC activity

The study of autophagy in stem cells in an active research line. In the present work, we found that *LAMP2A* downregulation reduced self-renewal and proliferation, and induced apoptosis in two patient-derived GSCs, as well as in the GSC subpopulation of

conventional glioma cells. Although a possible limitation of our study is that we used a single shRNA for targeting *LAMP2A*, it is noteworthy to say that this shRNA was extensively compared with two additional ones in a previous study [185]. In fact, these three shRNAs lead to similar changes in cell proliferation and cell death in response to stressors, minimizing concerns about unintended off-target effects of our shRNA. Moreover, an additional study reported that *LAMP2A* silencing in conventional U87 cells enhanced apoptosis and reduced tumor growth [335], further validating the effect of CMA in GB. The first study that described that CMA contributes to cancer cell proliferation was performed in lung cancer and melanoma [206]. Since then, studies performed in gastric cancer, and cervical and hepatocellular carcinoma, among others, have shown that CMA degrades cell cycle-related proteins RND3/RhoE [339] or HIF1α [341], as well as apoptosis-related proteins cyclin D1 [342] or HMGB1 [343]. However, all these studies analyze tumor-bulk, being our work the first describing the effect of CMA in CSC activity.

With the aim of further characterizing the intrinsic role of CMA in GSC activity, we performed *LAMP2A* overexpression experiments, where we demonstrated that self-renewal was increased in control cells and rescued in *shL2A* cells. The role of autophagy, and specifically CMA, in stem cells is being addressed recently. In the case of MA, it is activated in oocyte to embryo transition, embryo-to-neonate transition and cell differentiation, among others [344]. In fact, the knock out of some MA-related genes in mice leads to lethality during mid-embryonic development, and those that survive the postnatal period display some developmental abnormalities [344]. In the adulthood, MA may be required for the maintenance of quiescence, self-renewal, differentiation and multipotency of hematopoietic, cardiac and NSCs [345]. Not only in physiological status, but MA also plays a crucial role in the origin, maintenance, and systemic distribution of CSCs [345]. In fact, both MA inhibitors, such as chloroquine, and promoters, such as mTOR inhibitors, block tumorigenesis and cancer progression by eliminating CSCs [345]. On the contrary, no one had studied the role of CMA in any CSCs type, and the studies in embryonic and adult stem cells showed different results. The study of CMA in embryonic development has recently started to emerge, with a recent paper in which authors report that low CMA activity promotes ESC self-renewal, while its upregulation enhances differentiation [194]. In fact, this study shows that *Lamp2a* expression is suppressed by Oct4 and Sox2 for the maintenance of stemness [194]. Moreover, CMA is required for protein quality control and metabolism in HSC upon activation [195]. Thus, CMA deficiency impairs HSC activation in young and more notably, in aged mice [195].

Overall, our work, together with these data, indicate that CMA activity regulates stem cell maintenance not only under physiological state in a time- and context-dependent manner, but also in pathological conditions.

GSCs are considered responsible for tumor initiation, progression, recurrence, and therapy resistance in GB patients [86]. DNA alkylating agents, such as TMZ, target proliferating cells, but do not attack quiescent GSCs. In the present work we show that TMZ treatment non-responder patients present higher expression of *LAMP2* compared to responder ones. In line with this, it has been previously shown that tissues from GB patients present higher expression of LAMP2A protein after TMZ treatment comparing to their pre-treated status [214]. Besides showing that the levels of LAMP2A correlated with TMZ resistance, we experimentally demonstrated that LAMP2A was functionally involved in resistance, as its knock down sensitized GSCs to TMZ treatment. Several reports have associated CMA with resistance to therapy in various types of cancer, such as hepatocellular carcinoma, colorectal cancer, or hepatitis B virus-associated cancer [205], but with no mention of the presence of CSCs. Thus, our work reveals that the role of CMA in therapy resistance is in part mediated by the intrinsic control of CSC subpopulation.

1.3. *LAMP2A* knock down alters proteomic and transcriptomic pathways in GSCs

Having identified for the first time the role of CMA in CSCs, we characterized the molecular pathways regulated by CMA process, related to GSC activity. Proteomic and transcriptomic analysis revealed a variety of pathways and processes by which CMA could control GSC activity. They seem to be modulated at distinct regulatory levels, as anticipated by the variety of functional protein groups normally degraded by this pathway [177].

High throughput proteome analysis in *LAMP2A* knocked down GSC and bulk glioma cells presented alterations in chaperone function and protein translation associated pathways. In particular, CCT/TriC chaperonin complex function appeared to be dysregulated in CMA impaired GSCs, whose potential as a prognostic biomarker in GB has been previously reported [346]. Of note, it has been shown that CCT/TriC complex regulates MA functionality [347], but no evidence had linked this complex to CMA. Together with protein synthesis and folding regulation, our study identified differential expression of proteins involved in ECM interaction, IFN signaling, mitochondrial function, response to stress and mRNA processing in *LAMP2A* downregulated GSCs. Although CMA downregulation altered common processes

in both GSCs and tumor-bulk glioma cells, the vast majority of dysregulated proteins were different, indicating a distinct regulatory level of CMA among cell types.

Transcriptomic analysis of *LAMP2A* knocked down GSCs similarly showed alterations in ECM interaction associated processes, as well as dysregulated PI3K-AKT and p53 signaling pathways, widely associated with GSC maintenance [315, 316]. In this line, several reports have characterized proteomic and transcriptomic processes regulated by CMA in certain cellular and animal models. In this line, *LAMP2A* knocked out murine HSC have shown alterations in cellular metabolism, motility, cell cycle and proliferation [195], which are partly observed in our study. On the contrary, enrichment analysis of proteins altered in neuronal specific *LAMP2A* knock out mice model showed dysregulation in protein trafficking, cation homeostasis and metabolism [348]. Alterations in protein translation have been similarly identified upon CMA modulation in ovarian, breast, fibrosarcoma and lung cancer, together with intercellular transport, RNA regulation processes, or heat shock protein response, among others [349, 350]. Altogether, these data suggest a cell-type-dependent regulation of CMA, with important distinctions between differentiated and stem cells.

1.3.1. *LAMP2A* knock down impairs mitochondrial function in GSCs

Besides the role in protein quality control, CMA has been associated with the control of cellular energetics [189]. In this line, our proteome analysis performed in *LAMP2A* knocked down GSCs revealed differential expression of proteins regulating mitochondrial functionality. Accordingly, we unraveled that this molecular signature was further observed functionally, as *LAMP2A* knock down significantly diminished OXPHOS function in GSCs. A growing body of literature reports that OXPHOS plays an important role in addressing the energy demands of CSCs [351]. Not only in CSCs, but OXPHOS impairment has been also observed in lung cancer cells after CMA blockage [206], extending our result to other cell types. Of note, assembly of OXPHOS complexes is largely regulated by mitoribosomes [351], which appeared to be downregulated in *LAMP2A* knocked down GSCs. Indeed, the specific inhibition of mitochondrial translation by targeting the function of mitoribosomes has been previously shown to dysregulate OXPHOS and suppress GSCs growth [351]. Together with OXPHOS impairment, we identified that *LAMP2A* knock down in GSCs increased in the amount of mitochondrial ROS and membrane depolarization, both indicators of impaired mitochondrial integrity and function [352]. All these data reveal that CMA regulates mitochondrial function in GSCs.

GSCs are metabolically heterogeneous and adaptive, able to shift between glycolytic and oxidative phenotypes [124, 353]. In fact, our study revealed that GSCs upregulated glycolysis upon *LAMP2A* downregulation. The use of glycolysis by cancer cells is known as 'Warburg effect', which provides survival and proliferative advantage by decreasing their reliance on aerobic respiration [354]. Thus, this evidence could originally indicate a more aggressive metabolic phenotype of tumor cells. However, the impaired activity of GSCs observed in all functional and molecular studies performed in this doctoral thesis suggest that this metabolic change might represent a potential but failed compensatory mechanism to cope with mitochondrial impairment. In contrast to our results, a previous study in lung cancer demonstrated that *LAMP2A* knock down reduced glycolysis, together with the expression of glycolytic enzymes [206]. In the same line, both dopaminergic neurons and HSCs from *LAMP2A* cell-type-specific knock out mice presented impaired glycolysis [195, 348]. This evidence could indicate a cell-type and context dependent modulation of metabolic pathways upon CMA downregulation.

1.3.2. *LAMP2A* knock down reduces ECM content and interactions in GSCs

The analysis of both proteomic and transcriptomic data performed in *LAMP2A* knocked down GSCs revealed an impairment on ECM interaction pathways. ECM provides both structural and biochemical support to regulate proliferation, self-renewal and differentiation of CSCs [355]. In fact, important ECM associated proteins such as integrins or ECM content proteins have been described as regulators of the maintenance of GSCs and their niche [356, 357] [355, 358], which indeed were decreased in our model. Of note, ECM remodeling has been shown to be crucial for the extensive infiltrative capacity of GSCs [319]. Our study showed that the observed molecular alterations were accompanied by reduced migration and collagen invading capacities of *LAMP2A* knocked down GSCs. Similarly, *LAMP2A* knock down had shown to impair migration of human lung cancer cells [206] and colorectal cancer cells [359]. Thus, our work shows the regulatory role of CMA in the remodeling of ECM interaction in GSCs, therefore modulating their migration and invasion properties.

1.3.3. *LAMP2A* knock down alters inflammatory and immune response in GSCs

Interaction of GB cells with the microenvironment leads to an extrinsic heterogeneity that enhances tumor immune evasion [318]. In this respect, our proteomic

study revealed upregulated IFN signaling and reduced MHC class II antigen-presentation, suggesting a role of CMA in immune response.

IFNs are a family of endogenous antiviral proteins which also present anti-oncogenic activity [360]. In particular, *LAMP2A* downregulated GSCs showed elevated mRNA levels of IFN-γ, which has been described to inhibit proliferation and self-renewal of GSCs [360]. Notably, the key mediators in IFN signaling STAT1 and MX1 appeared to be upregulated in CMA depleted GSCs. In this line, previous studies revealed that overexpression of STAT1 decreases proliferation, migration and invasion of GB cells [361]. Moreover, it has been shown that GSCs present reduced expression of STAT1 comparing to non-stem tumor cells [362], suggesting that CMA knock down-mediated STAT1 upregulation could induce the differentiation of GSCs. Interestingly, several studies have linked reduced expression of STAT1 and MX1 to hypoxic conditions [361, 363] and irradiation [364], both important features in GSC maintenance [133, 365]. Intriguingly, clinical trials evaluating the administration of IFN in recurrent glioma have shown promising results [366]. All these data may indicate that the upregulation of IFN signaling by *LAMP2A* downregulation could impair self-renewal of GSCs.

Although genes associated with MHC class II molecules are constitutively expressed primarily by mature professional antigen presenting cells, they can be also induced in tumor cells [367]. In this regard, *LAMP2A* knocked down GSCs presented a reduction in the protein abundance of key regulators of this process [368-370]. By contrast, it has been shown that IFN-γ induces the expression of MHC-II [367], which could be indirectly opposite to the effect that we observe in our model. Thus, our results indicate that CMA may modulate MHC class II presentation in GSCs, but further evidence are needed to elucidate the specific mechanism of this modulation and its controversial link with IFN signaling.

Interestingly, our work extends the relevance of *LAMP2A* in IFN and MHC class II antigen presentation pathways to a general alteration in cytokine secretion. Indeed, *LAMP2A* knocked down GSCs showed reduced abundance of a set of pro-inflammatory cytokines in their supernatant, which was accompanied by a downregulation of the phosphorylated active form of STAT3, pivotal effector of glioma tumorigenesis and anti-tumor immunity [318]. Future work should be done to clarify which cytokines are critical and to elicit their regulatory pathway, since some of the factors were not validated at mRNA level. Despite this, the diminished secretion of angiogenic factors, such as ANG or VEGF, by CMA depleted GSCs was of special interest since a previous study demonstrated the implication of CMA in the

crosstalk between glioma cells and pericytes [215], functional and critical contributors of tumor angiogenesis. Indeed, there are evidence demonstrating that GSCs can transdifferentiate into pericyte-like cells, supporting the interaction between these cell types [371]. Thus, our results might suggest that high levels of CMA in GSCs could contribute to the secretion of angiogenic factors, inducing the interactions with tumor-associated pericytes, and thus, possibly contributing to tumor survival.

Overall, we found that CMA activity is enriched in GSC population, and we reveal a novel role of LAMP2A controlling intrinsic tumorigenic activity of GSCs (***Figure D1***). Additionally, we unravel pathways and processes that are differentially altered at proteomic and/or transcriptomic level in *LAMP2A* knocked down GSCs. Among them, we highlight IFN signaling, MHC class II antigen presentation, cytokine secretion, mitochondrial function, glycolysis rate and ECM interactions (***Figure D1***). Future studies should investigate whether the regulatory role of CMA described in this work is specific of GSCs, or whether it is common among all CSC types.

Cellular functions regulated by CMA in GSCs

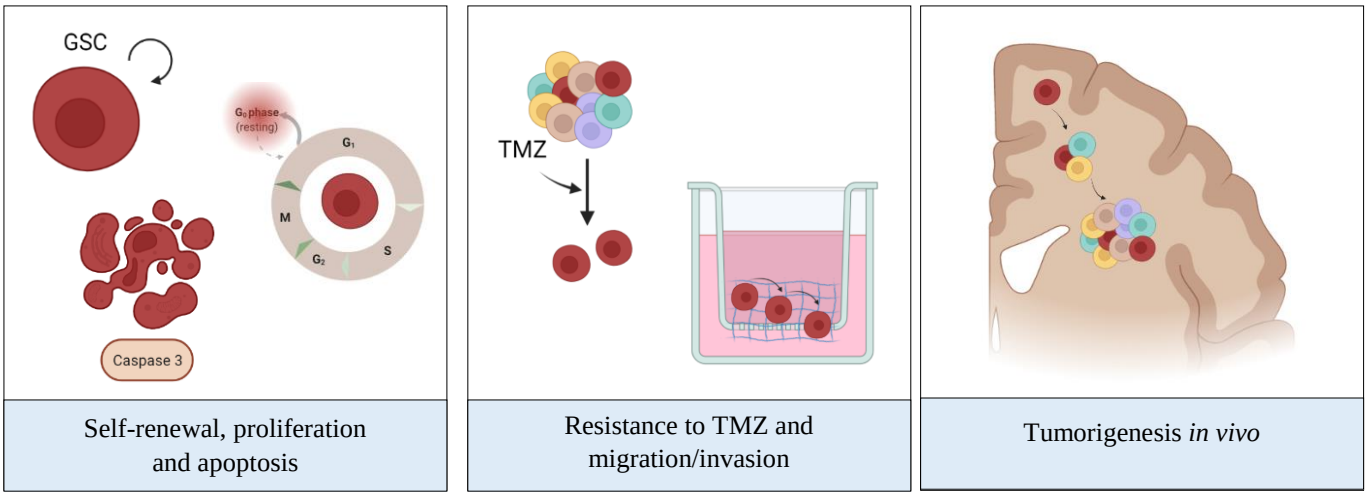

Main pathways regulated by CMA in GSCs

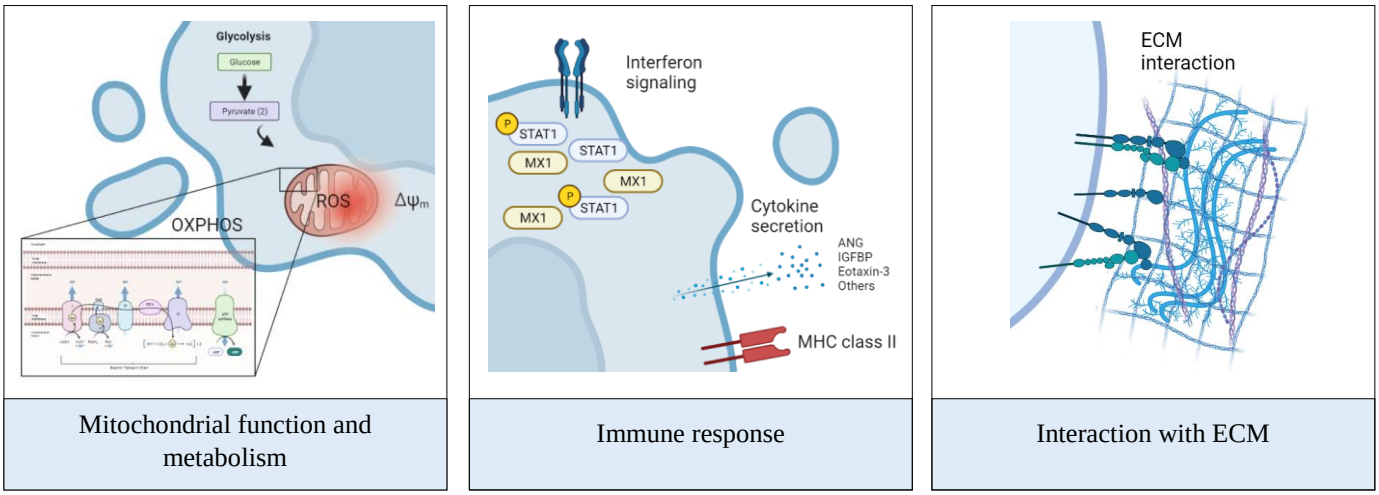

Figure D1. CMA process regulates crucial cellular functions and pathways in GSC activity. Created with BioRender.com. GSC: glioma stem cell; TMZ: temozolomide; ROS: reactive oxygen species; OXPHOS: oxidative phosphorylation; ECM:extracellular matrix.

2. Characterization of a new small-molecule inhibitor of HDAC6 in GB

As highlighted within this doctoral thesis, GBs are notorious for resistance to therapy, which has been linked to genetic and cellular heterogeneity, as well as limited drug delivery into the brain [82, 372-374]. Despite numerous efforts, the addition of compounds against specific genetic driver targets or biological hallmarks of GB have largely failed [375].

Therefore, new molecules and targets for GB effective treatment constitute an unmet medical need.

The application of HDACi for treating several types of cancer is an active research field. To date, various HDACi compounds have been tested in preclinical or clinical studies in GB [376]. However, most of them are considered pan-inhibitors, due to their lack of selectivity against a specific HDAC isoform. Among them, Vorinostat, also known as SAHA, is the first FDA-approved compound for the treatment of relapsed and refractory cutaneous T-cell lymphoma [377]. In GB, besides showing a strong preclinical effect, it has been tested in various clinical trials, showing acceptable tolerability profile, but still with some side effects, such as fatigue, vomiting, hyperglycemia, neutropenia, or anemia [274]. Thus, the use of selective HDACi could reduce non-desirable side-effects, improving the efficacy of the treatment. HDAC6 is a member of class IIb HDAC family, and it is becoming an attractive pharmacological target in cancer [378]. In fact, *HDAC6* knocked down mice have been shown to be viable and fertile, suggesting that its inhibition could be a relatively safe approach.

2.1. HDAC6 is overexpressed in GB and GSCs

In the present work we characterized the mRNA expression of 11 human classical *HDACs* in two large and independent cohorts. Herein, GB samples showed an overexpression of *HDAC1, 3, 6* and *7* compared to control tissue. In line with our results, a previous publication showed upregulated levels of *HDACs* such as *HDAC1, 3* and *6* in a small number of GB samples compared to non-neoplastic brain control samples [379], extending our results into an additional cohort. In this direction, a large-scale sequencing of protein coding genes has described missense mutations in *HDAC2* and *HDAC9* genes in human GB samples [380], but their impact on HDAC expression and functionality remains to be elucidated.

Translating gene expression into patient survival, our work revealed that patients with high expression of *HDAC1* and *HDAC6* presented worse prognosis than the ones with low expression, in three independent cohorts. HDAC6 has been found to be upregulated in various types of cancer, such as ovarian [381], oral squamous [382] or acute myeloid leukemia [383], among others. In fact, HDAC6 regulates crucial processes in cancer such as cell cycle, apoptosis or motility [384]. Moreover, a very recent publication that analyses multiple publicly available datasets shows similar results for the case of *HDAC1* and extends its prognostic value to increased immune infiltration [385].

HDAC6 has been associated with GB cell proliferation and TMZ resistance [386]. In this line, in our work we found that HDAC6 expression was enriched in patient-derived GSCs and GSC population within conventional glioma cells, in a greater extent than HDAC1. In fact, *HDAC6* positively correlated with GSC markers in GB patients, whereas *HDAC1* did not. Accordingly, a previous study reported that the expression HDAC6 was upregulated in leukemic stem cells comparing to non-stem leukemic cells [387]. Altogether, these data indicate that HDAC6 is highly expressed in GSCs and GB, becoming an interesting therapeutical target for attacking GSC and thus, have an impact on patient survival.

2.2. The novel HDAC6 inhibitor JOC1 presents a superior efficacy as a therapeutic agent in GB

Next, we characterized the effect of a new small-molecule inhibitor of HDAC6, named as JOC1 in GB [300]. Notably, we found that JOC1 significantly reduced proliferation and induced apoptosis in GB cells. Interestingly, this *in vitro* effect was translated into *in vivo* scenario, as JOC1 reduced tumor growth, even when the treatment started once tumors were formed. Importantly, JOC1 presented greater inhibitory effect of HDAC6, stronger cytotoxic effect and more potent activation of signaling pathways compared to SAHA and Tubastatin A. Similar results were observed when testing this compound in mantle cell lymphoma [299], highlighting its applicability in various types of cancer.

Besides, we unraveled that JOC1 was able to target GSCs, as it impaired their proliferation and self-renewal, and induced apoptosis. These cellular effects were similarly observed at molecular level, as microarray analysis and its validation showed augmented differentiation and cell death, and diminished cell-cycle regulators in GSCs treated with JOC1. In fact, these features are typically modulated by HDACis [274], including SAHA and Tubastatin A, whose regulatory role on the activity of GSCs has been previously reported [388] [389]. In fact, it has been demonstrated that SAHA reduces stem cell markers such as CD133 and NESTIN in GSCs [388] or SOX2 in melanoma [390], and induces *TUJ1* in GSCs [388], among others.

The molecular studies performed in this work revealed an altered expression of critical genes upon JOC1 treatment. In this sense, MKP1 is a relevant mediator of GSCs activity, and its expression is induced by HDACis [302]. Indeed, genetic, and pharmacological activation of MKP1 promotes GSC differentiation and reduces tumorigenic activity [302]. In

line with this, JOC1 induced *MKP1* expression in GSCs, and its overexpression sensitized GSCs against combined therapy of TMZ plus JOC1, indicating that MKP1 could mediate JOC1 response. Together with this, we revealed that JOC1 diminished BMI-1, SOX2 and SOX9 stem cell markers. The molecular impairment of stem cell markers was similarly observed in tumorigenic embryonic carcinoma CSC models with *HDAC6* knock down [391]. In this line, a very recent study identified that HDAC1/2/6, together Sp1 transcription factor, a novel nuclear substrate of HDAC6, promote self-renewal by upregulating BMI-1 [266]. Besides differentiation and stemness, cell-cycle arrest markers were also dysregulated upon JOC1 treatment, as it is the case of $p21^{CIP1}$. The transcriptional regulation of $p21^{CIP1}$ by HDACis has been widely described [274], in part by altering the accessibility of regulatory proteins to its promoter [392]. As an example, it has been reported that HDAC6 inhibition modulates p53 acetylation [393], one of the tumor suppressing transcription factors that regulates $p21^{CIP1}$ expression and whose relevance in GB has been widely explored [394]. In this line, SAHA has shown preferential cytotoxicity in mutant p53 cells by destabilizing it through the inhibition of HDAC6 [395]. In our study, we did not observe significant differences between wild-type and mutated p53 cell lines, which could be explained, in part, by the strong cytotoxicity of JOC1 in all of them.

HDAC6 activity has been associated with TMZ resistance in GB [386]. In this line, our data show that the combination of TMZ plus JOC1 had greater cytotoxic effect than the combination between TMZ and SAHA. The synergistic effect of the combination between TMZ and SAHA had been previously studied preclinically not only in GB [396], but also in other types of cancer, such as melanoma [397]. The fact that JOC1 shows a stronger effect as anti-oncogenic drug than SAHA, both as monotherapy and in combination with TMZ, highlights its promising therapeutical capacity in GB. A future *in vivo* experiment should study the combination of TMZ and JOC1. This experiment would allow us to test the possible effect of JOC1 differentiating GSCs, while TMZ would target all proliferating GB cells.

2.3. JOC1 presents anti-tumor effect in GB *in vivo*

In regard to safety and cytotoxic effect, GB cells were more sensitive to JOC1 than control normal human astrocytes. Besides, JOC1 presented higher IC_{50} values in normal peripheral mononuclear cells, and thus, less cytotoxic effect, than in mantle cell lymphoma cells [299]. Besides, mice treated with JOC1 intraperitoneally did not present significant

alterations in their weight. Of note, the doses used in our study were similar or even lower than the ones reported for the case of SAHA in previous GB studies [388, 398]. These data show first insights regarding the tolerability of the compound.

As a step forward, the next experiment would be an orthotopic xenograft model, but JOC1 molecular structure still presents some solubility issues, and it is not able to cross the BBB. This latter issue is the most important obstacle that any drug must overcome for the treatment of GB. Of note, it has been popularized that BBB is uniformly disrupted in GB patients, but clinical evidence demonstrates that there is still a significant tumor burden with intact BBB [399]. Thus, we next worked in this point, carrying out a nanoparticle-based vehiculation of JOC1. We developed BSA-based nanoparticles for the vehiculation of JOC1, obtaining a nanoformulation with homogeneous size distribution and high encapsulation yields. Interestingly, the vehiculation of JOC1 presented a tendency for improving the efficacy of the free compound *in vitro*, which indicates that the binding of albumin does not alter the functionality of the compound, but even seems to improve it. This strategy has been shown to be successful in the clinical scenario, as FDA has already approved an albumin-bound nanoparticle of paclitaxel, named as *Abraxane* ®, as the first line therapy for metastatic breast cancer, advanced non-small cell lung cancer and last-stage metastatic pancreatic cancer [400]. Albumin possesses encouraging bioconjugation capability, biocompatibility, and *in vivo* half-life in blood circulation [401]. Indeed, it has been shown that compounds bound to albumin present increased half-life, which could increase the availability of a construct to target the tumor [401]. Importantly, albumin can cross brain capillary endothelial cells barrier by interacting with albumin-binding proteins, such as gp60 and SPARC [402]. Remarkably, these two molecules are overexpressed in glioma [402], supporting the potential success of the vehiculation of a compound by albumin-based nanoparticles for crossing the BBB.

As BBB shields the brain from most systemically administrated compounds, doses are increased with the aim of achieving intracranial therapeutic drug levels [403]. However, as discussed before, the dose-related toxicity affects directly to the efficacy of the treatment. We tried to move to an *in vivo* scenario with the vehiculation of JOC1, but we could not generate the amount of nanoparticle necessary for performing this type of experiment. Thus, future efforts should optimize this point.

Overall, our data reveal that *HDAC6* expression is upregulated and associated with poor prognosis in GB. Notably, its expression is enriched in patient-derived GSCs and we show that the novel HDAC6 inhibitor, JOC1, reduces GSC self-renewal and proliferation, and diminishes tumor growth even after tumor formation (***Figure D2***). Importantly, JOC1 effect is greater than other currently available pan-HDACi SAHA and the selective HDAC6 inhibitor Tubastatin A. For its delivery into the brain, we have developed a vehiculation strategy based on albumin nanoparticles which shows promising *in vitro* results.

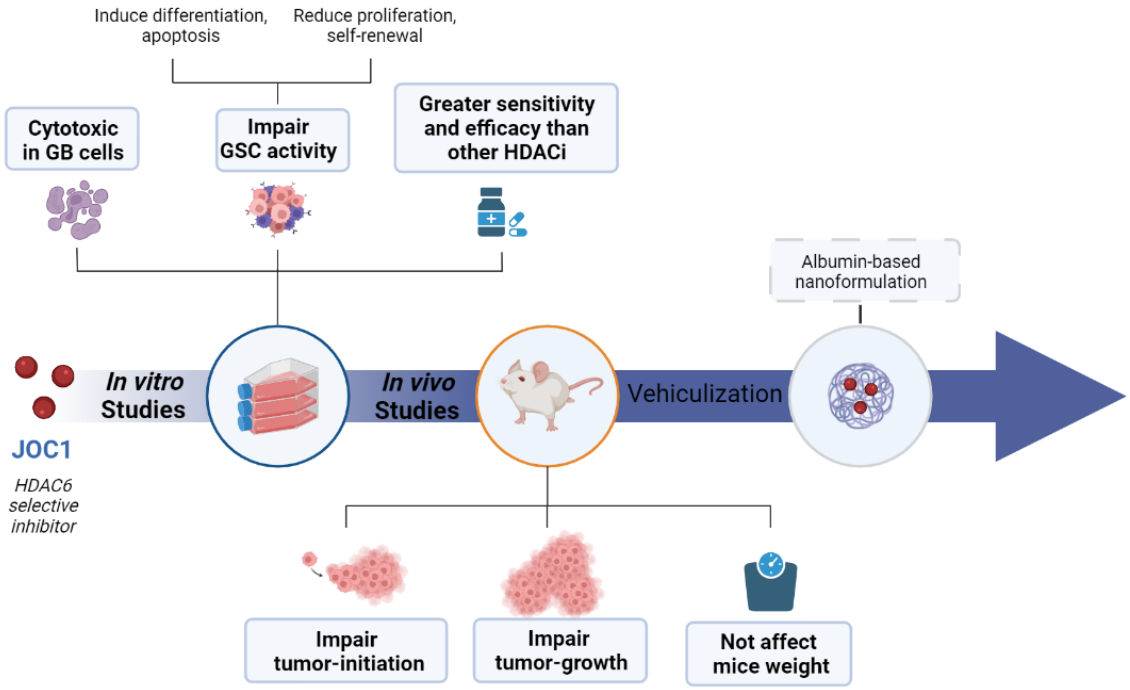

Figure D2. The novel inhibitor of HDAC6 JOC1 reduces tumorigenic properties of GSC *in vitro* and *in vivo*. Created with BioRender.com.NHA, normal human astrocytes. HDACi, histone deacetylase inhibitor.

3. HDAC expression correlates with microglia in aging

In addition to the study of HDACs in GB, we were also interested in studying their expression in brain aging. Taking advantage of Allen Brain Atlas, we observed that the expression of *Hdac1, 2, 3, 6, 7* and *Sirt3* was specifically intense in DG from adult mice. In line with this, we found that aged murine DG tend to present upregulated levels of *Hdac1, 2, 3, 6, 7* and *Sirt1* compared to young mice, suggesting the relevance of their activity in this brain

region. Differences were only significant for the case of *Hdac3*, which could be attributed, at least in part, to the reduced number of samples and the heterogeneity between them. Similarly, previous studies in rodent models show that *Hdac2* expression [277, 278] and overall HDAC enzymatic activity [279] increase with age in the hippocampus, supporting our preliminary data. The dysregulation of HDAC activity has been associated with memory and learning cognitive impairments [284, 404, 405], features that are directly associated with an age-related decline in adult neurogenesis within DG [406]. In particular, during learning, aged mice display a specific deregulation of histone H4 lysine 12 acetylation and fail to initiate a hippocampal gene expression program associated with memory consolidation [404]. Besides, HDAC2-overexpressing mice presented reduced synapse number and learning impairment, which were ameliorated by chronic HDACi treatment [284].

Importantly, our work further extends these results into human samples, wherein we observed significant elevation of *HDAC1, 3* and *7* in hippocampus from aged individuals compared to young ones. Of note, a similar but not significant tendency was observed in *HDAC2*, suggesting a generalized upregulation of *HDAC* expression. Accordingly, a study based on *in vivo* neuroimaging of aged human individuals reported not significant, but upregulated expression of *HDAC1, 2* and *3* in human hippocampus [407]. Herein, authors employed MR-PET technique with [^{11}C] Martinostat, a radiotracer selective for HDAC paralogs 1,2,3 and putatively 6 [407]. Thus, this methodology could not detect expression of other isoforms of HDACs such as *HDAC7*, which seem to be also promising in our study. Altogether, these data suggest that the expression of HDACs is elevated in DG during aging. In the same line, at organismal level, *HDAC* knock down or the use of HDACis have previously shown lifespan and healthspan extending properties in yeast, worm, fly and rodent models [259, 408]. The exact mechanism by which HDACis exert these actions has not been fully resolved. One of the hypotheses claims that, while high doses of HDACis may be toxic, low doses would elicit activation of protective genes to regain homeostasis, improving function [408].

Cellular senescence, a stable arrest of the cell cycle coupled to phenotypic changes, is one of the main hallmarks of aging [137]. Expression of $p16^{Ink4a}$ [409] and $p21^{Cip1}$ [410] has been associated with senescent phenotype, markers that, together with HDACs, appeared to be increased in aged hippocampus analyzed in our work. In fact, genetically manipulated mice with increased, but otherwise normally regulated, levels of Arf/p53

pathway presented significantly elongated lifespan and delayed organismal aging [411, 412]. Regarding the brain, these mice also displayed enhanced NSC self-renewal activity, increased neurogenesis and enhanced behavioral and neuromuscular coordination activity [412]. The fact that HDACs regulate p53 pathway [252] supports the relevance of HDACs in the context of aging.

NSCs in neurogenic niches are very likely to be primed by signals in their microenvironment [22]. In fact, a correct microglial activity is relevant for adult neurogenesis in the hippocampus during aging [24, 413]. In this line, the dysregulated activity of HDACs has been linked to alterations in intercellular communication [408]. Microglia is the most abundant immune cell type within the brain and HDAC seem to be involved on their regulation [288]. In particular, the deletion of *Hdac1* and *Hdac2* in mice leads to apoptosis and reduced survival of microglia in developmental stages [288]. In this same study, authors found that the deletion of *Hdac1* and *Hdac2* did not affect survival of adult microglia during homeostasis, but it enhanced microglial amyloid phagocytosis in a mouse model of Alzheimer's disease [288]. However, no studies have characterized the role of HDACs in microglial aging.

As a first approach of studying microglial aging, we found that bleomycin-induced senescent microglia showed significant upregulation of ~20% in the levels of *HDAC1*, *HDAC3* and *Sirt1*. In fact, the ectopic overexpression of *HDAC1* or its homologous *HDAC2* [328] in microglia cells *in vitro* tend to promote the upregulation of cell-cycle inhibitor $p21^{CIP1}$. In line with our results, HDAC1 has been previously associated with senescent phenotype in melanocytes [414]. Although observed alterations were slight, it is noteworthy to say that due to pleiotropic effects of HDACs, small changes could have a large impact [407]. As an example, genetic knock down of *Hdac2* expression by 25-30% increased transcription of memory-related genes and improved spatial memory in an Alzheimer's disease rodent model [415]. When analyzing *in vivo* samples, we unraveled that the expression of microglial markers *CD68, ITGAM* and *AIF1* was increased in aged hippocampal murine and human samples. Intriguingly, all studied HDACs were positively associated with microglial markers in human hippocampal samples in different cohorts. Our data suggest that elevated HDAC expression could be associated with microglial aging.

To further extend the link between HDACs and microglia in aging, we characterized them in the white matter (WM), which is damaged upon aging [416]. Herein,

aged samples showed an enriched expression of *HDAC1, 2, 6, 7*, *SIRT1* and microglial markers in the WM of forebrain. Similarly, in the previously mentioned *in vivo* neuroimaging study, authors found a significant increase in the protein expression of HDAC1 and 2 with age in cerebral WM [407], but no mention was done regarding any specific cell-type. Of note, WM is mainly composed of myelinated or unmyelinated axons, and glial cells. Microglial density [417] and diversity [416] greatly increases in WM of aged brains. Indeed, reduced expression of HDAC2 in microglia has been shown to promote neurological functional recovery and to reduce WM injury after intracerebral hemorrhage [418]. Moreover, WM hyperintensities, common age-associated findings that impact cognition [419], have been associated with decreased prefrontal cortex (PFC) activity in elderly individuals [420]. Intriguingly, data in the present doctoral thesis show that microglia from dorsolateral PFC of aged individuals present enriched expression of *HDAC1, 2* and *3* compared to bulk tissue. These evidence suggest the elevated expression of HDACs in microglial aging in different brain regions.

Altogether, our work reveals that both HDAC and microglial marker expression are elevated by age in murine and human DG neurogenic niche, and that this positive correlation is extended into other human brain regions such as WM and PFC (***Figure D3***). Indeed, our results indicate that the upregulation of HDAC expression seems to be associated with *in vitro* models of microglial aging, such as microglial senescence. These evidence suggest that alterations in the expression of HDACs could play a role in brain aging.

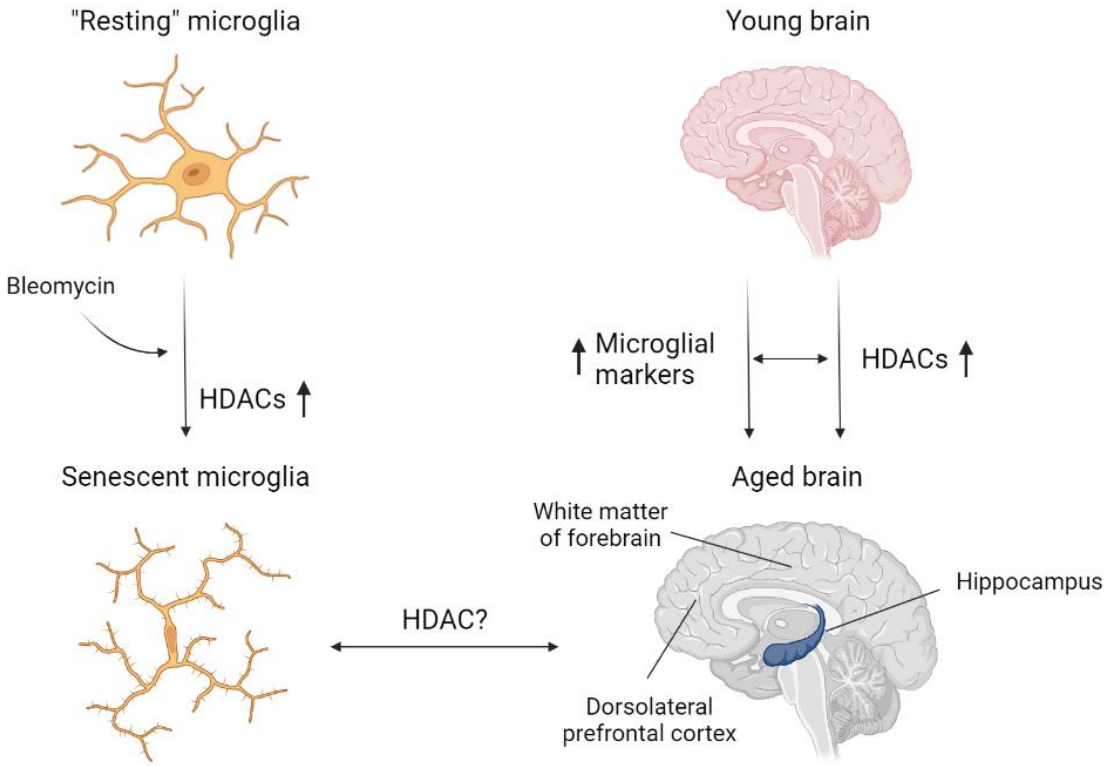

Figure D3. HDAC expression is upregulated in aged brain and correlates with microglial senescence. Created with BioRender.com. HDAC: histone deacetylase.

Concluding remarks

1. LAMP2A expression is enriched in GSC subpopulation and elevated in GB, correlating with malignancy grade, TMZ resistance and poor patient survival.

2. CMA is crucial for GSC activity, regulating processes such as proliferation, self-renewal and apoptosis.

3. CMA selectively controls several proteomic and transcriptomic pathways in GSCs, affecting to the mitochondrial function, IFN signaling and ECM interactions. Such alterations provoke changes in the metabolism, cytokine secretion and migration and invasion of GSCs.

4. HDAC6 and HDAC1 expression is upregulated in GB, being HDAC6, but not HDAC1, enriched in GSC subpopulation.

5. A novel HDAC6 inhibitor presents greater target specificity and cytotoxic effect in GB than other currently available HDACis in the preclinical scenario.

6. The novel HDAC6 inhibitor also targets GSC subpopulation, by transcriptionally inducing their differentiation and cell death, and reducing cell cycle progression.

7. HDAC expression is elevated in human microglia with aging *in vitro* and *in vivo*.

8. HDAC expression correlates with microglial signature in murine and human brain regions, including DG neurogenic niche, with aging.

References

1. Maldonado, K.A. and K. Alsayouri, *Physiology, Brain*, in *StatPearls*. 2022, StatPearls Publishing

2. Jiang, X. and J. Nardelli, *Cellular and molecular introduction to brain development.* Neurobiol Dis, 2016. **92**(Pt A): p. 3-17.
3. Ding, J., et al., *A metabolome atlas of the aging mouse brain.* Nat Commun, 2021. **12**(1): p. 6021.
4. Herculano-Houzel, S., *The human brain in numbers: a linearly scaled-up primate brain.* Front Hum Neurosci, 2009. **3**: p. 31.
5. von Bartheld, C.S., J. Bahney, and S. Herculano-Houzel, *The search for true numbers of neurons and glial cells in the human brain: A review of 150 years of cell counting.* J Comp Neurol, 2016. **524**(18): p. 3865-3895.
6. Jäkel, S. and L. Dimou, *Glial Cells and Their Function in the Adult Brain: A Journey through the History of Their Ablation.* Front Cell Neurosci, 2017. **11**: p. 24.
7. Matute, C., *Mechanisms of glial death and protection*, in *Primer on Cerebrovascular Diseases*. 2017, Elsevier. p. 215-219.
8. Kovacs, G.G., *Cellular reactions of the central nervous system.* Handb Clin Neurol, 2017. **145**: p. 13-23.
9. Oberheim, N.A., et al., *Astrocytic complexity distinguishes the human brain.* Trends Neurosci, 2006. **29**(10): p. 547-53.
10. Santello, M., N. Toni, and A. Volterra, *Astrocyte function from information processing to cognition and cognitive impairment.* Nat Neurosci, 2019. **22**(2): p. 154-166.
11. Molofsky, A.V. and B. Deneen, *Astrocyte development: A Guide for the Perplexed.* Glia, 2015. **63**(8): p. 1320-9.
12. Sabogal-Guáqueta, A.M., et al., *Microglia alterations in neurodegenerative diseases and their modeling with human induced pluripotent stem cell and other platforms.* Prog Neurobiol, 2020. **190**: p. 101805.
13. Wake, H., A.J. Moorhouse, and J. Nabekura, *Functions of microglia in the central nervous system--beyond the immune response.* Neuron Glia Biol, 2011. **7**(1): p. 47-53.
14. Ginhoux, F. and M. Prinz, *Origin of microglia: current concepts and past controversies.* Cold Spring Harb Perspect Biol, 2015. **7**(8): p. a020537.
15. Duncan, G.J., et al., *The fate and function of oligodendrocyte progenitor cells after traumatic spinal cord injury.* Glia, 2020. **68**(2): p. 227-245.
16. Malatesta, P., I. Appolloni, and F. Calzolari, *Radial glia and neural stem cells.* Cell Tissue Res, 2008. **331**(1): p. 165-78.
17. Zahr, S.K., D.R. Kaplan, and F.D. Miller, *Translating neural stem cells to neurons in the mammalian brain.* Cell Death Differ, 2019. **26**(12): p. 2495-2512.
18. Falk, S. and M. Götz, *Glial control of neurogenesis.* Curr Opin Neurobiol, 2017. **47**: p. 188-195.
19. Li, L. and H. Clevers, *Coexistence of quiescent and active adult stem cells in mammals.* Science, 2010. **327**(5965): p. 542-5.
20. Andreotti, J.P., et al., *Neural stem cell niche heterogeneity.* Semin Cell Dev Biol, 2019. **95**: p. 42-53.
21. Bond, A.M., G.L. Ming, and H. Song, *Adult Mammalian Neural Stem Cells and Neurogenesis: Five Decades Later.* Cell Stem Cell, 2015. **17**(4): p. 385-95.
22. Aimone, J.B., et al., *Regulation and function of adult neurogenesis: from genes to cognition.* Physiol Rev, 2014. **94**(4): p. 991-1026.
23. Sierra, A., et al., *Microglia shape adult hippocampal neurogenesis through apoptosis-coupled phagocytosis.* Cell Stem Cell, 2010. **7**(4): p. 483-95.
24. Diaz-Aparicio, I., et al., *Microglia Actively Remodel Adult Hippocampal Neurogenesis through the Phagocytosis Secretome.* J Neurosci, 2020. **40**(7): p. 1453-1482.

25. Daneman, R. and A. Prat, *The blood-brain barrier.* Cold Spring Harb Perspect Biol, 2015. **7**(1): p. a020412.
26. Gawdi, R. and P.D. Emmady, *Physiology, Blood Brain Barrier*, in *StatPearls*. 2022, StatPearls Publishing

27. Weller, M., et al., *Glioma.* Nat Rev Dis Primers, 2015. **1**: p. 15017.
28. Scherer, H.J., *A CRITICAL REVIEW: THE PATHOLOGY OF CEREBRAL GLIOMAS.* J Neurol Psychiatry, 1940. **3**(2): p. 147-77.
29. DeAngelis, L.M. and I.K. Mellinghoff, *Virchow 2011 or how to ID(H) human glioblastoma.* J Clin Oncol, 2011. **29**(34): p. 4473-4.
30. *A classification of the tumours of the glioma group on a histogenetic basis, with a correlated study of prognosis. By Percival Bailey and Harvey Cushing. Medium 8vo. Pp. 175, with 108 illustrations. 1926. Philadelphia, London, and Montreal: J. B. Lippincott Company. 21s. net %J British Journal of Surgery.* 1927. **14**(55): p. 554-555.
31. Ferguson, S. and M.S. Lesniak, *Percival Bailey and the classification of brain tumors.* Neurosurg Focus, 2005. **18**(4): p. e7.
32. Louis, D.N., et al., *The 2021 WHO Classification of Tumors of the Central Nervous System: a summary.* Neuro Oncol, 2021. **23**(8): p. 1231-1251.
33. Louis, D.N., et al., *The 2007 WHO classification of tumours of the central nervous system.* Acta Neuropathol, 2007. **114**(2): p. 97-109.
34. GLOBUS, J.H. and I. STRAUSS, *SPONGIOBLASTOMA MULTIFORME: A PRIMARY MALIGNANT FORM OF BRAIN NEOPLASM: ITS CLINICAL AND ANATOMIC FEATURES.* Archives of Neurology & Psychiatry, 1925. **14**(2): p. 139-191.
35. Bailey, P. and H. Cushing, *A classification of the tumors of the glioma group on a histogenetic basis with a correlated study of prognosis*. 1926: Lippincott.
36. Oronsky, B., et al., *A Review of Newly Diagnosed Glioblastoma.* Front Oncol, 2020. **10**: p. 574012.
37. Thakkar, J.P., et al., *Epidemiologic and molecular prognostic review of glioblastoma.* Cancer Epidemiol Biomarkers Prev, 2014. **23**(10): p. 1985-96.
38. Stupp, R., et al., *Radiotherapy plus concomitant and adjuvant temozolomide for glioblastoma.* N Engl J Med, 2005. **352**(10): p. 987-96.
39. Scott, J.G., et al., *Aggressive treatment is appropriate for glioblastoma multiforme patients 70 years old or older: a retrospective review of 206 cases.* Neuro Oncol, 2011. **13**(4): p. 428-36.
40. Harrison, R.A. and J.F. de Groot, *Treatment of Glioblastoma in the Elderly.* Drugs Aging, 2018. **35**(8): p. 707-718.
41. Ostrom, Q.T., et al., *CBTRUS Statistical Report: Primary Brain and Other Central Nervous System Tumors Diagnosed in the United States in 2012-2016.* Neuro Oncol, 2019. **21**(Suppl 5): p. v1-v100.
42. Sadetzki, S., et al., *Description of selected characteristics of familial glioma patients - results from the Gliogene Consortium.* Eur J Cancer, 2013. **49**(6): p. 1335-45.
43. Fisher, J.L., et al., *Epidemiology of brain tumors.* Neurol Clin, 2007. **25**(4): p. 867-90, vii.
44. Ellor, S.V., T.A. Pagano-Young, and N.G. Avgeropoulos, *Glioblastoma: background, standard treatment paradigms, and supportive care considerations.* J Law Med Ethics, 2014. **42**(2): p. 171-82.
45. Bhattacharjee, B., N. Renzette, and T.F. Kowalik, *Genetic analysis of cytomegalovirus in malignant gliomas.* J Virol, 2012. **86**(12): p. 6815-24.
46. Akhtar, S., et al., *Epstein-Barr Virus in Gliomas: Cause, Association, or Artifact?* Front Oncol, 2018. **8**: p. 123.
47. Ohgaki, H. and P. Kleihues, *The definition of primary and secondary glioblastoma.* Clin Cancer Res, 2013. **19**(4): p. 764-72.

48. Stoyanov, G.S. and D.L. Dzhenkov, *On the Concepts and History of Glioblastoma Multiforme - Morphology, Genetics and Epigenetics.* Folia Med (Plovdiv), 2018. **60**(1): p. 48-66.
49. Wen, P.Y., et al., *Glioblastoma in adults: a Society for Neuro-Oncology (SNO) and European Society of Neuro-Oncology (EANO) consensus review on current management and future directions.* Neuro Oncol, 2020. **22**(8): p. 1073-1113.
50. Clarke, C., *Neurological diseases in Kumar & Clark Clinical Medicine. Kumar P and Clark M*. 2005, Elsevier Saunders, Edinburgh.
51. Alexander, B.M. and T.F. Cloughesy, *Adult Glioblastoma.* J Clin Oncol, 2017. **35**(21): p. 2402-2409.
52. Wen, P.Y., et al., *Updated response assessment criteria for high-grade gliomas: response assessment in neuro-oncology working group.* J Clin Oncol, 2010. **28**(11): p. 1963-72.
53. Davis, M.E., *Glioblastoma: Overview of Disease and Treatment.* Clin J Oncol Nurs, 2016. **20**(5 Suppl): p. S2-8.
54. Johnson, D.R., et al., *Case-Based Review: newly diagnosed glioblastoma.* Neurooncol Pract, 2015. **2**(3): p. 106-121.
55. Siegal, T., *Clinical impact of molecular biomarkers in gliomas.* J Clin Neurosci, 2015. **22**(3): p. 437-44.
56. Weller, M., et al., *Molecular neuro-oncology in clinical practice: a new horizon.* Lancet Oncol, 2013. **14**(9): p. e370-9.
57. Liu, L., et al., *Clinical significance of EGFR amplification and the aberrant EGFRvIII transcript in conventionally treated astrocytic gliomas.* J Mol Med (Berl), 2005. **83**(11): p. 917-26.
58. Nagane, M., et al., *A common mutant epidermal growth factor receptor confers enhanced tumorigenicity on human glioblastoma cells by increasing proliferation and reducing apoptosis.* Cancer Res, 1996. **56**(21): p. 5079-86.
59. Armocida, D., et al., *Is Ki-67 index overexpression in IDH wild type glioblastoma a predictor of shorter Progression Free survival? A clinical and Molecular analytic investigation.* Clin Neurol Neurosurg, 2020. **198**: p. 106126.
60. Stupp, R., et al., *Effects of radiotherapy with concomitant and adjuvant temozolomide versus radiotherapy alone on survival in glioblastoma in a randomised phase III study: 5-year analysis of the EORTC-NCIC trial.* Lancet Oncol, 2009. **10**(5): p. 459-66.
61. Fan, C.H., et al., *O6-methylguanine DNA methyltransferase as a promising target for the treatment of temozolomide-resistant gliomas.* Cell Death Dis, 2013. **4**(10): p. e876.
62. Watts, G.S., et al., *Methylation of discrete regions of the O6-methylguanine DNA methyltransferase (MGMT) CpG island is associated with heterochromatinization of the MGMT transcription start site and silencing of the gene.* Mol Cell Biol, 1997. **17**(9): p. 5612-9.
63. Pandith, A.A., et al., *Concordant association validates MGMT methylation and protein expression as favorable prognostic factors in glioma patients on alkylating chemotherapy (Temozolomide).* Sci Rep, 2018. **8**(1): p. 6704.
64. *Comprehensive genomic characterization defines human glioblastoma genes and core pathways.* Nature, 2008. **455**(7216): p. 1061-8.
65. Egaña, L., et al., *Methylation of MGMT promoter does not predict response to temozolomide in patients with glioblastoma in Donostia Hospital.* Sci Rep, 2020. **10**(1): p. 18445.
66. Cohen, M.H., et al., *FDA drug approval summary: bevacizumab (Avastin) as treatment of recurrent glioblastoma multiforme.* Oncologist, 2009. **14**(11): p. 1131-8.
67. Stupp, R., et al., *Maintenance Therapy With Tumor-Treating Fields Plus Temozolomide vs Temozolomide Alone for Glioblastoma: A Randomized Clinical Trial.* Jama, 2015. **314**(23): p. 2535-43.

68. Stupp, R., et al., *Effect of Tumor-Treating Fields Plus Maintenance Temozolomide vs Maintenance Temozolomide Alone on Survival in Patients With Glioblastoma: A Randomized Clinical Trial.* Jama, 2017. **318**(23): p. 2306-2316.
69. Branter, J., S. Basu, and S. Smith, *Tumour treating fields in a combinational therapeutic approach.* Oncotarget, 2018. **9**(93): p. 36631-36644.
70. Wick, W., *TTFields: where does all the skepticism come from?* Neuro Oncol, 2016. **18**(3): p. 303-5.
71. Shergalis, A., et al., *Current Challenges and Opportunities in Treating Glioblastoma.* Pharmacol Rev, 2018. **70**(3): p. 412-445.
72. Comba, A., et al., *Uncovering Spatiotemporal Heterogeneity of High-Grade Gliomas: From Disease Biology to Therapeutic Implications.* Front Oncol, 2021. **11**: p. 703764.
73. Verhaak, R.G., et al., *Integrated genomic analysis identifies clinically relevant subtypes of glioblastoma characterized by abnormalities in PDGFRA, IDH1, EGFR, and NF1.* Cancer Cell, 2010. **17**(1): p. 98-110.
74. Phillips, H.S., et al., *Molecular subclasses of high-grade glioma predict prognosis, delineate a pattern of disease progression, and resemble stages in neurogenesis.* Cancer Cell, 2006. **9**(3): p. 157-73.
75. Wang, Q., et al., *Tumor Evolution of Glioma-Intrinsic Gene Expression Subtypes Associates with Immunological Changes in the Microenvironment.* Cancer Cell, 2017. **32**(1): p. 42-56.e6.
76. Yan, H., et al., *IDH1 and IDH2 mutations in gliomas.* N Engl J Med, 2009. **360**(8): p. 765-73.
77. Furnari, F.B., et al., *Malignant astrocytic glioma: genetics, biology, and paths to treatment.* Genes Dev, 2007. **21**(21): p. 2683-710.
78. Arjona, D., J.A. Rey, and S.M. Taylor, *Early genetic changes involved in low-grade astrocytic tumor development.* Curr Mol Med, 2006. **6**(6): p. 645-50.
79. Brat, D.J., et al., *cIMPACT-NOW update 5: recommended grading criteria and terminologies for IDH-mutant astrocytomas.* Acta Neuropathol, 2020. **139**(3): p. 603-608.
80. Bhat, K.P.L., et al., *Mesenchymal differentiation mediated by NF-κB promotes radiation resistance in glioblastoma.* Cancer Cell, 2013. **24**(3): p. 331-46.
81. Neftel, C., et al., *An Integrative Model of Cellular States, Plasticity, and Genetics for Glioblastoma.* Cell, 2019. **178**(4): p. 835-849.e21.
82. Brennan, C.W., et al., *The somatic genomic landscape of glioblastoma.* Cell, 2013. **155**(2): p. 462-77.
83. Ma, H., et al., *Specific glioblastoma multiforme prognostic-subtype distinctions based on DNA methylation patterns.* Cancer Gene Ther, 2020. **27**(9): p. 702-714.
84. Garofano, L., et al., *Pathway-based classification of glioblastoma uncovers a mitochondrial subtype with therapeutic vulnerabilities.* Nat Cancer, 2021. **2**(2): p. 141-156.
85. Prasetyanti, P.R. and J.P. Medema, *Intra-tumor heterogeneity from a cancer stem cell perspective.* Mol Cancer, 2017. **16**(1): p. 41.
86. Muftuoglu, Y. and F. Pajonk, *Targeting Glioma Stem Cells.* Neurosurg Clin N Am, 2021. **32**(2): p. 283-289.
87. Medema, J.P., *Cancer stem cells: the challenges ahead.* Nat Cell Biol, 2013. **15**(4): p. 338-44.
88. Meacham, C.E. and S.J. Morrison, *Tumour heterogeneity and cancer cell plasticity.* Nature, 2013. **501**(7467): p. 328-37.
89. Silver, D.J. and D.A. Steindler, *Common astrocytic programs during brain development, injury and cancer.* Trends Neurosci, 2009. **32**(6): p. 303-11.
90. Lapidot, T., et al., *A cell initiating human acute myeloid leukaemia after transplantation into SCID mice.* Nature, 1994. **367**(6464): p. 645-8.

91. Al-Hajj, M., et al., *Prospective identification of tumorigenic breast cancer cells.* Proc Natl Acad Sci U S A, 2003. **100**(7): p. 3983-8.
92. Collins, A.T., et al., *Prospective identification of tumorigenic prostate cancer stem cells.* Cancer Res, 2005. **65**(23): p. 10946-51.
93. O'Brien, C.A., et al., *A human colon cancer cell capable of initiating tumour growth in immunodeficient mice.* Nature, 2007. **445**(7123): p. 106-10.
94. Ricci-Vitiani, L., et al., *Identification and expansion of human colon-cancer-initiating cells.* Nature, 2007. **445**(7123): p. 111-5.
95. Li, C., et al., *Identification of pancreatic cancer stem cells.* Cancer Res, 2007. **67**(3): p. 1030-7.
96. Ignatova, T.N., et al., *Human cortical glial tumors contain neural stem-like cells expressing astroglial and neuronal markers in vitro.* Glia, 2002. **39**(3): p. 193-206.
97. Singh, S.K., et al., *Identification of a cancer stem cell in human brain tumors.* Cancer Res, 2003. **63**(18): p. 5821-8.
98. Singh, S.K., et al., *Identification of human brain tumour initiating cells.* Nature, 2004. **432**(7015): p. 396-401.
99. Galli, R., et al., *Isolation and characterization of tumorigenic, stem-like neural precursors from human glioblastoma.* Cancer Res, 2004. **64**(19): p. 7011-21.
100. Lathia, J.D., et al., *Direct in vivo evidence for tumor propagation by glioblastoma cancer stem cells.* PLoS One, 2011. **6**(9): p. e24807.
101. Hu, B., et al., *Epigenetic Activation of WNT5A Drives Glioblastoma Stem Cell Differentiation and Invasive Growth.* Cell, 2016. **167**(5): p. 1281-1295.e18.
102. Chen, J., et al., *A restricted cell population propagates glioblastoma growth after chemotherapy.* Nature, 2012. **488**(7412): p. 522-6.
103. Nakai, E., et al., *Enhanced MDR1 expression and chemoresistance of cancer stem cells derived from glioblastoma.* Cancer Invest, 2009. **27**(9): p. 901-8.
104. Bao, S., et al., *Glioma stem cells promote radioresistance by preferential activation of the DNA damage response.* Nature, 2006. **444**(7120): p. 756-60.
105. Lobo, N.A., et al., *The biology of cancer stem cells.* Annu Rev Cell Dev Biol, 2007. **23**: p. 675-99.
106. Li, Q., et al., *Cancer stem cells and cell size: A causal link?* Semin Cancer Biol, 2015. **35**: p. 191-9.
107. Lombard, A., et al., *The Subventricular Zone, a Hideout for Adult and Pediatric High-Grade Glioma Stem Cells.* Front Oncol, 2020. **10**: p. 614930.
108. Sarkar, A. and K. Hochedlinger, *The sox family of transcription factors: versatile regulators of stem and progenitor cell fate.* Cell Stem Cell, 2013. **12**(1): p. 15-30.
109. de la Rocha, A.M., et al., *Role of SOX family of transcription factors in central nervous system tumors.* Am J Cancer Res, 2014. **4**(4): p. 312-24.
110. Stevanovic, M., et al., *SOX transcription factors and glioma stem cells: Choosing between stemness and differentiation.* World J Stem Cells, 2021. **13**(10): p. 1417-1445.
111. Garros-Regulez, L., et al., *mTOR inhibition decreases SOX2-SOX9 mediated glioma stem cell activity and temozolomide resistance.* Expert Opin Ther Targets, 2016. **20**(4): p. 393-405.
112. Bachoo, R.M., et al., *Epidermal growth factor receptor and Ink4a/Arf: convergent mechanisms governing terminal differentiation and transformation along the neural stem cell to astrocyte axis.* Cancer Cell, 2002. **1**(3): p. 269-77.
113. Holland, E.C., et al., *Combined activation of Ras and Akt in neural progenitors induces glioblastoma formation in mice.* Nat Genet, 2000. **25**(1): p. 55-7.
114. Huse, J.T. and E.C. Holland, *Genetically engineered mouse models of brain cancer and the promise of preclinical testing.* Brain Pathol, 2009. **19**(1): p. 132-43.
115. Kwon, C.H., et al., *Pten haploinsufficiency accelerates formation of high-grade astrocytomas.* Cancer Res, 2008. **68**(9): p. 3286-94.

116. Zhu, Y., et al., *Early inactivation of p53 tumor suppressor gene cooperating with NF1 loss induces malignant astrocytoma.* Cancer Cell, 2005. **8**(2): p. 119-30.
117. Alcantara Llaguno, S., et al., *Malignant astrocytomas originate from neural stem/progenitor cells in a somatic tumor suppressor mouse model.* Cancer Cell, 2009. **15**(1): p. 45-56.
118. Lee, J.H., et al., *Human glioblastoma arises from subventricular zone cells with low-level driver mutations.* Nature, 2018. **560**(7717): p. 243-247.
119. Mistry, A.M., *On the subventricular zone origin of human glioblastoma.* Transl Cancer Res, 2019. **8**(1): p. 11-13.
120. Lee, J.S., et al., *Brain cancer stem-like cell genesis from p53-deficient mouse astrocytes by oncogenic Ras.* Biochem Biophys Res Commun, 2008. **365**(3): p. 496-502.
121. Moon, J.H., et al., *Nanog-induced dedifferentiation of p53-deficient mouse astrocytes into brain cancer stem-like cells.* Biochem Biophys Res Commun, 2011. **412**(1): p. 175-81.
122. Friedmann-Morvinski, D., et al., *Dedifferentiation of neurons and astrocytes by oncogenes can induce gliomas in mice.* Science, 2012. **338**(6110): p. 1080-4.
123. Suvà, M.L., N. Riggi, and B.E. Bernstein, *Epigenetic reprogramming in cancer.* Science, 2013. **339**(6127): p. 1567-70.
124. Shibao, S., et al., *Metabolic heterogeneity and plasticity of glioma stem cells in a mouse glioblastoma model.* Neuro Oncol, 2018. **20**(3): p. 343-354.
125. Gilbertson, R.J. and J.N. Rich, *Making a tumour's bed: glioblastoma stem cells and the vascular niche.* Nat Rev Cancer, 2007. **7**(10): p. 733-6.
126. Codrici, E., et al., *Glioma Stem Cells and Their Microenvironments: Providers of Challenging Therapeutic Targets.* Stem Cells Int, 2016. **2016**: p. 5728438.
127. Niibori-Nambu, A., et al., *Glioma initiating cells form a differentiation niche via the induction of extracellular matrices and integrin αV.* PLoS One, 2013. **8**(5): p. e59558.
128. Boyd, N.H., et al., *Glioma stem cells and their roles within the hypoxic tumor microenvironment.* Theranostics, 2021. **11**(2): p. 665-683.
129. Biserova, K., et al., *Cancer Stem Cells: Significance in Origin, Pathogenesis and Treatment of Glioblastoma.* Cells, 2021. **10**(3).
130. Soda, Y., et al., *Transdifferentiation of glioblastoma cells into vascular endothelial cells.* Proc Natl Acad Sci U S A, 2011. **108**(11): p. 4274-80.
131. Hjelmeland, A.B., et al., *Acidic stress promotes a glioma stem cell phenotype.* Cell Death Differ, 2011. **18**(5): p. 829-40.
132. Flavahan, W.A., et al., *Brain tumor initiating cells adapt to restricted nutrition through preferential glucose uptake.* Nat Neurosci, 2013. **16**(10): p. 1373-82.
133. Heddleston, J.M., et al., *The hypoxic microenvironment maintains glioblastoma stem cells and promotes reprogramming towards a cancer stem cell phenotype.* Cell Cycle, 2009. **8**(20): p. 3274-84.
134. Filatova, A., T. Acker, and B.K. Garvalov, *The cancer stem cell niche(s): the crosstalk between glioma stem cells and their microenvironment.* Biochim Biophys Acta, 2013. **1830**(2): p. 2496-508.
135. Nayak, L. and F.M. Iwamoto, *Primary brain tumors in the elderly.* Curr Neurol Neurosci Rep, 2010. **10**(4): p. 252-8.
136. Wu, S., et al., *Evaluating intrinsic and non-intrinsic cancer risk factors.* Nat Commun, 2018. **9**(1): p. 3490.
137. López-Otín, C., et al., *The hallmarks of aging.* Cell, 2013. **153**(6): p. 1194-217.
138. Hanahan, D., *Hallmarks of Cancer: New Dimensions.* Cancer Discov, 2022. **12**(1): p. 31-46.
139. Kennedy, B.K., et al., *Geroscience: linking aging to chronic disease.* Cell, 2014. **159**(4): p. 709-13.
140. Isaev, N.K., E.V. Stelmashook, and E.E. Genrikhs, *Neurogenesis and brain aging.* Rev Neurosci, 2019. **30**(6): p. 573-580.

141. Oeppen, J. and J.W. Vaupel, *Demography. Broken limits to life expectancy.* Science, 2002. **296**(5570): p. 1029-31.
142. Partridge, L., J. Deelen, and P.E. Slagboom, *Facing up to the global challenges of ageing.* Nature, 2018. **561**(7721): p. 45-56.
143. Drayer, B.P., *Imaging of the aging brain. Part I. Normal findings.* Radiology, 1988. **166**(3): p. 785-96.
144. Isaev, N.K., et al., *Accelerated aging and aging process in the brain.* Rev Neurosci, 2018. **29**(3): p. 233-240.
145. Navarro Negredo, P., R.W. Yeo, and A. Brunet, *Aging and Rejuvenation of Neural Stem Cells and Their Niches.* Cell Stem Cell, 2020. **27**(2): p. 202-223.
146. Soreq, L., et al., *Major Shifts in Glial Regional Identity Are a Transcriptional Hallmark of Human Brain Aging.* Cell Rep, 2017. **18**(2): p. 557-570.
147. Salas, I.H., J. Burgado, and N.J. Allen, *Glia: victims or villains of the aging brain?* Neurobiol Dis, 2020. **143**: p. 105008.
148. Bouab, M., et al., *Aging of the subventricular zone neural stem cell niche: evidence for quiescence-associated changes between early and mid-adulthood.* Neuroscience, 2011. **173**: p. 135-49.
149. Sorrells, S.F., et al., *Human hippocampal neurogenesis drops sharply in children to undetectable levels in adults.* Nature, 2018. **555**(7696): p. 377-381.
150. Spalding, K.L., et al., *Dynamics of hippocampal neurogenesis in adult humans.* Cell, 2013. **153**(6): p. 1219-1227.
151. Boldrini, M., et al., *Human Hippocampal Neurogenesis Persists throughout Aging.* Cell Stem Cell, 2018. **22**(4): p. 589-599.e5.
152. Ernst, A., et al., *Neurogenesis in the striatum of the adult human brain.* Cell, 2014. **156**(5): p. 1072-83.
153. Vaughan, D.W. and A. Peters, *Neuroglial cells in the cerebral cortex of rats from young adulthood to old age: an electron microscope study.* J Neurocytol, 1974. **3**(4): p. 405-29.
154. Peters, A., K. Josephson, and S.L. Vincent, *Effects of aging on the neuroglial cells and pericytes within area 17 of the rhesus monkey cerebral cortex.* Anat Rec, 1991. **229**(3): p. 384-98.
155. Hefendehl, J.K., et al., *Homeostatic and injury-induced microglia behavior in the aging brain.* Aging Cell, 2014. **13**(1): p. 60-9.
156. Streit, W.J., et al., *Dystrophic microglia in the aging human brain.* Glia, 2004. **45**(2): p. 208-12.
157. Streit, W.J., et al., *Microglial pathology.* Acta Neuropathol Commun, 2014. **2**: p. 142.
158. Marschallinger, J., et al., *Lipid-droplet-accumulating microglia represent a dysfunctional and proinflammatory state in the aging brain.* Nat Neurosci, 2020. **23**(2): p. 194-208.
159. Suhonen, J.O., et al., *Differentiation of adult hippocampus-derived progenitors into olfactory neurons in vivo.* Nature, 1996. **383**(6601): p. 624-7.
160. Bachstetter, A.D., et al., *Fractalkine and CX 3 CR1 regulate hippocampal neurogenesis in adult and aged rats.* Neurobiol Aging, 2011. **32**(11): p. 2030-44.
161. Monje, M.L., H. Toda, and T.D. Palmer, *Inflammatory blockade restores adult hippocampal neurogenesis.* Science, 2003. **302**(5651): p. 1760-5.
162. Solano Fonseca, R., et al., *Neurogenic Niche Microglia Undergo Positional Remodeling and Progressive Activation Contributing to Age-Associated Reductions in Neurogenesis.* Stem Cells Dev, 2016. **25**(7): p. 542-55.
163. Elmore, M.R.P., et al., *Replacement of microglia in the aged brain reverses cognitive, synaptic, and neuronal deficits in mice.* Aging Cell, 2018. **17**(6): p. e12832.
164. Balch, W.E., et al., *Adapting proteostasis for disease intervention.* Science, 2008. **319**(5865): p. 916-9.
165. Laskowska, E., D. Kuczyńska-Wiśnik, and B. Lipińska, *Proteomic analysis of protein homeostasis and aggregation.* J Proteomics, 2019. **198**: p. 98-112.

166. Yang, Z. and D.J. Klionsky, *Eaten alive: a history of macroautophagy.* Nat Cell Biol, 2010. **12**(9): p. 814-22.
167. Boya, P., F. Reggiori, and P. Codogno, *Emerging regulation and functions of autophagy.* Nat Cell Biol, 2013. **15**(7): p. 713-20.
168. De Duve, C., *The lysosome.* Sci Am, 1963. **208**: p. 64-72.
169. Levy, J.M.M., C.G. Towers, and A. Thorburn, *Targeting autophagy in cancer.* Nat Rev Cancer, 2017. **17**(9): p. 528-542.
170. Aman, Y., et al., *Autophagy in healthy aging and disease.* Nat Aging, 2021. **1**(8): p. 634-650.
171. De Duve, C. and R. Wattiaux, *Functions of lysosomes.* Annu Rev Physiol, 1966. **28**: p. 435-92.
172. Marzella, L., J. Ahlberg, and H. Glaumann, *Autophagy, heterophagy, microautophagy and crinophagy as the means for intracellular degradation.* Virchows Arch B Cell Pathol Incl Mol Pathol, 1981. **36**(2-3): p. 219-34.
173. Klionsky, D.J., et al., *Guidelines for the use and interpretation of assays for monitoring autophagy (3rd edition).* Autophagy, 2016. **12**(1): p. 1-222.
174. Arndt, V., et al., *Chaperone-assisted selective autophagy is essential for muscle maintenance.* Curr Biol, 2010. **20**(2): p. 143-8.
175. Sahu, R., et al., *Microautophagy of cytosolic proteins by late endosomes.* Dev Cell, 2011. **20**(1): p. 131-9.
176. Dice, J.F., et al., *Regulation of catabolism of microinjected ribonuclease A. Identification of residues 7-11 as the essential pentapeptide.* J Biol Chem, 1986. **261**(15): p. 6853-9.
177. Kaushik, S. and A.M. Cuervo, *The coming of age of chaperone-mediated autophagy.* Nat Rev Mol Cell Biol, 2018. **19**(6): p. 365-381.
178. Ferreira, J.V., et al., *K63 linked ubiquitin chain formation is a signal for HIF1A degradation by Chaperone-Mediated Autophagy.* Sci Rep, 2015. **5**: p. 10210.
179. Dice, J.F., *Peptide sequences that target cytosolic proteins for lysosomal proteolysis.* Trends Biochem Sci, 1990. **15**(8): p. 305-9.
180. Cuervo, A.M. and J.F. Dice, *A receptor for the selective uptake and degradation of proteins by lysosomes.* Science, 1996. **273**(5274): p. 501-3.
181. Salvador, N., et al., *Import of a cytosolic protein into lysosomes by chaperone-mediated autophagy depends on its folding state.* J Biol Chem, 2000. **275**(35): p. 27447-56.
182. Cuervo, A.M. and E. Wong, *Chaperone-mediated autophagy: roles in disease and aging.* Cell Res, 2014. **24**(1): p. 92-104.
183. Bandyopadhyay, U., et al., *The chaperone-mediated autophagy receptor organizes in dynamic protein complexes at the lysosomal membrane.* Mol Cell Biol, 2008. **28**(18): p. 5747-63.
184. Agarraberes, F.A. and J.F. Dice, *A molecular chaperone complex at the lysosomal membrane is required for protein translocation.* J Cell Sci, 2001. **114**(Pt 13): p. 2491-9.
185. Massey, A.C., et al., *Consequences of the selective blockage of chaperone-mediated autophagy.* Proc Natl Acad Sci U S A, 2006. **103**(15): p. 5805-10.
186. Kiffin, R., et al., *Activation of chaperone-mediated autophagy during oxidative stress.* Mol Biol Cell, 2004. **15**(11): p. 4829-40.
187. Schneider, J.L., et al., *Loss of hepatic chaperone-mediated autophagy accelerates proteostasis failure in aging.* Aging Cell, 2015. **14**(2): p. 249-64.
188. Backer, J.M. and J.F. Dice, *Covalent linkage of ribonuclease S-peptide to microinjected proteins causes their intracellular degradation to be enhanced during serum withdrawal.* Proc Natl Acad Sci U S A, 1986. **83**(16): p. 5830-4.
189. Tasset, I. and A.M. Cuervo, *Role of chaperone-mediated autophagy in metabolism.* Febs j, 2016. **283**(13): p. 2403-13.
190. Park, C., Y. Suh, and A.M. Cuervo, *Regulated degradation of Chk1 by chaperone-mediated autophagy in response to DNA damage.* Nat Commun, 2015. **6**: p. 6823.

191. Ferreira, J.V., et al., *STUB1/CHIP is required for HIF1A degradation by chaperone-mediated autophagy.* Autophagy, 2013. **9**(9): p. 1349-66.
192. Hubbi, M.E., et al., *Chaperone-mediated autophagy targets hypoxia-inducible factor-1α (HIF-1α) for lysosomal degradation.* J Biol Chem, 2013. **288**(15): p. 10703-14.
193. Valdor, R., et al., *Chaperone-mediated autophagy regulates T cell responses through targeted degradation of negative regulators of T cell activation.* Nat Immunol, 2014. **15**(11): p. 1046-54.
194. Xu, Y., et al., *Chaperone-mediated autophagy regulates the pluripotency of embryonic stem cells.* Science, 2020. **369**(6502): p. 397-403.
195. Dong, S., et al., *Chaperone-mediated autophagy sustains haematopoietic stem-cell function.* Nature, 2021. **591**(7848): p. 117-123.
196. Cuervo, A.M. and J.F. Dice, *Unique properties of lamp2a compared to other lamp2 isoforms.* J Cell Sci, 2000. **113 Pt 24**: p. 4441-50.
197. Pajares, M., et al., *Transcription factor NFE2L2/NRF2 modulates chaperone-mediated autophagy through the regulation of LAMP2A.* Autophagy, 2018. **14**(8): p. 1310-1322.
198. Zhang, J., et al., *Cystinosin, the small GTPase Rab11, and the Rab7 effector RILP regulate intracellular trafficking of the chaperone-mediated autophagy receptor LAMP2A.* J Biol Chem, 2017. **292**(25): p. 10328-10346.
199. Kaushik, S., A.C. Massey, and A.M. Cuervo, *Lysosome membrane lipid microdomains: novel regulators of chaperone-mediated autophagy.* Embo j, 2006. **25**(17): p. 3921-33.
200. Bandyopadhyay, U., et al., *Identification of regulators of chaperone-mediated autophagy.* Mol Cell, 2010. **39**(4): p. 535-47.
201. Arias, E., et al., *Lysosomal mTORC2/PHLPP1/Akt Regulate Chaperone-Mediated Autophagy.* Mol Cell, 2015. **59**(2): p. 270-84.
202. Auzmendi-Iriarte, J. and A. Matheu, *Impact of Chaperone-Mediated Autophagy in Brain Aging: Neurodegenerative Diseases and Glioblastoma.* Front Aging Neurosci, 2020. **12**: p. 630743.
203. Cuervo, A.M. and J.F. Dice, *Age-related decline in chaperone-mediated autophagy.* J Biol Chem, 2000. **275**(40): p. 31505-13.
204. Zhang, C. and A.M. Cuervo, *Restoration of chaperone-mediated autophagy in aging liver improves cellular maintenance and hepatic function.* Nat Med, 2008. **14**(9): p. 959-65.
205. Arias, E. and A.M. Cuervo, *Pros and Cons of Chaperone-Mediated Autophagy in Cancer Biology.* Trends Endocrinol Metab, 2020. **31**(1): p. 53-66.
206. Kon, M., et al., *Chaperone-mediated autophagy is required for tumor growth.* Sci Transl Med, 2011. **3**(109): p. 109ra117.
207. Loeffler, D.A., *Influence of Normal Aging on Brain Autophagy: A Complex Scenario.* Front Aging Neurosci, 2019. **11**: p. 49.
208. Loeffler, D.A., et al., *Age-Related Decrease in Heat Shock 70-kDa Protein 8 in Cerebrospinal Fluid Is Associated with Increased Oxidative Stress.* Front Aging Neurosci, 2016. **8**: p. 178.
209. Loeffler, D.A., et al., *Cerebrospinal Fluid Concentration of Key Autophagy Protein Lamp2 Changes Little During Normal Aging.* Front Aging Neurosci, 2018. **10**: p. 130.
210. Escamilla-Ramírez, A., et al., *Autophagy as a Potential Therapy for Malignant Glioma.* Pharmaceuticals (Basel), 2020. **13**(7).
211. Yang, K., et al., *Glioblastoma: Targeting the autophagy in tumorigenesis.* Brain Res Bull, 2019. **153**: p. 334-340.
212. Liu, W.T., et al., *Inhibition of glioma growth by minocycline is mediated through endoplasmic reticulum stress-induced apoptosis and autophagic cell death.* Neuro Oncol, 2013. **15**(9): p. 1127-41.
213. Gammoh, N., et al., *Suppression of autophagy impedes glioblastoma development and induces senescence.* Autophagy, 2016. **12**(9): p. 1431-9.

214. Natsumeda, M., et al., *Induction of autophagy in temozolomide treated malignant gliomas.* Neuropathology, 2011. **31**(5): p. 486-93.
215. Valdor, R., et al., *Glioblastoma ablates pericytes antitumor immune function through aberrant up-regulation of chaperone-mediated autophagy.* Proc Natl Acad Sci U S A, 2019. **116**(41): p. 20655-20665.
216. Ryskalin, L., et al., *The Autophagy Status of Cancer Stem Cells in Gliobastoma Multiforme: From Cancer Promotion to Therapeutic Strategies.* Int J Mol Sci, 2019. **20**(15).
217. Nazio, F., et al., *Autophagy and cancer stem cells: molecular mechanisms and therapeutic applications.* Cell Death Differ, 2019. **26**(4): p. 690-702.
218. Allis, C.D. and T. Jenuwein, *The molecular hallmarks of epigenetic control.* Nat Rev Genet, 2016. **17**(8): p. 487-500.
219. Cavalli, G. and E. Heard, *Advances in epigenetics link genetics to the environment and disease.* Nature, 2019. **571**(7766): p. 489-499.
220. Benayoun, B.A., E.A. Pollina, and A. Brunet, *Epigenetic regulation of ageing: linking environmental inputs to genomic stability.* Nat Rev Mol Cell Biol, 2015. **16**(10): p. 593-610.
221. Barter, J.D. and T.C. Foster, *Aging in the Brain: New Roles of Epigenetics in Cognitive Decline.* Neuroscientist, 2018. **24**(5): p. 516-525.
222. Shireby, G.L., et al., *Recalibrating the epigenetic clock: implications for assessing biological age in the human cortex.* Brain, 2020. **143**(12): p. 3763-3775.
223. Shahzad, U., et al., *Noncoding RNAs in Glioblastoma: Emerging Biological Concepts and Potential Therapeutic Implications.* Cancers (Basel), 2021. **13**(7).
224. Houston, I., et al., *Epigenetics in the human brain.* Neuropsychopharmacology, 2013. **38**(1): p. 183-97.
225. Hwang, J.Y., K.A. Aromolaran, and R.S. Zukin, *The emerging field of epigenetics in neurodegeneration and neuroprotection.* Nat Rev Neurosci, 2017. **18**(6): p. 347-361.
226. Suter, R.K., J. Rodriguez-Blanco, and N.G. Ayad, *Epigenetic pathways and plasticity in brain tumors.* Neurobiol Dis, 2020. **145**: p. 105060.
227. Chaligne, R., et al., *Epigenetic encoding, heritability and plasticity of glioma transcriptional cell states.* Nat Genet, 2021. **53**(10): p. 1469-1479.
228. Daniel, M. and T.O. Tollefsbol, *Epigenetic linkage of aging, cancer and nutrition.* J Exp Biol, 2015. **218**(Pt 1): p. 59-70.
229. Kouzarides, T., *Chromatin modifications and their function.* Cell, 2007. **128**(4): p. 693-705.
230. Dupont, C., D.R. Armant, and C.A. Brenner, *Epigenetics: definition, mechanisms and clinical perspective.* Semin Reprod Med, 2009. **27**(5): p. 351-7.
231. Li, G., Y. Tian, and W.G. Zhu, *The Roles of Histone Deacetylases and Their Inhibitors in Cancer Therapy.* Front Cell Dev Biol, 2020. **8**: p. 576946.
232. Xu, Y., et al., *WERAM: a database of writers, erasers and readers of histone acetylation and methylation in eukaryotes.* Nucleic Acids Res, 2017. **45**(D1): p. D264-d270.
233. Allfrey, V.G., R. Faulkner, and A.E. Mirsky, *ACETYLATION AND METHYLATION OF HISTONES AND THEIR POSSIBLE ROLE IN THE REGULATION OF RNA SYNTHESIS.* Proc Natl Acad Sci U S A, 1964. **51**(5): p. 786-94.
234. Alonso, W.R. and D.A. Nelson, *A novel yeast histone deacetylase: partial characterization and development of an activity assay.* Biochim Biophys Acta, 1986. **866**(2-3): p. 161-9.
235. Stiegler, P., et al., *The COOH-terminal region of pRb2/p130 binds to histone deacetylase 1 (HDAC1), enhancing transcriptional repression of the E2F-dependent cyclin A promoter.* Cancer Res, 1998. **58**(22): p. 5049-52.
236. Gao, L., et al., *Cloning and functional characterization of HDAC11, a novel member of the human histone deacetylase family.* J Biol Chem, 2002. **277**(28): p. 25748-55.
237. Milazzo, G., et al., *Histone Deacetylases (HDACs): Evolution, Specificity, Role in Transcriptional Complexes, and Pharmacological Actionability.* Genes (Basel), 2020. **11**(5).

238. Witt, O., et al., *HDAC family: What are the cancer relevant targets?* Cancer Lett, 2009. **277**(1): p. 8-21.
239. Hubbert, C., et al., *HDAC6 is a microtubule-associated deacetylase.* Nature, 2002. **417**(6887): p. 455-8.
240. Juan, L.J., et al., *Histone deacetylases specifically down-regulate p53-dependent gene activation.* J Biol Chem, 2000. **275**(27): p. 20436-43.
241. Shukla, S. and B.L. Tekwani, *Histone Deacetylases Inhibitors in Neurodegenerative Diseases, Neuroprotection and Neuronal Differentiation.* Front Pharmacol, 2020. **11**: p. 537.
242. Hai, Y. and D.W. Christianson, *Histone deacetylase 6 structure and molecular basis of catalysis and inhibition.* Nat Chem Biol, 2016. **12**(9): p. 741-7.
243. Boyault, C., et al., *HDAC6-p97/VCP controlled polyubiquitin chain turnover.* Embo j, 2006. **25**(14): p. 3357-66.
244. Guardiola, A.R. and T.P. Yao, *Molecular cloning and characterization of a novel histone deacetylase HDAC10.* J Biol Chem, 2002. **277**(5): p. 3350-6.
245. Tanno, M., et al., *Nucleocytoplasmic shuttling of the NAD+-dependent histone deacetylase SIRT1.* J Biol Chem, 2007. **282**(9): p. 6823-32.
246. Onyango, P., et al., *SIRT3, a human SIR2 homologue, is an NAD-dependent deacetylase localized to mitochondria.* Proc Natl Acad Sci U S A, 2002. **99**(21): p. 13653-8.
247. Kutil, Z., et al., *Histone Deacetylase 11 Is a Fatty-Acid Deacylase.* ACS Chem Biol, 2018. **13**(3): p. 685-693.
248. Xu, W.S., R.B. Parmigiani, and P.A. Marks, *Histone deacetylase inhibitors: molecular mechanisms of action.* Oncogene, 2007. **26**(37): p. 5541-52.
249. Zhang, Y., et al., *Mice lacking histone deacetylase 6 have hyperacetylated tubulin but are viable and develop normally.* Mol Cell Biol, 2008. **28**(5): p. 1688-701.
250. Grunstein, M., *Histone acetylation in chromatin structure and transcription.* Nature, 1997. **389**(6649): p. 349-52.
251. Harms, K.L. and X. Chen, *Histone deacetylase 2 modulates p53 transcriptional activities through regulation of p53-DNA binding activity.* Cancer Res, 2007. **67**(7): p. 3145-52.
252. Brochier, C., et al., *Specific acetylation of p53 by HDAC inhibition prevents DNA damage-induced apoptosis in neurons.* J Neurosci, 2013. **33**(20): p. 8621-32.
253. Gryder, B.E., et al., *Chemical genomics reveals histone deacetylases are required for core regulatory transcription.* Nat Commun, 2019. **10**(1): p. 3004.
254. Ju, R. and M.T. Muller, *Histone deacetylase inhibitors activate p21(WAF1) expression via ATM.* Cancer Res, 2003. **63**(11): p. 2891-7.
255. Yamaguchi, T., et al., *Histone deacetylases 1 and 2 act in concert to promote the G1-to-S progression.* Genes Dev, 2010. **24**(5): p. 455-69.
256. Bai, J., et al., *Down-regulation of deacetylase HDAC6 inhibits the melanoma cell line A375.S2 growth through ROS-dependent mitochondrial pathway.* PLoS One, 2015. **10**(3): p. e0121247.
257. Reddy, R.G., et al., *Advances in histone deacetylase inhibitors in targeting glioblastoma stem cells.* Cancer Chemother Pharmacol, 2020. **86**(2): p. 165-179.
258. Li, H., et al., *p27(Kip1) directly represses Sox2 during embryonic stem cell differentiation.* Cell Stem Cell, 2012. **11**(6): p. 845-52.
259. Pasyukova, E.G. and A.M. Vaiserman, *HDAC inhibitors: A new promising drug class in anti-aging research.* Mech Ageing Dev, 2017. **166**: p. 6-15.
260. Boffa, L.C., et al., *Suppression of histone deacetylation in vivo and in vitro by sodium butyrate.* J Biol Chem, 1978. **253**(10): p. 3364-6.
261. Fraga, M.F., et al., *Loss of acetylation at Lys16 and trimethylation at Lys20 of histone H4 is a common hallmark of human cancer.* Nat Genet, 2005. **37**(4): p. 391-400.
262. Dell'Aversana, C., I. Lepore, and L. Altucci, *HDAC modulation and cell death in the clinic.* Exp Cell Res, 2012. **318**(11): p. 1229-44.

263. Li, S., et al., *Histone deacetylase 1 promotes glioblastoma cell proliferation and invasion via activation of PI3K/AKT and MEK/ERK signaling pathways.* Brain Res, 2018. **1692**: p. 154-162.
264. Huang, Z., et al., *Histone deacetylase 6 promotes growth of glioblastoma through the MKK7/JNK/c-Jun signaling pathway.* J Neurochem, 2020. **152**(2): p. 221-234.
265. Li, S., et al., *Histone deacetylase 6 promotes growth of glioblastoma through inhibition of SMAD2 signaling.* Tumour Biol, 2015. **36**(12): p. 9661-5.
266. Yang, W.B., et al., *Increased activation of HDAC1/2/6 and Sp1 underlies therapeutic resistance and tumor growth in glioblastoma.* Neuro Oncol, 2020. **22**(10): p. 1439-1451.
267. Kim, G.W., et al., *Temozolomide-resistant Glioblastoma Depends on HDAC6 Activity Through Regulation of DNA Mismatch Repair.* Anticancer Res, 2019. **39**(12): p. 6731-6741.
268. Marampon, F., et al., *HDAC4 and HDAC6 sustain DNA double strand break repair and stem-like phenotype by promoting radioresistance in glioblastoma cells.* Cancer Lett, 2017. **397**: p. 1-11.
269. Yang, W., et al., *HDAC6 inhibition induces glioma stem cells differentiation and enhances cellular radiation sensitivity through the SHH/Gli1 signaling pathway.* Cancer Lett, 2018. **415**: p. 164-176.
270. Chang, C.J., et al., *Enhanced radiosensitivity and radiation-induced apoptosis in glioma CD133-positive cells by knockdown of SirT1 expression.* Biochem Biophys Res Commun, 2009. **380**(2): p. 236-42.
271. Sayd, S., et al., *Sirtuin-2 activity is required for glioma stem cell proliferation arrest but not necrosis induced by resveratrol.* Stem Cell Rev Rep, 2014. **10**(1): p. 103-13.
272. Hsu, C.C., et al., *Suberoylanilide hydroxamic acid represses glioma stem-like cells.* J Biomed Sci, 2016. **23**(1): p. 81.
273. Alvarez, A.A., et al., *The effects of histone deacetylase inhibitors on glioblastoma-derived stem cells.* J Mol Neurosci, 2015. **55**(1): p. 7-20.
274. Bezecny, P., *Histone deacetylase inhibitors in glioblastoma: pre-clinical and clinical experience.* Med Oncol, 2014. **31**(6): p. 985.
275. Booth, L.N. and A. Brunet, *The Aging Epigenome.* Mol Cell, 2016. **62**(5): p. 728-44.
276. Satoh, A., S.I. Imai, and L. Guarente, *The brain, sirtuins, and ageing.* Nat Rev Neurosci, 2017. **18**(6): p. 362-374.
277. Singh, P. and M.K. Thakur, *Reduced recognition memory is correlated with decrease in DNA methyltransferase1 and increase in histone deacetylase2 protein expression in old male mice.* Biogerontology, 2014. **15**(4): p. 339-46.
278. Chouliaras, L., et al., *Histone deacetylase 2 in the mouse hippocampus: attenuation of age-related increase by caloric restriction.* Curr Alzheimer Res, 2013. **10**(8): p. 868-76.
279. Dos Santos Sant' Anna, G., et al., *Histone deacetylase activity is altered in brain areas from aged rats.* Neurosci Lett, 2013. **556**: p. 152-4.
280. Sun, G., et al., *Orphan nuclear receptor TLX recruits histone deacetylases to repress transcription and regulate neural stem cell proliferation.* Proc Natl Acad Sci U S A, 2007. **104**(39): p. 15282-7.
281. MacDonald, J.L. and A.J. Roskams, *Histone deacetylases 1 and 2 are expressed at distinct stages of neuro-glial development.* Dev Dyn, 2008. **237**(8): p. 2256-67.
282. Sun, G., et al., *Histone deacetylases in neural stem cells and induced pluripotent stem cells.* J Biomed Biotechnol, 2011. **2011**: p. 835968.
283. Bahari-Javan, S., et al., *HDAC1 regulates fear extinction in mice.* J Neurosci, 2012. **32**(15): p. 5062-73.
284. Guan, J.S., et al., *HDAC2 negatively regulates memory formation and synaptic plasticity.* Nature, 2009. **459**(7243): p. 55-60.
285. McQuown, S.C., et al., *HDAC3 is a critical negative regulator of long-term memory formation.* J Neurosci, 2011. **31**(2): p. 764-74.

286. Kim, M.S., et al., *An essential role for histone deacetylase 4 in synaptic plasticity and memory formation.* J Neurosci, 2012. **32**(32): p. 10879-86.
287. LoPresti, P., *HDAC6 in Diseases of Cognition and of Neurons.* Cells, 2020. **10**(1).
288. Datta, M., et al., *Histone Deacetylases 1 and 2 Regulate Microglia Function during Development, Homeostasis, and Neurodegeneration in a Context-Dependent Manner.* Immunity, 2018. **48**(3): p. 514-529.e6.
289. Bowman, R.L., et al., *GlioVis data portal for visualization and analysis of brain tumor expression datasets.* Neuro Oncol, 2017. **19**(1): p. 139-141.
290. Müller, S., et al., *A single-cell atlas of human glioblastoma reveals a single axis of phenotype in tumor-propagating cells.* 2018: p. 377606.
291. Menyhárt, O., J.T. Fekete, and B. Győrffy, *Gene expression-based biomarkers designating glioblastomas resistant to multiple treatment strategies.* Carcinogenesis, 2021. **42**(6): p. 804-813.
292. Gao, J., et al., *Integrative analysis of complex cancer genomics and clinical profiles using the cBioPortal.* Sci Signal, 2013. **6**(269): p. pl1.
293. Cerami, E., et al., *The cBio cancer genomics portal: an open platform for exploring multidimensional cancer genomics data.* Cancer Discov, 2012. **2**(5): p. 401-4.
294. Louis, D.N., et al., *The 2016 World Health Organization Classification of Tumors of the Central Nervous System: a summary.* Acta Neuropathol, 2016. **131**(6): p. 803-20.
295. Miller, J.A., et al., *Neuropathological and transcriptomic characteristics of the aged brain.* Elife, 2017. **6**.
296. Olah, M., et al., *A transcriptomic atlas of aged human microglia.* Nat Commun, 2018. **9**(1): p. 539.
297. Morton, D.B. and P.H. Griffiths, *Guidelines on the recognition of pain, distress and discomfort in experimental animals and an hypothesis for assessment.* Vet Rec, 1985. **116**(16): p. 431-6.
298. Lein, E.S., et al., *Genome-wide atlas of gene expression in the adult mouse brain.* Nature, 2007. **445**(7124): p. 168-76.
299. Pérez-Salvia, M., et al., *In vitro and in vivo activity of a new small-molecule inhibitor of HDAC6 in mantle cell lymphoma.* Haematologica, 2018. **103**(11): p. e537-e540.
300. Auzmendi-Iriarte, J., et al., *Characterization of a new small-molecule inhibitor of HDAC6 in glioblastoma.* Cell Death Dis, 2020. **11**(6): p. 417.
301. Storp, B., et al., *Albumin nanoparticles with predictable size by desolvation procedure.* J Microencapsul, 2012. **29**(2): p. 138-46.
302. Arrizabalaga, O., et al., *High expression of MKP1/DUSP1 counteracts glioma stem cell activity and mediates HDAC inhibitor response.* Oncogenesis, 2017. **6**(12): p. 401.
303. Yang, W.M., et al., *Isolation and characterization of cDNAs corresponding to an additional member of the human histone deacetylase gene family.* J Biol Chem, 1997. **272**(44): p. 28001-7.
304. Wiśniewski, J.R., et al., *Universal sample preparation method for proteome analysis.* Nat Methods, 2009. **6**(5): p. 359-62.
305. Tyanova, S., et al., *The Perseus computational platform for comprehensive analysis of (prote)omics data.* Nat Methods, 2016. **13**(9): p. 731-40.
306. G., C., *Protein Array Analyze for ImageJ* ImageJ News, 2010.
307. Koga, H., et al., *A photoconvertible fluorescent reporter to track chaperone-mediated autophagy.* Nat Commun, 2011. **2**: p. 386.
308. Lal, S., et al., *An implantable guide-screw system for brain tumor studies in small animals.* J Neurosurg, 2000. **92**(2): p. 326-33.
309. Donoghue, J.F., O. Bogler, and T.G. Johns, *A simple guide screw method for intracranial xenograft studies in mice.* J Vis Exp, 2011(55).
310. Cuervo, A.M., et al., *Selective degradation of annexins by chaperone-mediated autophagy.* J Biol Chem, 2000. **275**(43): p. 33329-35.

311. Kaushik, S., et al., *Chaperone-mediated autophagy at a glance.* J Cell Sci, 2011. **124**(Pt 4): p. 495-9.
312. Brown, D.V., et al., *Expression of CD133 and CD44 in glioblastoma stem cells correlates with cell proliferation, phenotype stability and intra-tumor heterogeneity.* PLoS One, 2017. **12**(2): p. e0172791.
313. Silver, D.J. and J.D. Lathia, *Revealing the glioma cancer stem cell interactome, one niche at a time.* J Pathol, 2018. **244**(3): p. 260-264.
314. Talukdar, S., et al., *EGFR: An essential receptor tyrosine kinase-regulator of cancer stem cells.* Adv Cancer Res, 2020. **147**: p. 161-188.
315. Bleau, A.M., et al., *PTEN/PI3K/Akt pathway regulates the side population phenotype and ABCG2 activity in glioma tumor stem-like cells.* Cell Stem Cell, 2009. **4**(3): p. 226-35.
316. Zheng, H., et al., *p53 and Pten control neural and glioma stem/progenitor cell renewal and differentiation.* Nature, 2008. **455**(7216): p. 1129-33.
317. Sack, M.N., *Mitochondrial depolarization and the role of uncoupling proteins in ischemia tolerance.* Cardiovasc Res, 2006. **72**(2): p. 210-9.
318. Piperi, C., K.A. Papavassiliou, and A.G. Papavassiliou, *Pivotal Role of STAT3 in Shaping Glioblastoma Immune Microenvironment.* Cells, 2019. **8**(11).
319. Herrera-Perez, M., S.L. Voytik-Harbin, and J.L. Rickus, *Extracellular Matrix Properties Regulate the Migratory Response of Glioblastoma Stem Cells in Three-Dimensional Culture.* Tissue Eng Part A, 2015. **21**(19-20): p. 2572-82.
320. Brelstaff, J.H., et al., *Microglia become hypofunctional and release metalloproteases and tau seeds when phagocytosing live neurons with P301S tau aggregates.* Sci Adv, 2021. **7**(43): p. eabg4980.
321. Angelova, D.M. and D.R. Brown, *Microglia and the aging brain: are senescent microglia the key to neurodegeneration?* J Neurochem, 2019. **151**(6): p. 676-688.
322. Zupkovitz, G., et al., *Histone deacetylase 1 expression is inversely correlated with age in the short-lived fish Nothobranchius furzeri.* Histochem Cell Biol, 2018. **150**(3): p. 255-269.
323. Mahady, L., et al., *HDAC2 dysregulation in the nucleus basalis of Meynert during the progression of Alzheimer's disease.* Neuropathol Appl Neurobiol, 2019. **45**(4): p. 380-397.
324. Trzeciakiewicz, H., et al., *An HDAC6-dependent surveillance mechanism suppresses tau-mediated neurodegeneration and cognitive decline.* Nat Commun, 2020. **11**(1): p. 5522.
325. Khurana, A. and C.A. Dlugos, *Age-related alterations in histone deacetylase expression in Purkinje neurons of ethanol-fed rats.* Brain Res, 2017. **1675**: p. 8-19.
326. Jing, X., et al., *HDAC7 Ubiquitination by the E3 Ligase CBX4 Is Involved in Contextual Fear Conditioning Memory Formation.* J Neurosci, 2017. **37**(14): p. 3848-3863.
327. Schultz, M.B., et al., *Molecular and Cellular Characterization of SIRT1 Allosteric Activators.* Methods Mol Biol, 2019. **1983**: p. 133-149.
328. Kelly, R.D. and S.M. Cowley, *The physiological roles of histone deacetylase (HDAC) 1 and 2: complex co-stars with multiple leading parts.* Biochem Soc Trans, 2013. **41**(3): p. 741-9.
329. Thangaraj, A., et al., *HIV TAT-mediated microglial senescence: Role of SIRT3-dependent mitochondrial oxidative stress.* Redox Biol, 2021. **40**: p. 101843.
330. Hanahan, D. and R.A. Weinberg, *Hallmarks of cancer: the next generation.* Cell, 2011. **144**(5): p. 646-74.
331. Tamimi, A.F. and M. Juweid, *Epidemiology and Outcome of Glioblastoma*, in *Glioblastoma*, S. De Vleeschouwer, Editor. 2017, Codon Publications

Copyright: The Authors.: Brisbane (AU).
332. Gillotin, S., et al., *Targeting impaired adult hippocampal neurogenesis in ageing by leveraging intrinsic mechanisms regulating Neural Stem Cell activity.* Ageing Res Rev, 2021. **71**: p. 101447.

333. Hassell, K.N., *Histone Deacetylases and their Inhibitors in Cancer Epigenetics.* Diseases, 2019. **7**(4).
334. Patel, B. and A.M. Cuervo, *Methods to study chaperone-mediated autophagy.* Methods, 2015. **75**: p. 133-40.
335. Wang, Y., et al., *Discovery of LAMP-2A as potential biomarkers for glioblastoma development by modulating apoptosis through N-CoR degradation.* Cell Commun Signal, 2021. **19**(1): p. 40.
336. Giatromanolaki, A., et al., *Autophagy and lysosomal related protein expression patterns in human glioblastoma.* Cancer Biol Ther, 2014. **15**(11): p. 1468-78.
337. Chi, C., et al., *LAMP-2B regulates human cardiomyocyte function by mediating autophagosome-lysosome fusion.* Proc Natl Acad Sci U S A, 2019. **116**(2): p. 556-565.
338. Jovčevska, I., *Sequencing the next generation of glioblastomas.* Crit Rev Clin Lab Sci, 2018. **55**(4): p. 264-282.
339. Zhou, J., et al., *Chaperone-mediated autophagy regulates proliferation by targeting RND3 in gastric cancer.* Autophagy, 2016. **12**(3): p. 515-28.
340. Han, Q., et al., *Downregulation of ATG5-dependent macroautophagy by chaperone-mediated autophagy promotes breast cancer cell metastasis.* Sci Rep, 2017. **7**(1): p. 4759.
341. Hubbi, M.E., et al., *Cyclin-dependent kinases regulate lysosomal degradation of hypoxia-inducible factor 1α to promote cell-cycle progression.* Proc Natl Acad Sci U S A, 2014. **111**(32): p. E3325-34.
342. Guo, B., et al., *M2 tumor-associated macrophages produce interleukin-17 to suppress oxaliplatin-induced apoptosis in hepatocellular carcinoma.* Oncotarget, 2017. **8**(27): p. 44465-44476.
343. Wu, J.H., et al., *CMA down-regulates p53 expression through degradation of HMGB1 protein to inhibit irradiation-triggered apoptosis in hepatocellular carcinoma.* World J Gastroenterol, 2017. **23**(13): p. 2308-2317.
344. Mizushima, N. and B. Levine, *Autophagy in mammalian development and differentiation.* Nat Cell Biol, 2010. **12**(9): p. 823-30.
345. Guan, J.L., et al., *Autophagy in stem cells.* Autophagy, 2013. **9**(6): p. 830-49.
346. Hallal, S., et al., *Extracellular Vesicles from Neurosurgical Aspirates Identifies Chaperonin Containing TCP1 Subunit 6A as a Potential Glioblastoma Biomarker with Prognostic Significance.* Proteomics, 2019. **19**(1-2): p. e1800157.
347. Pavel, M., et al., *CCT complex restricts neuropathogenic protein aggregation via autophagy.* Nat Commun, 2016. **7**: p. 13821.
348. Bourdenx, M., et al., *Chaperone-mediated autophagy prevents collapse of the neuronal metastable proteome.* Cell, 2021. **184**(10): p. 2696-2714.e25.
349. Hao, Y., et al., *Targetome analysis of chaperone-mediated autophagy in cancer cells.* Autophagy, 2019. **15**(9): p. 1558-1571.
350. Kacal, M., et al., *Quantitative proteomic analysis of temporal lysosomal proteome and the impact of the KFERQ-like motif and LAMP2A in lysosomal targeting.* Autophagy, 2021. **17**(11): p. 3865-3874.
351. Sighel, D., et al., *Inhibition of mitochondrial translation suppresses glioblastoma stem cell growth.* Cell Rep, 2021. **35**(4): p. 109024.
352. Modica-Napolitano, J.S. and J.R. Aprille, *Delocalized lipophilic cations selectively target the mitochondria of carcinoma cells.* Adv Drug Deliv Rev, 2001. **49**(1-2): p. 63-70.
353. Saga, I., et al., *Integrated analysis identifies different metabolic signatures for tumor-initiating cells in a murine glioblastoma model.* Neuro Oncol, 2014. **16**(8): p. 1048-56.
354. Yuen, C.A., et al., *Cancer stem cell molecular reprogramming of the Warburg effect in glioblastomas: a new target gleaned from an old concept.* CNS Oncol, 2016. **5**(2): p. 101-8.
355. Nallanthighal, S., J.P. Heiserman, and D.J. Cheon, *The Role of the Extracellular Matrix in Cancer Stemness.* Front Cell Dev Biol, 2019. **7**: p. 86.

356. Paolillo, M., M. Serra, and S. Schinelli, *Integrins in glioblastoma: Still an attractive target?* Pharmacol Res, 2016. **113**(Pt A): p. 55-61.
357. Lathia, J.D., et al., *Integrin alpha 6 regulates glioblastoma stem cells.* Cell Stem Cell, 2010. **6**(5): p. 421-32.
358. Motegi, H., et al., *Type 1 collagen as a potential niche component for CD133-positive glioblastoma cells.* Neuropathology, 2014. **34**(4): p. 378-85.
359. Xuan, Y., et al., *Inhibition of chaperone-mediated autophagy reduces tumor growth and metastasis and promotes drug sensitivity in colorectal cancer.* Mol Med Rep, 2021. **23**(5).
360. Du, Z., et al., *The effects of type I interferon on glioblastoma cancer stem cells.* Biochem Biophys Res Commun, 2017. **491**(2): p. 343-348.
361. Zhang, Y., et al., *Overexpression of STAT1 suppresses angiogenesis under hypoxia by regulating VEGF-A in human glioma cells.* Biomed Pharmacother, 2018. **104**: p. 566-575.
362. Zhan, X., et al., *Glioma stem-like cells evade interferon suppression through MBD3/NuRD complex-mediated STAT1 downregulation.* J Exp Med, 2020. **217**(5).
363. Zhang, K., et al., *Proteome Analysis of Hypoxic Glioblastoma Cells Reveals Sequential Metabolic Adaptation of One-Carbon Metabolic Pathways.* Mol Cell Proteomics, 2017. **16**(11): p. 1906-1921.
364. Nguyen, H.S., et al., *Molecular Markers of Therapy-Resistant Glioblastoma and Potential Strategy to Combat Resistance.* Int J Mol Sci, 2018. **19**(6).
365. Arnold, C.R., et al., *The Role of Cancer Stem Cells in Radiation Resistance.* Front Oncol, 2020. **10**: p. 164.
366. Fine, H.A., et al., *A phase I trial of a new recombinant human beta-interferon (BG9015) for the treatment of patients with recurrent gliomas.* Clin Cancer Res, 1997. **3**(3): p. 381-7.
367. Axelrod, M.L., et al., *Biological Consequences of MHC-II Expression by Tumor Cells in Cancer.* Clin Cancer Res, 2019. **25**(8): p. 2392-2402.
368. McCormick, P.J., J.A. Martina, and J.S. Bonifacino, *Involvement of clathrin and AP-2 in the trafficking of MHC class II molecules to antigen-processing compartments.* Proc Natl Acad Sci U S A, 2005. **102**(22): p. 7910-5.
369. Belabed, M., et al., *Kinesin-1 regulates antigen cross-presentation through the scission of tubulations from early endosomes in dendritic cells.* Nat Commun, 2020. **11**(1): p. 1817.
370. Riese, R.J. and H.A. Chapman, *Cathepsins and compartmentalization in antigen presentation.* Curr Opin Immunol, 2000. **12**(1): p. 107-13.
371. Guelfi, S., et al., *Vascular Transdifferentiation in the CNS: A Focus on Neural and Glioblastoma Stem-Like Cells.* Stem Cells Int, 2016. **2016**: p. 2759403.
372. Patel, A.P., et al., *Single-cell RNA-seq highlights intratumoral heterogeneity in primary glioblastoma.* Science, 2014. **344**(6190): p. 1396-401.
373. van Tellingen, O., et al., *Overcoming the blood-brain tumor barrier for effective glioblastoma treatment.* Drug Resist Updat, 2015. **19**: p. 1-12.
374. Parada, L.F., P.B. Dirks, and R.J. Wechsler-Reya, *Brain Tumor Stem Cells Remain in Play.* J Clin Oncol, 2017. **35**(21): p. 2428-2431.
375. Touat, M., et al., *Glioblastoma targeted therapy: updated approaches from recent biological insights.* Ann Oncol, 2017. **28**(7): p. 1457-1472.
376. Kunadis, E., et al., *Targeting post-translational histone modifying enzymes in glioblastoma.* Pharmacol Ther, 2021. **220**: p. 107721.
377. Eckschlager, T., et al., *Histone Deacetylase Inhibitors as Anticancer Drugs.* Int J Mol Sci, 2017. **18**(7).
378. Seidel, C., et al., *Histone deacetylase 6 in health and disease.* Epigenomics, 2015. **7**(1): p. 103-18.
379. Staberg, M., et al., *Inhibition of histone deacetylases sensitizes glioblastoma cells to lomustine.* Cell Oncol (Dordr), 2017. **40**(1): p. 21-32.

380. Parsons, D.W., et al., *An integrated genomic analysis of human glioblastoma multiforme.* Science, 2008. **321**(5897): p. 1807-12.
381. Bazzaro, M., et al., *Ubiquitin proteasome system stress underlies synergistic killing of ovarian cancer cells by bortezomib and a novel HDAC6 inhibitor.* Clin Cancer Res, 2008. **14**(22): p. 7340-7.
382. Sakuma, T., et al., *Aberrant expression of histone deacetylase 6 in oral squamous cell carcinoma.* Int J Oncol, 2006. **29**(1): p. 117-24.
383. Bradbury, C.A., et al., *Histone deacetylases in acute myeloid leukaemia show a distinctive pattern of expression that changes selectively in response to deacetylase inhibitors.* Leukemia, 2005. **19**(10): p. 1751-9.
384. Aldana-Masangkay, G.I. and K.M. Sakamoto, *The role of HDAC6 in cancer.* J Biomed Biotechnol, 2011. **2011**: p. 875824.
385. Fan, Y., et al., *Comprehensive Analysis of HDAC Family Identifies HDAC1 as a Prognostic and Immune Infiltration Indicator and HDAC1-Related Signature for Prognosis in Glioma.* Front Mol Biosci, 2021. **8**: p. 720020.
386. Wang, Z., et al., *HDAC6 promotes cell proliferation and confers resistance to temozolomide in glioblastoma.* Cancer Lett, 2016. **379**(1): p. 134-42.
387. Bamodu, O.A., et al., *HDAC inhibitor suppresses proliferation and tumorigenicity of drug-resistant chronic myeloid leukemia stem cells through regulation of hsa-miR-196a targeting BCR/ABL1.* Experimental cell research, 2018. **370**(2): p. 519-530.
388. Chiao, M.T., et al., *Suberoylanilide hydroxamic acid (SAHA) causes tumor growth slowdown and triggers autophagy in glioblastoma stem cells.* Autophagy, 2013. **9**(10): p. 1509-26.
389. Urdiciain, A., et al., *Tubastatin A, an inhibitor of HDAC6, enhances temozolomide-induced apoptosis and reverses the malignant phenotype of glioblastoma cells.* Int J Oncol, 2019. **54**(5): p. 1797-1808.
390. Wu, R., et al., *SOX2 promotes resistance of melanoma with PD-L1 high expression to T-cell-mediated cytotoxicity that can be reversed by SAHA.* J Immunother Cancer, 2020. **8**(2).
391. Sharif, T., et al., *HDAC6 differentially regulates autophagy in stem-like versus differentiated cancer cells.* Autophagy, 2019. **15**(4): p. 686-706.
392. Gui, C.Y., et al., *Histone deacetylase (HDAC) inhibitor activation of p21WAF1 involves changes in promoter-associated proteins, including HDAC1.* Proc Natl Acad Sci U S A, 2004. **101**(5): p. 1241-6.
393. Ryu, H.W., et al., *HDAC6 deacetylates p53 at lysines 381/382 and differentially coordinates p53-induced apoptosis.* Cancer Lett, 2017. **391**: p. 162-171.
394. Zhang, Y., et al., *The p53 Pathway in Glioblastoma.* Cancers (Basel), 2018. **10**(9).
395. Li, D., N.D. Marchenko, and U.M. Moll, *SAHA shows preferential cytotoxicity in mutant p53 cancer cells by destabilizing mutant p53 through inhibition of the HDAC6-Hsp90 chaperone axis.* Cell Death Differ, 2011. **18**(12): p. 1904-13.
396. Diss, E., et al., *Vorinostat(SAHA) Promotes Hyper-Radiosensitivity in Wild Type p53 Human Glioblastoma Cells.* J Clin Oncol Res, 2014. **2**(1).
397. Gatti, L., et al., *Histone deacetylase inhibitor-temozolomide co-treatment inhibits melanoma growth through suppression of Chemokine (C-C motif) ligand 2-driven signals.* Oncotarget, 2014. **5**(12): p. 4516-28.
398. Singh, M.M., et al., *Preclinical activity of combined HDAC and KDM1A inhibition in glioblastoma.* Neuro Oncol, 2015. **17**(11): p. 1463-73.
399. Sarkaria, J.N., et al., *Is the blood-brain barrier really disrupted in all glioblastomas? A critical assessment of existing clinical data.* Neuro Oncol, 2018. **20**(2): p. 184-191.
400. Yuan, H., et al., *Albumin Nanoparticle of Paclitaxel (Abraxane) Decreases while Taxol Increases Breast Cancer Stem Cells in Treatment of Triple Negative Breast Cancer.* Mol Pharm, 2020. **17**(7): p. 2275-2286.

401. Jung, B. and B. Anvari, *Synthesis and characterization of bovine serum albumin-coated nanocapsules loaded with indocyanine green as potential multifunctional nanoconstructs.* Biotechnol Prog, 2012. **28**(2): p. 533-9.
402. Lin, T., et al., *Blood-Brain-Barrier-Penetrating Albumin Nanoparticles for Biomimetic Drug Delivery via Albumin-Binding Protein Pathways for Antiglioma Therapy.* ACS Nano, 2016. **10**(11): p. 9999-10012.
403. Zhao, M., et al., *Nanocarrier-based drug combination therapy for glioblastoma.* Theranostics, 2020. **10**(3): p. 1355-1372.
404. Peleg, S., et al., *Altered histone acetylation is associated with age-dependent memory impairment in mice.* Science, 2010. **328**(5979): p. 753-6.
405. Penney, J. and L.H. Tsai, *Histone deacetylases in memory and cognition.* Sci Signal, 2014. **7**(355): p. re12.
406. Hainmueller, T. and M. Bartos, *Dentate gyrus circuits for encoding, retrieval and discrimination of episodic memories.* Nat Rev Neurosci, 2020. **21**(3): p. 153-168.
407. Gilbert, T.M., et al., *Neuroepigenetic signatures of age and sex in the living human brain.* Nat Commun, 2019. **10**(1): p. 2945.
408. McIntyre, R.L., et al., *From molecular promise to preclinical results: HDAC inhibitors in the race for healthy aging drugs.* EMBO Mol Med, 2019. **11**(9): p. e9854.
409. Baker, D.J., et al., *Opposing roles for p16Ink4a and p19Arf in senescence and ageing caused by BubR1 insufficiency.* Nat Cell Biol, 2008. **10**(7): p. 825-36.
410. Baker, D.J., R.L. Weaver, and J.M. van Deursen, *p21 both attenuates and drives senescence and aging in BubR1 progeroid mice.* Cell Rep, 2013. **3**(4): p. 1164-74.
411. Matheu, A., et al., *Delayed ageing through damage protection by the Arf/p53 pathway.* Nature, 2007. **448**(7151): p. 375-9.
412. Carrasco-Garcia, E., et al., *Increased gene dosage of Ink4/Arf and p53 delays age-associated central nervous system functional decline.* Aging Cell, 2015. **14**(4): p. 710-4.
413. Gebara, E., et al., *Adult hippocampal neurogenesis inversely correlates with microglia in conditions of voluntary running and aging.* Front Neurosci, 2013. **7**: p. 145.
414. Bandyopadhyay, D., et al., *Dynamic assembly of chromatin complexes during cellular senescence: implications for the growth arrest of human melanocytic nevi.* Aging Cell, 2007. **6**(4): p. 577-91.
415. Gräff, J., et al., *An epigenetic blockade of cognitive functions in the neurodegenerating brain.* Nature, 2012. **483**(7388): p. 222-6.
416. Safaiyan, S., et al., *White matter aging drives microglial diversity.* Neuron, 2021. **109**(7): p. 1100-1117.e10.
417. Liu, H., et al., *Aging of cerebral white matter.* Ageing Res Rev, 2017. **34**: p. 64-76.
418. Yang, H., et al., *HDAC inhibition reduces white matter injury after intracerebral hemorrhage.* J Cereb Blood Flow Metab, 2021. **41**(5): p. 958-974.
419. Fernández-Cabello, S., et al., *White matter hyperintensities and cognitive reserve during a working memory task: a functional magnetic resonance imaging study in cognitively normal older adults.* Neurobiol Aging, 2016. **48**: p. 23-33.
420. Nordahl, C.W., et al., *White matter changes compromise prefrontal cortex function in healthy elderly individuals.* J Cogn Neurosci, 2006. **18**(3): p. 418-29.

Publications during the PhD

1. **Auzmendi-Iriarte J**, Otaegi-Ugartemendia M, Carrasco-Garcia E, Azkargorta M, Diaz A, Saenz-Antoñanzas A, Andermatten JA, García-Puga M, Garcia I, Elua-Pinin A, Ruiz I, Samprón N, Elortza F, Cuervo AM, Matheu A. Chaperone-mediated autophagy controls proteomic and transcriptomic pathways to maintain glioma stem cell activity. **Cancer Research.** 2022 Feb 7:canres.2161.2021. doi: 10.1158/0008-5472.CAN-21-2161. Epub ahead of print. PMID: 35131870.

2. Saenz-Antoñanzas A, Moncho-Amor V, **Auzmendi-Iriarte J**, Elua-Pinin A, Rizzoti K, Lovell-Badge R, Matheu A. *CRISPR/Cas9 Deletion of SOX2 Regulatory Region 2 (SRR2) Decreases SOX2 Malignant Activity in Glioblastoma*. **Cancers (Basel)**. 2021 Mar 29;13(7):1574. doi: 10.3390/cancers13071574.

3. **Auzmendi-Iriarte J**, Matheu A. *Impact of Chaperone-Mediated autophagy in Brain Aging: Neurodegenerative Diseases and Glioblastoma.* **Frontiers in Aging Neuroscience**. 2021 Jan 28;12:630743. doi: 10.3389/fnagi.2020.630743.

4. Aldaz P, **Auzmendi-Iriarte J**, Durántez M, Lasheras-Otero I, Carrasco-Garcia E, Zelaya MV, Bragado L, Olías-Arjona A, Egaña L, Samprón N, Morilla I, Redondo-Muñoz M, Rico M, Squatrito M, Maria-Alonso M, Fernández-Irigoyen J, Santamaria E, Larráyoz IM, Wellbrock C, Matheu A, Arozarena I. *Identification of a Dexamethasone MediatedRadioprotection Mechanism Reveals New Therapeutic Vulnerabilities in Glioblastoma.* **Cancers (Basel).** 2021 Jan 19;13(2):361. doi: 10.3390/cancers13020361.

5. Egaña L, **Auzmendi-Iriarte J**, Andermatten J, Villanua J, Ruiz I, Elua-Pinin A, Aldaz P, Querejeta A, Sarasqueta C, Zubia F, Matheu A, Samprón N. *Methylation of MGMT promoter does not predict response to temozolomide in patients with glioblastoma in Donostia Hospital.* **Scientific Reports.** 2020 Oct 28;10(1):18445. doi: 10.1038/s41598-020-75477-9.

6. **Auzmendi-Iriarte J**, Saenz-Antoñanzas A, Mikelez-Alonso I, Carrasco-Garcia E, Tellaetxe-Abete M, Lawrie CH, Sampron N, Cortajarena AL, Matheu A. *Characterization of a new small-molecule inhibitor of HDAC6 in glioblastoma.* **Cell Death & Disease.** 2020 Jun 2;11(6):417. doi: 10.1038/s41419-020-2586-x.

7. Saenz-Antoñanzas A, **Auzmendi-Iriarte J**, Carrasco-Garcia E, Moreno-Cugnon L, Ruiz I, Villanua J, Egaña L, Otaegui D, Samprón N, Matheu A. *Liquid Biopsy in Glioblastoma: Opportunities, Applications and Challenges.* **Cancers (Basel).** 2019 Jul 5;11(7):950. doi: 10.3390/cancers11070950.

8. De Lope C, Martín-Alonso S, **Auzmendi-Iriarte J**, Escudero C, Mulet I, Larrasa-Alonso J, López-Antona I, Matheu A, Palmero I. *SIX1 represses senescence and promotes SOX2-mediatedcellular plasticity during tumorigenesis.* **Scientific Reports.** 2019 Feb 5;9(1):1412. doi: 10.1038/s41598-018-38176-0.

9. Torres-Bayona S, Aldaz P, **Auzmendi-Iriarte J**, Saenz-Antoñanzas A, Garcia I, Arrazola M, Gerovska D, Undabeitia J, Querejeta A, Egaña L, Villanúa J, Ruiz I, Sarasqueta C, Urculo E, Araúzo-Bravo MJ, Huarte M, Samprón N, Matheu A. *PR-LncRNA signature regulates glioma cell activity through expression of SOX factors.* **Scientific Reports.** 2018 Aug 24;8(1):12746. doi: 10.1038/s41598-018-30836-5.

10. Carrasco-Garcia E, **Auzmendi-Iriarte J**, Matheu A. *Integrin α7: a novel promising target in glioblastoma stem cells.* **Stem Cell Investigation.** 2018 Jan 13;5:2. doi: 10.21037/sci.2017.12.05.

11. Arrizabalaga O*, Moreno-Cugnon L*, **Auzmendi-Iriarte J**, Aldaz P, Ibanez de Caceres I, Garros-Regulez L, Moncho-Amor V, Torres-Bayona S, Pernía O, Pintado-Berninches L, Carrasco-Ramirez P, Cortes-Sempere M, Rosas R, Sanchez-Gomez P, Ruiz I, Caren H, Pollard S, Garcia I, Sacido AA, Lovell-Badge R, Belda-Iniesta C, Sampron N, Perona R, Matheu A. *High expression of MKP1/DUSP1 counteracts glioma stem cell activity and mediumtes HDAC inhibitor response.* **Oncogenesis.** 2017 Dec 14;6(12):401. doi: 10.1038/s41389-017-0003-9. *Equal contribution.